Global flood model assessment and flood risk evaluation

Mark Viktor Bernhofen

Submitted in accordance with the requirements for the degree of
Doctor of Philosophy

The University of Leeds
School of Civil Engineering

January 2022

The candidate confirms that the work submitted is his/her own, except where work which has formed part of jointly-authored publications has been included. The contribution of the candidate and the other authors to this work has been explicitly indicated below. The candidate confirms that appropriate credit has been given within the thesis where reference has been made to the work of others.

The rationale for submitting an alternative format thesis was that the work conducted in each chapter was deemed to be a significant contribution to the existing literature that warranted timely publication in academic journals. Each chapter has either been published or is currently under review for publication. As such, it was deemed appropriate to submit this work as a 'thesis by publication'. The four publications which form the main body of work in this thesis are outlined below, along with the contributions of each author.

The work in **Chapter 2** of this thesis has appeared in publication as follows: Trigg M. A., **Bernhofen, M. V.**, Marechal, D., Alfieri, L., Dottori, F., Hoch, J., Horritt, M., Sampson, C., Smith, A., Yamazaki, D., and Li, H. (2021). Global Flood Models. *In Global Drought and Flood* (eds. H. Wu, D.P. Lettenmaier, Q. Tang and P.J. Ward). https://doi.org/10.1002/9781119427339.ch10

M.V.B. developed the structure and expected contents of the publication with M.A.T. **M.V.B** created Figure 2.1 and Figure 2.3 and wrote section 2.3, section 2.4, and section 2.7 with input from all co-authors. M.A.T. wrote section 2.2 and 2.6 with input from all co-authors. D.M. wrote section 2.5. **M.V.B.** and M.A.T edited the manuscript for submission. **M.V.B** revised the manuscript after review.

The work in **Chapter 3** of this thesis has appeared in publication as follows: **Bernhofen, M. V.**, Whyman C., Trigg, M. A., Sleigh, P. A., Smith, A. M., Sampson, C. C., Yamazaki, D., Ward, P., Rudari, R., Pappenberger, F. (2018). A first collective validation of global fluvial flood models for major floods in Nigeria and Mozambique. *Environmental Research Letters*, Volume 13, Number 10. https://doi.org/10.1088/1748-9326/aae014

M.V.B. and M.A.T. conceived of the study. **M.V.B.** developed and carried out the analysis and drafted the manuscript. C.W. created the Chemba validation maps. All co-authors contributed towards the discussion and editing of the manuscript.

The work in **Chapter 4** of this thesis as appeared in publication as follows: **Bernhofen, M.V.**, Trigg, M. A., Sleigh, P. A., Sampson, C. C., Smith, A. M. (2021). Global flood exposure from different sized rivers. *Natural Hazards and Earth Systems Science*, 21, pp. 2829-2847. https://doi.org/10.5194/nhess-21-2829-2021

M.V.B. and M.A.T conceived of the study. **M.V.B.** designed and carried out the analysis and drafted the manuscript. All co-authors contributed towards the discussion and editing of the manuscript.

The work in **Chapter 5** is currently under review: **Bernhofen M.V.**, Cooper, S., Trigg, M.A., Mdee, A., Carr, A., Bhave, A., Solano-Correa, Y., Pencue-Fierro, E., Teferi, E., Haile, A. T., Yusop, Z., Alias, N., Sa'adi, Z., Bin Ramzan, M., Dhanya, C. T., Shukla, P. *under review*. The Role of Global Datasets for Flood Risk Management at National Scales. *Water Resources Research.*

M.V.B. and M.A.T conceived of the study comparing global flood risk datasets nationally. S.C. developed and carried out interviews to assess institutional capacity. **M.V.B.** developed and carried out the flood risk analysis and drafted the manuscript. S.C. wrote section 5.3.2 with contribution from Y.S-C., E.P-F., E.T., A.T.H., Z.Y., N.A., Z.S., .M.B.R., C.T.D. and P.S. and section 5.7.3 with contribution from A.M. A.B wrote section 5.7.2. All co-authors contributed towards the discussion and editing of the manuscript.

iv

Acknowledgements

I would like to thank my family for their encouragement and support throughout this PhD. I have been incredibly fortunate to be able to continue research discussions at home and your interest in my work has been an enormous encouragement. Thanks also to Harriet, who has shared an office with me the last two years and endured hours of mock presentations and reading aloud.

Abstract

Floods are the most frequent and damaging natural hazard globally. To adequately prepare for floods it is essential to know where they will occur and what their impacts will be. This can be done by developing a flood model. Traditionally, these models have been local in scale, limited to areas with the necessary expertise and data to develop a flood model. However, the last decade has seen the proliferation of several global flood models, which use global datasets and automated approaches to map flood hazard globally. When combined with global datasets of exposure and vulnerability, they can be used to assess global flood risk. The development of these global flood risk datasets marks a potential paradigm shift in flood risk analysis from the traditional "ad hoc" approach to global datasets which can be used to assess flood risk anywhere in the world. Despite this, these global flood risk datasets still need significant evaluation to understand the limits of their effective application.

This thesis furthers the evaluation and explores the potential applications of global flood risk datasets. The current state of global flood risk modelling is reviewed, highlighting the different models, their history, structure, and application. The models are then collectively validated for the first time against observed flood events, demonstrating the skill of some models and identifying model characteristics which influence performance. The impact of river size thresholds, a key difference identified between the models, are quantified by calculating flood exposure to different sized rivers globally. Both the chosen river size thresholds and the global population maps used to calculate exposure are found to have a significant impact on flood exposure estimates. The use of global flood risk data is then explored nationally as global datasets of hazard, exposure, and vulnerability are evaluated for flood risk management in five countries. While some global datasets are found to be of potential use, there is still significant uncertainty in their national flood risk estimates and potential issues are identified related to the capacity there is to use them nationally.

Abbreviations

1D	One Dimension
2D	Two Dimensions
CaMa-Flood	Catchment-Based Macro-scale Floodplain
CAT	Catastrophe (insurance)
CIESIN	Center for International Earth Science Information Network
CIMA	Centro Internazionale in Monitoraggio Ambientale
CMIP	Coupled Model Intercomparison Project
CNN	Convolutional Neural Networks
CSI	Critical Success Index
CWC	Central Water Commission
DEM	Digital Elevation Model
DFO	Dartmouth Flood Observatory
DID	Department of Irrigation and Drainage
DRIVE	Dominant River Tracing-Routing Integrated with VIC Environment
DRM	Disaster Risk Management
EA	Environment Agency
EAE	Expected Annual Exposure
EAI	Exposure Agreement Index
ECMWF	European Centre for Medium-Range Weather Forecasts
ENSO	El Niño Southern Oscillation
ESA	European Space Agency
EUR	Euros
EUWATCH	European Union Water and Global Change
FEMA	Federal Emergency Management Agency
FRM	Flood Risk Management
G3WBM	Global 3sec Water Body Map
GAR	Global Assessment Report
GCM	Global Circulation Model
GCRF	Global Challenges Research Fund
GDP	Gross Domestic Product
GEE	Google Earth Engine
GFD	Global Flood Database

GFM	Global Flood Model
GFMIP	Global Flood Model Intercomparison Project
GFMS	Global Flood Monitoring System
GFP	Global Flood Partnership
GHG	Greenhouse Gas
GHSL	Global Human Settlement Layer
GHS-POP	Global Human Settlement Population
GIS	Geographical Information System
GloFAS	Global Flood Awareness System
GLOFRIS	Global Flood Risk with IMAGE Scenarios
GOE	Government of Ethiopia
GPM	Global Precipitation Measurement
GPW	Gridded Population of the World
GRAF	Global Risk Assessment Framework
GRDC	Global Runoff Data Center
GRUMP	Global Rural-Urban Mapping Project
HAND	Height Above Nearest Drainage
HR	Hit Rate
HRSL	High Resolution Settlement Layer
HYDE	History Database of the Global Environment
IMERG	Integrated Multi-Satellite Retrievals for GPM
IPCC	Intergovernmental Panel on Climate Change
ISI-MIP	Inter-Sectoral Impact Model Intercomparison Project
ITCZ	Intertropical Convergence Zone
JRC	Joint Research Centre
LiDAR	Light Detecting and Ranging
LMF	Loss Modelling Framework
MAI	Model Agreement Index
MERIT	Multi Error-Removed Improved-Terrain
MIP	Model Intercomparison Project
MODIS	Moderate Resolution Imaging Spectroradiometer
MOSART	Model for Scale Adaptive River Transport
NADMA	National Disaster Management Agency
NaFRA	National Flood Risk Assessment
NASA	National Aeronautics and Space Administration
NDRF	National Disaster Response Force

NDRMC	National Disaster Risk Management Commission
NFHL	National Flood Hazard Layer
NFIP	National Flood Insurance Program
PAI	Population Agreement Index
QGIS	Quantum GIS
RFSM	River Flood Susceptibility Map
RRC	Relief and Rehabilitation Commission
RS	Remote Sensing
SDRF	State Disaster Response Fund
SPIF	Strategic Program and Investment Framework
SRTM	Shuttle Radar and Topography Mission
SWOT	Surface Water and Ocean Topography
TMPA	TRMM Multi-Satellite Precipitation Analysis
TRMM	Tropical Rainfall Measuring Mission
UDA	Upstream Drainage Area
UK	United Kingdom
UKRI	UK Research and Innovation
UNDRR	United Nations Office for Disaster Risk Reduction
UNEP	United Nations Environment Program
UNISDR	United Nations International Strategy for Disaster Reduction
US	United States
USD	US Dollars
USGS	US Geological Survey
VAI	Volume Agreement Index

Table of Contents

List of Tables

List of Figures

Chapter 1
Introduction

In the first two decades of the 21st century, over 1.6 billion people were affected by floods (CRED and UNDRR, 2020). A global problem has elicited solutions at a similar scale, and several global datasets of flood hazard, exposure, and vulnerability have been developed. This thesis evaluates and explores the applicability of these global flood risk datasets. In this introductory chapter, the novel work of this thesis is placed into context with respect to the existing literature. The chapter begins with an introduction to flooding in a more general sense, covering both historical and future flooding. It then reviews how floods are modelled at increasing spatial scales. Focus is then turned to global flood models, reviewing existing efforts at global flood model evaluation and intercomparison. The approaches to calculate global flood risk are then reviewed, covering both exposure and vulnerability. The chapter concludes with a discussion of global data applied nationally and the challenges this presents.

1.1 Flooding

There are three key natural mechanisms of flooding: fluvial, pluvial and coastal. Fluvial flooding occurs when a river overflows its banks, normally as a result of rainfall or snowmelt in the river catchment. Frequently flooded areas along the river are known as floodplains. These areas are ecologically important, but development within them risks both floodplain degradation and human exposure to potentially catastrophic flooding (Tockner and Stanford, 2002, Opperman et al., 2009). Pluvial flooding is rainfall induced flooding not associated with any river. This disconnect between 'flood' and 'source' makes pluvial flooding difficult to predict and prepare for (Houston et al., 2011). The effects of pluvial flooding are disproportionally felt in urban areas, where impervious surfaces and inadequate drainage systems often exacerbate flooding (Rosenzweig et al., 2018). Coastal flooding is caused by storms with intense wind speeds, where a combination of high tides and extreme wind drives sea-water onto the shore (Woodruff et al., 2013). The severity of coastal flooding is directly correlated to sea-level rise (Nicholls et al.,

1999, Church et al., 2006). There is a growing body of literature which recognizes the importance of the interaction of these different mechanisms during flood events (Wahl et al., 2015, Ward et al., 2018, Eilander et al., 2020, Bates et al., 2021). These 'compound' events can often increase the magnitude of experienced impacts (Zscheischler et al., 2018). The work in this thesis is primarily concerned with fluvial flooding.

1.1.1 Historical Flooding

Throughout history, there has been a tendency for settlements to form in flood-prone areas (Di Baldassarre et al., 2013). Floodplains provide fertile soil for agriculture (Crawford et al., 1998), while rivers are important sources of fresh water (Kummu et al., 2011) and act as navigation routes that facilitate economic development through trade (Rasul, 2015, Fang and Jawitz, 2019). Rivers have influenced historic human migration patterns (Campos et al., 2006, Bertuzzo et al., 2007) and settlements have been shown to follow fractal river patterns globally (Fang et al., 2018). Current global estimates suggest that over one billion people reside within floodplains (Di Baldassarre et al., 2013, Rentschler and Salhab, 2020).

Continental and global studies examining historical trends in flood impacts have shown increases in both economic and human exposure to flooding over the past 50 to 150 years (Mills, 2005, Barredo, 2007, Paprotny et al., 2018, Jonkman, 2005). At the same time, there is evidence of increased adaptation to floods reflected in declining global vulnerability (Jongman et al., 2015, Tanoue et al., 2016, Formetta and Feyen, 2019). Flood adaptation measures can be 'hard' (dikes and levees) or 'soft' (early warning systems, land-use planning, and insurance). Hard flood adaptation measures are often the most cost-effective solutions for high-risk areas (Jongman, 2018). However, the implementation of such measures can counterintuitively increase flood risk, a phenomenon known as the 'levee effect' (White, 1942). The levee effect is experienced when a physical measure is constructed that reduces the frequency of flooding. Over time this reduces the public perception of risk and encourages increased economic development and settlement within the protected area increasing the number of assets and people exposed to potentially devastating low-probability flood events (Ludy and Kondolf, 2012). Hurricane Katrina in 2005 is an example of such a rare and devastating event, where constructed levees were overtopped resulting in the deaths of over 1,000 people and

economic damages in the hundreds of billions for the state of Louisiana, USA (Hoople, 2013).

There is a plethora of evidence and research that points to demographic changes as one of the key drivers of historical increases in flood exposure (Changnon et al., 2000, Pielke et al., 2005, Di Baldassarre et al., 2010, Bouwer, 2011, Tellman et al., 2021). Less clear is the historical impact of climate change on flood exposure, largely due to the different processes driving river flooding (Blöschl et al., 2017). Extreme rainfall has increased with warming global temperatures (Westra et al., 2013, Asadieh and Krakauer, 2015), but this has not resulted in increased extreme floods (Sharma et al., 2018). Ivancic and Shaw (2015) show that extreme precipitation is not a good proxy for extreme river discharge if watershed soil moisture is not also accounted for. As such, historical trends in extreme floods are less obvious than trends in precipitation. For example, Hodgkins et al. (2017) found that any significant trends in North American and European extreme floods were a result of chance, while Slater et al. (2021) found both increases and decreases in extreme flood probability globally. Najibi and Devineni (2018) found global increases in both extreme flood frequency and duration, but these were attributed to climate variability rather than climate warming. Linking historical flooding to a warming climate is difficult due to poor quality historical record data (Wilby et al., 2017) and by short windows of observation which are often smaller than the timescale of climatic variability (Hall et al., 2014). Beyond observing the historical trends of extremes, there are a growing number of studies dedicated to extreme event attribution, where researchers try to determine the causal relationship between a warming climate and a single extreme event (Marjanac et al., 2017). This is typically done by running two climate model simulations. One which simulates the historical climate in the Anthropocene and another which simulates a historical climate without human influence. By comparing the extreme event in question under the two scenarios, the likelihood that it was made more extreme due to climate change can be calculated (Swain et al., 2020). An attribution study by Wehner and Sampson (2021) found that thirteen billion dollars of damage caused by Hurricane Harvey to the city of Houston, Texas could be attributed to global warming. Similarly, the devastating floods that affected western Europe in the summer of

2021 were found by to be between 1.2 and 9 times more likely to occur due to climate change (Kreienkamp et al., 2021).

1.1.2 Future Flooding

There is an urgent need to understand how flooding, and its impacts, will change in the future. Future changes in flood risk will be driven by both changes in the global climate and changes in global demographics. The Intergovernmental Panel on Climate Change (IPCC) was established in 1988 and has released six assessment reports every five to six years collating the latest science on climate change (IPCC, 2021). With each iteration of the IPCC report, the global outlook on climate change becomes bleaker. In the most recent report, new climate models predict greater increases in global surface temperature (compared to previous models) and increased frequency and severity of extreme events (precipitation, heat, and drought) (Masson-Delmotte et al., 2021). The report presents results from simulations of various emission scenarios (ranging from very low to very high greenhouse gas (GHG) emissions) run through the latest climate models from the Coupled Model Intercomparison Project Phase 6 (CMIP6) (Eyring et al., 2016). In a moderate emissions scenario, the climate models predict that the 1.5°C warming limit set in the Paris agreement (UNFCCC, 2015) will be passed before 2040 and by 2100 global temperatures will rise to between 2.3°C and 4.1°C above pre-industrial levels (Tollefson, 2021).

The new CMIP6 climate models were used to project future global changes in fluvial flooding by Hirabayashi et al. (2021). The study extended similar work done using the previous generation (CMIP5) of climate models (Hirabayashi et al., 2013) and aimed to compare the future flood projections under a high emission scenario from both studies. The future flood projections between the two generations of climate models were found to be largely similar, both in terms of magnitude and regionality. Flood frequency increased in large parts of Asia, Africa, and South America; and decreased in large parts of Europe, North America, central Asia and southern South America (Hirabayashi et al., 2021). Regional variations in future flood risk are a common theme in a number of global studies. Using climate predictions from the CMIP3 model catalogue, Arnell and Gosling (2016) found similar regional directional trends in flood frequency as Hirabayashi et al. (2021). Seven different climate models were used by Alfieri et al. (2017) to estimate future

flood exposure and damages under different warming scenarios. The study estimates the largest increases in flood exposure and damages will occur in Asia, the US, and Europe; some countries in Africa and Eastern Europe will experience decreases, while statistically insignificant changes will occur in a number of countries globally. The future flood risk projections outlined in Alfieri et al. (2017) considered exposure to be static in time, but there is a large body of work showing the implications of demographic and socio-economic change on future flood risk.

By combining models of socio-economic growth and climate change, Winsemius et al. (2016) were able to differentiate the impacts of demographic change and climate change on future flood risk. They found that without interventions, global damages as a result of both socio-economic and climate change may increase by up to a factor of 50 by 2100. In south-east Asia, where future flooding studies are unanimous on climate change's impact on increased flood frequency (Hirabayashi et al., 2008, Hirabayashi et al., 2013, Dankers et al., 2014, Arnell and Gosling, 2016, Alfieri et al., 2017, Hirabayashi et al., 2021), they found that socio-economic change will have a larger impact (by several orders of magnitude) on future flood risk (Winsemius et al., 2016). Similarly, Kam et al. (2021) found that the risk of future global flood displacement was further increased when socio-economic change was considered alongside climate change. A number of studies have shown that population growth is expected to occur in areas of flood risk. When exploring historical and future trends in exposure to floods, Jongman et al. (2012b) found that the global gross domestic product (GDP) exposed to flooding in 2050 would be roughly triple that of 2010. They also found that population growth in flood zones was larger than total population growth. Similarly, in nearly half (57) of the 119 countries examined by Tellman et al. (2021) flood exposure by 2030 was projected to increase at a greater rate than population growth. This is a trend seen at the national level too. Wing et al. (2018) found that population growth in the US would result in large increases of exposure by 2100 and, interestingly, exposure increases were greater in low return period (higher frequency) flood zones than high return period (low frequency) flood zones.

It's important to address the uncertainty associated with estimating future flooding and its impacts. These estimates are based on models and projections, rife with epistemic uncertainties. Although each iteration of the IPCC report brings with

it a narrowing of the uncertainty bounds (likely temperature range was reduced from 1.5-4.5°C in IPCC5 to 2.5-4°C in IPCC6) (Arias et al., 2021), rainfall is still coarsely represented in the models. Additionally, the fluvial response to rainfall, as covered in the previous section, is not straightforward (Sharma et al., 2018) and this is reflected in the differences between the results of studies of future river flooding (Hirabayashi et al., 2021, Arnell and Gosling, 2016, Alfieri et al., 2017). Similarly, future population estimates are inherently uncertain as they are reliant on accurate data and projections of fertility, mortality, and international migration (DESA, 2019). As the models and science continue to improve, one would expect to observe a convergence in estimates of future flooding and its impacts. Regardless, it is well established that flood risk will increase in the future for more of the world than it won't.

1.2 Modelling Floods

Our knowledge of flooding has developed significantly over the last half-century, due in no small part to the continued development of simulation techniques and datasets that allow us to model flooding in greater detail, at higher speed, and over a larger spatial domain.

1.2.1 Model Structure

Flooding can be modelled to varying degrees of complexity. Models can represent inundation in either one, two, or three dimensions. Three dimensional flood models are typically limited to smaller scales and represent phenomena unimportant to floodplain flow dynamics (Teng et al., 2017) and are therefore beyond the scope of this thesis. Both one and two dimensional models solve some formulation of the shallow water equations (also known as the Saint-Venant equations). In one-dimensional models, flow is assumed unidirectional along the river channel and the one-dimensional shallow-water equations are solved at cross-sections perpendicular to the river channel (Brunner, 1995, Md Ali et al., 2015). These models are typically computationally efficient and can be run over large spatial scales. Two-dimensional flood models solve the two-dimensional shallow-water equations across two-dimensional space represented either by a grid or a mesh (Neelz and Pender, 2009). These models are more computationally complex than one-dimensional models and have runtimes several orders of magnitude longer (Lin

et al., 2006). Both one-dimensional and two-dimensional model types can be coupled into 1D/2D models to capitalize on their respective advantages. In these coupled models, which are more computationally efficient than two-dimensional models, channel flow is represented in one-dimension and floodplain flow is represented in two-dimensions (Bates et al., 2005, Vozinaki et al., 2017). Using a coupled approach also allows for explicit representation of channels below the resolution of the two-dimensional grid (Neal et al., 2012a).

In order to improve runtimes or increase the spatial domain of the analysis, simplifications are often made to the shallow water equations (Hunter et al., 2007). Ordered in increasing levels of complexity, the kinematic simplification considers only the friction and gravity terms of the shallow water equations; the diffusive simplification considers the pressure, friction, and gravity terms (Ponce et al., 1978); and the inertial simplification considers the local acceleration, pressure, friction, and gravity terms (Bates et al., 2010). The choice of shallow water simplification is often made considering the context of the modelling study and whether the chosen simplification scheme would lead to an erroneous output. The kinematic simplification is useful for modelling slow rising flood waves, where wave velocity is determined by friction and gravity (Ponce et al., 1978, Neal et al., 2012a). The diffusive simplification is necessary to simulate backwater effects, and produces better results in areas of low relief compared with the kinematic approach (Trigg et al., 2009, Neal et al., 2012a, Bates et al., 2013). To represent momentum conservation, the inertial simplification is needed, and it has been shown to be more computationally efficient than the diffusive simplification (Bates et al., 2010, Neal et al., 2012b). The implementation of the full shallow water equations is necessary to model super-critical flows such as in mountainous rivers or during dam-breaks (Neal et al., 2012b, Neelz and Pender, 2013, de Almeida and Bates, 2013).

Modelling approaches that don't consider the physics of fluid flow, colloquially referred to as zero-dimensional models (Pender, 2006), are often applied in data-sparse regions and as initial scoping studies due to their low computational demand (Di Baldassarre et al., 2020). They can be either volume spreading models (Lhomme et al., 2008) or geomorphic (terrain based) models (Nobre et al., 2016, Samela et al., 2017b, Nardi et al., 2019). These zero-dimensional models produce credible results in well-defined floodplains, however

care should be taken when interpreting results across complex topographies and where the representation of momentum conservation is important (Teng et al., 2017)

1.2.2 Modelling across spatial scales

Flood models are developed for, and applied to, different scales. The scale of application normally determines the inputs, approach, and intended use of a model. Below, model application has been split into five different scales, ranging from local to global. These are not definitive classifications and there will be considerable overlap of model inputs, approaches, and uses across scales.

1.2.2.1 Local scale

Local scale models are typically confined to a small river reach. They are custom built by technical experts, normally to aid the design of flood defences or to carry out detailed flood risk assessments for local development and infrastructure (SEPA, 2017). These models require detailed data as input, as outlined in Mason et al. (2010). The elevation data used is typically the best available (normally Light Detecting And Ranging (LiDAR) data). The bathymetry of the channel (collected through surveyed channel cross sections) and hydraulicly relevant structures (flood defences, bridges, culverts, etc.) are explicitly represented. Local scale models are run using the full formulation of the shallow-water equations with boundary condition information (discharge and stage data) from local gauging stations. Gauge data is also used for model calibration (of the friction parameters) and validation. Where observational data is available, it too is used for model validation (Schumann et al., 2009).

1.2.2.2 Catchment scale

Catchment scale models share a number of similarities with local scale models, over a slightly larger spatial domain: the river catchment. They are typically used for options appraisal and planning, rather than to inform design (SEPA, 2017). The models are often fully hydrodynamic (solving the full shallow-water equations) and incorporate surveyed river cross sections. The representation of hydraulicly relevant structures is less explicit than local scale models and often some hydrological assumptions are made (Hankin et al., 2016). Catchment scale models are run for a number of different plausible scenarios using regionally available

rainfall data and hydrological models to simulate the catchment response (Hankin et al., 2017).

1.2.2.3 National scale

National scale flood maps are used to raise awareness of flooding, support flood risk management, and to inform insurance (de Moel et al., 2009). There are two distinctive approaches to national scale flood modelling. The first, involves combining individual catchment scale flood maps into an 'agglomerated' national flood map. This approach has been used in the UK, by the Environment Agency (EA), for their 'flood map for planning' (Environment Agency, 2018) and in the US, by the Federal Emergency Management Agency (FEMA), for the maps that underpin their National Flood Insurance Program (NFIP) (Federal Emergency Planning Agency, 2019). The other national approach involves modelling flooding for the country in its entirety. This approach benefits from a consistent methodology and overcomes the pitfalls of data gaps and outdated maps that plague the agglomerated approach (Horn and Brown, 2017, Wing et al., 2017). To model flooding for an entire country, however, certain sacrifices have to be made with regards to detail and hydrodynamic representation (de Moel et al., 2015). The river channel is assumed to be rectangular, flood defences are only sometimes represented (either explicitly or implicitly), and a simplified version of the shallow water equations is used to simulate flooding in order to make the model computationally viable. National level flood models have been developed in the UK (Hall et al., 2003, Hall et al., 2005, Bradbrook et al., 2005) and in the US (Wing et al., 2017, Bates et al., 2021)

1.2.2.4 Transboundary and continental scale

Often large river basins that span multiple countries are modelled in their entirety. Examples of this include the Rhine (ICPR, 2019), the Elbe (IKSE, 2016), and the Danube (ICPDR, 2015). Efforts have also been made to model flooding at the continental scale; predominantly in regions where the necessary data is available such as Europe (Dankers and Feyen, 2009, Alfieri et al., 2014), the US (Wing et al., 2017, Bates et al., 2021), and Australia (Schumann et al., 2016). Models at this scale have to make further simplifications to their frameworks to allow for data and computational limitations. The models are often coarser in resolution and make

simplifications to the hydrodynamic simulations, even so-far as being zero-dimensional (see Lugeri et al. (2010) for Europe and Jafarzadegan et al. (2018) and Samela et al. (2017a) for the US). These continental scale models are typically used to assess both present day and future risks (Feyen et al., 2012, Rojas et al., 2013, Alfieri et al., 2015, Alfieri et al., 2018b, Wing et al., 2018) and to evaluate potential adaptation measures (Jongman et al., 2014, Johnson et al., 2020). Continental scale models are also used extensively by the insurance industry, however their modelling approaches and outputs are proprietary (JBA, 2019, JBA, 2021).

1.2.2.5 Global scale

The proliferation of the necessary datasets for flood modelling at the global scale (Farr et al., 2007, Lehner et al., 2008, Scussolini et al., 2016, Yamazaki et al., 2017, Yamazaki et al., 2019) and the formulation of efficient hydrodynamic codes (Bates and De Roo, 2000, Bates et al., 2010, Dottori and Todini, 2011, Yamazaki et al., 2013) has led to the development of a number of different global flood models (GFMs) over the last decade (Yamazaki et al., 2011, Pappenberger et al., 2012, Winsemius et al., 2013, Ward et al., 2013, Rudari et al., 2015, Sampson et al., 2015, Dottori et al., 2016). In their seminal paper, Sampson et al. (2015) identified six key challenges that must be addressed to model flooding globally: accurate global terrain data, extreme flow generation, accurate global hydrography data, representation of flood defences, computationally efficient hydrodynamics, and an automated framework. These were challenges faced by all groups developing global flood models, and the different solutions to the challenges proposed by each model group led to the development of a number of very different GFMs (Bates et al., 2018).

The global scale of the models, their wide-ranging applicability, and their potential to fill data-gaps in previously unmodelled regions has seen the GFMs implemented across a number of different sectors and use cases. The models have been used to simulate the impacts of climate change on flooding (Alfieri et al., 2017, Dottori et al., 2018, Winsemius et al., 2016, Hirabayashi et al., 2021), to evaluate the effectiveness of flood protection investments (Ward et al., 2017), to assess business risks (Ward et al., 2020b), to inform (re)insurance (Wing et al., 2020b), and to aid in disaster response (Emerton et al., 2020). Despite their far-ranging use, the models still have their limits, which often aren't realized by the end-user (Ward et al., 2015). To appropriately use these models, prospective users need some understanding of

their formulation and limitations. At present, this would require users to disseminate and compare a number of different model description papers. There is a need for a comprehensive, combined, literature review of all GFMs; covering their development, structure, use cases, and limitations. Such a literature review could be the reference point for prospective users of the different GFMs and help to inform them of the most appropriate model to use and the extent to which the outputs of the model can be relied upon.

1.3 Global Flood Model Intercomparison

To better understand the strengths, weaknesses, similarities, and dissimilarities of the GFMs, intercomparison is needed. Model intercomparison projects have been central to the climate modelling community for years, with the semi-decadal CMIP organized by the IPCC and various other IPCC endorsed model intercomparison projects (Meehl et al., 2005). The Global Flood Partnership (GFP), a voluntary organization that brings together academics, research institutes, companies, and practitioners in the field of global flood risk recognized the need for a similar, GFM intercomparison project (De Groeve et al., 2015, Alfieri et al., 2018a).

1.3.1 Comparing model outputs

In the first global flood model intercomparison project (GFMIP), Trigg et al. (2016) compared the output of six different GFMs across the African continent. The study found significant differences between the models; continental agreement between the modelled flood extents ranged between 30-40%. In a subsequent study, Aerts et al. (2020), compared the output of the same six GFMs, along with two additional proprietary insurance models in China, and found similar levels of disagreement as Trigg et al. (2016) found in Africa. Both studies posit GFM characteristics and elements in the modelling chain that contribute towards disagreement. These include extreme flow generation, hydrodynamic representation, output resolution, and river network representation. The studies were limited in the definitive conclusions they could make as the models were being evaluated on the intercomparison of their outputs alone. Both Trigg et al. (2016) and Aerts et al. (2020) called for future work to include the comparison of elements of the internal

model chain—to evaluate the quality of individual model components; and for the incorporation of validation into intercomparison studies so that the comparative performance of GFMs could be assessed.

1.3.2 Comparative model validation

Model validation is an important part of model development. A key issue facing GFM developers is a lack of global validation data. This means that GFMs have had limited validation; and where the models have been validated has been largely regulated by data availability. To compound this, each GFM developer has validated their model in different ways, in different locations, and using different data: making it impossible to compare model performance. Hoch and Trigg (2019) provided a detailed summary of the different approaches, datasets, and locations used by the GFMs for validation. GFM validation can be split into three distinct approaches. The first approach is the validation of flood extents: GFM outputs are compared either to satellite derived footprints of historic flood events (Yamazaki et al., 2011, Winsemius et al., 2013, Rudari et al., 2015, Dottori et al., 2016, Wing et al., 2021, Yamazaki et al., 2012) or to existing modelled flood maps (Pappenberger et al., 2012, Sampson et al., 2015, Wing et al., 2017). The second validation approach is the comparison of modelled extreme flows with observed discharge (Yamazaki et al., 2011, Dottori et al., 2016, Rudari et al., 2015). The third approach is the comparison of modelled and observed water surface elevation (Yamazaki et al., 2012, Yamazaki et al., 2014, Wing et al., 2021).

There is little geographical overlap between the GFM validation locations. Only Sampson et al. (2015) and Dottori et al. (2016) explicitly compare the performance of their GFMs with one-another in the Severn and Thames basins in England. In the remaining regions of overlap, differences in either the validation data or metrics render the results incomparable. For example, both Winsemius et al. (2013) and Dottori et al. (2016) use observational data from the Dartmouth Flood Observatory (DFO) (Brakenridge and Anderson, 2006) to validate their models over much of south-east Asia. However, while Dottori et al. (2016) use fit metrics to evaluate the performance of their model relative to the observed extents, Winsemius et al. (2013) only perform a visual validation. The lack of consistent, comparable validation results with which to compare all the GFMs presents a significant gap in our understanding of the models. In order for the GFMs to be used most effectively,

a model needs to be chosen by prospective users with an understanding of their comparative performance relative to the other available models. This can only be achieved through comparative validation. The results of a comparative validation would also benefit model developers by identifying where their chosen modelling approaches do (and do not) work well.

1.3.3   Comparing model structure

There are limits to the conclusions that can be drawn from studies which only compare GFM outputs (Trigg et al., 2016, Aerts et al., 2020). GFMs are modelling chains; each link in the modelling chain introduces uncertainty, which can only be quantified by examining the internal elements of the models. Hoch and Trigg (2019) proposed a framework for GFM validation and intercomparison that employs standardized model inputs and test conditions, which would allow for a more direct comparison of model design. The framework is promising, but requires buy-in and cooperation across the different modelling groups, which has so far been lacking.

A number of studies have begun to independently look at the different stages of the global modelling chain to try and quantify the influence of different modelling inputs and approaches on uncertainty. The focus of several recent studies has been on the uncertainty of extreme flow generation in GFMs (Zhou et al., 2020, Mester et al., 2021, Devitt et al., 2021). In Zhou et al. (2020), the authors explore the effect of different variables, fitting distributions, and hydrological models on extreme flow uncertainty and find that the choice of hydrological model is the biggest contributor to uncertainty. In a subsequent related study, Mester et al. (2021) also explored the use of different hydrological models, but include multiple climate forcings, and found that both inputs were equally important to model performance. Devitt et al. (2021) took this one step further by comparing the extreme flows generated by hydrological models and those generated using a regionalized flood frequency approach—a key difference between the GFMs identified in Trigg et al. (2016). No single approach was found to be the best globally (Devitt et al., 2021). Extreme flow generation harbours significant uncertainty in the GFM modelling chain, but accurate terrain data is the greatest limit on continued GFM development (Schumann, 2014). Currently all GFMs use terrain data derived from the 20-year old Shuttle Radar and Topography Mission (SRTM) (Farr et al., 2007). The impact of

using different terrain datasets on model accuracy was explored by Archer et al. (2018) who compared hydrodynamic simulations using two digital elevation models (DEMs) used extensively by the GFMs (Farr et al., 2007, Yamazaki et al., 2017) and a new generation of DEM (Rizzoli et al., 2017). Differences in model performance were substantial for the two commonly used DEMs, while the new DEM needed significant pre-processing to produce accurate results; limiting its potential uptake at the global scale (Archer et al., 2018). The impact of spatial resolution on global flood model performance has also been assessed. Fleischmann et al. (2019) found the resolution of the input DEM to be important to model performance, while Mateo et al. (2017) found model performance improved with finer spatial resolution, but only if the model was sufficient in its physical representation of flow connectivity.

A key GFM assumption, which has so-far gone unassessed, is model boundary delimitation. Each GFM has a different pre-defined river size threshold (normally expressed as upstream drainage area or Strahler stream order) below which they won't model flooding. These thresholds are often determined by the spatial resolution and accuracy of the model inputs (Dottori et al., 2016) but they vary significantly (by several orders of magnitude) across the GFMs. Both Trigg et al. (2016) and Aerts et al. (2020) note the impact that these different river size thresholds may have had on the GFM flood extents, but are unable to quantify their influence on model disagreement. Further work should explore the impact of boundary delimitation on GFM outputs, following a *ceteris paribus* approach employed by a number of the studies referenced in this section. The results of such a study would have implications beyond furthering model intercomparison work and help inform GFM end-users on the appropriate selection of their model.

1.4 Global Flood Risk

Risk is defined in the Sendai Framework for Disaster Risk Reduction as the product of hazard, exposure, and vulnerability (UNISDR, 2015). In a flooding context, hazard refers to the modelled (or observed) flooding, exposure is the quantification of who (or what) is exposed to the hazard, and vulnerability is the susceptibility of the exposure to experience loss. Flood risk assessments are vital for understanding the impacts of flooding and for implementing disaster risk reduction measures (Ward et al., 2020a). The preceding sections have detailed the global

datasets available for flood hazard (GFMs); a number of global datasets and approaches have also been developed and applied to assess exposure and vulnerability.

1.4.1 Exposure

Flood exposure can refer to any number of things affected by a hazard. Infrastructure, assets, buildings, and people can all be exposed to floods. The most common quantification of exposure is the number of people exposed. Data on human populations is plentiful and has been collected for millennia. Records of censuses in China date back to 2,000 BC during the Xia dynasty (Durand, 1960). In the last three decades, the value of gridded population data has been realized and efforts have been made to transform population data collected at the census tract to a regularly spaced grid (Clarke and Rhind, 1992, Tobler et al., 1997, Liverman et al., 1998). Gridded population datasets represent a significant development in the study of flood exposure, harmonizing data types (flood model outputs are gridded) and allowing for easy integration and analysis in geographical information systems (GIS).

Several different global population datasets have been developed over the last three decades varying in complexity, approach, and intended use (Leyk et al., 2019). In their simplest form, gridded population datasets simply distribute census population totals evenly across a gridded area equivalent to the size and dimensions of the census tract (Doxsey-Whitfield et al., 2015). A number of population datasets use ancillary datasets as proxies of human presence to weight the distribution of census population totals across gridded space. Common ancillary datasets include satellite imagery of human settlements, land cover data, roads, topography, climate, protected areas, and water bodies (Leyk et al., 2019). The degree of complexity to which these ancillary datasets are used to weight population distribution varies significantly. Satellite imagery of human settlements are frequently used in isolation to binarily classify gridded cells as 'populated' or 'unpopulated', with census data then distributed evenly across populated cells (Balk et al., 2006, Freire et al., 2016, Tiecke, 2017). More complex approaches use multiple ancillary datasets and statistical techniques to dynamically weight the distribution of population across the grid (Klein Goldewijk et al., 2010, Stevens et al., 2015). The different approaches and ancillary datasets employed by the different global population datasets result in

global population maps with substantial differences. These datasets are approximations of the global human population distribution. There is no single 'best' approach and each makes assumptions that both benefit and hinder the accuracy of the final population product in different ways. A useful example of this is the difference between constrained and unconstrained population datasets (Reed et al., 2018, Stevens et al., 2020). These two approaches address a major quandary in global population mapping — the accurate representation of rural populations — in very different ways. Constrained population datasets distribute census data only across satellite identified settlements (hence population distribution is 'constrained' by the settlements), while unconstrained population datasets will distribute some census data across 'uninhabited' areas. The unconstrained approach operates under the assumption that not all settlements can be identified in the satellite imagery and cedes that in accounting for these 'missed settlements' some unpopulated cells will be misallocated as populated (WorldPop, n.d.). Conversely, the constrained approach assumes the accuracy of satellite identified rural settlements, at risk of underrepresenting rural populations. In the end, it is up to the users of these datasets to decide which approaches and assumptions best align with their intended use (Leyk et al., 2019).

The use of these global population datasets is widespread in studies of global flood exposure. However, in many studies only one global population dataset is used, with little to no consideration of how the chosen population dataset contributes towards the uncertainty of the estimated flood exposure (Jongman et al., 2012b, Ward et al., 2013, Arnell and Gosling, 2016, Trigg et al., 2016, Willner et al., 2018, Eilander et al., 2020, Gu et al., 2020). Recently, some studies have begun to address population data as a source of uncertainty in global flood exposure estimates. Dottori et al. (2018) dedicate a section of their Supplementary Material to the discussion of various sources of uncertainty in their modelling framework, population data being one of them. This uncertainty was specifically quantified by Smith et al. (2019), who compared national flood exposure estimates calculated using three global population datasets in 18 developing countries and found significant differences between the exposure estimates. The Smith et al. (2019) study has prompted subsequent global flood exposure studies to rationalize their choice of population data (Rentschler and Salhab, 2020, Dryden et al., 2021) and even to use multiple population datasets in their analysis (Tellman et al., 2021,

Lindersson et al., 2021). What is currently still lacking from the literature is a study which compares exposure estimates at the global scale. The existing studies comparing global population datasets for flood exposure are geographically limited, constrained by either the availability of data (Smith et al., 2019, Tellman et al., 2021) or the motive of the study (Lindersson et al., 2021). Furthermore, these studies have only looked at a small number of populations datasets; either two (Tellman et al., 2021) or three (Smith et al., 2019, Lindersson et al., 2021). To fully understand the implications of using different global population datasets to calculate flood exposure, the entire catalogue of population data that has been used in previous studies of global flood exposure needs to be compared.

1.4.2 Vulnerability

Vulnerability is a complex and multifaceted concept, both in how it is defined and how it is measured. Birkmann et al. (2006) identified 25 different definitions of vulnerability. For the sake of brevity, the United Nations Office for Disaster Risk Reduction (UNDRR) definition of vulnerability is used, as it aligns most closely with the subject of this thesis: "the conditions determined by physical, social, economic, and environmental factors or processes which increase the susceptibility of an individual, a community, assets, or system to the impacts of hazards" (UNDRR, 2017).

Vulnerability changes with the scale of the analysis. A vulnerability assessment at the local or regional scale will have different aims and require different data than a vulnerability assessment at the national or global scale (de Moel et al., 2015). In their review of global flood risk assessments, Ward et al. (2020a) found that while all studies of global flood risk considered flood hazard and exposure, only some considered vulnerability. Vulnerability at the global scale has been assessed through a human-social, physical, and economic lens. Human vulnerability to flooding has been assessed by both Jongman et al. (2015) and Tanoue et al. (2016). Both studies used historical data on annual flood fatalities and compared these to modelled annual flood exposure. The mortality ratio (fatalities divided by modelled exposure) was used as an indicator of human vulnerability to flooding. Jongman et al. (2015) found declining global river flood vulnerability from 1980-2010, while Tanoue et al. (2016) found less linear global trends over a longer time period (1960-2013). Human-social vulnerability is frequently assessed at

smaller scales through a vulnerability index, which is constructed by considering a number of different indicators—each contributing to a final measure of flood vulnerability (Moreira et al., 2021). Vulnerability indices at the global scale have been fairly limited. In developing a more general global disaster risk index, Peduzzi et al. (2009) develop a flood vulnerability index based on three indicators: recorded fatalities, GDP, and people living in floodplains. A more detailed global flood vulnerability index, based on 48 indicators, was developed by Okazawa et al. (2011). The most common approach to measuring vulnerability at the global scale is through direct physical damages, using what are known as intensity-damage functions. These intensity-damage functions relate some aspect of flood intensity (depth, velocity, duration) to a degree of damage caused to the object at risk. Intensity-damage functions can be derived empirically (using historical flood damage data or expert judgement) or analytically (based on engineering design criteria) (van Westen, 2014). These functions are typically developed at the national level (e.g. the Multi-Coloured Manual in the UK (Penning-Rowsell et al., 2013) and HAZUS-MH in the US (Scawthorn et al., 2006)) making it difficult to assess damages at larger scales. This issue was addressed by Huizinga et al. (2017) who collected and normalized intensity-damage functions from countries across six different continents to produce a comprehensive and consistent global database of depth-damage functions. Current global studies which assess vulnerability through direct physical damages do so using either the Huizinga et al. (2017) global database of depth-damage functions (Alfieri et al., 2017, Dottori et al., 2018, Ward et al., 2020b) or by applying nationally derived intensity-damage functions globally (Ward et al., 2013, Winsemius et al., 2016, Ward et al., 2017). A few global studies have also begun to address vulnerability from an economic perspective, using economic models to assess both the direct and indirect economic losses of river flooding (Dottori et al., 2018, Willner et al., 2018).

While studies have begun to compare global approaches to model flood hazard and exposure (as outlined in the previous sections), none so-far have compared global approaches to measuring vulnerability. Studies comparing and evaluating national scale approaches for calculating direct physical damages have been fairly extensive. Significant differences have been noted both in the different methodologies applied (Meyer and Messner, 2005, Merz et al., 2010b, Jongman et al., 2012a) and in the damage model outputs; owing to uncertainties including the

spatial allocation of assets, the pricing of assets, and the construction of intensity-damage functions (de Moel and Aerts, 2011, Jongman et al., 2012a, Wing et al., 2020a). Global approaches to calculate vulnerability deserve the same level of scrutiny, as the same uncertainties identified in national scale damage models are often inflated at the global scale; due to coarser data, wider-ranging assumptions, and less-detailed validation.

1.6 Global Data Used Nationally

Global flood risk data has the potential to be useful at national scales to inform flood risk management decisions. These decisions, which have historically been reliant on the availability of national data (de Moel et al., 2009), are now being made in 'data-poor' countries; informed by global datasets of flood risk (Ward et al., 2015). It has also been shown that the global flood modelling frameworks can ingest detailed local data (where available) to produce flood maps which are comparable to existing national level maps (Wing et al., 2017, Bates et al., 2021). A question often posed when working across different scales is: what level of detail is necessary? Apel et al. (2009) tried to answer this for a flood event on the river Mulde in the town of Eilenberg, Germany; a scale which would be commensurate (or just below) the level required to assess national flood risk. In comparing three hydraulic models and three vulnerability methods of increasing complexity to reference flood maps and damage data, Apel et al. (2009) found that both the 'moderate' complexity hydraulic model and vulnerability approach produced the best results. This moderate complexity hydraulic model follows a similar approach and makes the same assumptions as many of the global flood models (Bates and De Roo, 2000) — demonstrating their potential applicability at these scales. A global hydrological model, similar to those which force many of the GFMs, was shown by Gusyev et al. (2016) to produce comparable results to a local-scale hydrological model in the Rhine river basin. In a similar cross-scale comparison, Fleischmann et al. (2019) compared local, regional, and global approaches to modelling flood hazard in the Itajaí-Açu basin in Brazil and found that many global model components (reach length, cross sections, DEM resolution) limit their local relevance. These studies have demonstrated both the potential and possible limits of global data used nationally. However, the studies have all typically looked at one modelling approach

(at differing degrees of complexity). Previous intercomparison work has shown that the GFMs use very different approaches — each potentially relevant in different contexts (Trigg et al., 2016, Aerts et al., 2020). To properly assess the national credibility of global flood models, all existing modelling approaches should be compared. Furthermore, this comparison should involve global datasets encompassing all components of flood risk (hazard, exposure, and vulnerability) — something that has so-far been lacking in these cross-scale comparisons.

Further to evaluating how these global datasets actually perform at the national level is understanding how they can, and should, be used in a national flood risk management context. Depending on the country in question, national flood risk management differs in its approach, implementation, and objectives (Morrison et al., 2018). Where, how, and if data is used to inform decision making will depend on the national flood risk management structure and determine the degree to which global data could be used to complement the process. There has been a shift in approach to flood risk management from an assumption of stationarity to a realization that future changes in climate and demographics need to be accounted for (Milly et al., 2008, Merz et al., 2010a, Biesbroek et al., 2010, Jonkman and Dawson, 2012, Browder et al., 2021). It would pre-suppose that these global datasets, which have been used extensively in academic studies of future flood risk, could benefit non-stationary national flood risk management. However, questions still remain about the accuracy of global data at these scales—and whether this data has the potential to be misused (Venot et al., 2021). To properly evaluate global flood risk data for use nationally a cross-disciplinary approach needs to be taken; their applicability at these scales is equally dependent on the accuracy of the global data as it is on the national context in which they would be used.

1.7 Thesis Aims and Objectives

The aim of this thesis is to further the evaluation of global flood risk datasets. Despite their widespread use, there has been limited intercomparison and evaluation of these datasets, hampering their effective and informed implementation by end-users. In developing and building upon an intercomparison framework of global flood risk data, this thesis will address gaps in our current understanding of global flood risk; informing users about the applicability of global data and

identifying future directions for global dataset development. To achieve this aim, four main objectives have been identified:

- Review and summarize the existing global flood model literature including their history, development, methodologies, use, and future directions.

- Develop and test a framework for global flood model validation intercomparison.

- Develop a methodology for exploring the differences in global flood model river network size and apply this methodology to quantify the impacts that both river network size and choice of global population data have on global and national flood exposure estimates.

- Develop and apply an intercomparison framework for assessing the suitability of global flood risk data (hazard, exposure, and vulnerability) for use at the national scale while also considering the national flood risk management context in each country.

1.8 Thesis Structure

The remainder of this thesis will be structured as follows. In **Chapter 2,** a literature review of global flood models will be presented. This literature review will cover the history and development of the models, different model structures and approaches, their wide-ranging application, existing model intercomparison work, and future research directions. This review will be the first to consolidate the literature on all existing global flood models. In **Chapter 3**, six different global flood models will be validated against satellite observed flood events in three hydraulically diverse regions in Nigeria and Mozambique. This work will introduce a framework for global flood model validation intercomparison, producing and publishing open validation data for future use. In **Chapter 4**, the issue of river network size in global flood models will be addressed. A model-independent geomorphological flood map will be developed and used to calculate global and national flood exposure using three different global population datasets. This work will quantify the impact of both the choice of global flood model (in terms of river network size) and the choice of global population dataset on flood exposure estimates. In **Chapter 5**, the use of global data for national flood risk management

in Colombia, England, Ethiopia, India, and Malaysia will be assessed. In total, 16 different global datasets encompassing hazard, exposure, and vulnerability will be compared for use at the national scale. This work will also review the national flood risk management approaches in each country and assess the suitability of the global datasets used nationally within this context. In **Chapter 6**, the work in the preceding four chapters will be discussed within the context of the wider global flood risk literature, the key findings will be identified, and opportunities for further research will be discussed.

References

AERTS, J. P. M., UHLEMANN-ELMER, S., EILANDER, D. & WARD, P. J. 2020. Comparison of estimates of global flood models for flood hazard and exposed gross domestic product: a China case study. *Nat. Hazards Earth Syst. Sci.,* 20**,** 3245-3260.

ALFIERI, L., BISSELINK, B., DOTTORI, F., NAUMANN, G., DE ROO, A., SALAMON, P., WYSER, K. & FEYEN, L. 2017. Global projections of river flood risk in a warmer world. *Earths Future,* 5**,** 171-182.

ALFIERI, L., COHEN, S., GALANTOWICZ, J., SCHUMANN, G. J. P., TRIGG, M. A., ZSOTER, E., PRUDHOMME, C., KRUCZKIEWICZ, A., COUGHLAN DE PEREZ, E., FLAMIG, Z., RUDARI, R., WU, H., ADLER, R. F., BRAKENRIDGE, R. G., KETTNER, A., WEERTS, A., MATGEN, P., ISLAM, S. A. K. M., DE GROEVE, T. & SALAMON, P. 2018a. A global network for operational flood risk reduction. *Environmental Science & Policy,* 84**,** 149-158.

ALFIERI, L., DOTTORI, F., BETTS, R., SALAMON, P. & FEYEN, L. 2018b. Multi-Model Projections of River Flood Risk in Europe under Global Warming. 6**,** 6.

ALFIERI, L., FEYEN, L., DOTTORI, F. & BIANCHI, A. 2015. Ensemble flood risk assessment in Europe under high end climate scenarios. *Global Environmental Change-Human and Policy Dimensions,* 35**,** 199-212.

ALFIERI, L., SALAMON, P., BIANCHI, A., NEAL, J., BATES, P. & FEYEN, L. 2014. Advances in pan-European flood hazard mapping. *Hydrological Processes,* 28**,** 4067-4077.

APEL, H., ARONICA, G. T., KREIBICH, H. & THIEKEN, A. H. 2009. Flood risk analyses—how detailed do we need to be? *Natural Hazards,* 49**,** 79-98.

ARCHER, L., NEAL, J. C., BATES, P. D. & HOUSE, J. I. 2018. Comparing TanDEM-X Data With Frequently Used DEMs for Flood Inundation Modeling. 54**,** 10,205-10,222.

ARIAS, P. A., BELLOUIN, N., COPPOLA, E., JONES, R. H., KRINNER, G., MAROTZKE, J., NAIK, V., PALMER, M. D., PLATTNER, G. K., ROGELJ, J., ROJAS, M., SILLMAN, J., STORELVMO, T., THORNE, P. W., TREWIN, B., ACHUTA RAO, K., ADHIKARY, B., ALLAN, R. P., ARMOUR, K., BALA, G., BARIMALALA, R., BERGER, S., CANADELL, J. G., CASSOU, C., CHERCHI, A., COLLINS, W., COLLINS, W. D., CONNORS, S. L., CORTI, S., CRUZ, F., DENTENER,

F. J., DERECZYNSKI, C., DI LUCA, A., DIONGUE NIANG, A.,
DOBLAS-REYES, F. J., DOSIO, A., DOUVILLE, H., ENGELBRECHT,
F., EYRING, V., FISCHER, E., FORSTER, P., FOX-KEMPER, B.,
FUGLESTVEDT, J. S., FYFE, J. C., GILLET, N. P., GOLDFARD, L.,
GORODETSKAYA, I., GUTIERREZ, J. M., HAMDI, R., HAWKINS, E.,
HEWITT, H. T., HOPE, P., ISLAM, A. S., JONES, C., KAUFMAN, D. S.,
KOPP, R. E., KOSAKA, Y., KOSSIN, J., KRAKOVSKA, S., LEE, J. Y., LI,
J., MAURITSEN, T., MAYCOCK, T. K., MEINSHAUSEN, M., MIN, S.
K., MONTEIRO, P. M. S., NGO-DUC, T., OTTO, F., PINTO, I., PIRANI,
A., RAGHAVAN, K., RANASINGHE, R., RUANE, A. C., RUIZ, L.,
SALLÉE, J. B., SAMSET, B. H., SATHYENDRANATH, S.,
SENEVIRATNE, S. I., SÖRENSSON, A. A., SZOPA, S., TAKAYABU, I.,
TRÉGUIER, A. M., VAN DEN HURK, B., VAUTARD, R., VON
SCHUCKMANN, K., ZAEHLE, S., ZHANG, X. & ZICKFIELD, K. 2021.
Technical Summary. *In:* MASSON-DELMOTTE, V., ZHAI, P., PIRANI,
A., CONNORS, S. L., PÉAN, C., BERGER, S., CAUD, N., CHEN, Y.,
GOLDFARD, L., GOMIS, M. I., HUANG, M., LEITZELL, K., LONNOY,
E., MATTHEW, J. B. R., MAYCOCK, T. K., WATERFIELD, T.,
YELEKÇI, O., YU, R. & ZHOU, B. (eds.) *Climate Change 2021: The
Physical Science Basis, Contribution of Working Group 1 to the Sixth
Assessment Report of the Intergovernmental Panel on Climate Change.*
Intergovernmental Panel on Climate Change.

ARNELL, N. W. & GOSLING, S. N. 2016. The impacts of climate change on river
flood risk at the global scale. *Climatic Change,* 134**,** 387-401.

ASADIEH, B. & KRAKAUER, N. Y. 2015. Global trends in extreme precipitation:
climate models versus observations. *Hydrol. Earth Syst. Sci.,* 19**,** 877-891.

BALK, D. L., DEICHMANN, U., YETMAN, G., POZZI, F., HAY, S. I. &
NELSON, A. 2006. Determining Global Population Distribution: Methods,
Applications and Data. *In:* HAY, S. I., GRAHAM, A. & ROGERS, D. J.
(eds.) *Advances in Parasitology.* Academic Press.

BARREDO, J. I. 2007. Major flood disasters in Europe: 1950–2005. *Natural
Hazards,* 42**,** 125-148.

BATES, P., TRIGG, M. A., NEAL, J. & DABROWA, A. 2013. LISFLOOD-FP
User Manual. University of Bristol.

BATES, P. D. & DE ROO, A. P. J. 2000. A simple raster-based model for flood
inundation simulation. *Journal of Hydrology,* 236**,** 54-77.

BATES, P. D., HORRITT, M. S. & FEWTRELL, T. J. 2010. A simple inertial
formulation of the shallow water equations for efficient two-dimensional
flood inundation modelling. *Journal of Hydrology,* 387**,** 33-45.

BATES, P. D., HORRITT, M. S., HUNTER, N. M., MASON, D. & COBBY, D.
2005. Numerical Modelling of Floodplain Flow. *Computational Fluid
Dynamics.*

BATES, P. D., NEAL, J., SAMPSON, C., SMITH, A. & TRIGG, M. 2018. Chapter
9 - Progress Toward Hyperresolution Models of Global Flood Hazard. *In:*
MICHEL, G. (ed.) *Risk Modeling for Hazards and Disasters.* Elsevier.

BATES, P. D., QUINN, N., SAMPSON, C., SMITH, A., WING, O., SOSA, J.,
SAVAGE, J., OLCESE, G., NEAL, J., SCHUMANN, G., GIUSTARINI, L.,
COXON, G., PORTER, J. R., AMODEO, M. F., CHU, Z., LEWIS-GRUSS,
S., FREEMAN, N. B., HOUSER, T., DELGADO, M., HAMIDI, A.,
BOLLIGER, I., E. MCCUSKER, K., EMANUEL, K., FERREIRA, C. M.,

KHALID, A., HAIGH, I. D., COUASNON, A., E. KOPP, R., HSIANG, S. & KRAJEWSKI, W. F. 2021. Combined Modeling of US Fluvial, Pluvial, and Coastal Flood Hazard Under Current and Future Climates. 57**,** e2020WR028673.

BERTUZZO, E., MARITAN, A., GATTO, M., RODRIGUEZ-ITURBE, I. & RINALDO, A. 2007. River networks and ecological corridors: Reactive transport on fractals, migration fronts, hydrochory. 43.

BIESBROEK, G. R., SWART, R. J., CARTER, T. R., COWAN, C., HENRICHS, T., MELA, H., MORECROFT, M. D. & REY, D. 2010. Europe adapts to climate change: Comparing National Adaptation Strategies. *Global Environmental Change,* 20**,** 440-450.

BIRKMANN, J., DECH, S., HIRZINGER, G., KLEIN, R., KLÜPFEL, H., LEHMANN, F., MOTT, C., NAGEL, K., SCHLURMANN, T., SETIADI, N., SIEGERT, F. & STRUNZ, G. Measuring vulnerability to promote disaster-resilient societies: Conceptual frameworks and definitions. 2006.

BLÖSCHL, G., HALL, J., PARAJKA, J., PERDIGÃO, R. A. P., MERZ, B., ARHEIMER, B., ARONICA, G. T., BILIBASHI, A., BONACCI, O., BORGA, M., ČANJEVAC, I., CASTELLARIN, A., CHIRICO, G. B., CLAPS, P., FIALA, K., FROLOVA, N., GORBACHOVA, L., GÜL, A., HANNAFORD, J., HARRIGAN, S., KIREEVA, M., KISS, A., KJELDSEN, T. R., KOHNOVÁ, S., KOSKELA, J. J., LEDVINKA, O., MACDONALD, N., MAVROVA-GUIRGUINOVA, M., MEDIERO, L., MERZ, R., MOLNAR, P., MONTANARI, A., MURPHY, C., OSUCH, M., OVCHARUK, V., RADEVSKI, I., ROGGER, M., SALINAS, J. L., SAUQUET, E., ŠRAJ, M., SZOLGAY, J., VIGLIONE, A., VOLPI, E., WILSON, D., ZAIMI, K. & ŽIVKOVIĆ, N. 2017. Changing climate shifts timing of European floods. 357**,** 588-590.

BOUWER, L. M. 2011. Have Disaster Losses Increased Due to Anthropogenic Climate Change? %J Bulletin of the American Meteorological Society. 92**,** 39-46.

BRADBROOK, K., WALLER, S. & MORRIS, D. 2005. National floodplain mapping: datasets and methods–160,000 km in 12 months. *Natural hazards,* 36**,** 103-123.

BRAKENRIDGE, R. & ANDERSON, E. 2006. Modis-based flood detection, mapping and measurement: The potential for operational hydrological applications. *In:* MARSALEK, J., STANCALIE, G. & BALINT, G. (eds.) *Transboundary Floods: Reducing Risks through Flood Management.* Dordrecht: Springer.

BROWDER, G., NUNEZ SANCHEZ, A., JONGMAN, B., ENGLE, N., VAN BEEK, E., CASTERA ERREA, M. & HODGSON, S. 2021. An EPIC Response.

BRUNNER, G. W. 1995. HEC-RAS River Analysis System. Hydraulic Reference Manual. Version 1.0. Hydrologic Engineering Center Davis CA.

CAMPOS, D., FORT, J. & MÉNDEZ, V. 2006. Transport on fractal river networks: Application to migration fronts. *Theoretical Population Biology,* 69**,** 88-93.

CHANGNON, S. A., PIELKE, R. A., CHANGNON, D., SYLVES, R. T. & PULWARTY, R. 2000. Human Factors Explain the Increased Losses from Weather and Climate Extremes. *Bulletin of the American Meteorological Society,* 81**,** 437-442.

CHURCH, J. A., HUNTER, J. R., MCINNES, K. L. & WHITE, N. J. J. A. M. M. 2006. Sea-level rise around the Australian coastline and the changing frequency of extreme sea-level events. 55, 253-260.

CLARKE, J. I. & RHIND, D. W. 1992. Human dimensions of global environmental change.

CRAWFORD, G. W., SMITH, D. G., DESLOGES, J. R. & DAVIS, A. M. 1998. Floodplains and Agricultural Origins: A Case Study in South-Central Ontario, Canada. *Journal of Field Archaeology,* 25, 123-137.

CRED & UNDRR 2020. *The Human Cost of Natural Disasters - An overview of the last 20 years 2000-2019.*

DANKERS, R., ARNELL, N. W., CLARK, D. B., FALLOON, P. D., FEKETE, B. M., GOSLING, S. N., HEINKE, J., KIM, H., MASAKI, Y., SATOH, Y., STACKE, T., WADA, Y. & WISSER, D. 2014. First look at changes in flood hazard in the Inter-Sectoral Impact Model Intercomparison Project ensemble. *Proc Natl Acad Sci U S A,* 111, 3257-61.

DANKERS, R. & FEYEN, L. 2009. Flood hazard in Europe in an ensemble of regional climate scenarios. 114.

DE ALMEIDA, G. A. M. & BATES, P. 2013. Applicability of the local inertial approximation of the shallow water equations to flood modeling. *Water Resources Research,* 49, 4833-4844.

DE GROEVE, T., THIELEN-DEL POZO, J., BRAKENRIDGE, R., ADLER, R., ALFIERI, L., KULL, D., LINDSAY, F., IMPERIALI, O., PAPPENBERGER, F., RUDARI, R., SALAMON, P., VILLARS, N. & WYJAD, K. 2015. Joining Forces in a Global Flood Partnership. *Bulletin of the American Meteorological Society,* 96, ES97-ES100.

DE MOEL, H. & AERTS, J. C. J. H. 2011. Effect of uncertainty in land use, damage models and inundation depth on flood damage estimates. *Natural Hazards,* 58, 407-425.

DE MOEL, H., JONGMAN, B., KREIBICH, H., MERZ, B., PENNING-ROWSELL, E. & WARD, P. J. 2015. Flood risk assessments at different spatial scales. *Mitigation and Adaptation Strategies for Global Change,* 20, 865-890.

DE MOEL, H., VAN ALPHEN, J. & AERTS, J. C. J. H. 2009. Flood maps in Europe – methods, availability and use. *Nat. Hazards Earth Syst. Sci.,* 9, 289-301.

DESA 2019. Population Facts. Population Division of the United Nations Department of Economic and Social Affaris.

DEVITT, L., NEAL, J., WAGENER, T. & COXON, G. 2021. Uncertainty in the extreme flood magnitude estimates of large-scale flood hazard models. *Environmental Research Letters,* 16, 064013.

DI BALDASSARRE, G., MONTANARI, A., LINS, H., KOUTSOYIANNIS, D., BRANDIMARTE, L. & BLÖSCHL, G. 2010. Flood fatalities in Africa: From diagnosis to mitigation. *Geophysical Research Letters,* 37.

DI BALDASSARRE, G., NARDI, F., ANNIS, A., ODONGO, V., RUSCA, M. & GRIMALDI, S. 2020. Brief communication: Comparing hydrological and hydrogeomorphic paradigms for global flood hazard mapping. *Nat. Hazards Earth Syst. Sci.,* 20, 1415-1419.

DI BALDASSARRE, G., VIGLIONE, A., CARR, G., KUIL, L., SALINAS, J. L. & BLÖSCHL, G. 2013. Socio-hydrology: conceptualising human-flood interactions. *Hydrol. Earth Syst. Sci.,* 17, 3295-3303.

DOTTORI, F., SALAMON, P., BIANCHI, A., ALFIERI, L., HIRPA, F. A. & FEYEN, L. 2016. Development and evaluation of a framework for global flood hazard mapping. *Advances in Water Resources,* 94**,** 87-102.

DOTTORI, F., SZEWCZYK, W., CISCAR, J. C., ZHAO, F., ALFIERI, L., HIRABAYASHI, Y., BIANCHI, A., MONGELLI, I., FRIELER, K., BETTS, R. A. & FEYEN, L. 2018. Increased human and economic losses from river flooding with anthropogenic warming. *Nature Climate Change,* 8**,** 781-+.

DOTTORI, F. & TODINI, E. 2011. Developments of a flood inundation model based on the cellular automata approach: Testing different methods to improve model performance. *Physics and Chemistry of the Earth, Parts A/B/C,* 36**,** 266-280.

DOXSEY-WHITFIELD, E., MACMANUS, K., ADAMO, S. B., PISTOLESI, L., SQUIRES, J., BORKOVSKA, O. & BAPTISTA, S. R. 2015. Taking Advantage of the Improved Availability of Census Data: A First Look at the Gridded Population of the World, Version 4. *Papers in Applied Geography,* 1**,** 226-234.

DRYDEN, R., ANAND, M., LEHNER, B. & FLUET-CHOUINARD, E. 2021. Do we prioritize floodplains for development and farming? Mapping global dependence and exposure to inundation. *Global Environmental Change,* 71**,** 102370.

DURAND, J. D. 1960. The Population Statistics of China, A.D. 2-1953. *Population Studies,* 13**,** 209-256.

EILANDER, D., COUASNON, A., IKEUCHI, H., MUIS, S., YAMAZAKI, D., WINSEMIUS, H. C. & WARD, P. J. 2020. The effect of surge on riverine flood hazard and impact in deltas globally. *Environmental Research Letters,* 15**,** 104007.

EMERTON, R., CLOKE, H., FICCHI, A., HAWKER, L., DE WIT, S., SPEIGHT, L., PRUDHOMME, C., RUNDELL, P., WEST, R., NEAL, J., CUNA, J., HARRIGAN, S., TITLEY, H., MAGNUSSON, L., PAPPENBERGER, F., KLINGAMAN, N. & STEPHENS, E. 2020. Emergency flood bulletins for Cyclones Idai and Kenneth: A critical evaluation of the use of global flood forecasts for international humanitarian preparedness and response. *International Journal of Disaster Risk Reduction,* 50**,** 101811.

ENVIRONMENT AGENCY 2018. Preliminary Flood Risk Assessment for England. Environment Agency.

EYRING, V., BONY, S., MEEHL, G. A., SENIOR, C. A., STEVENS, B., STOUFFER, R. J. & TAYLOR, K. E. 2016. Overview of the Coupled Model Intercomparison Project Phase 6 (CMIP6) experimental design and organization. *Geosci. Model Dev.,* 9**,** 1937-1958.

FANG, Y., CEOLA, S., PAIK, K., MCGRATH, G., RAO, P. S. C., MONTANARI, A. & JAWITZ, J. W. 2018. Globally Universal Fractal Pattern of Human Settlements in River Networks. *Earth's Future,* 6**,** 1134-1145.

FANG, Y. & JAWITZ, J. W. 2019. The evolution of human population distance to water in the USA from 1790 to 2010. *Nature Communications,* 10**,** 430.

FARR, T. G., ROSEN, P. A., CARO, E., CRIPPEN, R., DUREN, R., HENSLEY, S., KOBRICK, M., PALLER, M., RODRIGUEZ, E., ROTH, L., SEAL, D., SHAFFER, S., SHIMADA, J., UMLAND, J., WERNER, M., OSKIN, M., BURBANK, D. & ALSDORF, D. 2007. The shuttle radar topography mission. *Reviews of Geophysics,* 45**,** 33.

FEDERAL EMERGENCY PLANNING AGENCY 2019. Flood Risk Analysis and
    Mapping (Rev. 11). Federal Emergency Planning Agency.
FEYEN, L., DANKERS, R., BÓDIS, K., SALAMON, P. & BARREDO, J. I. 2012.
    Fluvial flood risk in Europe in present and future climates. *Climatic Change,*
    112**,** 47-62.
FLEISCHMANN, A., PAIVA, R. & COLLISCHONN, W. 2019. Can regional to
    continental river hydrodynamic models be locally relevant? A cross-scale
    comparison. *Journal of Hydrology X,* 3**,** 100027.
FORMETTA, G. & FEYEN, L. 2019. Empirical evidence of declining global
    vulnerability to climate-related hazards. *Global Environmental Change,* 57**,**
    101920.
FREIRE, S., MACMANUS, K., PESARESI, M., DOXSEY-WHITFIELD, E. &
    MILLS, J. 2016. *Development of new open and free multi-temporal global
    population grids at 250 m resolution.*
GU, X., ZHANG, Q., LI, J., CHEN, D., SINGH, V. P., ZHANG, Y., LIU, J., SHEN,
    Z. & YU, H. 2020. Impacts of anthropogenic warming and uneven regional
    socio-economic development on global river flood risk. *Journal of
    Hydrology,* 590**,** 125262.
GUSYEV, M., GÄDEKE, A., CULLMANN, J., MAGOME, J., SUGIURA, A.,
    SAWANO, H. & TAKEUCHI, K. 2016. Connecting global- and local-scale
    flood risk assessment: a case study of the Rhine River basin flood hazard. 9**,**
    343-354.
HALL, J., ARHEIMER, B., BORGA, M., BRÁZDIL, R., CLAPS, P., KISS, A.,
    KJELDSEN, T. R., KRIAUČIŪNIENĖ, J., KUNDZEWICZ, Z. W., LANG,
    M., LLASAT, M. C., MACDONALD, N., MCINTYRE, N., MEDIERO, L.,
    MERZ, B., MERZ, R., MOLNAR, P., MONTANARI, A., NEUHOLD, C.,
    PARAJKA, J., PERDIGÃO, R. A. P., PLAVCOVÁ, L., ROGGER, M.,
    SALINAS, J. L., SAUQUET, E., SCHÄR, C., SZOLGAY, J., VIGLIONE,
    A. & BLÖSCHL, G. 2014. Understanding flood regime changes in Europe: a
    state-of-the-art assessment. *Hydrol. Earth Syst. Sci.,* 18**,** 2735-2772.
HALL, J. W., DAWSON, R. J., SAYERS, P. B., ROSU, C., CHATTERTON, J. B.
    & DEAKIN, R. 2003. A methodology for national-scale flood risk
    assessment. 156**,** 235-247.
HALL, J. W., SAYERS, P. B. & DAWSON, R. J. 2005. National-scale Assessment
    of Current and Future Flood Risk in England and Wales. *Natural Hazards,*
    36**,** 147-164.
HANKIN, B., BURGESS-GAMBLE, L., BENTLEY, S. & ROSE, S. 2016. How to
    model and map catchment processes when flood risk management planning.
    Environment Agency.
HANKIN, B., LAMB, R., CRAIGEN, I., PAGE, T., CHAPPELL, N. &
    METCALFE, P. 2017. A whole catchment approach to improve flood
    resilience in the Eden: Winning entry to the Defra Flood Modelling
    Competition 2016. JBA Consulting.
HIRABAYASHI, Y., KANAE, S., EMORI, S., OKI, T. & KIMOTO, M. 2008.
    Global projections of changing risks of floods and droughts in a changing
    climate. Hydrological Sciences Journal.
HIRABAYASHI, Y., MAHENDRAN, R., KOIRALA, S., KONOSHIMA, L.,
    YAMAZAKI, D., WATANABE, S., KIM, H. & KANAE, S. 2013. Global
    flood risk under climate change. *Nature Climate Change,* 3**,** 816-821.

HIRABAYASHI, Y., TANOUE, M., SASAKI, O., ZHOU, X. & YAMAZAKI, D. 2021. Global exposure to flooding from the new CMIP6 climate model projections. *Scientific Reports,* 11**,** 3740.

HOCH, J. M. & TRIGG, M. A. 2019. Advancing global flood hazard simulations by improving comparability, benchmarking, and integration of global flood models. *Environmental Research Letters,* 14**,** 034001.

HODGKINS, G. A., WHITFIELD, P. H., BURN, D. H., HANNAFORD, J., RENARD, B., STAHL, K., FLEIG, A. K., MADSEN, H., MEDIERO, L., KORHONEN, J., MURPHY, C. & WILSON, D. 2017. Climate-driven variability in the occurrence of major floods across North America and Europe. *Journal of Hydrology,* 552**,** 704-717.

HOOPLE, D. 2013. The Budgetary Impact of the Federal Government's Response to Disasters. *Congressional Budget Office Blog* [Online]. Available from: https://www.cbo.gov/publication/44601 [Accessed 29/09/2021 2021].

HORN, D. P. & BROWN, J. T. 2017. *Introduction to the national flood insurance program (nfip)*, Congressional Research Service Washington DC, USA.

HOUSTON, D., WERRITY, A., BASSETT, D., GEDDES, A., HOOLACHAN, A. & MCMILLAN, M. 2011. Pluvial (rain-related) flooding in urban areas: the invisible hazard.

HUIZINGA, K., DE MOEL, H. & SZEWCZYK, W. 2017. Global flood depth-damage functions. Methodology and the database with guidelines. JRC Technical Reports.

HUNTER, N. M., BATES, P. D., HORRITT, M. S. & WILSON, M. D. 2007. Simple spatially-distributed models for predicting flood inundation: A review. *Geomorphology,* 90**,** 208-225.

ICPDR 2015. Flood Risk Management Plan for the Danube River Basin District.

ICPR 2019. Update on the Flood Hazard and Flood Risk Maps in the International River Basin District 'Rhine' (Catchment > 2,500 km², Part A). Kaiserin-Augusta-Anlagen 15, D 56068 Koblenz: Internationale Kommission zum Schutz des Rheins,.

IKSE 2016. International Flood Risk Management Plan for the Elbe River Basin District. *In:* (IKSE), I. K. Z. S. D. E. (ed.) *Information Sheet 2016 on the European Flood Risk Management Directive.* Magdeburg.

IPCC. 2021. *IPCC FACTSHEET: Timeline - highlights of IPCC history* [Online]. Available: https://www.ipcc.ch/site/assets/uploads/2021/07/AR6_FS_timeline.pdf [Accessed Novermber 9th 2021].

IVANCIC, T. J. & SHAW, S. B. 2015. Examining why trends in very heavy precipitation should not be mistaken for trends in very high river discharge. *Climatic Change,* 133**,** 681-693.

JAFARZADEGAN, K., MERWADE, V. & SAKSENA, S. 2018. A geomorphic approach to 100-year floodplain mapping for the Conterminous United States. *Journal of Hydrology,* 561**,** 43-58.

JBA 2019. Continental China Flood Model. *In:* JBA (ed.).

JBA. 2021. Australia Flood Map Update 2021. *News & Blogs* [Online]. Available from: https://www.jbarisk.com/news-blogs/australia-flood-map-update-2021/ [Accessed November 18 2021].

JOHNSON, K. A., WING, O. E. J., BATES, P. D., FARGIONE, J., KROEGER, T., LARSON, W. D., SAMPSON, C. C. & SMITH, A. M. 2020. A benefit–cost analysis of floodplain land acquisition for US flood damage reduction. *Nature Sustainability,* 3**,** 56-62.

JONGMAN, B. 2018. Effective adaptation to rising flood risk. *Nature Communications,* 9**,** 1986.

JONGMAN, B., HOCHRAINER-STIGLER, S., FEYEN, L., AERTS, J. C. J. H., MECHLER, R., BOTZEN, W. J. W., BOUWER, L. M., PFLUG, G., ROJAS, R. & WARD, P. J. 2014. Increasing stress on disaster-risk finance due to large floods. *Nature Climate Change,* 4**,** 264-268.

JONGMAN, B., KREIBICH, H., APEL, H., BARREDO, J. I., BATES, P. D., FEYEN, L., GERICKE, A., NEAL, J., AERTS, J. C. J. H. & WARD, P. J. 2012a. Comparative flood damage model assessment: towards a European approach. *Nat. Hazards Earth Syst. Sci.,* 12**,** 3733-3752.

JONGMAN, B., WARD, P. J. & AERTS, J. 2012b. Global exposure to river and coastal flooding: Long term trends and changes. *Global Environmental Change-Human and Policy Dimensions,* 22**,** 823-835.

JONGMAN, B., WINSEMIUS, H. C., AERTS, J., DE PEREZ, E. C., VAN AALST, M. K., KRON, W. & WARD, P. J. 2015. Declining vulnerability to river floods and the global benefits of adaptation. *Proceedings of the National Academy of Sciences of the United States of America,* 112**,** E2271-E2280.

JONKMAN, S. N. 2005. Global perspectives on loss of human life caused by floods. *Natural Hazards,* 34**,** 151-175.

JONKMAN, S. N. & DAWSON, R. J. 2012. Issues and Challenges in Flood Risk Management *Editorial for the Special Issue on Flood Risk Management,* 4**,** 785-792.

KAM, P. M., AZNAR-SIGUAN, G., SCHEWE, J., MILANO, L., GINNETTI, J., WILLNER, S., MCCAUGHEY, J. W. & BRESCH, D. N. 2021. Global warming and population change both heighten future risk of human displacement due to river floods. *Environmental Research Letters,* 16**,** 044026.

KLEIN GOLDEWIJK, K., BEUSEN, A. & JANSSEN, P. 2010. Long-term dynamic modeling of global population and built-up area in a spatially explicit way: HYDE 3.1. 20**,** 565-573.

KREIENKAMP, F., PHILIP, S. Y., TRADOWSKY, J. S., KEW, S. F., LORENZ, P., ARRIGHT, J., BELLAFLAMME, A., BETTMAN, T., CALUWAERTS, S., CHAN, S. C., CIAVARELLA, A., DE CRUZ, L., DE VRIES, H., DEMUTH, N., FERRONE, A., FISCHER, E. M., FOWLER, H. J., GOERGEN, K., HEINRICH, D., HENRICHS, Y., LENDERINK, G., KASPAR, F., NILSON, E., OTTO, F. E. L., RAGONE, F., SENEVIRATNE, S. I., SINGH, R. K., SKALEVAG, A., TERMONIA, P., THALHEIMER, L., VAN AALST, M. K., VAN DE BERG, J., VAN DE VYER, H., VANNITSEM, S., VAN OLDENBORGH, G., VAN SCHAEYBROECK, B., VAUTARD, R., VONK, D. & WANDERS, N. 2021. Rapid attribution of heavy rainfall events in Western Europe July 2021. World Weather Attribution.

KUMMU, M., DE MOEL, H., WARD, P. J. & VARIS, O. 2011. How Close Do We Live to Water? A Global Analysis of Population Distance to Freshwater Bodies. *Plos One,* 6**,** 13.

LEHNER, B., VERDIN, K. & JARVIS, A. 2008. New Global Hydrography Derived From Spaceborne Elevation Data. *Eos, Transactions American Geophysical Union,* 89**,** 93-94.

LEYK, S., GAUGHAN, A. E., ADAMO, S. B., DE SHERBININ, A., BALK, D., FREIRE, S., ROSE, A., STEVENS, F. R., BLANKESPOOR, B., FRYE, C.,

COMENETZ, J., SORICHETTA, A., MACMANUS, K., PISTOLESI, L., LEVY, M., TATEM, A. J. & PESARESI, M. 2019. The spatial allocation of population: a review of large-scale gridded population data products and their fitness for use. *Earth Syst. Sci. Data,* 11**,** 1385-1409.

LHOMME, J., SAYERS, P., GOULDBY, B., SAMUELS, P. & WILLS, M. 2008. *Recent development and application of a rapid flood spreading method*.

LIN, B., WICKS, J. M., FALCONER, R. A. & ADAMS, K. 2006. Integrating 1D and 2D hydrodynamic models for flood simulation. 159**,** 19-25.

LINDERSSON, S., BRANDIMARTE, L., MÅRD, J. & DI BALDASSARRE, G. 2021. Global riverine flood risk – how do hydrogeomorphic floodplain maps compare to flood hazard maps? *Nat. Hazards Earth Syst. Sci.,* 21**,** 2921-2948.

LIVERMAN, D., MORAN, E., RINDFUSS, R. & STERN, P. 1998. *People and pixels: Linking remote sensing and social science,* Washington, D.C., National Academies Press.

LUDY, J. & KONDOLF, G. M. 2012. Flood risk perception in lands "protected" by 100-year levees. *Natural Hazards,* 61**,** 829-842.

LUGERI, N., KUNDZEWICZ, Z. W., GENOVESE, E., HOCHRAINER, S. & RADZIEJEWSKI, M. 2010. River flood risk and adaptation in Europe—assessment of the present status. *Mitigation and Adaptation Strategies for Global Change,* 15**,** 621-639.

MARJANAC, S., PATTON, L. & THORNTON, J. 2017. Acts of God, human influence and litigation. *Nature Geoscience,* 10**,** 616-619.

MASON, D. C., J-P. SCHUMANN, G. & BATES, P. D. 2010. Data Utilization in Flood Inundation Modelling. *Flood Risk Science and Management.*

MASSON-DELMOTTE, V., ZHAI, P., PIRANI, A., CONNORS, S. L., PÉAN, C., BERGER, S., CAUD, N., Y., C., GOLDFARD, L., GOMIS, M. I., HUANG, M., LEITZELL, K., LONNOY, E., MATTHEW, J. B. R., MAYCOCK, T. K., WATERFIELD, T., YELEKÇI, O., YU, R. & ZHOU, B. E. 2021. IPCC 2021: Summary for Policymakers. Cambridge University Press (In Press): Intergovernmental Panel on Climate Change.

MATEO, C. M. R., YAMAZAKI, D., KIM, H., CHAMPATHONG, A., VAZE, J. & OKI, T. 2017. Impacts of spatial resolution and representation of flow connectivity on large-scale simulation of floods. *Hydrology and Earth System Sciences,* 21**,** 5143-5163.

MD ALI, A., DI BALDASSARRE, G. & SOLOMATINE, D. P. 2015. Testing different cross-section spacing in 1D hydraulic modelling: a case study on Johor River, Malaysia. *Hydrological Sciences Journal,* 60**,** 351-360.

MEEHL, G. A., COVEY, C., MCAVANEY, B., LATIF, M. & STOUFFER, R. J. 2005. Overview of the Coupled Model Intercomparison Project. *Bulletin of the American Meteorological Society,* 86**,** 89-93.

MERZ, B., HALL, J., DISSE, M. & SCHUMANN, A. 2010a. Fluvial flood risk management in a changing world. *Nat. Hazards Earth Syst. Sci.,* 10**,** 509-527.

MERZ, B., KREIBICH, H., SCHWARZE, R. & THIEKEN, A. 2010b. Review article "Assessment of economic flood damage". *Nat. Hazards Earth Syst. Sci.,* 10**,** 1697-1724.

MESTER, B., WILLNER, S. N., FRIELER, K. & SCHEWE, J. 2021. Evaluation of river flood extent simulated with multiple global hydrological models and climate forcings. *Environmental Research Letters,* 16**,** 094010.

MEYER, V. & MESSNER, F. 2005. National flood damage evaluation methods: A review of applied methods in England, the Netherlands, the Czech Republik and Germany. Helmholtz Centre for Environmental Research (UFZ), Division of Social Sciences (ÖKUS).

MILLS, E. 2005. Insurance in a Climate of Change. 309, 1040-1044.

MILLY, P. C. D., BETANCOURT, J., FALKENMARK, M., HIRSCH, R. M., KUNDZEWICZ, Z. W., LETTENMAIER, D. P. & STOUFFER, R. J. 2008. Stationarity Is Dead: Whither Water Management? 319, 573-574.

MOREIRA, L. L., DE BRITO, M. M. & KOBIYAMA, M. 2021. Review article: A systematic review and future prospects of flood vulnerability indices. *Nat. Hazards Earth Syst. Sci.,* 21, 1513-1530.

MORRISON, A., WESTBROOK, C. J. & NOBLE, B. F. 2018. A review of the flood risk management governance and resilience literature. *Journal of Flood Risk Management,* 11, 291-304.

NAJIBI, N. & DEVINENI, N. 2018. Recent trends in the frequency and duration of global floods. *Earth Syst. Dynam.,* 9, 757-783.

NARDI, F., ANNIS, A., DI BALDASSARRE, G., VIVONI, E. R. & GRIMALDI, S. 2019. GFPLAIN250m, a global high-resolution dataset of Earth's floodplains. *Scientific Data,* 6, 180309.

NEAL, J., SCHUMANN, G. & BATES, P. 2012a. A subgrid channel model for simulating river hydraulics and floodplain inundation over large and data sparse areas. *Water Resources Research,* 48, 16.

NEAL, J., VILLANUEVA, I., WRIGHT, N., WILLIS, T., FEWTRELL, T. & BATES, P. 2012b. How much physical complexity is needed to model flood inundation? 26, 2264-2282.

NEELZ, S. & PENDER, G. 2009. Desktop review of 2D hydraulic modelling packages. Bristol, UK: Environment Agency.

NEELZ, S. & PENDER, G. 2013. Benchmarking the latest generation of 2D hydraulic modelling packages. Environment Agency.

NICHOLLS, R. J., HOOZEMANS, F. M. J. & MARCHAND, M. 1999. Increasing flood risk and wetland losses due to global sea-level rise: regional and global analyses. *Global Environmental Change,* 9, S69-S87.

NOBRE, A. D., CUARTAS, L. A., MOMO, M. R., SEVERO, D. L., PINHEIRO, A. & NOBRE, C. A. 2016. HAND contour: a new proxy predictor of inundation extent. *Hydrological Processes,* 30, 320-333.

OKAZAWA, Y., YEH, P. J. F., KANAE, S. & OKI, T. 2011. Development of a global flood risk index based on natural and socio-economic factors. *Hydrological Sciences Journal,* 56, 789-804.

OPPERMAN, J. J., GALLOWAY, G. E., FARGIONE, J., MOUNT, J. F., RICHTER, B. D. & SECCHI, S. 2009. Sustainable Floodplains Through Large-Scale Reconnection to Rivers. 326, 1487-1488.

PAPPENBERGER, F., DUTRA, E., WETTERHALL, F. & CLOKE, H. L. 2012. Deriving global flood hazard maps of fluvial floods through a physical model cascade. *Hydrology and Earth System Sciences,* 16, 4143-4156.

PAPROTNY, D., SEBASTIAN, A., MORALES-NÁPOLES, O. & JONKMAN, S. N. 2018. Trends in flood losses in Europe over the past 150 years. *Nature Communications,* 9, 1985.

PEDUZZI, P., DAO, H., HEROLD, C. & MOUTON, F. 2009. Assessing global exposure and vulnerability towards natural hazards: the Disaster Risk Index. *Nat. Hazards Earth Syst. Sci.,* 9, 1149-1159.

PENDER, G. 2006. Briefing: Introducing the Flood Risk Management Research Consortium. 159**,** 3-8.

PENNING-ROWSELL, E. C., PRIEST, S. J., PARKER, D. J., MORRIS, J., TUNSTALL, S. M. V., VIAVATTENE, C., CHATTERTON, J. & OWEN, D. 2013. *Flood and coastal erosion risk management: a manual for economic appraisal,* London, U.K., Routledge, Taylor & Francis.

PIELKE, R., AGRAWALA, S., BOUWER, L., BURTON, I., GLANTZ, M., KLEIN, R., KUNKEL, K., MILETI, D., SAREWITZ, D., THOMPKINS, E., STEHR, N. & VON STORCH, H. 2005. Clarifying the attribution of recent disaster losses: a response to Epstein and McCarthy. *Bulletin of the American Meteorological Society,* 86**,** 1481-1483.

PONCE, V. M., SIMONS, D. B. & LI, R.-M. 1978. Applicability of Kinematic and Diffusion Models. 104**,** 353-360.

RASUL, G. 2015. Water for growth and development in the Ganges, Brahmaputra, and Meghna basins: an economic perspective. *International Journal of River Basin Management,* 13**,** 387-400.

REED, F. J., GAUGHAN, A. E., STEVENS, F. R., YETMAN, G., SORICHETTA, A. & TATEM, A. J. 2018. Gridded Population Maps Informed by Different Built Settlement Products. 3**,** 33.

RENTSCHLER, J. & SALHAB, M. 2020. People in Harm's Way: Flood Exposure and Poverty in 189 Countries. *Policy Research Wokring Paper.* Washington, D.C.: World Bank.

RIZZOLI, P., MARTONE, M., GONZALEZ, C., WECKLICH, C., BORLA TRIDON, D., BRÄUTIGAM, B., BACHMANN, M., SCHULZE, D., FRITZ, T., HUBER, M., WESSEL, B., KRIEGER, G., ZINK, M. & MOREIRA, A. 2017. Generation and performance assessment of the global TanDEM-X digital elevation model. *ISPRS Journal of Photogrammetry and Remote Sensing,* 132**,** 119-139.

ROJAS, R., FEYEN, L. & WATKISS, P. 2013. Climate change and river floods in the European Union: Socio-economic consequences and the costs and benefits of adaptation. *Global Environmental Change,* 23**,** 1737-1751.

ROSENZWEIG, B. R., MCPHILLIPS, L., CHANG, H., CHENG, C., WELTY, C., MATSLER, M., IWANIEC, D. & DAVIDSON, C. I. 2018. Pluvial flood risk and opportunities for resilience. *WIREs Water,* 5**,** e1302.

RUDARI, R., SILVESTRO, F., CAMPO, L., REBORA, N., BONI, G. & HEROLD, C. 2015. IMPROVEMENT OF THE GLOBAL FLOOD MODEL FOR THE GAR 2015.

SAMELA, C., MANFREDA, S. & TROY, T. J. 2017a. Dataset of 100-year flood susceptibility maps for the continental U.S. derived with a geomorphic method. *Data in Brief,* 12**,** 203-207.

SAMELA, C., TROY, T. J. & MANFREDA, S. 2017b. Geomorphic classifiers for flood-prone areas delineation for data-scarce environments. *Advances in Water Resources,* 102**,** 13-28.

SAMPSON, C. C., SMITH, A. M., BATES, P. B., NEAL, J. C., ALFIERI, L. & FREER, J. E. 2015. A high-resolution global flood hazard model. *Water Resources Research,* 51**,** 7358-7381.

SCAWTHORN, C., FLORES, P., BLAIS, N., SELIGSON, H., TATE, E., CHANG, S., MIFFLIN, E., THOMAS, W., MURPHY, J., JONES, C. & LAWRENCE, M. 2006. HAZUS-MH Flood Loss Estimation Methodology. II. Damage and Loss Assessment. *Natural hazards review,* 7**,** 72-81.

SCHUMANN, G., BALDASSARRE, G. D. & BATES, P. D. 2009. The Utility of
        Spaceborne Radar to Render Flood Inundation Maps Based on
        Multialgorithm Ensembles. *IEEE Transactions on Geoscience and Remote
        Sensing,* 47**,** 2801-2807.
SCHUMANN, G. J. P. 2014. Fight floods on a global scale. *Nature,* 507**,** 169.
SCHUMANN, G. J. P., STAMPOULIS, D., SMITH, A. M., SAMPSON, C. C.,
        ANDREADIS, K. M., NEAL, J. C. & BATES, P. D. 2016. Rethinking flood
        hazard at the global scale. *Geophysical Research Letters,* 43**,** 10249-10256.
SCUSSOLINI, P., AERTS, J., JONGMAN, B., BOUWER, L. M., WINSEMIUS, H.
        C., DE MOEL, H. & WARD, P. J. 2016. FLOPROS: an evolving global
        database of flood protection standards. *Natural Hazards and Earth System
        Sciences,* 16**,** 1049-1061.
SEPA 2017. Flood Modelling guidance for responsible authorities, version 1.1.
        Scottish Environment Protection Agency.
SHARMA, A., WASKO, C. & LETTENMAIER, D. P. 2018. If Precipitation
        Extremes Are Increasing, Why Aren't Floods? 54**,** 8545-8551.
SLATER, L., VILLARINI, G., ARCHFIELD, S., FAULKNER, D., LAMB, R.,
        KHOUAKHI, A. & YIN, J. 2021. Global Changes in 20-Year, 50-Year, and
        100-Year River Floods. *Geophysical Research Letters,* 48**,** e2020GL091824.
SMITH, A., BATES, P. D., WING, O., SAMPSON, C., QUINN, N. & NEAL, J.
        2019. New estimates of flood exposure in developing countries using high-
        resolution population data. *Nature Communications,* 10**,** 1814.
STEVENS, F. R., GAUGHAN, A. E., LINARD, C. & TATEM, A. J. 2015.
        Disaggregating Census Data for Population Mapping Using Random Forests
        with Remotely-Sensed and Ancillary Data. *Plos One,* 10**,** 22.
STEVENS, F. R., GAUGHAN, A. E., NIEVES, J. J., KING, A., SORICHETTA, A.,
        LINARD, C. & TATEM, A. J. 2020. Comparisons of two global built area
        land cover datasets in methods to disaggregate human population in eleven
        countries from the global South. *International Journal of Digital Earth,* 13**,**
        78-100.
SWAIN, D. L., SINGH, D., TOUMA, D. & DIFFENBAUGH, N. S. 2020.
        Attributing Extreme Events to Climate Change: A New Frontier in a
        Warming World. *One Earth,* 2**,** 522-527.
TANOUE, M., HIRABAYASHI, Y. & IKEUCHI, H. 2016. Global-scale river flood
        vulnerability in the last 50 years. *Scientific Reports,* 6**,** 36021.
TELLMAN, B., SULLIVAN, J. A., KUHN, C., KETTNER, A. J., DOYLE, C. S.,
        BRAKENRIDGE, G. R., ERICKSON, T. A. & SLAYBACK, D. A. 2021.
        Satellite imaging reveals increased proportion of population exposed to
        floods. *Nature,* 596**,** 80-86.
TENG, J., JAKEMAN, A. J., VAZE, J., CROKE, B. F. W., DUTTA, D. & KIM, S.
        2017. Flood inundation modelling: A review of methods, recent advances
        and uncertainty analysis. *Environmental Modelling & Software,* 90**,** 201-216.
TIECKE, T. G. L., XIANMING ZHANG, AMY GROS, ANDREAS LI, NAN
        YETMAN, GREGORY KILIC, TALIP MURRAY, SIOBHAN
        BLANKESPOOR, BRIAN PRYDZ, ESPEN B. DANG, HAI-ANH H. 2017.
        Mapping the World Population One Building at a Time.
TOBLER, W., DEICHMANN, U., GOTTSEGEN, J. & MALOY, K. 1997. World
        population in a grid of spherical quadrilaterals. 3**,** 203-225.
TOCKNER, K. & STANFORD, J. A. 2002. Riverine flood plains: present state and
        future trends. *Environmental Conservation,* 29**,** 308-330.

TOLLEFSON, J. 2021. *Diagnosing Earth: The science behind the IPCC's upcoming climate report* [Online]. [Accessed November 9th 2021].

TRIGG, M. A., BIRCH, C. E., NEAL, J. C., BATES, P. D., SMITH, A., SAMPSON, C. C., YAMAZAKI, D., HIRABAYASHI, Y., PAPPENBERGER, F., DUTRA, E., WARD, P. J., WINSEMIUS, H. C., SALAMON, P., DOTTORI, F., RUDARI, R., KAPPES, M. S., SIMPSON, A. L., HADZILACOS, G. & FEWTRELL, T. J. 2016. The credibility challenge for global fluvial flood risk analysis. *Environmental Research Letters,* 11**,** 10.

TRIGG, M. A., WILSON, M. D., BATES, P. D., HORRITT, M. S., ALSDORF, D. E., FORSBERG, B. R. & VEGA, M. C. 2009. Amazon flood wave hydraulics. *Journal of Hydrology,* 374**,** 92-105.

UNDRR 2017. Terminology of Disaster Risk Reduction. United Nations General Assmbly.

UNFCCC. Paris agreement. Report of the Conference of the Parties to the United Nations Framework Convention on Climate Change (21st Session, 2015). , 2015 Paris, France. 2017.

UNISDR 2015. Sendai Framework for Disaster Risk Reduction 2015-2030. United Nations - Headquarters (UN).

VAN WESTEN, C. J. 2014. Vulnerability. *Caribbean Handbook on Risk Management: Methodology Book.* Carribean Disaster Emergency Managment Agency.

VENOT, J.-P., BOWERS, S., BROCKINGTON, D., KOMAKECH, H., RYAN, C. M., VELDWISCH, G. J. & WOODHOUSE, P. J. W. A. 2021. Below the Radar: Data, Narratives and the Politics of Irrigation in Sub-Saharan Africa. 14**,** 546-572.

VOZINAKI, A.-E. K., MORIANOU, G. G., ALEXAKIS, D. D. & TSANIS, I. K. 2017. Comparing 1D and combined 1D/2D hydraulic simulations using high-resolution topographic data: a case study of the Koiliaris basin, Greece. *Hydrological Sciences Journal,* 62**,** 642-656.

WAHL, T., JAIN, S., BENDER, J., MEYERS, S. D. & LUTHER, M. E. 2015. Increasing risk of compound flooding from storm surge and rainfall for major US cities. *Nature Climate Change,* 5**,** 1093-1097.

WARD, P. J., BLAUHUT, V., BLOEMENDAAL, N., DANIELL, J. E., DE RUITER, M. C., DUNCAN, M. J., EMBERSON, R., JENKINS, S. F., KIRSCHBAUM, D., KUNZ, M., MOHR, S., MUIS, S., RIDDELL, G. A., SCHÄFER, A., STANLEY, T., VELDKAMP, T. I. E. & WINSEMIUS, H. C. 2020a. Review article: Natural hazard risk assessments at the global scale. *Nat. Hazards Earth Syst. Sci.,* 20**,** 1069-1096.

WARD, P. J., COUASNON, A., EILANDER, D., HAIGH, I. D., HENDRY, A., MUIS, S., VELDKAMP, T. I. E., WINSEMIUS, H. C. & WAHL, T. 2018. Dependence between high sea-level and high river discharge increases flood hazard in global deltas and estuaries. *Environmental Research Letters,* 13**,** 084012.

WARD, P. J., JONGMAN, B., AERTS, J., BATES, P. D., BOTZEN, W. J. W., LOAIZA, A. D., HALLEGATTE, S., KIND, J. M., KWADIJK, J., SCUSSOLINI, P. & WINSEMIUS, H. C. 2017. A global framework for future costs and benefits of river-flood protection in urban areas. *Nature Climate Change,* 7**,** 642-+.

WARD, P. J., JONGMAN, B., SALAMON, P., SIMPSON, A., BATES, P., DE GROEVE, T., MUIS, S., DE PEREZ, E. C., RUDARI, R., TRIGG, M. A. &

WINSEMIUS, H. C. 2015. Usefulness and limitations of global flood risk models. *Nature Climate Change,* 5**,** 712-715.

WARD, P. J., JONGMAN, B., WEILAND, F. S., BOUWMAN, A., VAN BEEK, R., BIERKENS, M. F. P., LIGTVOET, W. & WINSEMIUS, H. C. 2013. Assessing flood risk at the global scale: model setup, results, and sensitivity. *Environmental Research Letters,* 8**,** 10.

WARD, P. J., WINSEMIUS, H. C., KUZMA, S., BIERKENS, M. F. P., BOUWMAN, A., DE MOEL, H., DÍAZ LOAIZA, A., EILANDER, D., ENGLHARDT, J., ERKENS, G., TAFETE GEBTEMEDHIN, E., ICELAND, C., KOOI, H., LIGTVOET, W., MUIS, S., SCUSSOLINI, P., SUTANUDJAJA, E. H., VAN BEEK, R., VAN BEMMEL, B., VAN HUIJSTEE, J., VAN RIJN, F., VAN WESENBEECK, B., VATVANI, D., VERLAAN, M., TIGGELOVEN, T. & LUO, T. 2020b. Aqueduct Floods Methodology. Wasington D.C.: World Resources Institute.

WEHNER, M. & SAMPSON, C. 2021. Attributable human-induced changes in the magnitude of flooding in the Houston, Texas region during Hurricane Harvey. *Climatic Change,* 166**,** 20.

WESTRA, S., ALEXANDER, L. V. & ZWIERS, F. W. 2013. Global Increasing Trends in Annual Maximum Daily Precipitation %J Journal of Climate. 26**,** 3904-3918.

WHITE, G. F. 1942. *Human adjustment to floods: a geographical approach to the flood problem in the United States.* The University of Chicago.

WILBY, R. L., CLIFFORD, N. J., DE LUCA, P., HARRIGAN, S., HILLIER, J. K., HODGKINS, R., JOHNSON, M. F., MATTHEWS, T. K. R., MURPHY, C., NOONE, S. J., PARRY, S., PRUDHOMME, C., RICE, S. P., SLATER, L. J., SMITH, K. A. & WOOD, P. J. 2017. The 'dirty dozen' of freshwater science: detecting then reconciling hydrological data biases and errors. 4**,** e1209.

WILLNER, S. N., OTTO, C. & LEVERMANN, A. 2018. Global economic response to river floods. *Nature Climate Change,* 8**,** 594-598.

WING, O. E. J., BATES, P. D., SAMPSON, C. C., SMITH, A. M., JOHNSON, K. A. & ERICKSON, T. A. 2017. Validation of a 30 m resolution flood hazard model of the conterminous United States. *Water Resources Research,* 53**,** 7968-7986.

WING, O. E. J., BATES, P. D., SMITH, A. M., SAMPSON, C. C., JOHNSON, K. A., FARGIONE, J. & MOREFIELD, P. 2018. Estimates of present and future flood risk in the conterminous United States. *Environmental Research Letters,* 13**,** 7.

WING, O. E. J., PINTER, N., BATES, P. D. & KOUSKY, C. 2020a. New insights into US flood vulnerability revealed from flood insurance big data. *Nature Communications,* 11**,** 1444.

WING, O. E. J., QUINN, N., BATES, P. D., NEAL, J. C., SMITH, A. M., SAMPSON, C. C., COXON, G., YAMAZAKI, D., SUTANUDJAJA, E. H. & ALFIERI, L. 2020b. Toward Global Stochastic River Flood Modeling. 56**,** e2020WR027692.

WING, O. E. J., SMITH, A. M., MARSTON, M. L., PORTER, J. R., AMODEO, M. F., SAMPSON, C. C. & BATES, P. D. 2021. Simulating historical flood events at the continental scale: observational validation of a large-scale hydrodynamic model. *Nat. Hazards Earth Syst. Sci.,* 21**,** 559-575.

WINSEMIUS, H. C., AERTS, J., VAN BEEK, L. P. H., BIERKENS, M. F. P.,
        BOUWMAN, A., JONGMAN, B., KWADIJK, J. C. J., LIGTVOET, W.,
        LUCAS, P. L., VAN VUUREN, D. P. & WARD, P. J. 2016. Global drivers
        of future river flood risk. *Nature Climate Change,* 6**,** 381-385.
WINSEMIUS, H. C., VAN BEEK, L. P. H., JONGMAN, B., WARD, P. J. &
        BOUWMAN, A. 2013. A framework for global river flood risk assessments.
        Hydrology and Earth System Sciences, 17**,** 1871-1892.
WOODRUFF, J. D., IRISH, J. L. & CAMARGO, S. J. 2013. Coastal flooding by
        tropical cyclones and sea-level rise. *Nature,* 504**,** 44-52.
WORLDPOP. n.d. *Top-down estimation modelling: Constrained vs. Unconstrained*
        [Online]. WorldPop. Available:
        https://www.worldpop.org/methods/top_down_constrained_vs_unconstraine
        d [Accessed 23 November 2021].
YAMAZAKI, D., BAUGH, C. A., BATES, P. D., KANAE, S., ALSDORF, D. E. &
        OKI, T. 2012. Adjustment of a spaceborne DEM for use in floodplain
        hydrodynamic modeling. *Journal of Hydrology,* 436**,** 81-91.
YAMAZAKI, D., DE ALMEIDA, G. A. M. & BATES, P. D. 2013. Improving
        computational efficiency in global river models by implementing the local
        inertial flow equation and a vector-based river network map. Water
        Resources Research.
YAMAZAKI, D., IKESHIMA, D., SOSA, J., BATES, P. D., ALLEN, G. H. &
        PAVELSKY, T. M. 2019. MERIT Hydro: A High-Resolution Global
        Hydrography Map Based on Latest Topography Dataset. *Water Resources
        Research,* 55**,** 5053-5073.
YAMAZAKI, D., IKESHIMA, D., TAWATARI, R., YAMAGUCHI, T.,
        O'LOUGHLIN, F., NEAL, J. C., SAMPSON, C. C., KANAE, S. & BATES,
        P. D. 2017. A high-accuracy map of global terrain elevations. *Geophysical
        Research Letters,* 44**,** 5844-5853.
YAMAZAKI, D., KANAE, S., KIM, H. & OKI, T. 2011. A physically based
        description of floodplain inundation dynamics in a global river routing
        model. *Water Resources Research,* 47**,** 21.
YAMAZAKI, D., SATO, T., KANAE, S., HIRABAYASHI, Y. & BATES, P. D.
        2014. Regional flood dynamics in a bifurcating mega delta simulated in a
        global river model. *Geophysical Research Letters,* 41**,** 3127-3135.
ZHOU, X., MA, W., ECHIZENYA, W. & YAMAZAKI, D. 2020. Uncertainty in
        flood frequency analysis of hydrodynamic model simulations. *Nat. Hazards
        Earth Syst. Sci. Discuss.,* 2020**,** 1-31.
ZSCHEISCHLER, J., WESTRA, S., VAN DEN HURK, B. J. J. M.,
        SENEVIRATNE, S. I., WARD, P. J., PITMAN, A., AGHAKOUCHAK, A.,
        BRESCH, D. N., LEONARD, M., WAHL, T. & ZHANG, X. 2018. Future
        climate risk from compound events. *Nature Climate Change,* 8**,** 469-477.

Chapter 2
Global Flood Models

2.1 Abstract

Flooding is the most damaging natural hazard, both economically and by population affected. Flood models are important tools for evaluating the risks associated with flooding. Historically, the modelling domain has been limited in scale; however, advancements in computing power and global datasets have led to the development of global flood models (GFMs). This global modelling capability has benefited scientific studies of exposure and climate change impact, the insurance industry, and intergovernmental disaster risk reduction efforts. Global flood modelling has now progressed beyond its infancy to a point where coordinated and targeted model development can take place based on collective studies. This chapter provides a detailed summary of the current global flood modelling state-of-affairs. It begins with a summary of the history and challenges of GFM development. This is followed by a review of current GFMs and their structures, applications, and credibility. A section is also dedicated to describing global flood modelling in the context of the insurance catastrophe model, an important GFM category that is less visible due to their proprietary nature. The chapter concludes by looking to the future and highlighting how GFMs need to improve and the new datasets and methods that could contribute to their continued development.

2.2 Introduction

Global flood model (GFM) initiatives have developed rapidly over the past decade and have matured from research experiments into usable tools that are reshaping our understanding of global flood risk (Ward et al., 2015). This chapter explores how GFMs have become a recent reality and why they are important. It will also look at the different types of GFM, the differences between a GFM and more traditional flood modelling and look at some examples of how GFMs are being used, including the cross-overs with insurance catastrophe models. It will finish with

a look at current GFM credibility and where GFMs might develop in the future. The focus in this chapter will be mainly on models used to derive flood hazard globally, rather than those used for flood forecasting; which is a related use and many of the models discussed are used for both purposes.

While flooding is often experienced first-hand as a local impact and has traditionally been tackled at the relevant local catchment or reach scale, there is a growing understanding that many flood events are connected to, or driven by, short and long term global weather systems (Fan et al., 2015, Hagos et al., 2016). In addition, due to our increasingly interconnected global community, flood events in all parts of the globe are now having significant economic and social impacts in all parts of the world (Trigg et al., 2013). Together with the extra challenge of addressing the effects of climate change, which are felt globally, these drivers have led to a need for assessments of flood risk at a global scale. This global need has become evident on several fronts; scientific studies to simulate the impact effects of general circulation modelling, insurance catastrophe modelling to understand risk and exposure (Bates et al., 2018), and intergovernmental efforts in disaster risk reduction (UNISDR, 2005, UNISDR, 2009, UNISDR, 2011, UNISDR, 2013, UNISDR, 2015b). This collective challenge has resulted in the formation of the Global Flood Partnership (GFP), which brings together organizations involved in all these fronts. The overall objective of the GFP is the development of flood observational and modelling infrastructure, leveraging on existing initiatives for better predicting and managing flood disaster impacts and flood risk globally (De Groeve et al., 2015).

2.2.1 The Challenges and History of GFM Development

Despite the growing need for a better understanding of global flood risk, it was not immediately evident how this could be achieved and what a resulting GFM would look like. Any GFM needs to be able to provide realistic and reliable estimates of flood hazard for a range of probabilities (return periods). For estimates of risk exposure, at a bare minimum, flood extent is required, and ideally flood depth is also needed to estimate risk from vulnerability. These outputs need to be at a sufficient resolution to be commensurate with global exposure datasets, which are also an active research field.

Traditional flood risk modelling has filled these needs at a local scale. However, these require significant amounts of high resolution data and computation resources, as well as technical expertise to build and run the models (Table 2.1). Scaling this approach up to a global level seemed almost an impossible challenge and therefore a different approach was required. Thus, multiple parallel initiatives emerged from different sectors, leading to a rich diversity of GFMs approaches, which we detail in the next section. However, despite the initial variety, there were several common primary challenges to surmount for all developers (Sampson et al., 2015) and there is therefore a common development timeline as data and methods became available (Figure 2.1).

The challenges facing developers fall into the following five categories: terrain data, channel location and size, river discharge, computational efficiency, and automation. The first challenge facing developers was the availability of global data with which to build the models. Flood models require information about the topography of the terrain that controls flooding. It was not until the advent and adoption of Shuttle Radar Topography Mission (SRTM) digital elevation data (hereafter DEM), that data of sufficient resolution and quality was available with a near global coverage. The second challenge, correctly identifying channel location and size, is inherently linked to the first; as the channel is derived from the DEM. The HydroSHEDS hydrography dataset, developed using the SRTM DEM, is essential to modelling flooding globally. The third challenge was to derive extreme flood flows at multiple locations for every river on earth, with limited gauged data. There are two distinct approaches to solving river discharge in GFMs, regionalization growth curve methods using data from the Global Runoff Data Center (GRDC) database (Smith et al., 2015) and land surface modelling of flows from global circulation models (GCMs). The latter approach, which enables the models to produce nowcasts, forecasts, and future predictions also introduces additional uncertainties into the modelling framework. Precipitation, a major source of uncertainty in GCMs, often dominates the uncertainty of flood simulations in GCM-driven models (Chen et al., 2014). The fourth challenge was to be able to computationally model the hydraulics of the flood flows in the rivers and on the floodplains with sufficient speed to undertake this for all rivers, for multiple probability scenarios. This was achieved through simplification of the hydraulics

Table 2.1 Characteristics of Global Flood Models Relative to Traditional Local
Flood Models

Characteristic	Global flood model	Local flood model
Digital elevation model (DEM)	Coverage is key, needs to be global. Potentially can be composite from different sources but difficulties in merging different data sources seamlessly	Best available, typically three-dimensional laser scanning (LiDAR)
Geographical coverage	Global	Typically tens of kilometres
Floodplain hydraulics	Limited equation base, sacrificing accuracy for speed, knowing that errors due to neglecting, e.g., advection terms are small compared to errors from lower quality DEM. Also related to resolution, as larger model cells make some terms less significant (see Hunter et al. (2007))	Typically full shallow water
Channel hydraulics	Sometimes ignored completely; allowance for channel capacity made by, e.g., removing bankfull discharge from flow estimate; or simple representation in DEM or submodel grid	Full representation in two-dimensional or as on-dimensional submodel from bespoke topographical survey
Outputs	Typically extent only, vertical errors in DEM can prevent useful depth prediction	Extent-depth-velocity-duration
Hydrology	Regional growth-curve methods or large-scale land surface runoff modelling	Led by hydrologist, making best use of local data
Build and run process	Fully automated	Manual. Requiring experienced modellers
Hardware	Supercomputer, cluster, and cloud	Desktop computer
Flood sources	Mostly only fluvial, some now include coastal and surface water	Fluvial, coastal, surface water; sometimes dam break, groundwater, natural flood management, urban drainage systems
Resolution	1 km to ~ 90 m for two-dimensional models. 5-50 km and postprocess downscaling for one-dimensional models	~5 m or less
Catchment size	All large rivers. Smallest scale dependent on model, i.e., 50-5000 km^2 catchment size	Down to ~1 km^2 for fluvial, smaller catchments in surface water models
Dynamics	Steady state or partially dynamic, but increasingly fully dynamic	Fully dynamic

and the development of rapid parallel computational algorithms (Bates et al., 2010) and sub-grid modelling approaches to solve multi-scale hydrodynamic process in rivers and floodplains (Yamazaki et al., 2011, Neal et al., 2012, Wu et al., 2014), as well as with the help of continuous computation speed improvements. The final, not insignificant, challenge for developers was to put these data and methods into an automatic functional framework that allowed specific hazard and forecasting outputs to be generated as required and in a format and resolution that was useable.

It should also be noted here that there have been parallel efforts to develop regional flood model approaches that share similar scale challenges with GFMs but may have access to better regional data. For example, the United Kingdom has undertaken national risk assessments using simple none hydraulic methods, due to computational cost (Hall et al., 2003), but later used two-dimensional diffusive wave hydraulic models (Bradbrook et al., 2004, Bradbrook et al., 2005). In the United States, the recent focus has been on the dynamic, unsteady river routing methods for quasi-real-time, event-based flood extent mapping (Adams, 2016).

Once a GFM is functioning, there may be a number of other secondary follow on challenges that require development, depending upon the use intended. Many of these are active research areas in themselves and specific approaches are outlined in the model detail section. For example, most current GFMs do not include infrastructure that may locally affect flood hazard, e.g. bridges, dams, flood defences and urban drainage networks. They often do not yet include other, maybe only locally important, sources of flood hazard other than fluvial (river source), such as pluvial, coastal or groundwater.

The GFM community has succeeded in overcoming these primary challenges and in developing a range of usable flood models. The rest of the chapter focuses on describing the models and their uses in more detail, while also looking at their testing and how developers are addressing the secondary challenges that will ultimately improve their credibility and usability.
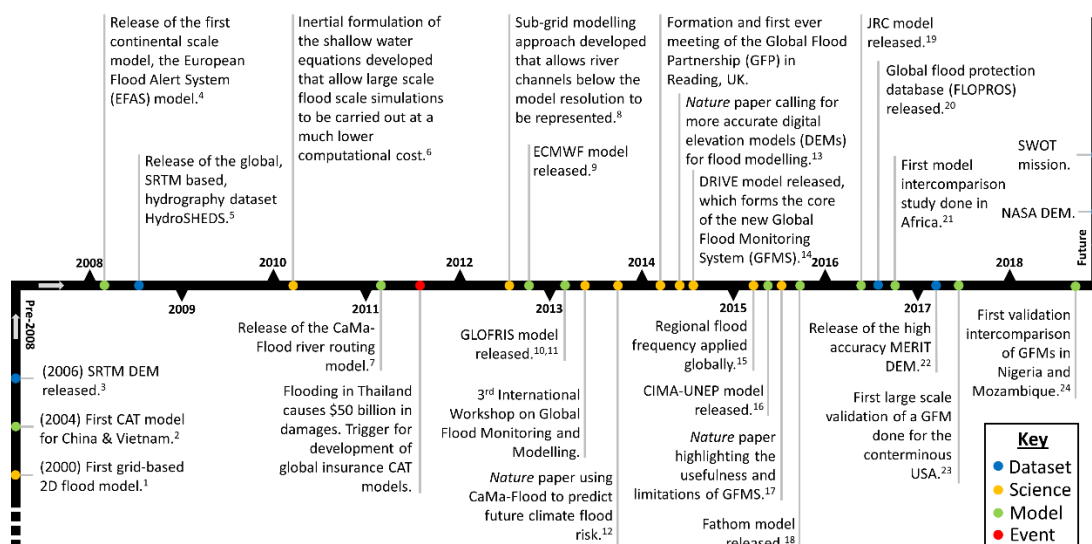
Figure 2.1 Timeline of global flood model (GFM) development highlighting key data set releases, scientific meetings and publications, model releases and testing, and flood events.

1, Bates and De Roo (2000); 2, Hall (2014); 3, Rodriguez et al. (2006); 4, Thielen et al. (2008); 5, Lehner et al. (2008); 6, Bates et al. (2010); 7, Yamazaki et al. (2011); 8, Neal et al. (2012); 9, Pappenberger et al. (2012); 10, Winsemius et al. (2013); 11, Ward et al. (2013); 12, Hirabayashi et al. (2013); 13, Schumann et al. (2014); 14, Wu et al. (2014); 15, Smith et al. (2015); 16, Rudari et al. (2015); 17, Ward et al. (2015); 18, Sampson et al. (2015); 19, Dottori et al. (2016); 20, Scussolini et al. (2016); 21, Trigg et al. (2016); 22, Yamazaki et al. (2017); 23, Wing et al. (2017); 24, Bernhofen et al. (2018)

2.3 Types of GFM and Specific Examples

The palpable benefit of being able to model flood hazard anywhere in the world meant that as soon as the necessary inputs for a GFM became available, a number of different groups began developing models simultaneously. Flood modelling on such a large scale had never been undertaken before and brought with it challenges that had not previously been encountered. Each model developer approached these new challenges differently, resulting in a broad selection of GFMs with varying model structures.

This section will begin by highlighting the key differences in model configuration of six well known GFMs, for which there is extensive documentation. These models include U-Tokyo (previously called CaMa-UT), a research model from the University of Tokyo (Yamazaki et al., 2011); Centro Internazionale in Monitoraggio Ambientale and United Nations Environment Program (CIMA-

UNEP), a model developed for the 2015 United Nations International Strategy for Disaster Reduction (UNISDR) Global Assessment Report (GAR; Rudari et al. (2015)); ECMWF, a model developed by the European Centre for Medium-Range Weather Forecasts (Pappenberger et al., 2012); GLOFRIS, a model developed by Deltares (Winsemius et al., 2013); JRC, a model developed by the Joint Research Centre in Italy (Dottori et al., 2016); and Fathom (previously called SSBN), a commercial model that arose out of research from the University of Bristol (Sampson et al., 2015).

Categorizing GFMs based on their characteristics is not a straightforward task. A previous study grouped the models into two types by extreme flow method: cascade model types and gauged flow data types (Trigg et al., 2016). A schematic of these two model groups is shown in Figure 2.2. This section will elaborate on additional model differences by looking at five different aspects: scale characteristics, model forcing, probability estimation methods, calibration, and hydraulic methods. Before highlighting the differences between the models, it should be noted that there are also many common underlying datasets, in particular, the HydroSHEDS global hydrography dataset (Lehner et al., 2008) and the SRTM DEM from which it is derived (Rodriguez et al., 2006). This section concludes by describing other global hydrology models that may also develop into GFMs in the future or add to process improvements in GFMs. The GFMs used for insurance purposes are described separately, partly due to the lack of published information, but also due to the very specific risk framework within which they are used.

2.3.1 Scale Characteristic

The scale of GFMs can refer to a number of things: the minimum threshold size of rivers that are represented, the resolution at which the calculations are carried out, or the resolution of the actual flood hazard output. The question of scale is something that needs to consider both the accuracy and comprehensiveness of the flood hazard output alongside the computational efficiency of the model.

Communicating the scale of river representation in GFMs is typically done in terms of upstream catchment area. The threshold river size considered by the models varies significantly, from ~50 km^2 (Fathom Global) to ~5000 km^2 (JRC). The GFM output is contingent on the input datasets, and often, global datasets are

not resolved to a level where the smallest rivers can be easily represented. The coarse (~5000 km^2) upstream area threshold of the JRC's model comes as a result of using ERA-Interim climatology, where the coarse global resolution cannot accurately represent very local precipitation (Dottori et al., 2016).

Operating at a coarse resolution is not a detriment to these global models but rather a necessity. Many of the models run their computations at a coarser scale and then downscale these results to the output resolution. The process of downscaling makes modelling at such large scales more computationally viable (Bates et al., 2018). The Fathom model, however, no longer downscales and runs all calculations explicitly at either 30 m or 90 m resolution (depending on the DEM available). This shows how far GFMs have come in only a matter of years (Sampson et al., 2015). The principle, however, remains the same; global models cannot be run at 'engineering' level resolutions (< 5 m), even if the data were available.

The scale of GFMs is likely the characteristic that will see the most improvement over the coming years. As computational capacity improves through faster processors and parallelization, so too global datasets will see advancements in terms of accuracy and resolution; making it possible to accurately model the flood hazard of even the smallest streams at some point.

2.3.2 Model Forcing

Global flood models can be most easily categorized by their method for generating extreme flood flows. Models are either forced by climate reanalysis data or by global gauge data. The two methods for forecasting extreme flows differ significantly. See Figure 2.2 for a useful visualization of this model categorization and the different stages in analysis that occur as a result of beginning with an extreme flow methodology.

Those models forced by climate data combine a climate reanalysis data set with a land surface model to predict extreme flows. Climate reanalysis datasets contain measurements of global climate data that are collected and stored at a constant time step (often 6-12 h) over an extended period (30-40 years for the GFMs in question) (Dee et al., 2016). These rainfall data, along with other relevant climate data, are input into a land surface model that simulates the land surface response to the climate forcing (Pappenberger et al., 2012) and outputs the resultant rainfall discharge and volume.

The GFMs not forced by climate data are forced instead by regionalized analysis of global gauge data. The premise for these models is that the discharges measured in well-monitored catchments can be transferred to unmonitored catchments that share similar characteristics. The GFMs use data from sources like the Global Runoff Data Centre (GRDC), which collects discharge data from 9500 stations globally. Catchments are then categorized based on their Koppen-Geiger climate classification (Kottek et al., 2006) and their rainfall characteristics. The behaviour of similarly characterized gauged catchments is used to derive ungauged catchment flows so that extreme flows can then be calculated for all global catchments (Smith et al., 2015, Rudari et al., 2015).

Cascade model type
[U-Tokyo, GLOFRIS, ECMWF, JRC]

Gauged flow data model type
[Fathom, CIMA-UNEP]

Cascade model type	Gauged flow data model type
Climate reanalysis data	Global gauged flow data
Land surface model	Regional flow frequency analysis
Continuous river flow routing	Flood flow magnitude
Flood frequency analysis	Flood flow routing, rivers & floodplain
Downscaling or calculate flood extents and depths	Calculate flood extents & depths

Figure 2.2 A simplified schematic of the two main model structures used by the six different global flood models.

Source: Trigg et al. (2016)

2.3.3 Probability Estimate Methods

In order for GFMs to model flooding of a specific return period, some form of flood probability estimation needs to take place. All the models apply a Gumbel distribution (Generalized Extreme Value distribution Type I) to their forcing data to estimate the return period magnitude. The models differ, however, in the flood component that is output as a result of this probability estimation.

The JRC, Fathom, and CIMA-UNEP models return probability discharges. These discharges are then used as input for a hydraulic model, which simulates the flood extent and depth in the catchment for the given return period flow (Sampson et al., 2015, Rudari et al., 2015, Dottori et al., 2016). The ECMWF and U-Tokyo models return probability flood depths, derived from the Gumbel frequency analysis of river water storage, which is calculated by passing the climate forcing data through a river routing scheme. These probability flood depths are calculated for each river cell and are used to determine whether the surrounding cells are flooded or not (Yamazaki et al., 2011, Pappenberger et al., 2012). The GLOFRIS model operates under a similar 'flooded cell' probability scheme, but uses flood volume instead of flood depth to determine the probability of cell inundation (Ward et al., 2013, Winsemius et al., 2013).

2.3.4 Calibration

A major difference between GFMs and reach-scale flood models is the level to which they are calibrated. Reach-scale flood models are often calibrated against a multitude of different measurements and observations from historical flood events, these include: gauge flow records, gauge water level measurements, flood depth, flood extent, and flood frequency (Huxley and Ryan, 2016). Data availability, in addition to the scale and global applicability of GFMs, limits the feasibility of conventional flood model calibration. Variables traditionally derived at a regional scale through calibration, such as flow roughness parameter Manning's n, are either calculated based on a relationship with streamflow (Wu et al., 2017) to account for the relationship between roughness and flooded vegetation (Soong et al., 2012), or determined based on basin characteristics (Rudari et al., 2015), previous studies (Dottori et al., 2016), or even kept constant in the global domain (Yamazaki et al., 2011, Winsemius et al., 2013).

Many of the GFM input data sets have undertaken some form of correction. The forcing datasets for almost all of the models have received bias correction and the underlying SRTM-based (Rodriguez et al., 2006) based HydroSHEDS DEM (Lehner et al., 2008) has in some cases received vegetation canopy and urban bias correction (Yamazaki et al., 2012, Sampson et al., 2015, Dottori et al., 2016). Bias correcting the underlying DEM is of vital importance, as these areas of vegetation and high urban concentration see consistent elevation overestimation. This incorrect terrain representation, in turn, naturally affects the accuracy of the modelled flood extent.

2.3.5 Hydraulic Method

Central to each GFM is a hydraulic model that simulates, to varying degrees of complexity, the physics of fluid flow. To operate globally, these models often need to make assumptions about flow physics that simplify the governing equations, thereby considerably reducing computation time. Information about the set-up of each model, including the most up to date hydraulic method is provided in Table 2.2.

The CIMA-UNEP model is the only GFM that operates in one-dimension, solving Manning's equation (2.1) at regular points along the centreline of the river channel (Rudari et al., 2015):

$$Q = \frac{A}{n} R^{\frac{2}{3}} \sqrt{S} \tag{2.1}$$

where Q is the channel flow [$L^3 T^{-1}$], R is the hydraulic radius [L], S is the channel slope [L/L], A is channel cross-sectional flow area [L^2], and n is Manning's roughness coefficient [$T L^{1/3}$]. One-dimensional flow representation is the simplest form of flood modelling, but while it is computationally efficient, it can falsely represent connectivity in floodplains and cannot model the floodplain flow well, unless it is parallel to the main river channel (Neelz and Pender, 2009). However, on the large scales of global flood models it appears to perform reasonably well considering its limitations (Bernhofen et al., 2018).

Table 2.2 Global Flood Model Details

Model	Climate Forcing	Land surface model	River routing	Floodplain	Flood frequency	Downscaling	Output data resolution
GLOFRIS (Deltares, VU Amsterdam, University of Utrecht, PBL)	EU-WATCH reanalysis 1960–1999	Hydrological model PCR-GLOBWB, 0.5°	Kinematic 0.5°	30 arc s SRTM model	Flood volume Gumbel distribution for 1960-1999	Volume redistribution 30 arc s SRTM model	30 arc s ~900 m
U-Tokyo (U-Tokyo, JAMSTEC)	JRA-25 reanalysis 1979-2010 + GPCP rain gauge correction	MATSIRO-GW energy and water balance (1°)	Inertia 0.25°	Subgrid topography upscaled from 3 arc s HydroSHEDS and SRTM	Water level Gumbel distribution for 1979-2010	Flood depth downscaled onto 18 arc s DEM	18 arc s ~540 m
HTESSEL + CaMa-Flood (ECMWF)	ERA-Interim reanalysis 1979-2014	HTESSEL, T255 (~80 km)	Three methods: kinematic, inertia(x2) 0.25°	Subgrid topography upscaled from 3 arc s HydroSHEDS and SRTM	Flood depth GEV distribution for 1979-2014	Depth downscaled onto 18 arc s DEM	18 arc s ~540 m
JRC	GloFAS, ERA-Interim reanalysis 1980-2013	HTESSEL	LISFLOOD-Global (0.1°) + inertia (30 arc s)	Subgrid topography upscaled from 3 arc s HydroSHEDS and SRTM	Gumbel distribution for 1980-2013	N/A	30 arc s ~900 m
Fathom	Regional FFA from global gauge data	N/A	Inertia 1 or 3 arc s	MERIT or 1 arc s mixed (e.g., NED)	From FFA	N/A	3 arc s ~90 m or 1 arc s ~30 m
CIMA-UNEP, GAR2015	Regional FFA from global gauge data + ECEarth bias corrected	Continuum model to improve FFA	Manning's at multiple points	Reconditioned HydroSHEDS and SRTM	From FFA, GEV fitting	Native at 3 arc s	3 arc s ~90 m

Adapted from Trigg et al. (2016)

The remaining flood models all operate in two dimensions, solving some simplified form of the shallow-water equations, as the computational cost of running the full solvers would make modelling unfeasible with such large domains. The full one-dimensional shallow water equations for momentum and continuity are given in equations (2.2) and (2.3), respectively, below:

$$\frac{\partial Q_x}{\partial t} + \frac{\partial}{\partial x}\left(\frac{Q_x{}^2}{A}\right) + gA\frac{\partial(h+z)}{\partial x} + \frac{gn^2Q_x{}^2}{R^{4/3}A} = 0 \qquad (2.2)$$

$$\frac{\partial A}{\partial x} + \frac{\partial Q_x}{\partial x} = 0 \qquad (2.3)$$

where Q is the flow in the x direction [$L^3\,T^{-1}$], A is the cross-sectional flow area [L^2], h is the water depth [L], z is the bed elevation [L], g is the acceleration due to gravity [$L\,T^{-2}$], n is Manning's roughness coefficient [$T\,L^{1/3}$], R is the hydraulic radius [L], t is time [T], and x is the distance in the x Cartesian direction [L].

Channel flow is calculated in the two-dimensional models using kinematic wave, diffusive wave, or inertial simplifications of the shallow-water equations. The kinematic wave simplification, used in the GLOFRIS model, assumes that local and convective acceleration (the first and second terms of equation 2.2) are negligible and simplifies the water slope term (term three in equation 2) to consider only bed gradient (z) and not water depth (h). It retains the friction-slope term (term four in equation 2.2). The diffusive wave simplification differs from the kinematic wave simplification in that it includes water depth (h) in the water-slope term. This allows backwater effects to be simulated in models that apply the diffusive wave simplification. The inertial simplification to the shallow-water equations is an adapted form of the diffusive wave simplification that incorporates local acceleration (term one in equation 2.2) into the formulation (Bates et al., 2010). The remaining models have either updated their models to (U-Tokyo and ECMWF), or have always employed (Fathom and JRC), a form of the inertial simplifications for their hydraulic simulations.

Out of channel, or floodplain flow, in the GFMs is modelled in two dimensions; and while most solve some simplified form of the two-dimensional shallow-water equations, the GLOFRIS model represents out of bank floodplain flow using a simple water-level/volume relationship. Although floodplain flow in

the GLOFRIS model is technically modelled in two dimensions, the volume distribution approach does not represent conservation of momentum. This approach is often referred to as "pseudo-two-dimensional" because it omits any flow physics in two dimensions (Evans et al., 2007, Neelz and Pender, 2009). The remaining models solve floodplain flow using the two-dimensional shallow-water equations, which take the same general form as the one-dimensional equations but in two directions, and apply the same simplifications as outlined above for one dimension.

Some of the models are also able to incorporate features below the model grid resolution into the simulation. This subgrid representation can either explicitly include channels as in the Fathom and JRC GFMs, or incorporate subgrid scale topography through parameterization (Yamazaki et al., 2011), as in the ECMWF and U-Tokyo GFMs. The ability to model subgrid processes is important in a global flood modelling context, as it allows simulations to run at a coarse, computationally efficient, resolution while still capturing the relevant floodplain connectivity and inundation dynamics.

2.3.6 Other Relevant Models

Another field that is starting to impact the GFM scene is that of global hydrology models (Schellekens et al., 2017), which have the potential, if tuned to high flow regimes, to represent flood regimes.

One example of a global modelling framework that is similar to the models described so far is the Dominant River Tracing-Routing Integrated with VIC Environment (DRIVE) model (Wu et al., 2014). The DRIVE model applies the kinematic wave or diffusion wave equations both to dominant rivers at grid level and tributaries at subgrid level. The DRIVE model is the core component of the Global Flood Monitoring System (GFMS). The GFMS is a National Aeronautics and Space Administration (NASA) funded experimental system using real-time Tropical Rainfall Measuring Mission (TRMM) Multi-satellite Precipitation Analysis (TMPA) and Global Precipitation Measurement (GPM) Integrated Multi-satellitE Retrievals for GPM (IMERG) precipitation maps as input to the DRIVE model. The DRIVE model runs on a quasiglobal (50 °N–50 °S) grid for hydrological runoff and routing simulations. Flood detection and intensity estimates are based on 15 years of retrospective model runs with TMPA input, with flood thresholds derived for each grid location using surface water storage statistics. The GFMS flood forecast range

is 5 days, and the DRIVE model also includes a routine for determining forecast-based inundation extent at 1km.

The Model for Scale Adaptive River Transport (MOSART) is also an example of a global hydrology model that has the potential to model floods and has been used to study surface water dynamics of the Amazon basin (Luo et al., 2017). The MOSART was developed as a scalable framework for representing and studying riverine dynamics of water, energy, and biogeochemistry cycles across local, regional, and global scales from an integrated human-Earth system perspective (Li et al., 2013, Li et al., 2015). The MOSART receives runoff inputs from the land component of an Earth system model or a land surface model, routes the runoff across hillslope into tributary channels (within each spatial unit such as a latitude/longitude grid or subwatershed) then through river networks which connect all spatial units within a study domain. The kinematic wave method is used for the routing of runoff over hillslopes and in the channels with relatively steep topography, and a diffusion wave method is used for the channels with flat topography or those prone to inundation (Luo et al., 2017).

Finally, it is worth mentioning the risk modelling framework developed by Arnell and Gosling (2016). These authors assessed global river flood risk under climate change (flood-prone population and flood damage) using a global hydrological model with climate scenarios derived from 21 climate models, together with projections of future population. Flood hazard was calculated considering change in the flood frequency and magnitude.

2.4 Application of GFMs

Global flood models are multifaceted: they have applications in many different fields related to research, planning, insurance, commercial use and emergency support. Here we present a description of some of their main applications, which are also summarized in Table 2.3.

2.4.1 Flood Hazard Mapping

Many areas of the globe still lack reliable spatial information about the location and extent of flood prone areas; this absence has been one of the main drivers behind the development of GFMs. The main advantage of using GFMs to

characterize flood hazard is that resulting estimates are derived in a consistent way, using input datasets of the same accuracy and with the same modelling framework. This consistent approach provides a more realistic picture of exposure (Wing et al., 2018). Flood hazard evaluation is typically undertaken by deriving inundation maps for a range of return periods, although some GFMs calculate hazard from continuous climatological or meteorological information. These maps can be produced either for research (Pappenberger et al., 2012, Ward et al., 2013, Sampson et al., 2015, Dottori et al., 2016) or commercial purposes, and some models are used for both (Sampson et al., 2015).

Table 2.3 Different Possible Applications of Global Flood Models with Referenced Examples

Category	Model	References
Flood Hazard Mapping	ECMWF	Pappenberger et al. (2012)
	JRC	Dottori et al. (2016)
	GLOFRIS	Ward et al. (2013)
	Fathom (SSBN)	Sampson et al. (2015)
Flood risk analysis (climate change)	CIMA-UNEP	UNISDR (2015a)
	GLOFRIS	Ward et al. (2013); Winsemius et al. (2016)
	JRC	Alfieri et al. (2017)
	U-Tokyo	Yamazaki et al. (2011); Hirabayashi et al. (2013); Tanoue et al. (2016); Dottori et al. (2018)
	Fathom	Sampson et al. (2015)
	CAT models	
Flood forecasting	GFMS	Wu et al. (2014)
	GloFAS	Alfieri et al. (2013)

Adapted from Alfieri et al. (2018)

Global flood models are now also being used at a national scale, incorporating more accurate local data into their framework. Fathom have recently released a United States model that uses national U.S. Geological Survey (USGS) elevation data along with other national datasets to produce flood hazard output at 30 m resolution (Wing et al., 2017). They used the same approach in Belize, incorporating local data into their model to produce national flood hazard maps (http://www.charim.net/) (Ward et al., 2015, Trigg et al., 2017).

2.4.2 Flood Risk Analysis

A further step in the use of GFMs is using the flood hazard maps as an intermediate step to produce flood risk estimates at a global scale. Typically, risk is expressed considering expected annual economic losses and expected annual

number of people potentially affected (UNISDR, 2015a). These analyses can focus on current risk, how risk has changed historically, and how risk may change as a result of future climate and socioeconomic change. Risk estimates characterizing present risk conditions often do so at country level. The CIMA-UNEP model was used to predict average annual losses at national level for the GAR 2015 report (Rudari et al., 2015). Similarly, GLOFRIS is integrated into an online tool, AQUEDUCT (http://floods.wri.org/), which allows end-users to easily interact with flood hazard maps and assess impacts such as urban damage, affected GDP, and affected population at country scale.

Historical datasets can be incorporated into flood risk analysis to evaluate changes in vulnerability and risk over time. Databases such as the History Database of the Global Environment (HYDE) provide gridded time series of population and land use changes. Combining these time series with flood hazard maps reveal historical trends in flood risk exposure (Jongman et al., 2012, Tanoue et al., 2016).

Those models forced by climate data (as outlined in the section 2.3.2) benefit from the fact that future climate scenarios can be easily simulated within the model framework. Studies investigating future flood risk also incorporate socioeconomic and demographic changes into their analyses as these are seen as equally contributory to future risk. The JRC, GLOFRIS, and U-Tokyo models have all been integral to high impact research studies predicting future flood risk under various climatic, demographic, and socioeconomic projections (Hirabayashi et al., 2013, Winsemius et al., 2016, Alfieri et al., 2017, Dottori et al., 2018).

The flexible, semiautomatic framework of GFMs also lends them useful to flood management scenario modelling. The models can be run under different defence scenarios and coupled with exposure datasets to provide a cost-benefit analysis of various management schemes (Ward et al., 2017).

2.4.3 Flood Forecasting

Given the computational burden of deriving inundation maps, GFMs are currently not applied for real-time flood forecasting. The GFMS is a flood forecasting model that shares a similar framework to GFMs. However, instead of being forced by historical climate or gauge data, it is forced instead by real-time satellite-based precipitation data (Wu et al., 2014). The previously described global

flood hazard models can quasi-forecast flooding by producing and using static inundation maps as reference scenarios to evaluate potential flood-prone areas and flood impacts according to forecasts. The GFM modelling frameworks are already automated and built for speed, in the future we will likely see these frameworks used in forecasting over large scales. This potential use presents one the most promising GFM development areas in the near future.

2.4.4   Insurance Exposure

A key application for GFMs is in modelling insurance exposure. Some of the GFMs we have covered already, such those developed by Fathom, are being used to inform insurance companies about the exposure of their portfolio. The bulk of this insurance exposure analysis is undertaken within specialized insurance catastrophe model frameworks. The commercial nature of these models means that there is little published literature about their development and structure. The next section provides a summary of the current "public" state of knowledge for these commercial examples of GFMs.

2.5   Insurance Catastrophe Models

The insurance and reinsurance industry started considering natural catastrophe (CAT) models in the late 1980s at a time when modelling companies first appeared. The use of CAT models by property (re)insurers has grown since then. They are now commonly used for portfolio management (e.g., accumulation control, analysis of the key risk drivers) and risk transfer (e.g., structuring and pricing of risk transfer through reinsurance or alternative solutions). Property (re)insurers are also expected by regulators to use cat models in their risk management processes.

The CAT models are designed to quantify the financial impact of catastrophic scenarios for the risk carrier. Both the frequency and the severity of the scenario (also called "event") are estimated. One of the specificities of CAT models is that they adopt different financial perspectives for the loss computation: economic losses but also insured losses or reinsured losses, depending on the interest of the risk carrier. The structure of CAT models can be described in four main modules:

1. The hazard module: this is the core of cat models and it contains information specific to the peril.

2. The exposure module: all relevant information from the (re)insurance portfolio is captured. This includes the location of the properties; but also the occupancy, building type, and sums insured.

3. The vulnerability module: hazard intensities are translated into potential damages based on the local hazard, the physical characteristics of the properties at risk and the values insured by coverage (e.g., building, content or business-interruption). Vulnerability functions are one of the main sources of uncertainty in flood risk models (Metin et al., 2018) because of the large variabilities in damages. Vulnerability functions are therefore typically described with an uncertainty distribution around the mean damages.

4. The financial module: insured and reinsured losses are computed based on the (re)insurance terms and conditions. All the CAT model vendors have developed their proprietary CAT modelling platforms that include a financial module. Model users run the set of stochastic events on their portfolio of policies and obtain from the platform the list of losses for different financial perspectives and by stochastic event. In the past few years, a new initiative largely driven by the (re)insurance industry has developed an open source loss modelling platform: OASIS (https://oasislmf.org/) Loss Modelling Framework (LMF). The main objectives of the OASIS initiative are to improve risk assessment through more models by providing the modelling platform, more transparency, and innovation.

There are three main categories of companies developing CAT models: the modelling companies that license their products to insurers, reinsurers and reinsurance brokers; the reinsurance brokers that provide their CAT models as part of their service to their clients (insurance companies) or license them; and some large insurance and reinsurance companies that use their cat models internally.

Flood events in a CAT model stochastic event set are defined as flood footprints. The local hazard intensity of those footprints is generally the flood depth. Other indicators are usually not modelled. Three main components are necessary to build those stochastic footprints: flood hazard maps, stochastic precipitation and discharge scenarios, and flood defence information. The final footprints run in the

CAT models are a combination of these three components. The flood hazard maps are used to translate the precipitation and discharge scenarios into flood footprints by taking into account the local flood defence systems.

2.5.1 Flood Hazard Mapping

The objective with flood hazard mapping in the context of financial loss assessment is to have comprehensive and detailed flood hazard maps for different return periods, typically six return periods between 20 years and 1000 years. However, the challenges when mapping flood hazard are the resolution required and the spatial coverage. In fact, local topography conditions can significantly influence the damages sustained in the properties. Furthermore, it is estimated that around 30% of the National Flood Insurance Program (NFIP) claims in the United States are located outside of the 100-year flood zones (Wojtkiewicz et al., 2013). A standard flood mapping strategy has been adopted to overcome these two difficulties.

Detailed topography datasets are one of the main drivers for accurate flood mapping (Bhuyian and Kalyanapu, 2018). The nationally complete digital elevation data range in resolution from 5 m (e.g., in the United Kingdom) or 10 m (e.g., in the United States) to 90 m in other countries (e.g., in Asia). The resolution of the digital elevation data is, however, limited by the availability and cost of high-resolution topography data at very large scales, and by the run time cost of the hydraulic model. Developers of GFMs will often vary the digital elevation data used from country to country depending on the quality of data available at a national level.

The flows are propagated along the river network in order to obtain the extent and depth of the flooding by using hydraulic models solving the shallow-water equations. Different modelling solutions have been chosen: one-dimensional hydraulic models, two-dimensional hydraulic models, or a combination of both types of hydraulic model.

The flood frequency analysis approach is often applied to derive design discharges at all river locations for a set of return periods. Alternative techniques can also be used because of the global scale of some of the modelling. The rationale behind those alternative approaches is to make use of precipitation data as they are common and more comprehensive than discharge data in some parts of the world.

The analysis of historical insurance claims data from floods shows that a significant proportion of those claims come from outside of the large river floodplains. Consequently, both fluvial flooding and surface water flooding are modelled, and the fluvial flood maps cover the large and the small rivers draining a few square kilometres.

Some companies have developed global flood hazard map products based on the specifications and approaches described above. Those companies use approaches that they can apply anywhere, paralleling the GFMs described in the rest of the chapter.

2.5.2 Stochastic Precipitation and Discharge Scenarios

Realistic scenarios reproducing dependences across catchments are important to properly assess potential financial impacts for a (re)insurance company. These scenarios can be developed at the country or at the regional level and cover several countries.

The stochastic scenarios need to include both precipitation and river discharges in order for the CAT model to estimate claim amounts from both flood types. Precipitation modelling is the first component of the modelling chain for the stochastic scenarios in most of the models. In countries where tropical cyclones are present, precipitation is modelled as tropical cyclone induced and non-tropical cyclone induced. This requires a realistic catalogue of tropical cyclones tracks.

Temperature modelling is usually carried out along with precipitation to account for snow accumulation and snow melt in the runoff generation process for relevant regions. The precipitation and temperature simulations then drive rainfall-runoff models to compute river discharges at all river locations. The precipitation, temperature and hydrological modelling can be done on a continuous basis or as event based.

A key parameter for the evaluation of financial losses under reinsurance contracts is the definition of an event. It is often found in reinsurance contracts that a natural event has a physical definition, for instance that a flood event must come from a single weather system, but also has a maximum duration. This maximum duration is called the hours clause, and current practice in the United States is for this to be 168 h; clauses of 504 h are also common in Europe. However, those

clauses are not necessarily standard and can differ from one contract to another even for the same territory. This means that if the travel time of the flood wave along a river system is long enough, flooding can happen more than 168 h apart at two different locations. In that case, the flood claims would be considered as belonging to two different events. The hours clause can have an impact on the payment by the reinsurer to the insurer after an event depending on the details of the reinsurance contract. The hours clause is often taken into account in the definition of the events of the stochastic event set. Some models provide the flexibility to the cat model users to define their own relevant hours clause.

2.5.3 Flood Defences

Flood defence systems can have a significant impact on flooding. Developers of CAT models collect flood defence information from authorities and incorporate them into their models. However, this information is often incomplete and assumptions need to be made for places where no information exists or is not available. Flood defence data is another significant source of uncertainty in flood risk models (Metin et al., 2018).

2.6 GFM Credibility

2.6.1 The Importance of Model Credibility

Since the beginnings of the development and use of numerical models, there has always been an acknowledgment that models need to be applied carefully, lest their limitations lead users astray. As the famous quote from George Box states, "All models are wrong, but some are useful". This is no different for GFMs and it could be argued that it is even more pertinent, as in reality GFMs consist of a chain of models. Addressing aspects of model error and uncertainty has become a specific, and important, research field in the past few decades (Beven and Freer, 2001, Beven, 2006, Chatfield, 2006). Despite model uncertainty being a complex area of study in its own right, at its core has been the traditional process of model calibration and validation. Calibration is the tuning of model parameters to ensure model outputs match real-world observations as closely as is reasonably practicable. Validation is the testing of a calibrated model's outputs against observations to see how well they match non-calibration events. In essence, calibration and validation

allow us to test the models to see how useful they are, and they form an integral part of the scientific process (KlemeŠ, 1986).

Given that the ambitious aim of GFMs is to provide a quantification of flood hazard for all rivers through the application of a single consistent methodology, and that their outputs are being used by an increasing range of practitioners (Ward et al., 2015), ensuring they are fit for purpose is crucial. The very different scale and ambition of GFMs, as well as the difference of approach to traditional flood modelling, makes testing them a particularly challenging process, and therefore this is still a developing, but very important, research field.

As the improvements in data resolution and increasing computation abilities enable GFMs to move towards ever higher resolutions, there is a tendency for users' expectations to increase in line with this. This expectation is particularly prevalent where there is an existing lack of national-scale or reach-scale flood hazard information with which to compare. The expectation can lead to an unrealistic view that a GFM can replace engineering-grade hydraulic modelling methods and data and be applied to purposes for which they were never intended, for example to identify risks to individual properties.

After the initial excitement of being able to generate and use flood risk analysis at a global scale for the first time fades, users are beginning to demand more information about how good the models are in particular geographical locations or for particular purposes. Model developers are very aware of the importance of communicating the limitations of their models and are therefore also keen to gain constructive feedback from users in order to focus future efforts to improve the models. This user-developer dialogue has long been a regular topic at GFP annual meetings and led directly to the first multi-model intercomparison (Trigg et al., 2016) and collective validation exercise (Bernhofen et al., 2018) for GFMs.

2.6.2 Existing Model Testing

It is ultimately the model developer's responsibility to test their models to ensure they are fit for purpose, particularly where their results have been made openly accessible. There are plenty of studies showing that developers do take this responsibility seriously (Yamazaki et al., 2011, Yamazaki et al., 2012, Pappenberger

et al., 2012, Winsemius et al., 2013, Yamazaki et al., 2013, Yamazaki et al., 2014b, Wu et al., 2014, Rudari et al., 2015, Sampson et al., 2015, Dottori et al., 2016, Wing et al., 2017), although not all to the same extent, possibly due to resource limitations, data availability, and/or project funding cycle challenges.

Model outputs typically consist of flood extents and depths for multiple probabilities (or return periods). While methods of remote sensing of flooding have advanced significantly (Schumann and Neal, 2021), it is not possible to observe the full range of event probabilities for all rivers and therefore definitively validate all models for all locations, as these events will not necessarily have occurred in the limited time we have been observing the whole globe. Add to this the fact that the larger the river system scale, the less likely the same probability event will occur everywhere, ensuring a definitive calibration and validation for GFMs will remain elusive.

Due to the scale and complexity of GFMs and commensurate observational data challenges, GFMs do not necessarily have a full calibration of all components. Their hyper-distributed form, with multiple parameters and components ensure that model equifinality (Beven and Freer, 2001, Beven, 2006) is a serious challenge for any attempt at overall model calibration. However, developers often undertake a form of calibration and validation for subcomponents of the model, where observations are available. An example of this would be the testing of extreme flows for regionalized flow methods (Smith et al., 2015) or bias corrections for models that rely on precipitation inputs (Huffman et al., 2009). Where the GFM framework is sufficiently flexible to allow adjustment to locally available datasets, some GFMs have been applied at a national scale, such the Fathom model in Belize, where locally gauged rainfall and river flows were used to further regionalize the global method (Ward et al., 2015).

Hoch and Trigg (2019) provide a meta-study summary of GFM validations performed to date. They show that there have been a wide range in validation (also referred to as benchmarking) data sets used, maybe partly as a result of what data were available at the time of model development. Most GFMs are validated against some inundation extent in some basins, and only a few compare simulated discharge and water surface elevation with observations. The specific river systems used for

model validation differ between models as well as the number of studies documenting the model development over time (Figure 2.3) (Hoch and Trigg, 2019).

So we can see that GFMs have been validated for a range of case studies and model parameters. The fact that all models are validated "successfully" for non-identical settings may, from a model developers perspective, lead to the conclusion that the model performs well. However, it may also lead to the erroneous assumption that all models perform equally well (Hoch and Trigg, 2019). That this is not the case has been shown by grouped model intercomparison and validation studies (Trigg et al., 2016, Bernhofen et al., 2018).

2.6.3 Collective Testing

Trigg et al. (2016) performed the first intercomparison of GFMs and demonstrated that when six GFMs were compared with each other over the Continent of Africa, they only showed a 30-40% agreement in flood extent (Figure 2.4). So even at continental scales, there are significant differences in hazard magnitude and spatial pattern between models, notably in deltas, arid/semi-arid zones and wetlands (Trigg et al., 2016). Bernhofen et al. (2018) carried out the first group model validation against the same observed data for two major flood events in Africa. The flood events used were the floods of 2007 in Mozambique and of 2012 in Nigeria. These events were chosen as they were recent large-scale disasters with good observational validation data and of a scale where GFMs should perform reasonably well (Bernhofen et al., 2018). The critical success index of individual models ranged from 0.45 to 0.7 and the percentage of flood captured ranged from 52% to 97%. While this demonstrated a similar spread of model performance to that seen in Trigg et al. (2016), encouragingly it showed that the best individual models have an acceptable level of performance for these large rivers and demonstrated the importance of group validation.

Validation Type	JRC	Fathom	GLOFRIS	U-Tokyo	ECMWF	CIMA-UNEP
			Global Flood Model			
Discharge	✓[1]	✗	✗	✓[5,6,7,8]	✗	✗
Extent	✓[1]	✓[2,3]	✓[4]	✓[5,6]	✓[9]	✓[10]
Water Surface Level	✗	✗	✗	✓[6,8]	✗	✗
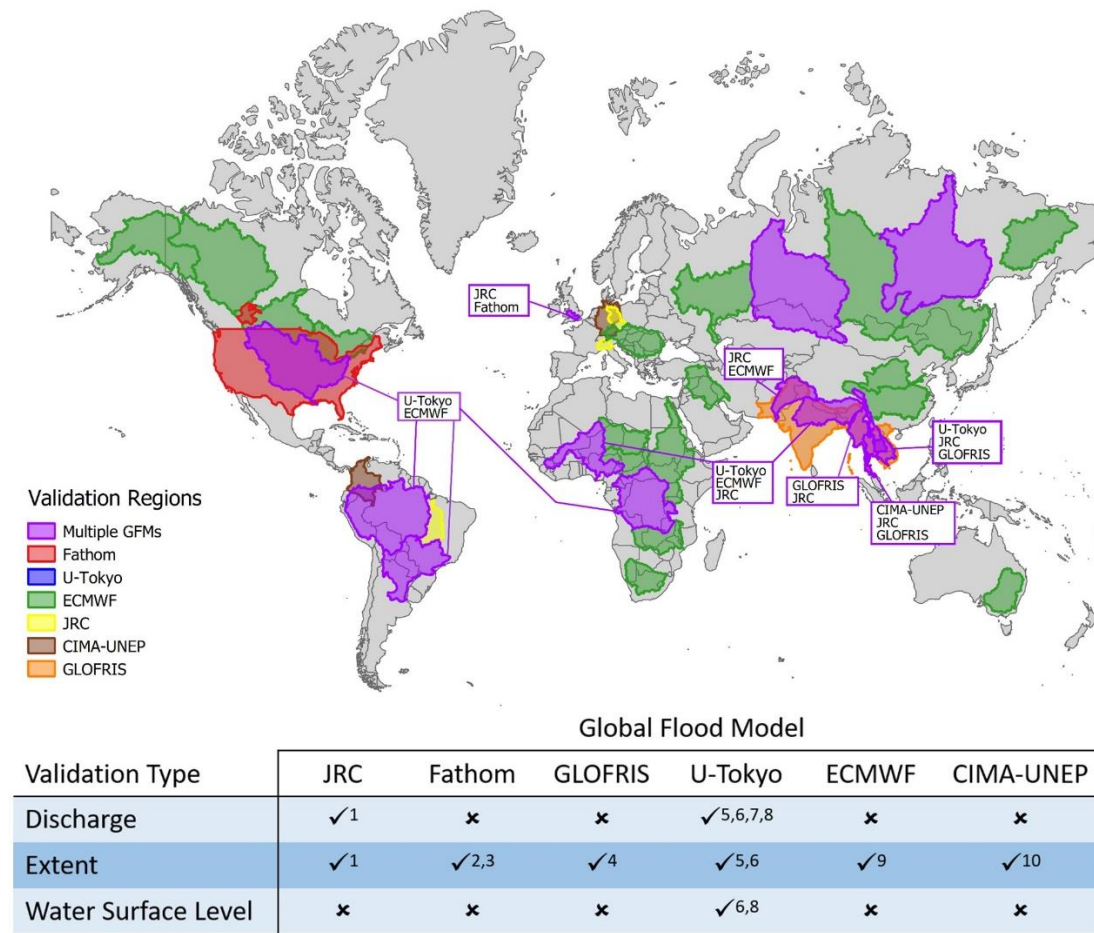
Figure 2.3 Map depicting the regions where each global flood model (GFM) validation model output against extents. Table summarizing the validation methods of each GFM

Regions depicted in purple are locations where multiple GFMs validated, all other colours refer to specific GFMs. (Note U-Tokyo has no unique validation locations). *Table adapted from Hoch and Trigg (2019)*

1, Dottori et al. (2016); 2, Sampson et al. (2015); 3, Wing et al. (2017); 4, Winsemius et al. (2013); 5, Yamazaki et al. (2012); 6, Yamazaki et al. (2013); 7, Yamazaki et al. (2011); 8, Yamazaki et al. (2014a); 9, Pappenberger et al. (2012); 10, Rudari et al. (2015)

It is encouraging to see this growing body of reports and publications recording the development and testing of GFMs, both individually and collectively, showing a growing maturity of the subject. However, there is a notable lack of record regarding one particularly important subgroup of GFMs: that of the global CAT model for insurance purposes. Proprietary modelling methods with associated intellectual property rights, as well as a unique application framework, make it difficult for these model groups to engage in this process in a fully open way. Nonetheless, given their important application worldwide they must not be excluded from the process and no doubt benefit from the open studies reported here.
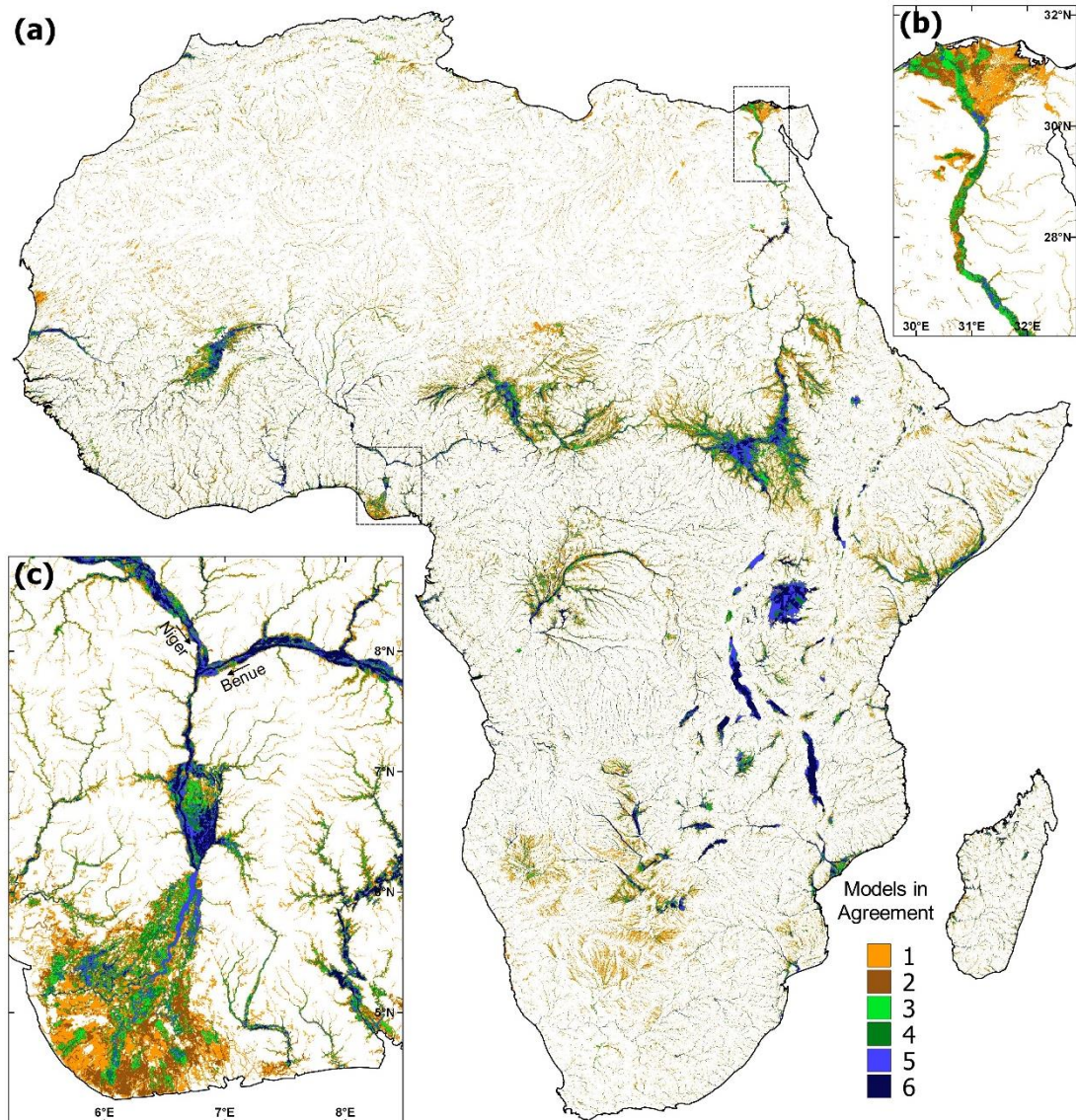
Figure 2.4 Global flood model agreement scores across Africa.

(a) Aggregated flood results for six models for a 1-in-100 year return period fluvial flood hazard for the African continent. Colour scale indicates how many models predict flooding. (b) Detail for the lower Nile. (c) Detail for the lower Niger, showing areas of strong agreement (narrow confined floodplains at the confluence of the Benue and Niger rivers) and areas of disagreement in the Niger coastal delta.

Source: Trigg et al. (2016)

Individual model validation procedures do not contribute to a better understanding why GFMs differ locally in their simulated inundation extent. The work of Trigg et al. (2016) and Bernhofen et al. (2018) demonstrates the value of a collective approach, but needs to be extended and undertaken routinely rather than on an ad hoc basis. What is really needed is more insight in the relative performance

of GFMs; that is, with identical boundary conditions and for the same set of validation data sets. It is only then that clearer conclusions can be drawn as to why results may differ between GFMs and where the greatest potential for improvement lies.

Up to now, GFMs have seen a rapid increase in number, their application, and acceptance (Ward et al., 2015). However, to further extend the dissemination of GFMs and their products, the testing of GFMs should become more standardized, as is already the case in other Earth science fields such as climate research. Model inter-comparison projects (MIPs) are a community-based way to compare models and their products with standardized objective functions and data sets, for instance, the Coupled Model Inter-comparison Project (CMIP) or the Inter-Sectoral Impact Model Inter-comparison Project (ISI-MIP) (Warszawski et al., 2014). Similar to these MIPs for general circulation models, establishing a MIP for GFMs should be a next development step. With such a Global Flood Model Inter-comparison Project (GFMIP) the uncertainties associated with model inputs, modelling cascade, parameterization, and so forth could be reduced and, consequently, the overall acceptance of models and their results would likely increase. That this is timely is shown by recent efforts benchmarking GFMs globally (Trigg et al., 2016, Bernhofen et al., 2018) or individual components such as DEMs (Hawker et al., 2018), numerical routing scheme (Hoch et al., 2017a, Hoch et al., 2017b, Zhao et al., 2017), or grid design and properties (Savage et al., 2016, Hoch et al., 2018). Besides, strong learning moments would be created which could additionally contribute to improvements of GFMs. Hoch and Trigg (2019) call for just such a project and outline how this may be achieved through a shared intercomparison framework, common forcing data, and validation data.

2.7 The Future of GFMs

Now that GFMs have most definitely "arrived" and are demonstrating their value, what is the next stage in their development? While many GFMs derive from scientific research projects to push the bounds of what is possible, these have ultimately translated into operational tools and this drives the interest in improving the models. Users also naturally begin to expect more of GFMs as their utility is demonstrated. Future steps will depend on where priorities lie for model

development groups and users and how these priorities align, with the GFP taking a central role in this dialogue. Flood is also not a standalone hazard and GFMs thus have a role as a subcomponent in integrated risk frameworks such as the upcoming UNISDR Global Risk Assessment Framework (GRAF) (Elsworth, 2018). Global flood models will certainly be around for the coming decades and development is likely to focus on three specific areas of improvement: (i) datasets, (ii) processes representation, and (iii) testing.

2.7.1   Improvements in Data Sets for Model Build and Testing

Advances in GFMs will be possible through future releases of higher resolution and more accurate data sets: whether through entirely new data sets or improvements to existing ones. Elevation data, in particular, strongly influences the performance of GFMs, as it is a representation of the terrain that controls flooding (Schumann, 2014). For example, the most anticipated near-future DEM release is the NASADEM Global Elevation Model (Crippen et al., 2016). Here, NASA will reprocess the entire SRTM dataset, which is used in all GFMs, and use new algorithms and ancillary data to produce a freely available global DEM at ~30 m resolution. Other DEMs, such as those produced by the Public-Private TanDEM-X mission, are able to resolve at up to ~12 m globally (Krieger et al., 2007). However, the commercial nature of the mission restricts the availability of the higher resolution data sets to paying customers and curtails their use in open GFMs. The trend is towards higher resolution DEM data sets and this will translate into better GFMs.

Derived from DEMs, hydrography datasets are a key component within GFMs, as they represent the river network. Global flood model hydrography is in urgent need of updating as all models still use the decade old HydroSHEDS dataset (Lehner et al., 2008). While HydroSHEDS has been particularly important in GFMs due to its structured data properties, it suffers from significant irregularities in flat terrains and urban areas, which affect the accurate location of river channels. Future hydrography datasets should incorporate accurate vector river data from observational sources, for example Sentinel 2 or OpenStreetMap, to compliment the traditional DEM-derived river delineation.

A future mission likely to have a major impact on GFMs is the NASA Surface Water and Ocean Topography (SWOT) mission (Durand et al., 2010). Scheduled for launch in 2021 and lasting three years, the SWOT mission will globally monitor Earth's surface water. Data related to the height, slope, and discharge of rivers will be invaluable from a hydraulic modelling testing perspective, while topographical ocean details should also improve the climate models that force many of the GFMs.

The measurement of river discharge using satellites is an emerging field of research that will benefit from the SWOT mission and could be incorporated into GFMs in the future. The Dartmouth Flood Observatory (DFO) already runs an experimental product called the River and Reservoir Watch that estimates river discharge using satellite microwave sensors (Brakenridge et al., 2016). Although still an experimental product, its relevance to GFMs is evident: remotely sensed river flows could become another method of model forcing as well as for validation.

Data sets used to measure flood exposure are equally as important as those ingested within the actual models. Traditionally, flood exposure has been measured using gridded datasets such as WorldPop, which represents population density within a 100 m x 100 m cell. Recently, a High Resolution Settlement Layer (HRSL) was released by Facebook in collaboration with the Center for International Earth Science Information Network (CIESIN) at Columbia University. The HRSL uses high-resolution (~0.5 m) commercial satellite data to identify individual settled cells at ~30 m resolution. Available in 22 countries, the HRSL can provide a more accurate picture of exposed population and should, in theory, result in better flood exposure estimates when used in tandem with GFMs. The limited global coverage of the HRSL warrants mentioning the Global Human Settlement Layer (GHSL), which relies on technology similar to that of the HRSL and has global coverage; though it is only available at 250 m resolution (Pesaresi et al., 2013).

Future GFM development will not only rely on new data, but also on existing data that has been adapted in a way that makes it more accessible and fit for purpose. An example of one of these "products" is the Global Flood Database being developed by Cloud to Street (https://www.cloudtostreet.ai/). Satellite images of historical flood events are vital for validating GFM output. The DFO has been the main source for this historical data. However, although the DFO maintains a

catalogue of around 5000 flood events dating back to 1985, only around 5% of the events have been mapped and the mapping methodology for these events has not always been consistent. The Global Flood Database uses the DFO's catalogue of events to map over 3,000 events since 2001 using a consistent algorithm and integrating it all within the Google Earth Engine (GEE) framework (Tellman et al., 2021). This consistent methodology as well as the accessibility provided by GEE opens the door to far more extensive future GFM validation studies.

2.7.2   Improvements in Processes Representation

In tandem with improved datasets for model build and testing, there is also a push to improve physical process representation within GFMs. Often this is through adding processes through subgrid representation, for example with improved river channel geometry (Neal et al., 2015). Further development in this area will rely on a combination of improved methods and bathymetry data, which are notoriously difficult to find. Another area which has seen improvement is in representation of river hydrography, such as the addition of bifurcating river channels (Yamazaki et al., 2014b), shown to be particularly important for flood mapping in delta regions (Trigg et al., 2016). Further developments in improving river hydrography are expected in the near future as this is an active research area for a number of GFP groups.

One particular current weakness of GFMs is in urban areas, where understanding flood exposure is particularly important. For example, the STRM DEM has not yet been corrected for urban areas to the same level as for vegetation (Baugh et al., 2013), although some model groups do a simple correction based on GDP (Sampson et al., 2015). Large urban areas also benefit from surface water drainage systems, which are not represented at all in GFMs. Urban areas can also benefit from flood defences and some models represent these through simple assumptions relating standards of defence linked with GDP (Sampson et al., 2015). However, there are notable efforts to build an open database of global defences that will be important in future GFMs (Scussolini et al., 2016).

As other global modelling efforts begin to overlap with GFMs, there are possibilities to explore compound flood events, which often occur together, such as coastal (Vousdoukas et al., 2016) and fluvial flood hazard. These additional hazard

components may either be included as an explicit model component such as with pluvial risk in Fathom's GFM (Sampson et al., 2015), or may be combined later in a general flood risk assessment framework.

2.7.3   Improved Model Testing

Thorough model testing and validation is key to guarantee model accuracy and as a basis for wider acceptance with end users. Currently, GFMs are validated and tested individually for different basins, with different data, and different objective functions. While this yields an estimate of how accurate a model performs in representing one or more specific flood events, it does not provide insight in its relative performance compared to other GFMs (Hoch and Trigg, 2019).

Hence, there is much potential in advancing GFMs by more thorough and streamlined validation procedures. Also needed for better testing is the integration of up-to-date observations of flood events. With remote sensing technology becoming more advanced and improved methods to account for uncertainties with such remotely sensed imagery, the overall accuracy of model testing will improve. This would not only require efforts from the GFM community, but also wider collaboration with adjacent fields such as data processing, cloud computing, and remote sensing, to provide the required cyberinfrastructure.

One possible approach might be a web-based platform created to facilitate a standardized validation of GFMs. By means of the platform, the external model properties (i.e., boundary conditions and forcing data) could be provided from a central location ensuring all models are applied under comparable settings. Model results could also be uploaded to the platform where validation with observed data (which could be updated regularly) and benchmarking with other model output would be performed in an automated manner.

Regardless of the way model testing will evolve, improvement is necessary. By subjecting GFMs to stricter guidelines, all involved can benefit: the wider community, through mutual learning moments, communication, and transparent scientific discourse; the developers, as they would learn where their model excels and where adjustments are required; and the end-users, as uncertainties surrounding flood maps would be reduced and quantified, leading to more actionable applications of GFMs.

References

ADAMS, T. E. 2016. Chapter 10 - Flood Forecasting in the United States NOAA/National Weather Service. *In:* ADAMS, T. E. & PAGANO, T. C. (eds.) *Flood Forecasting.* Boston: Academic Press.

ALFIERI, L., BISSELINK, B., DOTTORI, F., NAUMANN, G., DE ROO, A., SALAMON, P., WYSER, K. & FEYEN, L. 2017. Global projections of river flood risk in a warmer world. *Earths Future,* 5**,** 171-182.

ALFIERI, L., BUREK, P., DUTRA, E., KRZEMINSKI, B., MURARO, D., THIELEN, J. & PAPPENBERGER, F. 2013. GloFAS - global ensemble streamflow forecasting and flood early warning. *Hydrol. Earth Syst. Sci.,* 17**,** 1161-1175.

ALFIERI, L., COHEN, S., GALANTOWICZ, J., SCHUMANN, G. J. P., TRIGG, M. A., ZSOTER, E., PRUDHOMME, C., KRUCZKIEWICZ, A., COUGHLAN DE PEREZ, E., FLAMIG, Z., RUDARI, R., WU, H., ADLER, R. F., BRAKENRIDGE, R. G., KETTNER, A., WEERTS, A., MATGEN, P., ISLAM, S. A. K. M., DE GROEVE, T. & SALAMON, P. 2018. A global network for operational flood risk reduction. *Environmental Science & Policy,* 84**,** 149-158.

ARNELL, N. W. & GOSLING, S. N. 2016. The impacts of climate change on river flood risk at the global scale. *Climatic Change,* 134**,** 387-401.

BATES, P. D. & DE ROO, A. P. J. 2000. A simple raster-based model for flood inundation simulation. *Journal of Hydrology,* 236**,** 54-77.

BATES, P. D., HORRITT, M. S. & FEWTRELL, T. J. 2010. A simple inertial formulation of the shallow water equations for efficient two-dimensional flood inundation modelling. *Journal of Hydrology,* 387**,** 33-45.

BATES, P. D., NEAL, J., SAMPSON, C., SMITH, A. & TRIGG, M. 2018. Chapter 9 - Progress Toward Hyperresolution Models of Global Flood Hazard. *In:* MICHEL, G. (ed.) *Risk Modeling for Hazards and Disasters.* Elsevier.

BAUGH, C. A., BATES, P. D., SCHUMANN, G. & TRIGG, M. A. 2013. SRTM vegetation removal and hydrodynamic modeling accuracy. *Water Resources Research,* 49**,** 5276-5289.

BERNHOFEN, M. V., WHYMAN, C., TRIGG, M. A., SLEIGH, P. A., SMITH, A. M., SAMPSON, C. C., YAMAZAKI, D., WARD, P. J., RUDARI, R., PAPPENBERGER, F., DOTTORI, F., SALAMON, P. & WINSEMIUS, H. C. 2018. A first collective validation of global fluvial flood models for major floods in Nigeria and Mozambique. *Environmental Research Letters,* 13.

BEVEN, K. 2006. A manifesto for the equifinality thesis. *Journal of Hydrology,* 320**,** 18-36.

BEVEN, K. & FREER, J. 2001. Equifinality, data assimilation, and uncertainty estimation in mechanistic modelling of complex environmental systems using the GLUE methodology. *Journal of Hydrology,* 249**,** 11-29.

BHUYIAN, M. N. M. & KALYANAPU, A. 2018. Accounting digital elevation uncertainty for flood consequence assessment. *Journal of Flood Risk Management,* 11**,** S1051-S1062.

BRADBROOK, K., LANE, S., WALLER, S. & BATES, P. 2004. Two dimensional diffusion wave modelling of flood inundation using a simplified channel representation. *International Journal of River Basin Management,* 2**,** 211-223.

BRADBROOK, K., WALLER, S. & MORRIS, D. 2005. National floodplain mapping: datasets and methods–160,000 km in 12 months. *Natural hazards,* 36**,** 103-123.

BRAKENRIDGE, G. R., KETTNER, A. J., SYVITSKI, L., OVEREEM, I., DE GROEVE, T., COHEN, S. & NGHIEM, S. V. 2016. River and Reservoir Watch Version 3.5, Experimental Satellite-Based River Discharge and Reservoir Area Measurements: Technical Summary.

CHATFIELD, C. 2006. *Model Uncertainty.*

CHEN, S., LIU, H., YOU, Y., MULLENS, E., HU, J., YUAN, Y., HUANG, M., HE, L., LUO, Y., ZENG, X., TANG, G. & HONG, Y. 2014. Evaluation of high-resolution precipitation estimates from satellites during July 2012 Beijing flood event using dense rain gauge observations. *PLoS One,* 9**,** e89681.

CRIPPEN, R., BUCKLEY, S., AGRAM, P., BELZ, E., GURROLA, E., HENSLEY, S., KOBRICK, M., LAVALLE, M., MARTIN, J., NEUMANN, M., NGUYEN, Q., ROSEN, P., SHIMADA, J., SIMARD, M. & TUNG, W. 2016. NASADEM GLOBAL ELEVATION MODEL: METHODS AND PROGRESS. *In:* HALOUNOVA, L., SAFAR, V., JIANG, J., OLESOVSKA, H., DVORACEK, P., HOLLAND, D., SEREDOVICH, V. A., MULLER, J. P., RAO, E. P. R., VEENENDAAL, B., MU, L., ZLATANOVA, S., OBERST, J., YANG, C. P., BAN, Y., STYLIANIDIS, S., VOZENLEK, V., VONDRAKOVA, A., GARTNER, G., REMONDINO, F., DOYTSHER, Y., PERCIVALL, G., SCHREIER, G., DOWMAN, I., STREILEIN, A. & ERNST, J. (eds.) *XXIII ISPRS Congress, Commission IV.*

DE GROEVE, T., THIELEN-DEL POZO, J., BRAKENRIDGE, R., ADLER, R., ALFIERI, L., KULL, D., LINDSAY, F., IMPERIALI, O., PAPPENBERGER, F., RUDARI, R., SALAMON, P., VILLARS, N. & WYJAD, K. 2015. Joining Forces in a Global Flood Partnership. *Bulletin of the American Meteorological Society,* 96**,** ES97-ES100.

DEE, D., FASULLO, J., SHEA, D. & WALSH, J. 2016. *The Climate Data Guide: Atmospheric Reanalysis: Overview & Comparison Tables* [Online]. Available: https://climatedataguide.ucar.edu/climate-data/atmospheric-reanalysis-overview-comparison-tables [Accessed].

DOTTORI, F., SALAMON, P., BIANCHI, A., ALFIERI, L., HIRPA, F. A. & FEYEN, L. 2016. Development and evaluation of a framework for global flood hazard mapping. *Advances in Water Resources,* 94**,** 87-102.

DOTTORI, F., SZEWCZYK, W., CISCAR, J. C., ZHAO, F., ALFIERI, L., HIRABAYASHI, Y., BIANCHI, A., MONGELLI, I., FRIELER, K., BETTS, R. A. & FEYEN, L. 2018. Increased human and economic losses from river flooding with anthropogenic warming. *Nature Climate Change,* 8**,** 781-+.

DURAND, M., FU, L. L., LETTENMAIER, D. P., ALSDORF, D. E., RODRIGUEZ, E. & ESTEBAN-FERNANDEZ, D. 2010. The Surface Water and Ocean Topography Mission: Observing Terrestrial Surface Water and Oceanic Submesoscale Eddies. *Proceedings of the Ieee,* 98**,** 766-779.

ELSWORTH, J. 2018. *Putting science to work for resilience* [Online]. UNISDR. Available: https://www.unisdr.org/archive/58772 [Accessed November 11th 2018].

EVANS, E. P., WICKS, J. M., WHITLOW, C. D. & RAMSBOTTOM, D. M. 2007. The evolution of a river modelling system. *Proceedings of the Institution of Civil Engineers - Water Management,* 160**,** 3-13.

FAN, J. W., ROSENFELD, D., YANG, Y., ZHAO, C., LEUNG, L. R. & LI, Z. Q. 2015. Substantial contribution of anthropogenic air pollution to catastrophic floods in Southwest China. *Geophysical Research Letters,* 42**,** 6066-6075.

HAGOS, S. M., LEUNG, L. R., YOON, J.-H., LU, J. & GAO, Y. 2016. A projection of changes in landfalling atmospheric river frequency and extreme precipitation over western North America from the Large Ensemble CESM simulations. *Geophysical Research Letters,* 43**,** 1357-1363.

HALL, J. W. 2014. Editorial: steps towards global flood risk modelling. *Journal of Flood Risk Management,* 7**,** 193-194.

HALL, J. W., MEADOWCROFT, I. C., SAYERS, P. B. & BRAMLEY, M. E. 2003. Integrated Flood Risk Management in England and Wales. *Natural Hazards Review,* 4**,** 126-135.

HAWKER, L., ROUGIER, J., NEAL, J., BATES, P., ARCHER, L. & YAMAZAKI, D. 2018. Implications of Simulating Global Digital Elevation Models for Flood Inundation Studies. *Water Resources Research*.

HIRABAYASHI, Y., MAHENDRAN, R., KOIRALA, S., KONOSHIMA, L., YAMAZAKI, D., WATANABE, S., KIM, H. & KANAE, S. 2013. Global flood risk under climate change. *Nature Climate Change,* 3**,** 816-821.

HOCH, J. M., HAAG, A. V., VAN DAM, A., WINSEMIUS, H. C., VAN BEEK, L. P. H. & BIERKENS, M. F. P. 2017a. Assessing the impact of hydrodynamics on large-scale flood wave propagation – a case study for the Amazon Basin. *Hydrol. Earth Syst. Sci.,* 21**,** 117-132.

HOCH, J. M., NEAL, J. C., BAART, F., VAN BEEK, R., WINSEMIUS, H. C., BATES, P. D. & BIERKENS, M. F. P. 2017b. GLOFRIM v1.0-A globally applicable computational framework for integrated hydrological-hydrodynamic modelling. *Geoscientific Model Development,* 10**,** 3913-3929.

HOCH, J. M. & TRIGG, M. A. 2019. Advancing global flood hazard simulations by improving comparability, benchmarking, and integration of global flood models. *Environmental Research Letters,* 14**,** 034001.

HOCH, J. M., VAN BEEK, R., WINSEMIUS, H. C. & BIERKENS, M. F. P. 2018. Benchmarking flexible meshes and regular grids for large-scale fluvial inundation modelling. *Advances in Water Resources,* 121**,** 350-360.

HUFFMAN, G. J., ADLER, R. F., BOLVIN, D. T. & GU, G. 2009. Improving the global precipitation record: GPCP Version 2.1. *Geophysical Research Letters,* 36.

HUNTER, N. M., BATES, P. D., HORRITT, M. S. & WILSON, M. D. 2007. Simple spatially-distributed models for predicting flood inundation: A review. *Geomorphology,* 90**,** 208-225.

HUXLEY, C. & RYAN, P. 2016. Flood Modeling: How Accurate is Your Model? *Floodplain Management Association Newsletter*, November 2016.

JONGMAN, B., WARD, P. J. & AERTS, J. 2012. Global exposure to river and coastal flooding: Long term trends and changes. *Global Environmental Change-Human and Policy Dimensions,* 22**,** 823-835.

KLEMEŠ, V. 1986. Operational testing of hydrological simulation models. *Hydrological Sciences Journal,* 31**,** 13-24.

KOTTEK, M., GRIESER, J., BECK, C., RUDOLF, B. & RUBEL, F. 2006. World map of the Koppen-Geiger climate classification updated. *Meteorologische Zeitschrift,* 15**,** 259-263.

KRIEGER, G., MOREIRA, A., FIEDLER, H., HAJNSEK, I., WERNER, M., YOUNIS, M. & ZINK, M. 2007. TanDEM-X: A satellite formation for high-

resolution SAR interferometry. *Ieee Transactions on Geoscience and Remote Sensing,* 45**,** 3317-3341.

LEHNER, B., VERDIN, K. & JARVIS, A. 2008. New Global Hydrography Derived From Spaceborne Elevation Data. *Eos, Transactions American Geophysical Union,* 89**,** 93-94.

LI, H. Y., LEUNG, L. R., GETIRANA, A., HUANG, M. Y., WU, H., XU, Y. B., GUO, J. L. & VOISIN, N. 2015. Evaluating Global Streamflow Simulations by a Physically Based Routing Model Coupled with the Community Land Model. *Journal of Hydrometeorology,* 16**,** 948-971.

LI, H. Y., WIGMOSTA, M. S., WU, H., HUANG, M. Y., KE, Y. H., COLEMAN, A. M. & LEUNG, L. R. 2013. A Physically Based Runoff Routing Model for Land Surface and Earth System Models. *Journal of Hydrometeorology,* 14**,** 808-828.

LUO, X. Y., LI, H. Y., LEUNG, L. R., TESFA, T. K., GETIRANA, A., PAPA, F. & HESS, L. L. 2017. Modeling surface water dynamics in the Amazon Basin using MOSART-Inundation v1.0: impacts of geomorphological parameters and river flow representation. *Geoscientific Model Development,* 10**,** 1233-1259.

METIN, A. D., DUNG, N. V., SCHRÖTER, K., GUSE, B., APEL, H., KREIBICH, H., VOROGUSHYN, S. & MERZ, B. 2018. How do changes along the risk chain affect flood risk? *Nat. Hazards Earth Syst. Sci. Discuss.,* 2018**,** 1-29.

NEAL, J., SCHUMANN, G. & BATES, P. 2012. A subgrid channel model for simulating river hydraulics and floodplain inundation over large and data sparse areas. *Water Resources Research,* 48**,** 16.

NEAL, J. C., ODONI, N. A., TRIGG, M. A., FREER, J. E., GARCIA-PINTADO, J., MASON, D. C., WOOD, M. & BATES, P. D. 2015. Efficient incorporation of channel cross-section geometry uncertainty into regional and global scale flood inundation models. *Journal of Hydrology,* 529**,** 169-183.

NEELZ, S. & PENDER, G. 2009. Desktop review of 2D hydraulic modelling packages. Bristol, UK: Environment Agency.

PAPPENBERGER, F., DUTRA, E., WETTERHALL, F. & CLOKE, H. L. 2012. Deriving global flood hazard maps of fluvial floods through a physical model cascade. *Hydrology and Earth System Sciences,* 16**,** 4143-4156.

PESARESI, M., HUADONG, G., BLAES, X., EHRLICH, D., FERRI, S., GUEGUEN, L., HALKIA, M., KAUFFMANN, M., KEMPER, T., LU, L., MARIN-HERRERA, M. A., OUZOUNIS, G. K., SCAVAZZON, M., SOILLE, P., SYRRIS, V. & ZANCHETTA, L. 2013. A Global Human Settlement Layer From Optical HR/VHR RS Data: Concept and First Results. *IEEE Journal of Selected Topics in Applied Earth Observations and Remote Sensing,* 6**,** 2102-2131.

RODRIGUEZ, E., MORRIS, C. S. & BELZ, J. E. 2006. A global assessment of the SRTM performance. *Photogrammetric Engineering and Remote Sensing,* 72**,** 249-260.

RUDARI, R., SILVESTRO, F., CAMPO, L., REBORA, N., BONI, G. & HEROLD, C. 2015. IMPROVEMENT OF THE GLOBAL FLOOD MODEL FOR THE GAR 2015.

SAMPSON, C. C., SMITH, A. M., BATES, P. B., NEAL, J. C., ALFIERI, L. & FREER, J. E. 2015. A high-resolution global flood hazard model. *Water Resources Research,* 51**,** 7358-7381.

SAVAGE, J. T. S., BATES, P., FREER, J., NEAL, J. & ARONICA, G. 2016. When does spatial resolution become spurious in probabilistic flood inundation predictions? *Hydrological Processes,* 30**,** 2014-2032.

SCHELLEKENS, J., DUTRA, E., MARTINEZ-DE LA TORRE, A., BALSAMO, G., VAN DIJK, A., WEILAND, F. S., MINVIELLE, M., CALVET, J. C., DECHARME, B., EISNER, S., FINK, G., FLORKE, M., PESSENTEINER, S., VAN BEEK, R., POLCHER, J., BECK, H., ORTH, R., CALTON, B., BURKE, S., DORIGO, W. & WEEDON, G. P. 2017. A global water resources ensemble of hydrological models: the eartH2Observe Tier-1 dataset. *Earth System Science Data,* 9**,** 389-413.

SCHUMANN, G. J.-P., BATES, P. D., NEAL, J. C. & ANDREADIS, K. M. 2014. Technology: Fight Floods on a Global Scale. *Nature,* 507**,** 169-169.

SCHUMANN, G. J.-P. & NEAL, J. C. 2021. Integrating Earth Observation Data of Floods with Large-Scale Hydrodynamic Models. *Global Drought and Flood.*

SCHUMANN, G. J. P. 2014. Fight floods on a global scale. *Nature,* 507**,** 169.

SCUSSOLINI, P., AERTS, J., JONGMAN, B., BOUWER, L. M., WINSEMIUS, H. C., DE MOEL, H. & WARD, P. J. 2016. FLOPROS: an evolving global database of flood protection standards. *Natural Hazards and Earth System Sciences,* 16**,** 1049-1061.

SMITH, A., SAMPSON, C. & BATES, P. 2015. Regional flood frequency analysis at the global scale. *Water Resources Research,* 51**,** 539-553.

SOONG, D. T., PRATER, C. D., HALFAR, T. M. & WOBIG, L. A. 2012. Manning's roughness coefficient for Illinois streams. *Data Series.* Reston, VA.

TANOUE, M., HIRABAYASHI, Y. & IKEUCHI, H. 2016. Global-scale river flood vulnerability in the last 50 years. *Scientific Reports,* 6**,** 36021.

TELLMAN, B., SULLIVAN, J. A., KUHN, C., KETTNER, A. J., DOYLE, C. S., BRAKENRIDGE, G. R., ERICKSON, T. A. & SLAYBACK, D. A. 2021. Satellite imaging reveals increased proportion of population exposed to floods. *Nature,* 596**,** 80-86.

THIELEN, J., BARTHOLMES, J., RAMOS, M.-H. & DE ROO, A. 2008. The European Flood Alert System – Part 1: Concept and development. *Hydrology and Earth System Sciences Discussions,* 5**,** 257-287.

TRIGG, M. A., BIRCH, C. E., NEAL, J. C., BATES, P. D., SMITH, A., SAMPSON, C. C., YAMAZAKI, D., HIRABAYASHI, Y., PAPPENBERGER, F., DUTRA, E., WARD, P. J., WINSEMIUS, H. C., SALAMON, P., DOTTORI, F., RUDARI, R., KAPPES, M. S., SIMPSON, A. L., HADZILACOS, G. & FEWTRELL, T. J. 2016. The credibility challenge for global fluvial flood risk analysis. *Environmental Research Letters,* 11**,** 10.

TRIGG, M. A., MICHAELIDES, K., NEAL, J. C. & BATES, P. D. 2013. Surface water connectivity dynamics of a large scale extreme flood. *Journal of Hydrology,* 505**,** 138-149.

TRIGG, M. A., NEAL, J. & WARD, P. J. Special Session on Global Flood Models. 7th International Conference on Flood Management (ICFM7), 2017.

UNISDR. Hyogo Framework for Action 2005-2015: Building the Resilience of Naions and Communities to Disasters. The World Conference on Disaster Reduction, 2005 Kobe, Hyogo, Japan. United Nations (UN).

UNISDR 2009. Global Assessment Report on Disaster Risk Reduction.

UNISDR. 2011. Global Assessment Report (GAR) on Disaster Risk Reduction.

UNISDR. 2013. Global Assessment Report (GAR) on Disaster Risk Reduction. *From Shared Risk to Shared Value: The Business Case for Disaster Risk Reduction* [Online].

UNISDR 2015a. Making Development Sustainable: The Future of Disaster Risk Management. *Global Assessment Report on Disaster Risk Reduction.* Geneva, Switzerland: United Nations Office for Disaster Risk Reduction (UNISDR).

UNISDR 2015b. Sendai Framework for Disaster Risk Reduction 2015-2030. United Nations - Headquarters (UN).

VOUSDOUKAS, M. I., VOUKOUVALAS, E., MENTASCHI, L., DOTTORI, F., GIARDINO, A., BOUZIOTAS, D., BIANCHI, A., SALAMON, P. & FEYEN, L. 2016. Developments in large-scale coastal flood hazard mapping. *Natural Hazards and Earth System Sciences,* 16**,** 1841-1853.

WARD, P. J., JONGMAN, B., AERTS, J., BATES, P. D., BOTZEN, W. J. W., LOAIZA, A. D., HALLEGATTE, S., KIND, J. M., KWADIJK, J., SCUSSOLINI, P. & WINSEMIUS, H. C. 2017. A global framework for future costs and benefits of river-flood protection in urban areas. *Nature Climate Change,* 7**,** 642-+.

WARD, P. J., JONGMAN, B., SALAMON, P., SIMPSON, A., BATES, P., DE GROEVE, T., MUIS, S., DE PEREZ, E. C., RUDARI, R., TRIGG, M. A. & WINSEMIUS, H. C. 2015. Usefulness and limitations of global flood risk models. *Nature Climate Change,* 5**,** 712-715.

WARD, P. J., JONGMAN, B., WEILAND, F. S., BOUWMAN, A., VAN BEEK, R., BIERKENS, M. F. P., LIGTVOET, W. & WINSEMIUS, H. C. 2013. Assessing flood risk at the global scale: model setup, results, and sensitivity. *Environmental Research Letters,* 8**,** 10.

WARSZAWSKI, L., FRIELER, K., HUBER, V., PIONTEK, F., SERDECZNY, O. & SCHEWE, J. 2014. The Inter-Sectoral Impact Model Intercomparison Project (ISI–MIP): Project framework. *Proceedings of the National Academy of Sciences,* 111**,** 3228-3232.

WING, O. E. J., BATES, P. D., SAMPSON, C. C., SMITH, A. M., JOHNSON, K. A. & ERICKSON, T. A. 2017. Validation of a 30 m resolution flood hazard model of the conterminous United States. *Water Resources Research,* 53**,** 7968-7986.

WING, O. E. J., BATES, P. D., SMITH, A. M., SAMPSON, C. C., JOHNSON, K. A., FARGIONE, J. & MOREFIELD, P. 2018. Estimates of present and future flood risk in the conterminous United States. *Environmental Research Letters,* 13**,** 7.

WINSEMIUS, H. C., AERTS, J., VAN BEEK, L. P. H., BIERKENS, M. F. P., BOUWMAN, A., JONGMAN, B., KWADIJK, J. C. J., LIGTVOET, W., LUCAS, P. L., VAN VUUREN, D. P. & WARD, P. J. 2016. Global drivers of future river flood risk. *Nature Climate Change,* 6**,** 381-385.

WINSEMIUS, H. C., VAN BEEK, L. P. H., JONGMAN, B., WARD, P. J. & BOUWMAN, A. 2013. A framework for global river flood risk assessments. *Hydrology and Earth System Sciences,* 17**,** 1871-1892.

WOJTKIEWICZ, R., ROLLINS, J. & FOLEY, V. 2013. U.S. Flood Insurance - The NFIP and Beyond. Available: file:///C:/Users/cn13mvb/Downloads/U_S__Flood_Insurance%E2%80%94the_NFIP_and_Beyond.pdf.

WU, H., ADLER, R. F., TIAN, Y., GU, G. & HUFFMAN, G. J. 2017. Evaluation of Quantitative Precipitation Estimations through Hydrological Modeling in IFloodS River Basins. 18**,** 529-553.

WU, H., ADLER, R. F., TIAN, Y. D., HUFFMAN, G. J., LI, H. Y. & WANG, J. J. 2014. Real-time global flood estimation using satellite-based precipitation and a coupled land surface and routing model. *Water Resources Research,* 50**,** 2693-2717.

YAMAZAKI, D., BAUGH, C. A., BATES, P. D., KANAE, S., ALSDORF, D. E. & OKI, T. 2012. Adjustment of a spaceborne DEM for use in floodplain hydrodynamic modeling. *Journal of Hydrology,* 436**,** 81-91.

YAMAZAKI, D., DE ALMEIDA, G. A. M. & BATES, P. D. 2013. Improving computational efficiency in global river models by implementing the local inertial flow equation and a vector-based river network map. Water Resources Research.

YAMAZAKI, D., IKESHIMA, D., TAWATARI, R., YAMAGUCHI, T., O'LOUGHLIN, F., NEAL, J. C., SAMPSON, C. C., KANAE, S. & BATES, P. D. 2017. A high-accuracy map of global terrain elevations. *Geophysical Research Letters,* 44**,** 5844-5853.

YAMAZAKI, D., KANAE, S., KIM, H. & OKI, T. 2011. A physically based description of floodplain inundation dynamics in a global river routing model. *Water Resources Research,* 47**,** 21.

YAMAZAKI, D., O'LOUGHLIN, F., TRIGG, M. A., MILLER, Z. F., PAVELSKY, T. M. & BATES, P. D. 2014a. Development of the Global Width Database for Large Rivers. *Water Resources Research,* 50**,** 3467-3480.

YAMAZAKI, D., SATO, T., KANAE, S., HIRABAYASHI, Y. & BATES, P. D. 2014b. Regional flood dynamics in a bifurcating mega delta simulated in a global river model. *Geophysical Research Letters,* 41**,** 3127-3135.

ZHAO, F., VELDKAMP, T. I. E., FRIELER, K., SCHEWE, J., OSTBERG, S., WILLNER, S., SCHAUBERGER, B., GOSLING, S. N., SCHMIED, H. M., PORTMANN, F. T., LENG, G. Y., HUANG, M. Y., LIU, X. C., TANG, Q. H., HANASAKI, N., BIEMANS, H., GERTEN, D., SATOH, Y., POKHREL, Y., STACKE, T., CIAIS, P., CHANG, J. F., DUCHARNE, A., GUIMBERTEAU, M., WADA, Y., KIM, H. & YAMAZAKI, D. 2017. The critical role of the routing scheme in simulating peak river discharge in global hydrological models. *Environmental Research Letters,* 12**,** 14.

Chapter 3

A first collective validation of global fluvial flood models for major floods in Nigeria and Mozambique

3.1 Abstract

Global flood models (GFMs) are becoming increasingly important for disaster risk management internationally. However, these models have had little validation against observed flood events, making it difficult to compare model performance. In this paper, we introduce the first collective validation of multiple GFMs against the same events and we analyse how different model structures influence performance. We identify three hydraulically diverse regions in Africa with recent large scale flood events: Lokoja, Nigeria; Idah, Nigeria; and Chemba, Mozambique. We then evaluate the flood extent output provided by six GFMs against satellite observations of historical flood extents in these regions. The critical success index of individual models across the three regions ranges from 0.45 to 0.7 and the percentage of flood captured ranges from 52% to 97%. Site specific conditions influence performance as the models score better in the confined floodplain of Lokoja but score poorly in Idah's flat extensive floodplain. 2D hydrodynamic models are shown to perform favourably. The models forced by gauged flow data show a greater level of return period accuracy compared to those forced by climate reanalysis data. Using the results of our analysis, we create and validate a three-model ensemble to investigate the usefulness of ensemble modelling in a flood hazard context. We find the ensemble model performs similarly to the best individual and aggregated models. In the three study regions, we found no correlation between performance and the spatial resolution of the models. The best individual models show an acceptable level of performance for these large rivers.

3.1 Introduction

Flooding is the most frequent and the most damaging of natural disasters globally (Berz et al., 2001). From 1995-2015, floods affected 2.3 billion people, killing 157,000 (Wallemacq et al., 2015). Fluvial (river) flooding is the most

common type of flood event and with over half of the world's population living within 3 km of a freshwater body, it has truly global implications (Kummu et al., 2011). Flood impacts will continue to increase in severity, as the population exposed to fluvial flooding is expected to rise by 31% over the next 30 years. Certain vulnerable regions, such as Sub-Saharan Africa, are predicted to see an increase in exposed population by as much as 104% (Jongman et al., 2012). Given current CO_2 emission trends, global temperatures could rise by up to 4° C by 2100 (Sherwood et al., 2014). To put this into a fluvial flooding context, a temperature rise of 4° C could result in 70% of the global population experiencing a 500% increase in flood risk (Alfieri et al., 2017). Increased population exposure, coupled with the increased frequency and severity of flooding, means that reducing the risks associated with flooding is of vital importance to the United Nations Office for Disaster Risk Reduction (UNDRR) as outlined in their global assessment reports (UNISDR, 2015a). Reducing disaster vulnerability is a key target in goal 11 of the United Nation's Sustainable Development Goals (United Nations, 2015) and specific risk reduction targets, to be met by 2030, were introduced in the Sendai Framework for Disaster Risk Reduction (UNISDR, 2015b).

Flood models are an integral tool for managing and reducing the risks associated with flooding. In the past decade, increased computing power and precision of remote sensing data sets has led to the development of global flood models (GFMs) (Wood et al., 2011). These models are being developed by a number of different groups that include consultancies (Michel, 2018), research groups (Dottori et al., 2016), intergovernmental organizations (Rudari et al., 2015, Pappenberger et al., 2012), academia (Yamazaki et al., 2011), and academic affiliated companies (Sampson et al., 2015, Ward et al., 2013). GFMs are being actively used for disaster risk management: providing flood hazard maps in data-scarce countries where there is little local or national information about flood risk (Ward et al., 2015). They are also being used extensively in research: for evaluating the benefits of flood protection investments globally (Ward et al., 2017) and to determine changes in future flood risk due to climate change (Hirabayashi et al., 2013, Winsemius et al., 2016, Alfieri et al., 2017).

Despite their extensive applicability, each flood model has only had limited, internal, validation against either observed events, existing regional models, or reported fatalities and financial losses (Yamazaki et al., 2011, Pappenberger et al., 2012, Ward et al., 2013, Winsemius et al., 2013, Sampson et al., 2015, Rudari et al., 2015, Dottori et al., 2016, Ward et al., 2017). The Global Flood Partnership (GFP) (https://gfp.jrc.ec.europa.eu/), a cooperation framework between developers and users of global flood tools, made the comparison of GFMs a research priority at their annual meeting in 2014 (De Groeve et al., 2015). The resulting GFM Intercomparison Project (GFMIP) was the first study to compare the flood hazard output of six GFMs on the continent of Africa. Research from the GFMIP showed there was wide variation in the flood hazard output of the six GFMs (Trigg et al., 2016b). The GFMIP identified the need for collective validation of the GFMs against observed flood extents.

This study is a continuation to the GFMIP, using its outputs and original GFM model output data to validate against observed flood events and expand on the testing of collective model output. It is the first study to validate multiple GFMs under the same framework and against the same observed events, allowing model performance to be easily compared. This study should help identify which GFMs perform best and how different model structures influence performance. The results should also provide further insight into the reasons for model disagreement originally identified in the GFMIP (Hoch et al., 2017).

The collective validation presented in this paper expands the rigorous GFM comparison begun in the GFMIP. As the models are improved and are used more extensively for disaster risk reduction, the need to compare model performance becomes increasingly apparent. The results of a rigorous comparison provide both users and model developers with information pertinent to the potential applicability of GFMs.

In this study, we identify regions with recent, large scale flood events with good observational validation data. We then develop a validation framework under which we test the output of six GFMs and the aggregated output of the GFMIP. We aim to answer which models perform best and identify the most important model characteristics affecting GFM performance. We also investigate whether an ensemble of the best individual GFMs improves the predicted flood extent.

3.3 Data and Methodology

3.3.1 Models

The six GFMs compared in the GFMIP and in this study are the Catchment-Based Macro-scale Floodplain (CaMa-Flood) model (Yamazaki et al., 2011), the Centro Internazionale in Monitoraggio Ambientale and United Nations Environment Program (CIMA-UNEP) model (Rudari et al., 2015), the European Centre for Medium-Range Weather Forecasts (ECMWF) (Pappenberger et al., 2012) model, the Global Flood Risk with Image Scenarios (GLOFRIS) model (Winsemius et al., 2013, Ward et al., 2013), the Joint Research Centre (JRC) model (Dottori et al., 2016), and the SSBN model (now known as Fathom Global Ltd.) (Sampson et al., 2015). GFM output was provided for this study by each of the six developers in the form of flood extent maps. The models use different techniques to predict flood extent and depth for a given return period flow. These range in complexity from 1D hydraulic modelling (CIMA-UNEP) and simple 2D flood re-distribution methods (GLOFRIS) to more complex 2D (ECMWF and CaMa-Flood) and 2D hydrodynamic models (JRC and SSBN). GFM forcing can be split into cascade model type (CaMa-Flood, GLOFRIS, ECMWF, JRC) and gauged flow model type (SSBN, CIMA-UNEP) (Trigg et al., 2016b). Cascade models use climate reanalysis data over 40 years to determine the probability that a cell is flooded. Gauged flow models use a growth curve to determine extreme flow. This flow is then input into a hydraulic model that predicts the flood extent for a given return period flow. Model output resolutions at the equator vary between ~90 m (SSBN, CIMA-UNEP), ~540 m (CaMa-Flood, ECMWF), and ~900 m (GLOFRIS, JRC). All the GFMs use the Shuttle Radar Topography Mission (SRTM) Digital Elevation Model (DEM) as their input DEM. Further information regarding model setup and the differences in model forcing and computational engine can be found in Appendix A.2. The aggregated fluvial flood extent (Figure 3.1 (d)), an output of the GFMIP that shows the level of agreement in flood extent between all six models, was also validated in this study to assess the potential for using multiple model combinations for flood extent prediction (Trigg et al., 2016a, Trigg et al., 2016b).

3.3.2 Case Study

Three hydraulically varied regions in Africa were chosen for validation: two in Nigeria and one in Mozambique (Figure 3.1). Nigeria and Mozambique were identified in the GFMIP as countries with high exposure to flooding (Trigg et al., 2016b). An important factor in the choice of study regions was the size of the river. All the reaches contained rivers sufficiently large that they should be accurately represented in the GFMs regardless of the model spatial resolution. Validating model performance on rivers narrower than the resolution of the coarsest GFM would produce unfair results. In addition to this, delta regions were avoided for analysis to prevent issues associated with the demarcation of fluvial and coastal flooding, the latter of which is not currently represented in the GFMs, although recently CaMa-Flood was coupled with the results of a Global Tide and Surge Model (Muis et al., 2016) to simulate the influence of tide and surge on river levels (Ikeuchi et al., 2017).

The first region in Nigeria, referred to in this study as Lokoja, is at the confluence of the Niger and Benue rivers. It is a region with narrow, confined floodplains. The second region in Nigeria, located south of Lokoja between the cities of Idah and Onitsha, is referred to as Idah in this study. The Idah region is relatively flat and contains an extensive floodplain that has a number of smaller channels and streams. Downstream of the Idah floodplain is a tectonic constricted outlet. Located in central Mozambique, the final analysis region is referred to as Chemba and is situated in the lower Zambezi basin, upstream of the delta. The Zambezi River in the Chemba region can be classified as anabranching (more than one channel) with a very wide valley floor trough (Davies et al., 2000).

The flood events used as the benchmark validation datasets were the floods of 2007 in Mozambique and of 2012 in Nigeria. These events were chosen as they were recent large-scale disasters with good observational validation data. Torrential rain between December 2006 and February 2007, coupled with the landfall of Cyclone Favio in February 2007, caused flooding in Mozambique that affected more than 130,000 people (Rana, 2007). The 2012 flooding in Nigeria was even more devastating; affecting almost four million people (The Federal Government of Nigeria, 2013). The floods in Nigeria were caused by heavy rainfall between July and October 2012.
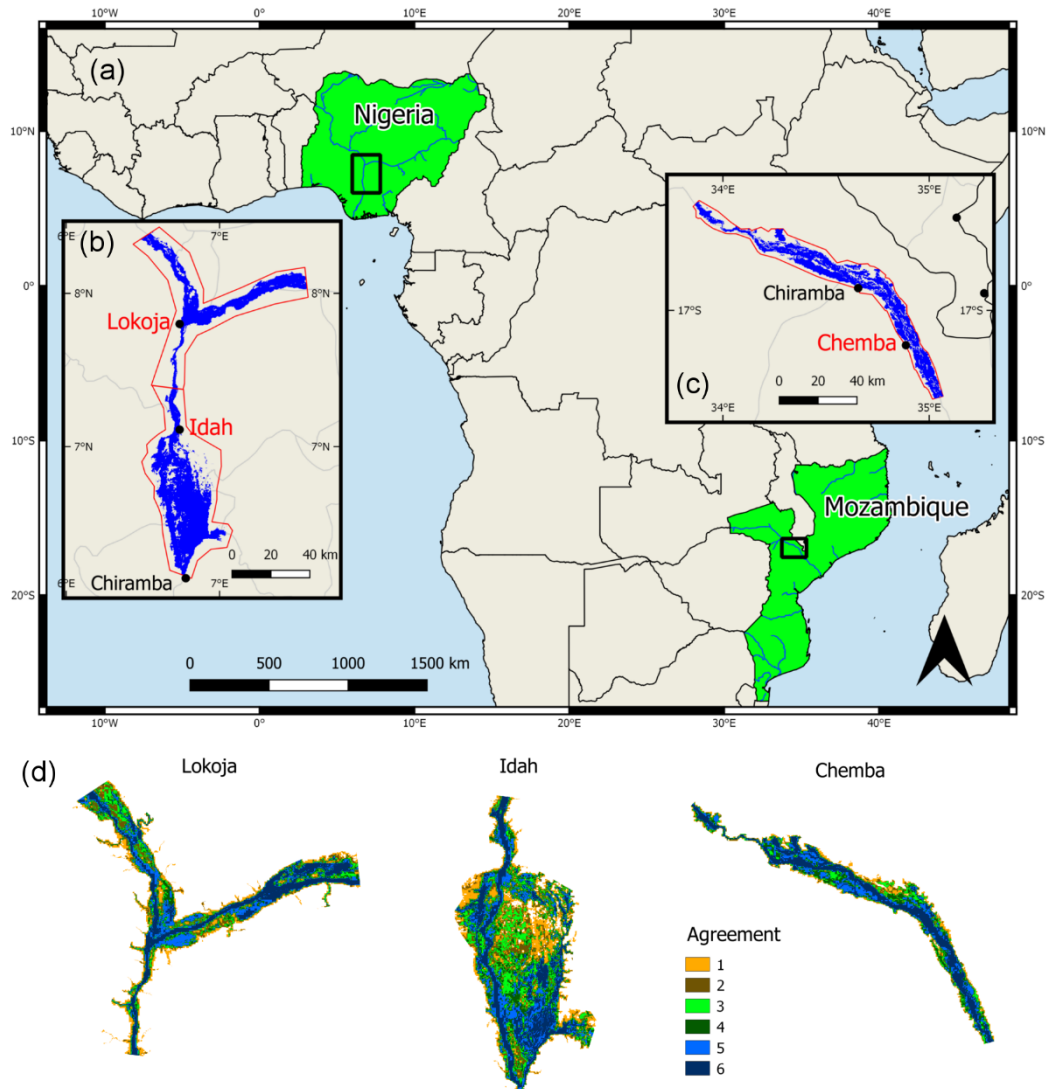
Figure 3.1 Global flood model validation study regions and data.

(a) Location of study regions in Africa. (b) Lokoja and Idah study regions with
MODIS imagery of 2012 flooding (Brakenridge, N.D.). (c) Chemba study
region with MODIS imagery of 2007 flooding (Brakenridge, N.D.). (d) Global
flood model aggregated fluvial flood extent output (25 year return period) for
each region where the cell colour represents the number of models that predict
it will flood in the corresponding cell (Trigg et al., 2016a).

3.3.3 Data

Flood imagery of both events was taken from the Dartmouth Flood
Observatory (DFO) archive (Brakenridge, N.D.). The DFO uses Moderate

Resolution Image Spectroradiometer (MODIS) imagery to capture flood events globally, and stores them online in an open-access archive. Vegetation bias was determined to have a negligible effect on the MODIS flood imagery in the three study regions (Nigro et al., 2014). The Chemba region is dominated by shrubbery and grasslands, and any woodland is sparse (CES, 2014) and although there are forests in both regions in Nigeria, these have not detrimentally affected the observed MODIS flood imagery. For the 2012 event in Nigeria, 45 days of imagery (September 15 – October 29) were downloaded from the DFO archive and merged into one flood extent. Using over six weeks of data ensured that the entire event (maximum extent) was captured. The flood extent for the 2007 event in Mozambique was taken from a flood map image on the DFO website. The process of georeferencing the image for analysis is outlined in Appendix A.1.

Both flood events had, very approximately, estimated return periods of around 50 years (BBC News, 2007, Reuters, 2012). The GFMIP compared the flood extent outputs of six return periods: 25, 100, 250, 500, and 1000 years. Not all of the individual GFMs had a 50 year return period output. Therefore, to ensure that the validation results best represent the skill of the models, two return periods were tested in the individual analysis: 25 and 100 years. For the aggregated analysis, only a 25 year return period was used. The return periods mentioned in this study, both reported and modelled, should be interpreted with an understanding of their associated uncertainties. Both events' 50 year flood return period was reported in news reports with no indication of how the value was calculated (BBC News, 2007, Reuters, 2012). Individual GFM return periods will not be consistent with one another due to the different approaches each takes to determine a given return period flood extent. Depending on the GFM model type, the climate model used, or the gauge data used, each GFM will have different estimated return period extents.

All the datasets used for validation in this study are open access, with the thought that the regions and events studied can be used for future GFM validation. The datasets are available from Research Data Leeds for academic research and education purposes (https://doi.org/10.5518/340).

3.3.4 Analysis

The analysis in this study was done in QGIS (v2.18). Individual GFM outputs were converted from extents with pixels indicating depth of flooding to

binary (wet/dry) water masks representing only flood extent. No specific flood depth threshold was used, only the wet/dry threshold of each individual GFM output. The modelled and observed extents were then overlapped in each of the study regions. The MODIS flood imagery used in this study was obtained in ~250 m resolution. In order to preserve the detail of the highest resolution models, and because comparison needs to be carried out at the same spatial resolution, the MODIS imagery and all GFM outputs that were not previously of ~90 m resolution were resampled using the nearest neighbour method to ~90 m resolution. Because the datasets are binary, false accuracy errors associated with resampling to a higher resolution are not introduced. This is because interpolation between binary pixels during resampling does not result in new values (as is the case when resampling a continuous value dataset). Resampling may have introduced geospatial overlap errors, however, these errors occur regardless of the resolution resampled to and they are unlikely to have affected the validation results. The degree of overlap between the modelled flood extents and the observed DFO extents was calculated in terms of the number of pixels that showed model agreement, overprediction, and underprediction. Maps visualizing this overlap were produced (Figure 3.3). The numerical data from these calculations was then used to calculate performance scores. The aggregated GFM output (Figure 3.1(d)) was extracted in six different model agreement levels. The extents ranged from largest to smallest: from any model agreement (≥1 models agree) to all model agreement (6 models agree). Each of the six model agreement levels was converted to a binary water mask and underwent the same analysis as the individual GFMs.

The performance metrics used in the analysis of the flood models are commonly used in flood model assessments and for forecast verification in the atmospheric sciences (Wilks, 2006). The scores were also used by a number of GFM providers for their own in-house validation (Wilks, 2006, Alfieri et al., 2014, Sampson et al., 2015, Dottori et al., 2016, Wing et al., 2017). The three performance scores were chosen as their results represent the most important aspects of model performance: model fit, model bias, and the proportion of total flood captured. The first, and most comprehensive, score is the $F^{<2>}$ score or the Critical Success Index (CSI) (Wilks, 2006):

$$CSI = \frac{F_m \cap F_o}{F_m \cup F_o} \qquad (3.1)$$

where $F_m \cap F_o$ is the intersection of the modelled and observed flood extent, or number of correct forecasts, and $F_m \cup F_o$ is the union of modelled and observed extent. The CSI ranges from 1 (best) to 0 (worst). The CSI has been shown to favourably bias larger floods (Stephens et al., 2014). However, because the floods compared in this study have a similar return period and because model performance is being compared within the same flood, CSI was deemed appropriate. The second score, the hit rate (HR) (Wilks, 2006), measures the proportion of the observed flood that was captured by the model:

$$HR = \frac{F_m \cap F_o}{F_o} \qquad (3.2)$$

where F_o is the total observed flood extent. The HR ranges from 1 (entire flood captured) to 0. The third score is the Bias score (Wilks, 2006), which measures whether a forecast is biased towards under-prediction or over-prediction:

$$Bias = \frac{(F_m \cap F_o) + F_m}{(F_m \cap F_o) + F_o} - 1 \qquad (3.3)$$

where F_m is the total modelled flood extent. A Bias score of 0 indicates an unbiased model. Positive and negative bias scores indicate bias towards overprediction and underprediction respectively.

Although there are a number of other forecast verification scores that could have been used, the three performance scores chosen for this study were deemed appropriate because they do not consider the dry area in the validation regions. Performance scores such as the Pierce skill score, false alarm rate, and F[1] that account for dry area in their formulae are not desirable in situations where correct 'no' forecasts dominate the analysis, as would be the case for the large validation regions in this study (Stephens et al., 2014).

The variation in flood hazard output between the GFMs identified in the GFMIP (Trigg et al., 2016b) raises the question of whether an ensemble model performs better than any individual flood model. Multiple model combinations have been used extensively in the atmospheric sciences in the form of model ensembles (Leith, 1974, Ehrendorfer, 1997, Gneiting and Raftery, 2005, Demeritt et al., 2007,

Siqueira et al., 2016, Schellekens et al., 2017). The ensemble model proposed in this study is a simple composite of the best performing individual models. In theory, this ensemble should reduce the uncertainty associated with using any individual model. Using a combination of the best performing individual models should reduce uncertainty as using multiple models with different modelling methods would negate any errors associated with a single modelling method. The best performing individual models to include in the ensemble are determined by the following Ensemble Score (ES):

$$ES = Average\ CSI - |0.2 * Average\ Bias| \qquad (3.4)$$

In order to have one common ensemble model output, the average of the 25 year return period performance scores across the regions was used to determine the ES. A Bias adjustment factor of 0.2 was added to the ES to penalise for any significant bias towards overprediction or underprediction. The value of 0.2 was chosen as it was large enough to penalize for bias, but small enough that the CSI remained the most important score in the ES. The bias adjustment factor reduces the likelihood that any GFM that is heavily biased towards over or under prediction is included in the ensemble model. Excessive overprediction is especially detrimental to the ensemble model as the resulting flood footprint would be dominated by the model that tends towards overprediction. The number of individual models to include in the ensemble model was decided based on the performance scores of the different model agreement levels in the aggregated model validation.

Once the best individual models to include in the ensemble model had been determined, the ensemble model was created in QGIS by combining the flood extents of the individual models into one, binary, ensemble flood extent. The ensemble extent was then validated using the same methodology as for the individual and aggregated models.

3.4 Results and Discussion

3.4.1 Individual Models

The performance scores are represented graphically in Figure 3.2 and the GFMs are arranged from left to right in order of resolution from coarsest to finest.

The results indicate that there is a significant variation between the GFMs ability in modelling the flood events in each region. The average CSI of the GFMs range from 0.45 (GLOFRIS) to 0.70 (JRC) for a 25 year flow. To put these scores into context, CSI scores from other flood validation literature, in different validation regions, range from 0.3-0.9 (Sampson et al., 2015, Dottori et al., 2016, Wing et al., 2017), with >0.7 considered good and < 0.5 poor.

Lokoja stands out as the region in which almost all of the models perform best. The higher CSI scores in Lokoja are likely a reflection of the region's narrow confined floodplain, and the relative simplicity of modelling the flood where extent is not sensitive to flood discharge magnitude. The increased complexity in flood modelling in flat extensive floodplains such as the one in Idah is reflected in the lower CSI scores for the region. The overlap of the observed and modelled extents (Figure 3.3) illustrates the varied success of the GFMs at modelling floodplain inundation in Idah.

GLOFRIS, which uses a simple flood volume distribution method for modelling inundation, had the lowest average CSI score across the three regions and showed very large regions of underprediction in Idah. The other 2D models, which have a more hydrodynamic flood modelling scheme scored better across the three regions. This could be due to a more accurate representation of the physics of floodplain flow or a better characterization of the river floodplain. This is evident in Idah, where CaMa-Flood, SSBN, and JRC performed better, possibly due to the greater connectivity modelled within the floodplain by their native sub-grid models. Although implementing similar schemes, the subtleties of their 2D model structures differ. This could explain why the JRC model had higher performance scores across the three regions. The benefits of CIMA-UNEP's simpler 1D cross-section approach to modelling floodplains proved successful at modelling much of the central floodplain missed by GFMs as the 1D section implicitly connects low areas along the cross-section. However, this can also lead to overprediction if the 1D approach models inundation in low lying floodplain areas with no connectivity to the channel.
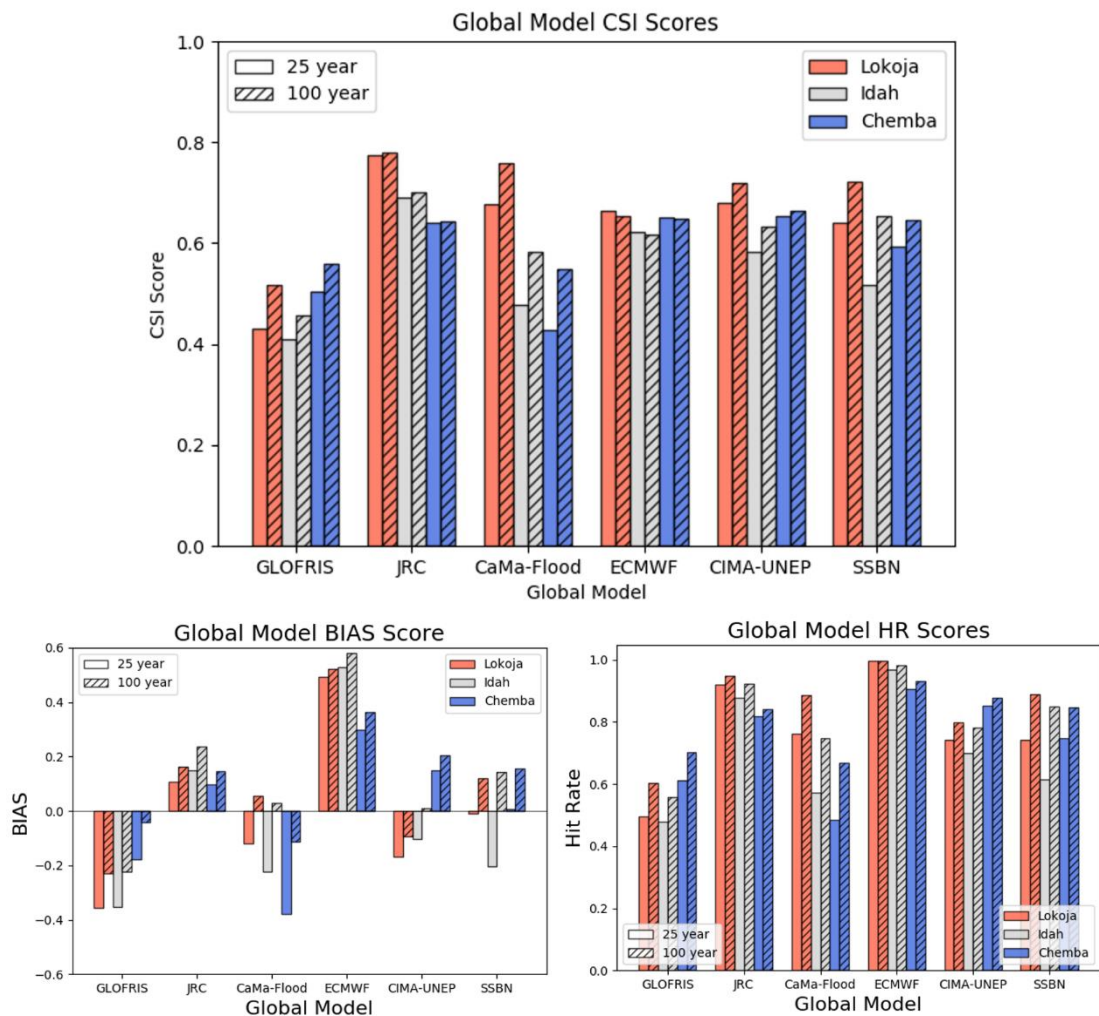
Figure 3.2 Individual global flood model (GFM) critical success index (CSI), Bias, and hit rate (HR) performance scores when compared against observed events in Lokoja, Idah, and Chemba.

Results shown for 25 and 100 year return period GFM output.

The GFM with one of the highest CSI scores in Chemba is ECMWF, whereas the GFM with the lowest CSI score in Chemba is CaMa-Flood. This highlights the importance of input flow in GFM performance: CaMa-Flood and ECMWF share the same core hydrodynamic model, but differ in their flow generation model. The performance of CaMa-Flood also significantly improves as the modelled return period is increased from 25 years to 100 years. This suggests that the input flow was the limiting factor affecting the performance scores of the 25 year output. Apart from ECMWF, increasing the return period from 25 years to 100 years generally increased the CSI scores of the GFMs. Increasing the GFM return period resulted in averaged CSI percentage increases of 14% (GLOFRIS), 0.1%

(JRC), 5% (CIMA-UNEP), 19% (CaMa-Flood), and 15% (SSBN). These findings show that in these three study areas, GLOFRIS, CaMa-Flood and SSBN are sensitive to input flow. However, the level of return period sensitivity could be exaggerated by the fact that these three models all showed higher bias towards underprediction at the 25 year return period than the rest of the models. Increasing the return period of an underpredicting and an unbiased flood model would likely result in a comparatively greater proportion of additional flooding being captured by the underpredicting model at the higher return period, thus leading to a larger increase in CSI. JRC continues to perform the best of all the models at either return period when averaged across the three regions. The variation in input flow is reflected in the HR and BIAS scores of the GFMs. Averaged across all three regions, ECMWF captures almost all the flooding, with an HR of 0.96 for a 25 year flood. However, it is the GFM that showed the largest bias in either direction: 0.44 for the 25 year return period and 0.49 for the 100 year return period. These results suggest that ECMWF is significantly overestimating input flow at both return periods.

The differences in model forcing (climate reanalysis data vs. gauged discharge data) is apparent in the bias scores of the GFMs. CIMA-UNEP and SSBN, both based on gauged discharge data, show an average bias towards underprediction at the 25 year return period and an average bias towards overprediction at the 100 year return period. This suggests that both gauge forced models are doing a good job at estimating the reported 50 year return period of the observed flooding. Three of the four models forced by climate reanalysis data show bias in only one direction at both return periods, suggesting that the climate forced models have greater difficulty predicting a representative return period. This could be due to the fact that the validation regions are in the tropics and reanalysis datasets have been found to poorly represent precipitation in the tropics (Beck et al., 2017). However, caution should be taken before drawing general conclusions because input flow is not the only parameter influencing floodplain extent (for instance, poorly represented floodplain connectivity might cause a systematic estimation bias on flood extent).
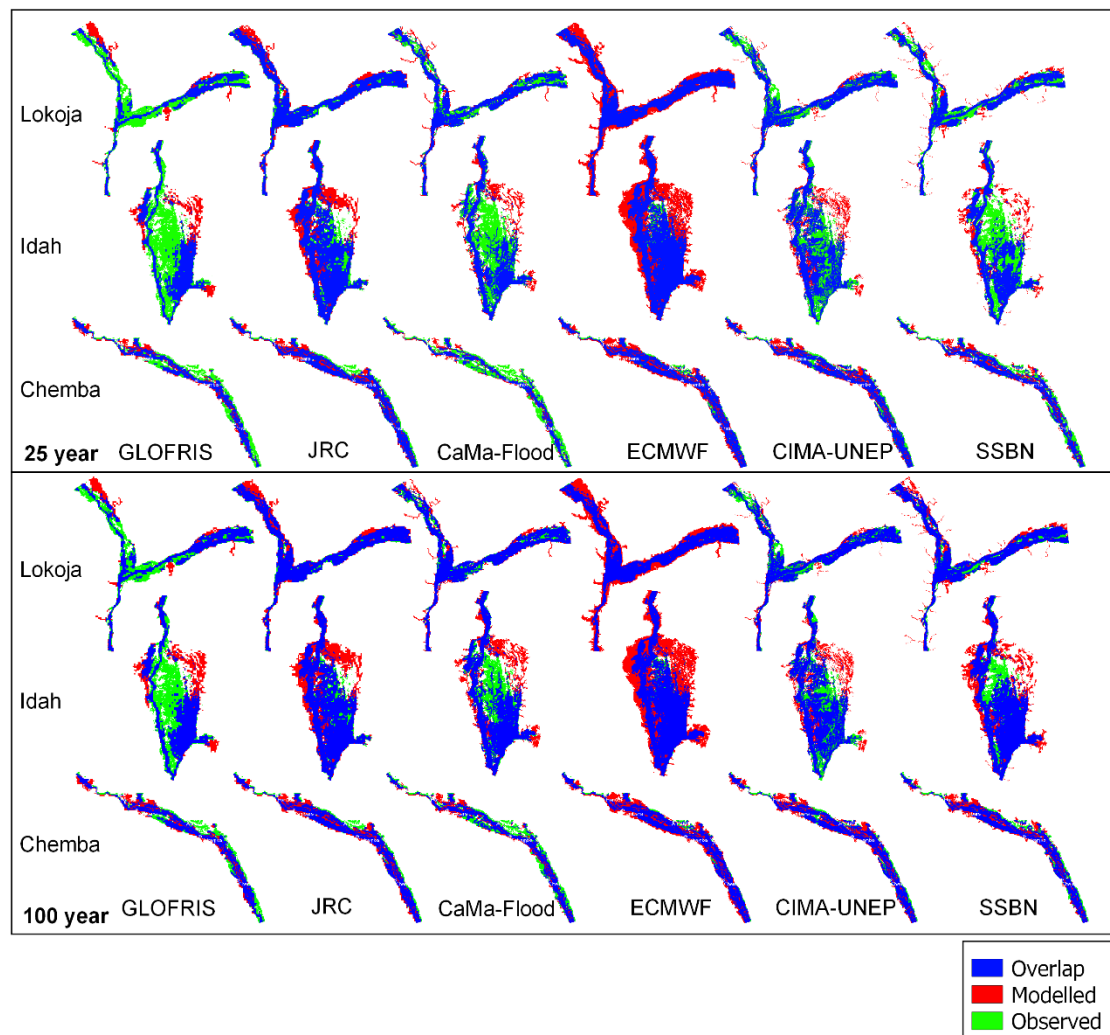
Figure 3.3 Overlap of individual global flood model extent for return period flows
of 25 and 100 years and MODIS observed flood extent for Lokoja, Idah, and
Chemba

The improved connectivity offered by higher spatial resolution GFMs is
evident in the Idah floodplain (Figure 3.3). CIMA-UNEP and SSBN, both with
outputs of 90 m resolution at the equator, are able to model some of the smaller
channels within the floodplain (either implicitly or explicitly). Despite the improved
connectivity representation, there is no discernible correlation between the
performance scores and GFM spatial resolution, indicating that the models still need
further improvements in capturing river/floodplain connectivity. At present, there is
currently no well-developed method to represent channel bifurcation in 1D fluvial
models. A better representation of bifurcation would improve the performance of
both 1D and 2D sub-grid models in areas of high bifurcation, such as floodplains
(Mateo et al., 2017).

The comparative usefulness of GFMs and regional flood models is a point of contention in flood modelling literature (WorldBank, 2014, Ward et al., 2015). Thomas (2017) developed a regional flood model for southern Nigeria and validated it against the 2012 floods. The model incorporated local bathymetric and hydrographic data. When compared with MODIS data of the flood event, the regional model's CSI scores were 0.73 and 0.53 for Lokoja and Idah, respectively. Comparison with the best GFM performance scores show that JRC and CaMa-Flood outperform the regional model in Lokoja with CSIs of 0.78 and 0.75, respectively. The case for the GFMs is even stronger in Idah as five GFMs outperform the regional model: JRC, SSBN, CaMa-Flood, ECMWF and CIMA-UNEP with CSI scores of 0.70, 0.65, 0.58, 0.62 and 0.58 respectively. Comparison of performance scores between the studies should be approached with some caution as the analysis areas in the Thomas (2017) study varied slightly compared with the ones used in this study. However, in the cases shown here, the performance of GFMs is comparable to, or in some cases better than, the performance of a locally calibrated regional model.

3.4.2 Aggregated Model

The performance scores of the different levels of model agreement for the 25 year return period aggregated model (Figure 3.4(a)) shows that the CSI peaks at ≥2 and ≥3 model agreement. These results correspond with the results of the individual model validation: two or three models consistently outperform the rest. A hit rate of 0.36 at 6 model agreement shows that all six models are correctly capturing at least 36% of the observed flood events. The bias trends steadily from overprediction to underprediction as the model agreement level increases. The least bias in either direction occurs at ≥3 and ≥4 model agreement, this is likely due to the fact that the opposite bias of the individual models shown in Figure 3.2 balanced one another out.
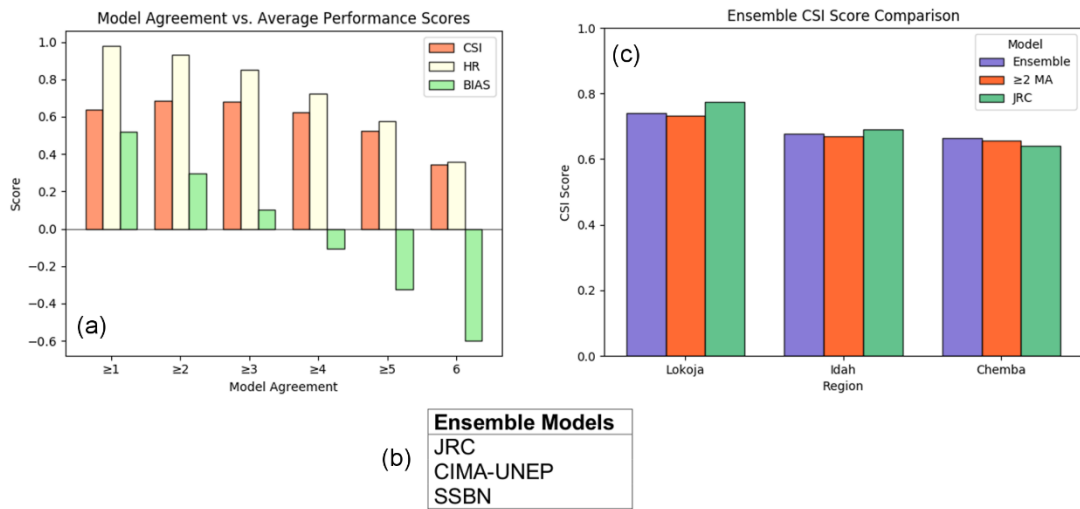
Figure 3.4 Aggregated and ensemble model performance scores.

(a) Critical success index (CSI), hit rate (HR), and Bias scores averaged across all three study regions for the six different levels of aggregated model agreement for a 25 year return period flood. (b) The three best performing individual global flood models (GFM) that are included in the ensemble model as determined by the ensemble score. (c) CSI scores for the ensemble model, the best performing individual GFM (JRC), and the best performing aggregated model agreement level ($\geq$ 2 Model Agreement) for a 25 year return period flood.

3.4.3 Ensemble Model

The aggregated model validation found that the $\geq$ 2 and $\geq$ 3 model agreement groups had the highest CSI scores. As a result, the number of models chosen to include in the ensemble model was three. The individual models included in the ensemble model, chosen using the ES, were JRC, CIMA-UNEP, and SSBN (Figure 3.4(b)). The validation performance scores of the ensemble model are compared (Figure 3.4(c)) with the best performing models from the individual and aggregate group: JRC and $\geq$ 2 model agreement. The results show that there is little difference between the CSI scores of the ensemble model, JRC, and $\geq$ 2 model agreement. Furthermore, the JRC GFM scores higher than the ensemble model in Lokoja and Idah. The aim of an ensemble model is to reduce the uncertainty associated with using a single model. For an ensemble model to perform better than individual models, the individual models that make up the ensemble model need to compensate for the uncertainty in the other models either through different input data or different modelling methods. Judging from the results of the analysis, it seems that the

combination of individual models did not improve the results as a whole. If anything, they added to the uncertainty in the form of increased overprediction, which resulted in the reduced CSI scores. Although the ensemble model did not outperform the best individual model, it did score comparably well. There are situations where this ensemble approach could be of use. For example, in regions where it is not possible to validate flood models to determine the best individual model, the use of a multiple model ensemble could reduce the uncertainty associated with using only one model, whilst not significantly reducing the flood extent prediction accuracy.

3.4.4   Observational Data

It is imprudent to discuss our validation findings without making some reference to the observational data used and the inherent uncertainty that is associated with flood observation mapping. This study used extents from the DFO archive, which is currently the most extensive global flood database. However, work is being done to develop a global database of historic flood events in Google Earth Engine (GEE) (Tellman et al., 2017, Tellman et al., 2018). The DFO flood extents used in this study and the equivalent extents from the new GEE global database (Tellman et al., 2018) were analysed to examine the agreement between the two data sources. The results of the analysis show that there is 12% disagreement in Lokoja (CSI 0.88), 11% disagreement in Idah (CSI 0.89), and 63% disagreement in Chemba (CSI 0.37) between the observed flood extents from the two data sources. The bias scores are also always in the direction of the DFO extents (Lokoja 0.02, Idah 0.01, and Chemba 1.32) indicating that the DFO extents are larger. Figures showing the observational agreement and disagreement are included in Appendix A.3. This observational disagreement between data sources highlights an underlying problem with flood mapping. Satellite imagery, both optical and radar, faces issues with observational bias. Optical imagery is affected by cloud cover and radar imagery is affected by vegetation. Data sources differ in the methods they use to reduce the effects of such observational bias. As a result, flood maps for the same event can differ if they are obtained from different sources. Neither source captures all of the flooding; each misses different parts. The task faced by the end user when confronted with the uncertainty associated with two disagreeing datasets is to decide which most closely represents the actual event. Even then, the chosen extent is used

under the assumption that it is entirely correct. If these observational uncertainties could be incorporated into flood maps, it would allow for a measure of confidence to be calculated relating to the accuracy of the observations and as a result, the accuracy of the validation findings.

3.5 Conclusions

This paper has outlined the first validation intercomparison between GFMs. Validation of the individual models against observed events in Nigeria and Mozambique showed that there is a significant variation in GFM performance, with average CSI scores ranging from 0.45 to 0.7. Site specific conditions played an important role in model performance. The GFMs scored well in Lokoja, where flood extents were restricted by a confined floodplain. Conversely, the models showed less skill in Idah, a flat extensive floodplain with complex morphology. The underlying hydraulic models showed varied success in modelling floodplain inundation. CIMA-UNEP's 1D approach was able to implicitly model greater connectivity within the Idah floodplain. Generally however, the connectivity provided by 2D models was evident in both the performance scores and the inundation maps. 2D hydrodynamic models showed significantly more skill at predicting inundation than 2D volume redistribution methods. Input flow was identified as a crucial factor in modeling a representative flood inundation extent and increasing the return period of the GFMs resulted in significant improvements for half of the GFMs. The GFMs forced by gauged data showed better return period accuracy than those forced by climate reanalysis data. This was attributed to the poor reanalysis representation of precipitation in the tropics. Spatial resolution, although showing some improvement in floodplain connectivity, did not obviously improve model performance.

Comparison of the GFMs with a regional flood model developed for Nigeria showed that some of the GFMs outperformed the regional model. Through validation, the three best models were identified and combined into a composite model. The validation of the composite model, showed that it performed similarly, but not better than the best individual GFM.

3.6 Outlook

This study has demonstrated the usefulness of a collective GFM validation procedure. The comparisons and conclusions that can be drawn from the common validation data cannot be made using the individual internal GFM validation data that has been available thus far. The focus area of this study has been limited to three regions in Africa and has looked only at flood extents. The GFMs tested in this study have a multitude of uses beyond only flood extent mapping. These include, but are not limited to: flood forecasting, estimating future impacts, and real time disaster response. Going further, a more extensive validation procedure that incorporates a comparison of flow velocity (Kreibich et al., 2009), inundated depth , and flood duration (Dang et al., 2011) would allow more conclusions to be drawn about both the performance and different uses of the models. The validation also needs to be extended across different climates and continents. To do this, a catalogue of appropriate validation regions needs to be developed and the observational data used for validation needs to be shared openly. Future studies should also incorporate more GFMs such as insurance catastrophe models to encourage the knowledge transfer between research and industry. Incorporating advanced methods of model output validation and applying them across more regions would allow for a truly global validation comparison study of GFMs.

3.7 Acknowledgements

References

ALFIERI, L., BISSELINK, B., DOTTORI, F., NAUMANN, G., DE ROO, A.,
    SALAMON, P., WYSER, K. & FEYEN, L. 2017. Global projections of river
    flood risk in a warmer world. *Earths Future,* 5**,** 171-182.
ALFIERI, L., SALAMON, P., BIANCHI, A., NEAL, J., BATES, P. & FEYEN, L.
    2014. Advances in pan-European flood hazard mapping. *Hydrological
    Processes,* 28**,** 4067-4077.
BBC NEWS. 2007. *Mozambique seeks urgent flood aid* [Online]. bbc.co.uk.
    Available: http://news.bbc.co.uk/go/pr/fr/-/2/hi/africa/6361957.stm
    [Accessed December 30th 2017].
BECK, H. E., VERGOPOLAN, N., PAN, M., LEVIZZANI, V., VAN DIJK, A.,
    WEEDON, G. P., BROCCA, L., PAPPENBERGER, F., HUFFMAN, G. J.
    & WOOD, E. F. 2017. Global-scale evaluation of 22 precipitation datasets
    using gauge observations and hydrological modeling. *Hydrology and Earth
    System Sciences,* 21**,** 6201-6217.
BERZ, G., KRON, W., LOSTER, T., RAUCH, E., SCHIMETSCHEK, J.,
    SCHMIEDER, J., SIEBERT, A., SMOLKA, A. & WIRTZ, A. 2001. World
    map of natural hazards - A global view of the distribution and intensity of
    significant exposures. *Natural Hazards,* 23**,** 443-465.
BRAKENRIDGE, G. R. N.D. Global Active Archive of Large Flood Events.
    Dartmouth Flood Observatory: University of Colorado.
CES 2014. Ecofarm Irrigation and Organic Sugarcane Project Mozambique,
    Botanical Specialist Study. Grahamstown.
DANG, N., BABEL, M. & LUONG, H. 2011. *Evaluation of food risk parameters in
    the Day River Flood Diversion Area, Red River Delta, Vietnam.*
DAVIES, B. R., BEILFUSS, R. D. & THOMS, M. C. 2000. Cahora Basin
    retrospective, 1974-1997: effects of flow regulation on the Lower Zambezi
    River. *Verh. Internat. Verein. Limnol.,* 27**,** 1-9.
DE GROEVE, T., THIELEN-DEL POZO, J., BRAKENRIDGE, R., ADLER, R.,
    ALFIERI, L., KULL, D., LINDSAY, F., IMPERIALI, O.,
    PAPPENBERGER, F., RUDARI, R., SALAMON, P., VILLARS, N. &
    WYJAD, K. 2015. Joining Forces in a Global Flood Partnership. *Bulletin of
    the American Meteorological Society,* 96**,** ES97-ES100.
DEMERITT, D., CLOKE, H., PAPPENBERGER, F., THIELEN, J.,
    BARTHOLMES, J. & RAMOS, M. 2007. Ensemble predictions and
    perceptions of risk, uncertainty, and error in flood forecasting.
    Environmental Hazards, 7**,** 115-127.
DOTTORI, F., SALAMON, P., BIANCHI, A., ALFIERI, L., HIRPA, F. A. &
    FEYEN, L. 2016. Development and evaluation of a framework for global
    flood hazard mapping. *Advances in Water Resources,* 94**,** 87-102.
EHRENDORFER, M. 1997. Predicting the uncertainty of numerical weather
    forecasts: a review. *Meteorologische Zeitschrift,* 6**,** 147-183.
GNEITING, T. & RAFTERY, A. E. 2005. Atmospheric science - Weather
    forecasting with ensemble methods. *Science,* 310**,** 248-249.
HIRABAYASHI, Y., MAHENDRAN, R., KOIRALA, S., KONOSHIMA, L.,
    YAMAZAKI, D., WATANABE, S., KIM, H. & KANAE, S. 2013. Global
    flood risk under climate change. *Nature Climate Change,* 3**,** 816-821.

HOCH, J. M., NEAL, J. C., BAART, F., VAN BEEK, R., WINSEMIUS, H. C., BATES, P. D. & BIERKENS, M. F. P. 2017. GLOFRIM v1.0-A globally applicable computational framework for integrated hydrological-hydrodynamic modelling. *Geoscientific Model Development,* 10**,** 3913-3929.

IKEUCHI, H., HIRABAYASHI, Y., YAMAZAKI, D., MUIS, S., WARD, P. J., WINSEMIUS, H. C., VERLAAN, M. & KANAE, S. 2017. Compound simulation of fluvial floods and storm surges in a global coupled river-coast flood model: Model development and its application to 2007 Cyclone Sidr in Bangladesh. *Journal of Advances in Modeling Earth Systems,* 9**,** 1847-1862.

JONGMAN, B., WARD, P. J. & AERTS, J. 2012. Global exposure to river and coastal flooding: Long term trends and changes. *Global Environmental Change-Human and Policy Dimensions,* 22**,** 823-835.

KREIBICH, H., PIROTH, K., SEIFERT, I., MAIWALD, H., KUNERT, U., SCHWARZ, J., MERZ, B. & THIEKEN, A. 2009. Is flow velocity a significant parameter in flood damage modelling?

KUMMU, M., DE MOEL, H., WARD, P. J. & VARIS, O. 2011. How Close Do We Live to Water? A Global Analysis of Population Distance to Freshwater Bodies. *Plos One,* 6**,** 13.

LEITH, C. E. 1974. THEORETICAL SKILL OF MONTE-CARLO FORECASTS. *Monthly Weather Review,* 102**,** 409-418.

MATEO, C. M. R., YAMAZAKI, D., KIM, H., CHAMPATHONG, A., VAZE, J. & OKI, T. 2017. Impacts of spatial resolution and representation of flow connectivity on large-scale simulation of floods. *Hydrology and Earth System Sciences,* 21**,** 5143-5163.

MICHEL, G. 2018. Introduction. *In:* MICHEL, G. (ed.) *Risk Modeling for Hazards and Disasters.* Elsevier.

MUIS, S., VERLAAN, M., WINSEMIUS, H. C., AERTS, J. & WARD, P. J. 2016. A global reanalysis of storm surges and extreme sea levels. *Nature Communications,* 7**,** 11.

NIGRO, J., SLAYBACK, D., POLICELLI, F. & BRAKENRIDGE, G. R. 2014. NASA/DFO MODIS Near Real-Time (NRT) Global Flood Mapping Product Evaluation of Flood and Permanent Water Detection.

PAPPENBERGER, F., DUTRA, E., WETTERHALL, F. & CLOKE, H. L. 2012. Deriving global flood hazard maps of fluvial floods through a physical model cascade. *Hydrology and Earth System Sciences,* 16**,** 4143-4156.

RANA, R. 2007. A Review of the Mozambique Floods Response Shelter Working Group. International Federation of Red Cross and Red Crescent Societies.

REUTERS. 2012. *Nigeria floods kill 363 people, displace 2.1 mln - agency* [Online]. reuters.com. Available: https://in.reuters.com/article/nigeria-floods/nigeria-floods-kill-363-people-displace-2-1-mln-agency-idINDEE8A40EH20121105 [Accessed December 30th 2017].

RUDARI, R., SILVESTRO, F., CAMPO, L., REBORA, N., BONI, G. & HEROLD, C. 2015. IMPROVEMENT OF THE GLOBAL FLOOD MODEL FOR THE GAR 2015.

SAMPSON, C. C., SMITH, A. M., BATES, P. B., NEAL, J. C., ALFIERI, L. & FREER, J. E. 2015. A high-resolution global flood hazard model. *Water Resources Research,* 51**,** 7358-7381.

SCHELLEKENS, J., DUTRA, E., MARTINEZ-DE LA TORRE, A., BALSAMO, G., VAN DIJK, A., WEILAND, F. S., MINVIELLE, M., CALVET, J. C., DECHARME, B., EISNER, S., FINK, G., FLORKE, M., PESSENTEINER,

S., VAN BEEK, R., POLCHER, J., BECK, H., ORTH, R., CALTON, B.,
     BURKE, S., DORIGO, W. & WEEDON, G. P. 2017. A global water
     resources ensemble of hydrological models: the eartH2Observe Tier-1
     dataset. *Earth System Science Data,* 9**,** 389-413.
SHERWOOD, S. C., BONY, S. & DUFRESNE, J. L. 2014. Spread in model climate
     sensitivity traced to atmospheric convective mixing. *Nature,* 505**,** 37-+.
SIQUEIRA, V. A., COLLISCHONN, W., FAN, F. M. & CHOU, S. C. 2016.
     Ensemble flood forecasting based on operational forecasts of the regional Eta
     EPS in the Taquari-Antas basin. *Rbrh-Revista Brasileira De Recursos
     Hidricos,* 21**,** 16.
STEPHENS, E., SCHUMANN, G. & BATES, P. 2014. Problems with binary
     pattern measures for flood model evaluation. *Hydrological Processes,* 28**,**
     4928-4937.
TELLMAN, B., SULLIVAN, J., DOYLE, C., KETTNER, A., BRAKENRIDGE, G.
     R., ERICKSON, T. & SLAYBACK, D. A Global Geospatial Database of
     5000+ Historic Flood Event Extents. American Geophysical Union, 2017
     New Orleans.
TELLMAN, B., SULLIVAN, J. A., KUHN, C., KETTNER, A. J., DOYLE, C. S.,
     BRAKENRIDGE, G. R., ERIKSEN, T. & SLAYBACK, D. 2018. A Global
     Inventory of Flood Events and Exposure Trends. *Manuscript in preperation.*
THE FEDERAL GOVERNMENT OF NIGERIA 2013. Nigeria: Post-Disaster
     Needs Assessment 2012 Floods.
THOMAS, E.-W. I. 2017. *Application of Open-access and 3rd Party Geospatial
     Technology for Integrated Flood Risk Management in Data Sparse Regions
     of Developing Countries.* Doctor of Philosophy, Lancaster University.
TRIGG, M. A., BIRCH, C. E., NEAL, J., BATES, P., SMITH, A., SAMPSON, C.,
     YAMAZAKI, D., HIRABAYASHI, Y., PAPPENBERGER, F., DUTRA, E.,
     WARD, P. J., WINSEMIUS, H. C., SALAMON, P., DOTTORI, F.,
     RUDARI, R., KAPPES, M. S., SIMPSON, A., HADZILACOS, G. &
     FEWTRELL, T. 2016a. Aggregated fluvial flood hazard output for six
     Global Flood Models for the African Continent. Research Data Leeds
     Repository.
TRIGG, M. A., BIRCH, C. E., NEAL, J. C., BATES, P. D., SMITH, A.,
     SAMPSON, C. C., YAMAZAKI, D., HIRABAYASHI, Y.,
     PAPPENBERGER, F., DUTRA, E., WARD, P. J., WINSEMIUS, H. C.,
     SALAMON, P., DOTTORI, F., RUDARI, R., KAPPES, M. S., SIMPSON,
     A. L., HADZILACOS, G. & FEWTRELL, T. J. 2016b. The credibility
     challenge for global fluvial flood risk analysis. *Environmental Research
     Letters,* 11**,** 10.
UNISDR 2015a. Making Development Sustainable: The Future of Disaster Risk
     Management. *Global Assessment Report on Disaster Risk Reduction.*
     Geneva, Switzerland: United Nations Office for Disaster Risk Reduction
     (UNISDR).
UNISDR 2015b. Sendai Framework for Disaster Risk Reduction 2015-2030.
UNITED NATIONS 2015. Transforming our World: The 2030 Agenda for
     Sustainable Development.
WALLEMACQ, P., GUHA-SAPIR, D., MCCLEAN, D., CRED & UNISDR 2015.
     The Human Cost of Natural Disasters - A global perspective.

WARD, P. J., JONGMAN, B., AERTS, J., BATES, P. D., BOTZEN, W. J. W.,
    LOAIZA, A. D., HALLEGATTE, S., KIND, J. M., KWADIJK, J.,
    SCUSSOLINI, P. & WINSEMIUS, H. C. 2017. A global framework for
    future costs and benefits of river-flood protection in urban areas. *Nature
    Climate Change,* 7**,** 642-+.
WARD, P. J., JONGMAN, B., SALAMON, P., SIMPSON, A., BATES, P., DE
    GROEVE, T., MUIS, S., DE PEREZ, E. C., RUDARI, R., TRIGG, M. A. &
    WINSEMIUS, H. C. 2015. Usefulness and limitations of global flood risk
    models. *Nature Climate Change,* 5**,** 712-715.
WARD, P. J., JONGMAN, B., WEILAND, F. S., BOUWMAN, A., VAN BEEK,
    R., BIERKENS, M. F. P., LIGTVOET, W. & WINSEMIUS, H. C. 2013.
    Assessing flood risk at the global scale: model setup, results, and sensitivity.
    Environmental Research Letters, 8**,** 10.
WILKS, D. 2006. *Statistical Methods in the Atmospheric Sciences,* United States of
    America, Elsevier.
WING, O. E. J., BATES, P. D., SAMPSON, C. C., SMITH, A. M., JOHNSON, K.
    A. & ERICKSON, T. A. 2017. Validation of a 30 m resolution flood hazard
    model of the conterminous United States. *Water Resources Research,* 53**,**
    7968-7986.
WINSEMIUS, H. C., AERTS, J., VAN BEEK, L. P. H., BIERKENS, M. F. P.,
    BOUWMAN, A., JONGMAN, B., KWADIJK, J. C. J., LIGTVOET, W.,
    LUCAS, P. L., VAN VUUREN, D. P. & WARD, P. J. 2016. Global drivers
    of future river flood risk. *Nature Climate Change,* 6**,** 381-385.
WINSEMIUS, H. C., VAN BEEK, L. P. H., JONGMAN, B., WARD, P. J. &
    BOUWMAN, A. 2013. A framework for global river flood risk assessments.
    Hydrology and Earth System Sciences, 17**,** 1871-1892.
WOOD, E. F., ROUNDY, J. K., TROY, T. J., VAN BEEK, L. P. H., BIERKENS,
    M. F. P., BLYTH, E., DE ROO, A., DOLL, P., EK, M., FAMIGLIETTI, J.,
    GOCHIS, D., VAN DE GIESEN, N., HOUSER, P., JAFFE, P. R., KOLLET,
    S., LEHNER, B., LETTENMAIER, D. P., PETERS-LIDARD, C.,
    SIVAPALAN, M., SHEFFIELD, J., WADE, A. & WHITEHEAD, P. 2011.
    Hyperresolution global land surface modeling: Meeting a grand challenge for
    monitoring Earth's terrestrial water. *Water Resources Research,* 47**,** 10.
WORLDBANK 2014. Understanding risk in an evolving world. Washington, D.C.:
    World Bank Group.
YAMAZAKI, D., KANAE, S., KIM, H. & OKI, T. 2011. A physically based
    description of floodplain inundation dynamics in a global river routing
    model. *Water Resources Research,* 47**,** 21.

Chapter 4

Global flood exposure from different sized rivers

4.1 Abstract

There is now a wealth of data to calculate global flood exposure. Available datasets differ in detail and representation of both global population distribution and global flood hazard. Previous studies of global flood risk have used datasets interchangeably without addressing the impacts using different datasets could have on exposure estimates. By calculating flood exposure to different sized rivers using a model-independent geomorphological river flood susceptibility map (RFSM), we show that limits placed on the size of river represented in global flood models result in global flood exposure estimates that differ by greater than a factor of 2. The choice of population dataset is found to be equally important and can have enormous impacts on national flood exposure estimates. Up-to-date, high-resolution population data are vital for accurately representing exposure to smaller rivers and will be key in improving the global flood risk picture. Our results inform the appropriate application of these datasets and where further development and research is needed.

4.2 Introduction

River floods are amongst the most frequent and damaging natural disasters globally (CRED and UNDRR, 2020). Considerable effort has gone into understanding global river flooding over the last decade, and a number of global flood models (GFMs) have been developed concurrently (Yamazaki et al., 2011, Pappenberger et al., 2012, Winsemius et al., 2013, Rudari et al., 2015, Sampson et al., 2015, Dottori et al., 2016c). The usefulness of these GFMs was initially limited to coarse scale flood risk assessments (Ward et al., 2015), largely due to global-scale data limitations. However, the incorporation of higher accuracy terrain data, available at the national level, has shown that their modelling frameworks are also suited to identifying more localized risk when utilising local data (Wing et al.,

2017). Previous studies comparing GFMs have shown there is disagreement between the global flood extents (Trigg et al., 2016b, Bernhofen et al., 2018b, Aerts et al., 2020). This disagreement between GFMs stems from different model structures and methods. One key difference between the models, which has not yet been explored, is the size of their river networks. The models have different river size thresholds at which they simulate fluvial events. These thresholds determine the size, and number, of rivers represented in GFMs, which can differ by several orders of magnitude. The size of a model's river network is contingent on both the quality and resolution of the model input datasets such as the underlying digital elevation model (DEM) and climatology (Dottori et al., 2016c) as well as the computational efficiency of the model, as the introduction of smaller rivers exponentially increases the modelled domain. Chosen thresholds also influence estimates of global flood exposure, as larger river networks result in higher simulated flood volumes and potential exposure. The effect that GFM river network size has on flood exposure estimates has not yet been quantified at the global scale. As remote sensing (RS) technologies continue to advance, so will the granularity at which rivers can be represented globally. Smaller rivers, previously unrepresented in coarse global datasets, will be able to be studied and modelled at large scales; potentially reframing current global flood exposure estimates. Limited work has been dedicated to the investigation of the human interaction with rivers of different size (Kummu et al., 2011). Understanding this interaction globally, particularly with respect to river flooding, will inform us about the completeness of current global flood exposure studies and identify where further study and development are needed.

A comprehensive understanding of flood risk requires information about the hazard, what or who is exposed, and their vulnerability. Exposure could include damages (both direct and indirect), exposed gross domestic product (GDP), exposed assets, and most commonly: exposed people (Ward et al., 2020). Identifying flood-exposed populations usually involves intersecting a flood hazard map with a population map. The methods and inputs used to produce population datasets differ, and so does their intended use (Leyk et al., 2019). Recently released population maps, which utilize commercial RS data and are an order of magnitude more resolved than existing population datasets (Tiecke, 2017) are already being used for disaster preparedness and response (Facebook, 2019). However, our current understanding of global flood exposure is based on existing global population

datasets, and these datasets have been used interchangeably in global studies (Tanoue et al., 2016, Jongman et al., 2012, Dottori et al., 2018) with little comment about their relative merit. The credibility of existing global flood exposure estimates in light of new, more detailed, population data and the implications of their interchangeable use in studies of global flood exposure needs to be explored. A recent study by Smith et al. (2019) reported large disagreement between flood exposure estimates calculated in 18 developing countries using three different population datasets. The identification of population data as one of the chief sources of uncertainty in global flood exposure studies warrants further investigation at the global scale. Understanding how both new and existing population datasets differ in their resulting exposure estimates, both regionally and within the hierarchy of the river network, can inform users about the most appropriate population dataset to use.

To explicitly explore the impact of river network size on global flood exposure estimates, we use a geomorphological measure of a river's flood susceptibility, which is independent from current GFMs and the additional uncertainties their different model structures bring. Fluvial processes contribute to the evolution of a landscape over time. The erosional action of flowing water has shaped the terrain of drainage basins to reflect the historical flow of water through them. Geomorphological approaches to mapping river flood susceptibility rely on the concept that the cumulative hydrogeomorphic effect of past flood events, evident in topography data, is indicative of a river's propensity to flood. Such approaches to flood mapping have been applied over a number of scales: from local (Nardi et al., 2006, Nobre et al., 2016, Dodov and Foufoula-Georgiou, 2006), to national (Jafarzadegan et al., 2018, Samela et al., 2017), to regional (Lugeri et al., 2010) and global (Nardi et al., 2019). The computational efficiency of geomorphic flood mapping, coupled with its reliance on only terrain data as input, make it useful for a 'first look' global scale analysis; intended to inform future development of higher accuracy hydrological flood mapping (Di Baldassarre et al., 2020).

Our geomorphological approach to mapping a river's flood susceptibility, herein referred to as the River Flood Susceptibility Map (RFSM) is based on new topography data (Yamazaki et al., 2017), which incorporate crowdsourced information to better represent the locations of rivers and streams (Yamazaki et al., 2019). Validation of our calibrated methodology (outlined in detail in Appendix B)

shows that the RFSM better replicates GFM hazard maps in Africa than an existing global geomorphological approach (Nardi et al., 2019). We also show that the RFSM performs similarly to the best GFMs (Dottori et al., 2016c, Sampson et al., 2015, Yamazaki et al., 2011) when validated against historical flood events (Bernhofen et al., 2018b). The RFSM allows us to easily discretize the flood map into different river sizes (independently of GFMs). We investigate the human interface with these different size rivers using three population datasets. Facebook's High Resolution Settlement Layer (HRSL), (1 arc-second, ~30 m resolution at the equator) (Tiecke, 2017) which is currently only available in 168 countries globally, and two population datasets used extensively in previous studies of global flood risk: the Global Human Settlement Population (GHS-POP) (9 arc-second, ~250 m resolution at the equator) (Freire et al., 2015, Schiavina, 2019) and WorldPop (3 arc-second, ~90 m resolution at the equator) (Stevens et al., 2015, Lloyd et al., 2019). We present a global picture of flood exposure to different size rivers, both in the present day, and how it has changed over the past 40 years. We then compare the flood exposure calculated using different population layers, exploring the implications this has on national level flood exposure estimates and examine the impact that river size has on any disagreement. Finally, we address the size of rivers represented in GFMs specifically and investigate how their chosen river network size impacts both global and national flood exposure estimates and what implications this has for previously published global flood risk assessments.

4.3 Methods

4.3.1 Mapping River Flood Susceptibility

We use a geomorphological approach to mapping river flood susceptibility, which is independent from the global flood models (GFMs). Previous GFM comparison studies found that multiple aspects of model structure contributed towards disagreement (Trigg et al., 2016b, Bernhofen et al., 2018b, Aerts et al., 2020). Using a geomorphological approach, we are able to explore just one aspect of disagreement: river network size. This approach allows us to explore all stream scales as drainage paths can be identified from the terrain alone. It is not influenced by the structure of the different GFMs and does not have the same computational restraints as a global hydrodynamic model. This approach is different from the

GFMs in that it does not measure the flood extent for a given return period flood, but rather a river and surrounding location's static susceptibility to flooding.

There are different approaches to geomorphic floodplain mapping. Three approaches were compared on the Tiber River in Central Italy by Manfreda et al. (2014). That study found that approaches utilizing morphological descriptors to delineate floodplains better replicate reference flood extents. The best morphological descriptor was found to be the relative elevation difference to the nearest channel (H). In a follow up study, Samela et al. (2017) investigated 11 different morphological descriptors in the Ohio River basin and then tested the best performing descriptors across the conterminous United States. While H was amongst the best four descriptors, it was shown to be highly variable across basins. The study found that the best morphological descriptor was a geomorphic index which relates H to a function of the nearest channel's contributing area. The method we use for delineating a river's flood susceptibility is based on the height above nearest drainage (HAND) methodology developed by Nobre et al. (2011). We use a variable H value (H_n), which changes depending on the Strahler stream order (Strahler, 1957) of the flooded channel (where n is the Strahler stream order). This geomorphic approach, requiring only terrain data as input, is computationally efficient, and can be easily modified to produce auxiliary data layers.

Our method, referred to as the river flood susceptibility map (RFSM) (Bernhofen et al., 2021), is illustrated in Figure 4.1 and takes three gridded datasets as input: a digital elevation model (DEM), its derived drainage directions, and its upstream drainage area (UDA). We use Multi Error-Removed Improved-Terrain (MERIT) hydro data (Yamazaki et al., 2019), a hydrography dataset based on the error improved SRTM (Shuttle Radar and Topography Mission) DEM: MERIT DEM (Yamazaki et al., 2017). MERIT Hydro is an improvement on previously available global hydrography datasets such as HydroSHEDs (Lehner et al., 2008) in terms of both spatial coverage and its representation of small streams. Its improved representation of small streams is enabled by its incorporation of global water body data and crowdsourced OpenStreetMap river data. This makes it particularly suited to this study; where we are interested in examining the flood susceptibility of rivers down to the smallest streams.
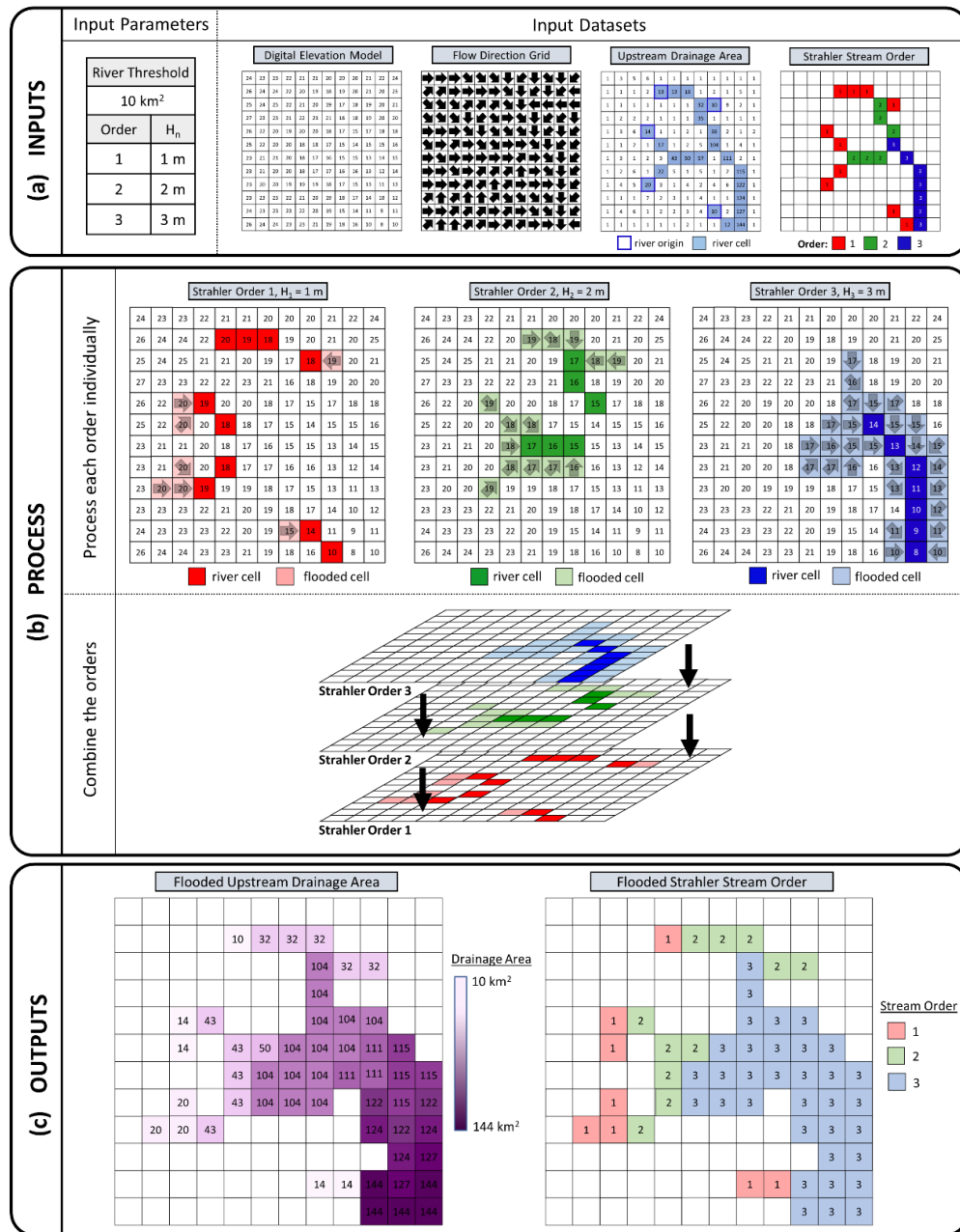
Figure 4.1 Illustrative example of the method for deriving the river flood susceptibility map (RFSM).

(a) User-defined input parameters include the minimum river size and the maximum relative elevation difference to the nearest draining channel, H_n, for each Strahler stream order. Dataset inputs include a digital elevation model (DEM), flow direction grid, and an upstream drainage area grid (represented on a 12 x 12 km^2 grid for illustrative purposes). Rivers (as defined by the minimum river size threshold) are classified into Strahler stream orders. (b) Each Strahler stream order is processed separately using the height above nearest drainage methods, and then the layers are combined. In areas of overlap the highest-order streams are retained. (c) Two outputs are produced: a map of the drainage are of the nearest flooded river and a map of the Strahler order of the nearest flooded river. See Figure 4.7 for an example of RFSM output in Bosnia and Herzegovina and Guinea-Bissau.

The river network is extracted from the upstream drainage area dataset by specifying a minimum threshold river size (in units of UDA). Identifying the headwater of a river is no trivial task, with regional and climatic factors playing a part (Montgomery and Dietrich, 1988, Tarboton et al., 1991). Previous work exploring optimal initiation thresholds for geomorphological floodplain mapping found that DEMs with a resolution of 1 arc second (~30 m) could use initiation thresholds less than 10 km^2 UDA. In the same study, a 3 arc second (~90 m) resolution DEM was used with a 100 km^2 UDA threshold (Annis et al., 2019). The MERIT Hydro data we use in this study has a resolution of 3 arc seconds (~90 m). But its incorporation of crowdsourced river data has optimized its representation of small streams and rivers. As such, we use a globally consistent river initiation threshold of 10 km^2 UDA for the RFSM. This is a large assumption, as in some locations globally there will be no visible channel at this location. However, we argue that removing areas of potential exposure to avoid overprediction in some areas goes against the premise of this study, which is to explore and identify 'missed' areas of exposure. The exposure calculations for small streams should therefore be interpreted with these limitations in mind.

Once the river network has been extracted, the rivers in the network are classified based on their Strahler stream orders (Strahler, 1957). The Strahler stream order is a dimensionless indicator of the magnitude of the river based on its hierarchy within the drainage basin.

4.3.1.1 Calibrating the River Flood Susceptibility Map

The maximum relative elevation difference to the nearest draining channel, H_n (see Figure 4.1(a)), for each Strahler stream order (n) is the only RFSM parameter requiring calibration. We use a variable H, which scales with Strahler stream order, to account for changes in flood depth as a river's size changes. In Samela et al. (2017), the best performing geomorphic index also accounts for variations in river size by scaling relative to the river's upstream contributing area.

To account for climatic variability in a river's flood susceptibility (Smith et al., 2015), we split the globe into five simplified Köppen-Geiger climate zones (Figure 4.2): Tropical, Arid, Temperate, Continental and Polar. Polar regions are excluded from our analysis as these regions are dominated by glacial but not fluvial

processes (Chen et al., 2019). The RFSM has uniquely calibrated H_n values in each of the four climate zones. We calibrate the H_n values in 19 different basins (see Figure 4.2), spanning 5 different continents across all four climate zones considered. Reference flood maps used for calibration are a mixture of national, continental, and global flood hazard maps. To maintain consistency across the calibration data, we use 100-year return period flood hazard maps. We use a combination of national, continental, and global flood hazard maps for calibration in each climate zone. This is to ensure that there is sufficient calibration data for each Strahler order river, as only the national flood hazard data captures flooding for low-order rivers. Two different national flood maps are used for calibration. The first is the National Flood Hazard Layer (NFHL) produced by the Federal Emergency Management Agency (FEMA). NFHL data are used for calibration in North American basins including Puerto Rico, Lower Gila, Upper Pecos, Lower Mississippi, Alabama, Muskingum, Rock, and Susquehanna. The second national flood map is the Environment Agency's 100-year flood map for planning, which is used for calibrating the RFSM in the Thames basin in England. The continental flood map for Europe (Dottori et al., 2016b), developed by the Joint Research Centre (JRC) is used to calibrate the RFSM in the Jucar river basin in Spain, the Loire river basin in France, the Po river basin in Italy and Switzerland, and the Oder river basin in Poland, Germany, and Czech Republic. A global flood hazard map (Dottori et al., 2016a), also developed by the JRC, is used to calibrate the RFSM in the Central Amazon basin in Brazil; the Lower Congo basin in the Democratic Republic of Congo and the Republic of Congo; the Lower Mekong basin in Thailand, Cambodia, Vietnam, and Laos; the Upper Nile basin in Egypt and Sudan, the Lower Lena basin in Russia and Kazakhstan; and the Central Lena basin in Russia. Maps of the reference flood maps used for calibration are shown in Figure B1 in Appendix B and further details about each calibration basin can be found in Table B1 in Appendix B.

Calibrated RFSM H_n Values (m)

H_n	Tr	Ar	Te	Co
H_1	1	0	0	0
H_2	2	0	1	0
H_3	4	0	2	2
H_4	6	1	4	4
H_5	8	3	5	5
H_6	8	3	7	6
H_7	9	5	9	8
H_8	10	5	10	9
H_9	10	12	10	10
H_{10}	10	13	13	11
H_{11}	13	14	-	12

Climate Zones
- Tropical (Tr)
- Arid (Ar)
- Temperate (Te)
- Continental (Co)
- Polar

Calibration Basins
1. Puerto Rico
2. Central Amazon
3. Lower Congo
4. Lower Mekong
5. Lower Gila
6. Upper Pecos
7. Jucar
8. Upper Nile
9. Lower Lena
10. Lower Mississippi
11. Alabama
12. Thames
13. Loire
14. Po
15. Muskingum
16. Rock
17. Susquehanna
18. Oder
19. Central Lena

Figure 4.2 The calibration basins shown on a map of simplified Köppen-Geiger climate zones and the calibrated maximum relative elevation difference to the nearest draining channel (H_n) for each Strahler stream order in the four climate zones considered (polar regions are excluded from the analysis).

The values are calibrated in each climate zone by running thousands of different combinations of H_n in each calibration basin. Optimal H_n values are determined by using three commonly used measure of fit scores: critical success index (CSI), hit rate (HR), and bias (Wilks, 2006). The H_n values retained are the ones that result in the best fit scores with respect to the reference flood maps within each climate zone. Final calibrated H_n values for each climate zone are shown in Figure 4.2. More detailed information on the calibration of the RFSM can be found in Appendix B.1.

Once H_n values for each order have been assigned, each stream order is processed separately (Figure 4.1(b)), and then merged together. In areas of overlap, the highest order stream retains the values. Two datasets are produced as output: a map of the flooded river's upstream drainage area, and a map of the flooded river's Strahler stream order. Illustrations of these two outputs are shown in Figure 4.1(c).

4.3.1.1 Validating the River Flood Susceptibility Map

The RFSM is validated against both existing GFMs and observed flood events. Validation against GFMs is carried out for the whole African continent using the 100-year return period aggregated output of six GFMs from a previous model intercomparison study (Trigg et al., 2016a). The six GFMs that make up the aggregated output include CIMA-UNEP (Rudari et al., 2015), ECMWF

(Pappenberger et al., 2012), Fathom (Sampson et al., 2015), GLOFRIS (Winsemius et al., 2013, Ward et al., 2013), JRC (Dottori et al., 2016c), and U-Tokyo (Yamazaki et al., 2011). To assess the credibility of the RFSM, it is also validated alongside an existing global geomorphological floodplain map (Nardi et al., 2019). For validation we split the African continent into eight major drainage basins (see Figure B.3 in Appendix B) according to the HydroBASIN Level 2 classification (Lehner and Grill, 2013). The results of the GFM validation show that the RFSM produces credible flood extents when compared with existing GFM outputs in Africa. The RFSM correctly captures over 90% of high agreement flood zones (where at least five out of six GFMs agree) in seven of the eight major drainage basins in Africa. In the East African basin, the RFSM captures 87% of this high-agreement flood zone. Comparing CSI, HR and bias scores for the RFSM and the existing global geomorphological floodplain map, the RFSM scores better in all the major drainage basins in Africa except for North Africa (where both maps score poorly due to the Sahara Desert). The RFSM is also validated against observed flood events in Nigeria and Mozambique. The 2012 flooding in Nigeria and the 2007 floods in Mozambique affected four million people and over one hundred thousand people respectively (Bernhofen et al., 2018b). Validation data for both these flood events used in a previous GFM validation comparison study (Bernhofen et al., 2018a) are also used to validate the RFSM. The RFSM is validated against observed data in three validation regions: Lokoja, which is a narrow, confined floodplain at the confluence of Niger and Benue rivers in Nigeria; Idah, which is a flat and extensive floodplain south of Lokoja; and Chemba, which is an anabranching stretch of the Zambezi river just upstream of the delta in Mozambique. Validation of the RFSM against observed data from these historical flood events show that it performs similarly to the best performing GFMs in each of the three validation regions. Further detail about the validation of the RFSM can be found in Appendix B.2.

It is important to note the limitations of our methodology and geomorphological approaches in general. The RFSM does not account for flood protection measures and cannot communicate the probability of flooding in any location. It consistently represents a river's flood susceptibility based on the surrounding terrain alone. In regions where the floodplain boundaries are less distinguishable from the terrain, such as flat and low-lying areas, geomorphological approaches are prone to overprediction as they do not represent mass and

momentum conservation. Our method's intended use is as a model-independent global 'first look' analysis to inform future hydrodynamic model development and use.

4.3.2 Measuring Exposure

We investigate the human exposure to river flood susceptibility. Human exposure is herein defined as the intersection of our river flood susceptibility map and a spatially distributed population layer. Three population datasets are used to measure exposure: Facebook's High Resolution Settlement Layer (HRSL) (Facebook and CIESIN, 2016), The European Commission Joint Research Centre's Global Human Settlement Population (GHS-POP) (Schiavina, 2019), and WorldPop (Stevens et al., 2015). These population datasets all use the same initial input census data, from Gridded Population of the World (GPW) v4 (Center for International Earth Science Information Network - CIESIN - Columbia University, 2016), but their methods for allocating the population across gridded cells differ. Facebook's HRSL is the only dataset of the three lacking full global coverage (at the time of writing 168 countries have been mapped). It is also the most recent, with work ongoing to map the remaining countries. HRSL uses ultra-high-resolution commercial satellite imagery (~ 50 cm resolution) and convolutional neural networks to detect individual buildings at the country level (Tiecke, 2017). Subnational census data for the year 2018 is then proportionally allocated to the identified buildings at 1 arc second resolution (~ 30 m at the equator).

Similarly to the HRSL in methodology, JRC's GHS-POP dataset identifies built-up areas from Landsat imagery and proportionally allocates census data to the built-up areas (Freire et al., 2015). In regions where no settlements can be identified, but where census data indicates there is a population, the population is evenly distributed across the census area using areal weighting (Freire et al., 2016). This can occur in some rural areas, where small settlements are not captured by the Landsat imagery. Despite being coarser in spatial resolution at 9 arc seconds (~250 m at the equator), GHS-POP provides consistent multi-temporal population estimates (for the years 1975, 1990, 2000, and 2015) allowing for accurate analyses over time (Freire et al., 2020).

Unlike the other two population datasets, which evenly spread census data over identified settlements, WorldPop uses a complex model to disaggregate population over an area (Leyk et al., 2019). It uses a random forest model and a number of ancillary datasets to dynamically weight the distribution of census data

over a 3 arc second (~90 m at the equator) gridded area (Stevens et al., 2015) to produce annual population estimates from 2000-2020.

Exposure calculations necessitate uniformity between the intersecting datasets in terms of spatial resolution. As such, the GHS-POP layer was resampled from 9 arc second resolution and the population evenly distributed to a 3 arc second resolution grid to allow for analysis with a flood map of the same resolution. Conversely, for the HRSL exposure calculations the RFSM was resampled from 3 arc second to 1 arc second resolution. When comparing the exposure results between population datasets the epoch used for comparison was 2015. National population totals for the HRSL and WorldPop datasets for the years 2018 and 2015, respectively, were scaled relative to GHS-POP 2015 national population totals.

4.4 Results and Discussion

4.4.1 Global Exposure to Different Sized Rivers from GHS-POP

Rivers were classified into six different sizes, expressed in upstream drainage area (UDA) (km^2), with the ranges increasing in powers of 10. River classifications based on UDA, depicted in Figure 4.3(b) for Nigeria, were as follows: stream (10-100 km^2), small river (100-1,000 km^2), medium river (1000-10,000 km^2), medium-large river (10,000-100,000 km^2), large river (100,000-1,000,000 km^2), and huge river (>1,000,000 km^2).

Flood exposure is first calculated using the GHS-POP layer. Globally, we find 1.94 billion people susceptible to flooding from rivers with a UDA greater than 10 km^2. Breaking this down by continent, Asia's flood exposure is 1.49 billion, Africa's is 203 million, Europe's is 104 million, North America's is 81 million, South America's is 59 million, and Oceania's is 3.5 million. Splitting global flood exposure by river size, of the total exposed: 18.2% are from streams, 26.4% from small rivers, 23.7% from medium rivers, 17.2% from medium-large rivers, 8.4% from large rivers, and 6.1% from huge rivers. Asia makes up over 75% of the total global flood exposure, the majority of this amount coming from India and China, which are by far the two most exposed countries (see Figure 4.3(a)). Roughly half of India's flood exposure is from streams and small rivers. Comparably, in China, this figure is closer to a third. This is likely due to the degree of urbanisation in both

countries; the percentage of China's urban population is double that of India's (WorldBank, 2018). Urban areas are disproportionately located on large rivers due to the historical tendency for settlements to form in areas fertile for farming and convenient for transport (McCool et al., 2009). As such, a greater proportion of flood exposure in China comes from larger rivers, whereas in India, a greater proportion comes from rural exposure to smaller rivers. Rivers classified as "huge" are only found in some countries, but often they make up a large proportion of the national flood risk. For example, the Brahmaputra in Bangladesh and the Nile in Egypt and Sudan are responsible for just under half of the national flood exposure in their respective countries.

To identify countries with the most acute flood risk, exposure was normalized against total national population (Figure 4.3(c)). Suriname has the highest normalized exposure, with 894 people exposed per 1000. The country's low elevation relief, and its capital city situated on the banks of the Suriname river near its outlet into the Atlantic Ocean, makes Suriname particularly vulnerable to flooding (WorldBank, 2019). A total of 4 of the top 10 most "normally" exposed countries are in south or southeast Asia. These include Bangladesh, Cambodia, Thailand, and Vietnam. Flooding in these countries is severe and annual, normally occurring each year during the monsoon season. In Europe, the Netherlands has a high normalized exposure, 738 exposed per 1000. The Netherlands has a long history of flooding due to its low elevation, flat terrain, and high population density. It also has the most advanced flood defence systems in the world, designed to contain river water levels with a probability of occurrence once every 1250 years (Stokkom et al., 2005). Geomorphological approaches to flood mapping, such as the RFSM, cannot model probabilities of occurrence; and are therefore unable to represent flood prevention measures (Scussolini et al., 2016) and distinguish defended and undefended floodplain zones. Much of the exposed population in the Netherlands, as well as other countries with flood protection, reside in the defended area of a floodplain. This does not eliminate their risk of flooding; just reduces the probability of it. The severity of a flood event when defences fail can be catastrophic, resulting in high velocity flows and rapid inundation with little to no warning.
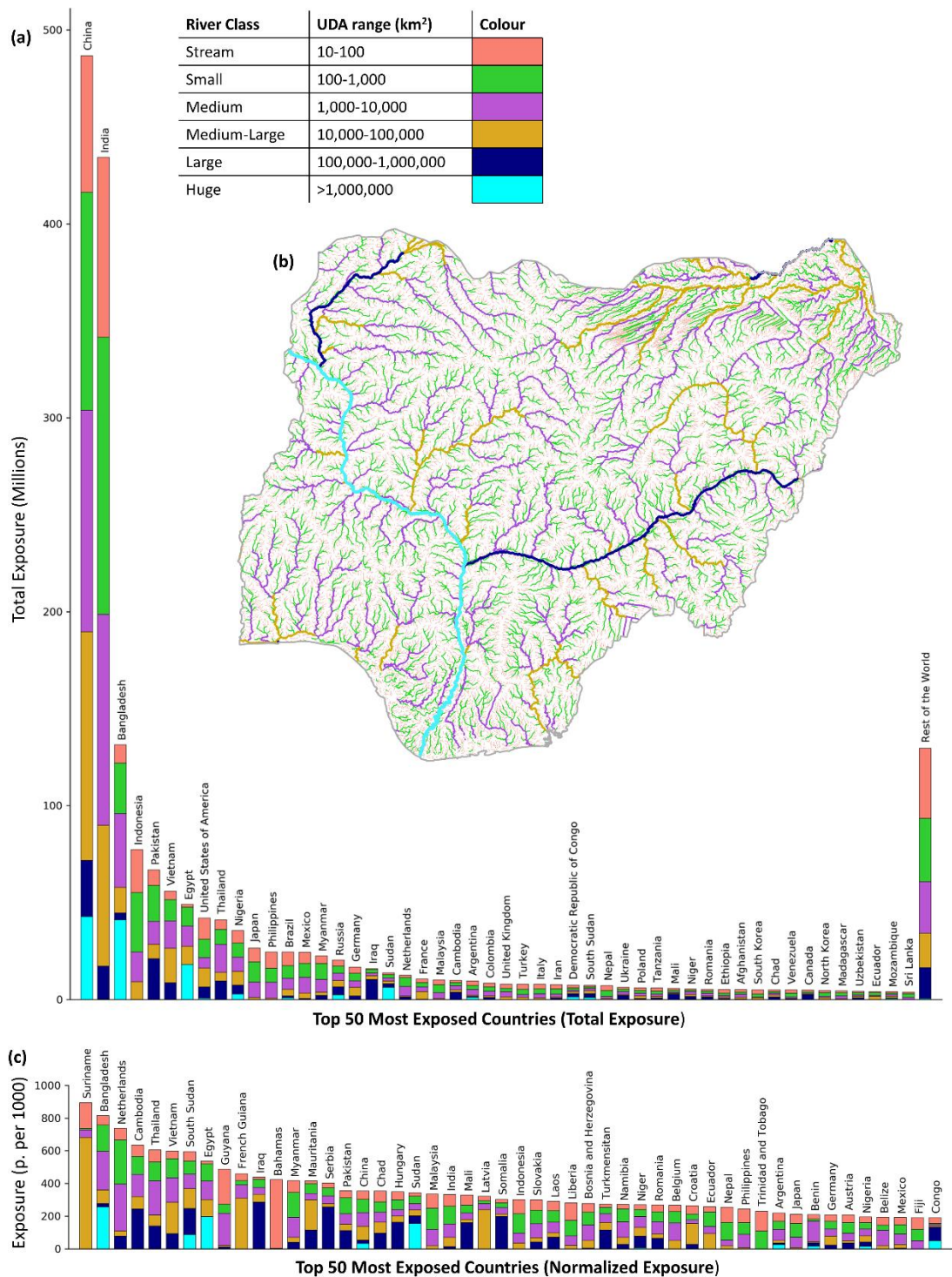
Figure 4.3 Flood exposure calculated with the Global Human Settlement
Population (GHS-POP) layer.

(a) Top 50 most exposed countries in terms of total flood exposure. (b) The
river size classification visualized in Nigeria. (c) Top 50 most exposed
countries in terms of normalized flood exposure (normalized to country's total
population).

The top 50 exposed countries calculated using the WorldPop and HRSL datasets are detailed in Figures B.13 and B.14 of Appendix B, respectively. We also compare continental and global flood exposure estimates from different sized rivers calculated using GHS-POP and WorldPop in Table 4.1. It's not possible to compare these global results with HRSL calculated exposure, as it does not yet have global coverage. Global flood exposure calculated using the WorldPop layer is 2.026 Billion, roughly 83 Million larger than the global figure calculated using GHS-POP. Differences in exposure between the two datasets are largest in Africa and Asia and Oceania. We explore the implications of using different population datasets for flood exposure calculations in greater detail in Section 4.4.3 of this chapter.

Table 4.1 Comparison of continental and global flood exposure estimates from different sized rivers calculated with the Global Human Settlement Population (GP) layer and WorldPop (WP).

Exposure is in millions of people.

River Class	Africa		Americas		Asia and Oceania		Europe		Global	
	GP	WP	GP	WP	GP	WP	GP	WP	GP	WP
Stream	33.2	42.1	38.88	38.45	260.53	274.69	20.65	20.07	353.26	275.31
Small	41.03	48.43	36.72	36.13	409.21	415.31	26.63	26.01	513.59	525.88
Medium	39.41	43.45	29.84	30.28	363.67	384.77	26.84	26.72	459.76	485.22
Medium-Large	34.23	35.91	20.94	20.65	260.44	268.13	18.64	18.6	334.25	343.29
Large	25.36	21.8	11.9	11.9	114.14	126.46	11.4	11.5	162.8	171.66
Huge	30.45	30.24	2.65	2.74	86.41	92.09	0	0	119.5	125.07
Total	**203.68**	**221.93**	**140.93**	**140.15**	**1494.4**	**1561.45**	**104.16**	**102.9**	**1943.17**	**2026.43**

4.4.2 Exposure Change from 1975-2015

An advantage of both the GHS-POP and WorldPop datasets is their population estimates across different time scales, allowing for exposure analysis over time. WorldPop has annual population maps from 2000-2020 and GHS-POP has population estimates across four epochs: 1975, 1990, 2000, and 2015. Here, using GHS-POP's multitemporal population layers, we calculate exposure change over a period of 40 years. Normalized flood exposure estimates were calculated for the years 1975, 1990, 2000, and 2015. These results are tabulated in Table B.10 in Appendix B. Population change is calculated by taking the difference between the normalized exposure estimates for the years considered. Globally, total flood exposure grew between 1975 and 2015 from 257 people per 1000 to 265 people per 1000. Interestingly, in both Tropical and Arid climates total flood exposure over this

40-year period grew by 11 people per 1000, but in Temperate and Continental climates total flood exposure decreased by 4 and 10 people per 1000, respectively. Developing countries are largely located in tropical and arid climates, conversely, developed economies are prevalent in temperate and continental climates. These findings correspond with previous work done by Jongman et al. (2012), which found developing countries had the largest increases in exposure relative to population growth in the period 1970-2010. At the continental level, normalized flood exposure saw the largest increase in Asia, growing by 15 people per 1000 from 1975-2015. It also grew in South America by 5 people per 1000. In Europe, changes in normalized exposure over this period were negligible; while in North America, Africa, and Oceania normalized exposure decreased by 3, 5, and 2 people per 1000, respectively. Comparing these results with a related study by Ceola et al. (2014), which used satellite night-time light intensity to explore changes in river flood exposure from 1992-2012, we find similar trends in North America, South America, Europe, and Asia. Exposure over the period 1975-2015 increased for streams, medium-large, large and huge rivers. There were slight reductions in exposure for small and medium sized rivers.

Exposure changes at the national level are depicted in Figure 4.4. The highest increase in overall flood exposure was seen in Nepal and French Guinea. In both countries, the proportion of exposed population grew by 200 people per 1000 in the period 1975-2015. In French Guinea, this sudden increase is largely due to the population growth of Saint-Laurent-du-Maroni, a town situated on the banks of the Maroni river. From 1975-2015 the town's population grew 1800% compared with the national population growth of 360%. In Nepal, one of the top 10 fastest urbanizing countries in the world (Bakrania, 2015), the flood exposure growth is a result of this fast urbanisation in cities such as Kathmandu, which is dissected by eight different rivers. An exposure decrease of 172 people per 1000 was seen in South Sudan. This is due to the growth of urban areas outside the Sudd swamp in cities such as Juba, Yei, Yambio, Nzara, and Wao. South Sudan has been hit by devastating floods in the past year, which displaced over 800,000 people (OCHA, 2020). Had relative population exposure in South Sudan grown, rather than shrunk, the recent flooding could have been even worse.

All Rivers (UDA >10 km²)

Change in normalized exposure 1975-2015 (p. per 1000)

| < -100 | -70 | -50 | -30 | -20 | -10 | -5 | -1 | 0 | NA | 0 | 1 | 5 | 10 | 20 | 30 | 50 | 70 | 100 < |

Streams (UDA 10-100 km²)   Small Rivers (UDA 100-1,000 km²)

Medium Rivers (UDA 1,000-10,000 km²)   Medium-Large Rivers (UDA 10,000-100,000 km²)

Large Rivers (UDA 100,000-1,000,000 km²)   Huge Rivers (UDA >1,000,000 km²)
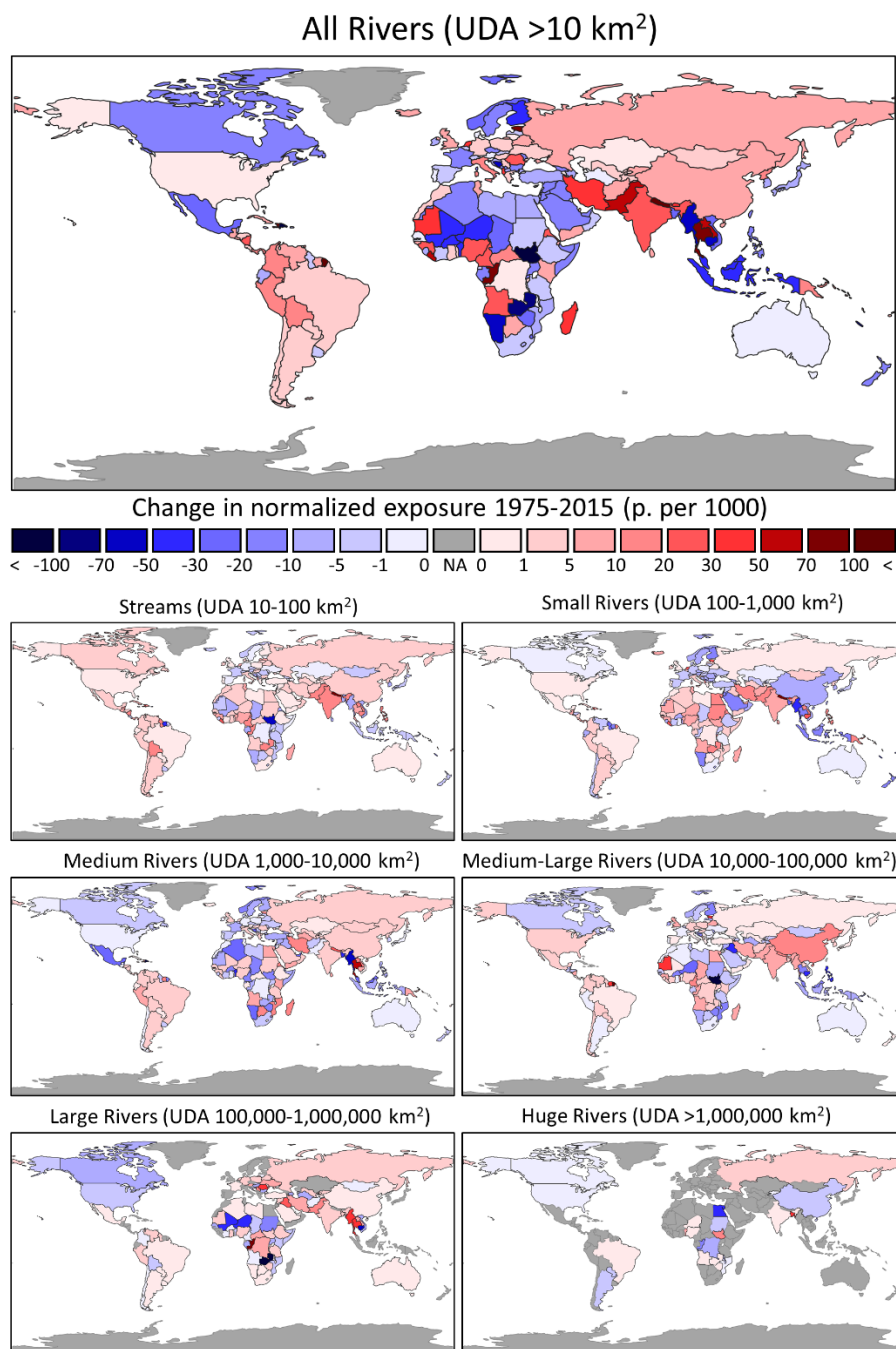
Figure 4.4 Country-level river flood exposure (population normalized) change from 1975-2015 calculated using the Global Human Settlement Population layer.

River size expressed in upstream drainage area (UDA)

4.4.3 Exposure Estimates from Different Population Datasets

Exposure differences arising from the use of different population layers were calculated for the 168 countries where all three population datasets are available (Figure 4.5*) (see Table B.11 in Appendix B for a list of the missing countries). In the countries examined, normalized exposure (with respect to the country's total

population) calculated with WorldPop data was the highest (270 exposed per 1000), followed by GHS-POP (256 exposed per 1000), and HRSL exposure was the lowest
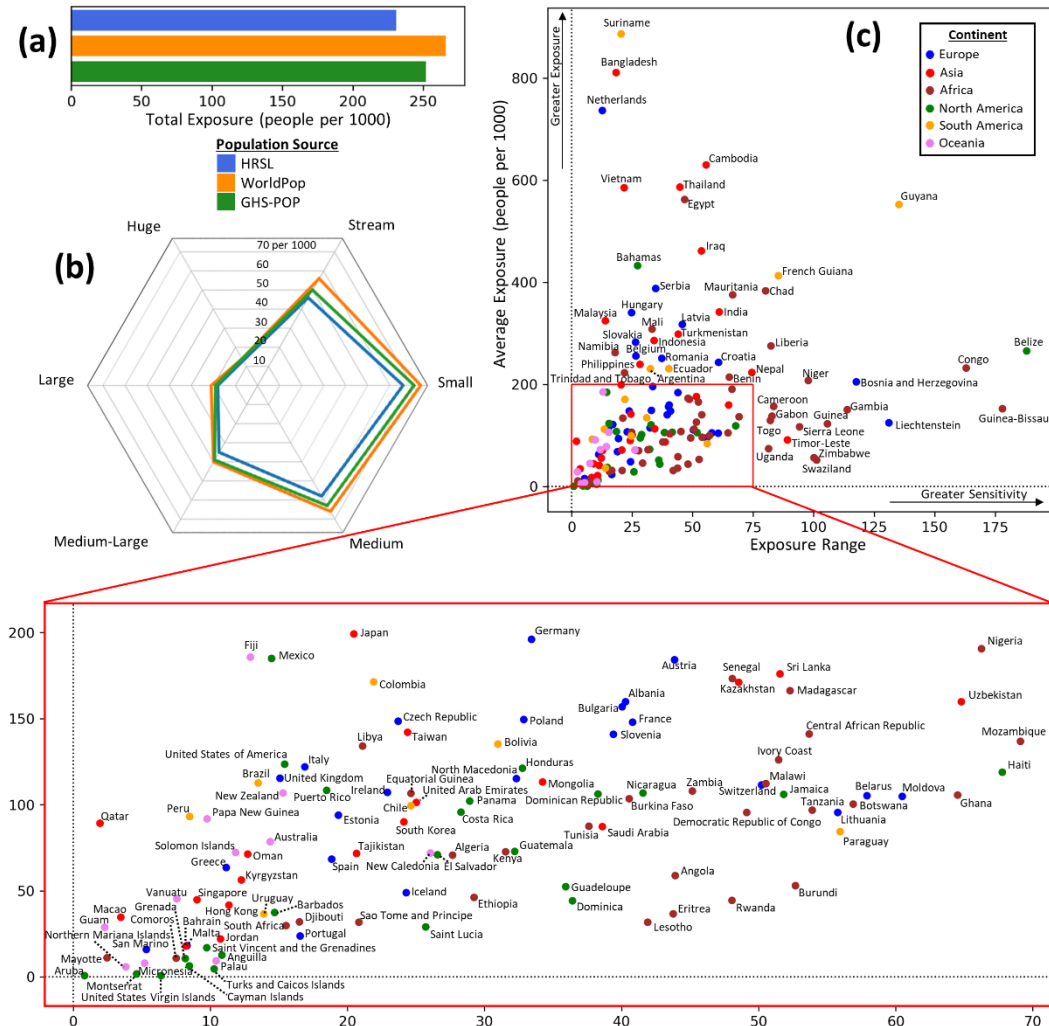
Figure 4.5 Flood exposure comparison in 168 countries using the High Resolution Settlement Layer (HRSL), WorldPop layer, and Global Human Settlement Population (GHS-POP) layer.

(a) Comparison of the total normalized flood exposure between the three population datasets in all available countries. (b) How the calculated exposure figures differ per river size classification. (c) Country-level statistics for average normalized exposure (calculated as the mean of the three national exposure estimates) and the sensitivity of the exposure calculation to the choice of population datasets (measured as the absolute range of the three national exposure estimates). The higher up the *y* axis and *x* axis a country is, the greater the average exposure and sensitivity will be to the choice of population dataset, respectively.

(235 exposed per 1000). These findings correlate with a previous study by Smith et al. (2019) which found WorldPop data overestimated flood exposure compared to HRSL data in each of the 18 developing countries examined.

Differences in calculated exposure across the river sizes are shown in Figure 4.5(b). Exposure differences were most pronounced for smaller rivers (streams, small, and medium rivers), while there was almost no exposure difference for the largest river class (huge). The overall trend across all river sizes consistently shows that WorldPop estimated the highest exposure, followed by GHS-POP, and HRSL estimated the lowest exposure.

The population mapping approaches of the three population layers can go some way towards explaining the differences in calculated exposure; these corresponding outputs are visualized in Figure 4.6, in which we qualitatively compare the population distribution of the three outputs with respect to the settlement distribution, manually identified from high-resolution satellite imagery, along the Likuala-aux-Herbes river in the Republic of Congo. WorldPop's population distribution algorithm dasymetrically redistributes the whole population across the grid, also in areas where no settlements have been identified. This is done under the assumption that not all "built up" areas will be picked up in the satellite imagery (TReNDS, 2020). When intersected with a flood extent, such a modelling approach can lead to mis-estimation of flood exposure in rural areas with respect to the other two population datasets. In the area examined in Figure 4.6, WorldPop estimates 1,167 people exposed, compared with 17,581 and 13,789 people exposed estimated by HRSL and GHS-POP, respectively. This is despite WorldPop exposure covering over 93% of the area examined, which far exceeds GHS-POP's 5% exposed area and HRSL's 1% exposed area. WorldPop's approach to rural population distribution can lead to underestimation of exposure in small rural settlements (such as in Figure 4.6) or overestimation of exposure across large expansive areas of flooding, as will be explored later in this section. Conversely, the approach implemented by both GHS-POP and HRSL (which spread census data only over identified "built up" areas) is more sensitive to omission and commission errors arising from the classification of settlements (Palacios-Lopez et al., 2019). For example, undetected settlements outside the flood extent would result in artificially higher flood exposure estimates as the underlying census data is only spread across the identified settlements (a greater proportion of which are now identified as being

within the flood extent). Similarly, commission errors (false positives) are common in sandy or rocky landscapes and often occur in coastal areas or along riverbanks. Commission and omission errors can lead to either artificial increases or decreases in flood exposure estimates, depending on the location of these errors with respect to the flood extent.

The resolution of the population layers should also be considered. GHS-POP's fairly coarse (9 arc second) resolution means that in some areas where the potential for flooding (or not) falls within the resolution of a 9 arc second grid cell, the settlement's avoidance (or not) of the flood risk cannot be accurately represented. This effect can be reduced by upsampling and proportionally reallocating the population to a grid that matches the resolution of the flooded data, as we have done in this study. Similarly, the spatial resolution of the underlying satellite imagery should be considered. Both GHS-POP and WorldPop identify settlements using Landsat imagery at 30 m resolution, while HRSL identifies settlements using DigitalGlobe imagery at 0.5 m resolution. Previous work by Tiecke (2017) showed that HRSL was able to identify buildings missed by GHS-POP, highlighting the importance of high-resolution imagery for comprehensive building classification.

The use of different population datasets had a negligible effect on exposure estimates for the huge river class. Large settlements tend to form around rivers of this size, and on coastlines where rivers of this size drain. Large urban areas are easily identifiable from remote sensing data, which means the population distribution (and resulting exposure estimates) for these urban centres show less variation between the datasets. Conversely, non-urban flood exposure estimates to smaller rivers show greater sensitvity to the choice of population layer. This is because the approach to non-urban population mapping between the three datasets differs. WorldPop, as mentioned previously, distributes administrative-level census data across all 3 arc second pixels in order to mitigate the impacts of potential omission and commission errors in the settlement data. This approach leads to some overestimation in rural populations (Smith et al., 2019, Wardrop et al., 2018). GHS-POP, which distributes census data over Landsat identified settlements (and in non built-up areas distributes population at the census unit by areal weighting), tends to underestimate rural populations. (Leyk et al., 2019, Liu et al., 2020). HRSL's use of

ultra-high-resolution sattelite imagery has been shown in previous studies to accurately identify rural settlements (Tiecke, 2017, Smith et al., 2019). However, the method of proportional allocation used to distribute the census data is relatively crude. Uncertainties in the underlying census data should also be considered, as the quality and detail of the data, as well as the frequency at which it is collected, varies significantly at the national level (Leyk et al., 2019). The three population datasets compared in this study share the same input census data (GPWv4) and therefore any associated census uncertainties are a common feature shared across the three datasets.
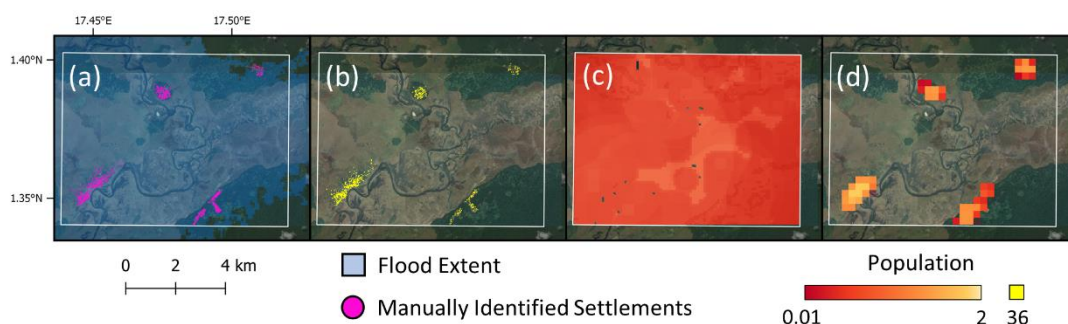
Figure 4.6 Qualitative comparison of settlement distributions on the Likoula aux Herbes river in the republic of Congo.

The white square in each panel is the pre-defined bounding box for which population totals are calculated. Population pixels in panels (b-d) range from low populated pixels (red) to high populated pixels (yellow). (a) River flood susceptibility map (RFSM) flood extent (blue pixels) along with manually identified settlements (pink circles) from high resolution Google Earth satellite imagery. (b) High Resolution Settlement Layer (HRSL) population distribution. A total of 17,581 people exposure. (c) WorldPop population distribution (resampled to 1 arc second for comparison). A total of 1,167 people exposed. (d) Global Human Settlement Population (GHS-POP) population distribution (resampled to 1 arc second for comparison). A total of 13,789 people exposed.

Map data: © Google, Maxar Technologies 2021.

Calculating the general trends of exposure between the population layers is useful for making broad conclusions about the suitability of a population layer. Understanding the variations of the data at the country level leads to more actionable information about the appropriate use of different population layers. We calculate both the severity of flooding in each country (as the mean of the normalized national flood exposure estimates calculated with the three population datasets) and the disagreement between the population exposure estimates in each country (as the absolute range of the three normalized national flood exposure estimates). The

disagreement between the population-layer exposure estimates for each country varies significantly (Figure 4.5(c)). In the three countries with the highest exposure disagreement (Belize, The Republic of Congo, and Guinea-Bissau) WorldPop estimates of exposure are far greater than either HRSL or GHS-POP estimates. In Belize, a country with large areas of inundated wetlands, WorldPop estimates 135,000 people exposed, while GHS-POP and HRSL estimate 70,000 and 80,000 exposed, respectively. In the Republic of Congo, a country with large areas of floodplain, WorldPop estimates 1.3 Million people exposed and GHS-POP and HRSL estimate 810,000 and 780,000 exposed respectively. WorldPop's method of distributing the population over a large area results in significant overestimation compared with HRSL or GHS-POP in these rural inundated areas. This can be seen in greater detail in Figure 4.7 for Guinea-Bissau. In Guinea-Bissau, GHS-POP and HRSL (which estimate exposures of 180,000 and 160,000 respectively) identify settlements largely situated outside the floodplains ("dry" cells in blue). Comparatively, WorldPop's modelling approach and assumptions leads to far more "wet" population cells and an estimate of exposure (480,000) more than double that of the other two population layers. The exposure disagreement in these three countries is compounded by the relatively large areas of inundation in each country. The percentage inundated area is 25%, 30%, and 26% for Guinea-Bissau, Belize, and The Republic of Congo, respectively. In comparison, the percentage of populated area defined by the population layers is less than 5% for GHS-POP and HRSL, but more than 95% for WorldPop in each of the three countries. As exposure in this study is defined as the intersection of the flooded area and the populated area, it is understandable that WorldPop's exposure estimates are more sensitive to the area of inundation. This is evident when examining a country with high exposure disagreement but with a comparatively smaller area of inundation. In Bosnia and Herzegovina (Figure 4.7), the percentage of flooded area is just 9% and the GHS-POP layer estimates far greater exposure (1 Million) than either WorldPop (680,000) or HRSL (610,000). Here, where much of the exposure occurs near the banks of the rivers, the coarse spatial resolution of GHS-POP is less able to precisely locate settlements situated just outside the floodplain. As a result, more populated cells are flagged 'at risk' compared to the higher-resolution HRSL layer.
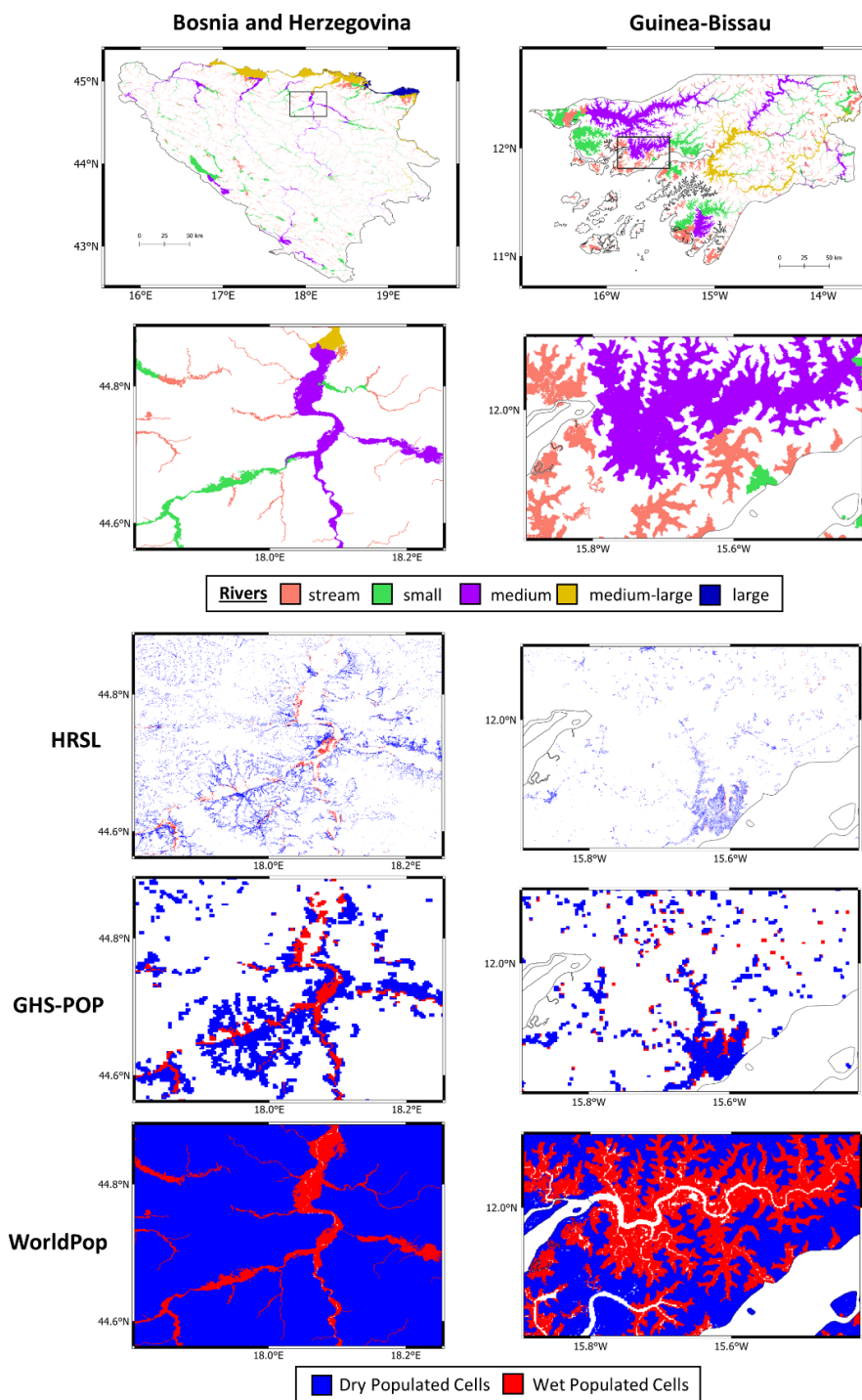
Figure 4.7 Comparison of population datasets and their intersection with the flood extent in Bosnia and Herzegovina and Guinea-Bissau.

The top two insets show the river flood susceptibility map (RFSM) split into the different river size categorise for the whole country (top panel) and for a smaller, more detailed area of both countries (second panel from top). The remaining insets show the three different population maps and their intersection with the flood map in the detailed areas of both countries. Blue cells indicate the population cells are dry (not exposed to flooding), and red cells indicate the population cells are wet (exposed to flooding).

These results have shown that the use of different population layers can lead to vastly different flood exposure estimates because of inherent differences in their spatial resolutions, methods used, and assumptions made to produce them. Our comparative analysis has identified in which countries exposure calculations are sensitive to the choice of population layer and shed light on some of the reasons for exposure disagreement. However, there is a limit to the conclusions that can be drawn from comparative analyses alone, and there is an urgent gap for more studies which validate the accuracy of these population layers using ground-truthed data.

It would be imprudent to definitively recommend one population dataset for use in flood exposure studies without extensive comparative global validation. However, previous studies have shown that HRSL performs better than existing population datasets at mapping reference building footprints, especially in rural areas (Tiecke, 2017, Smith et al., 2019). Our results also point to some of the benefits of using HRSL. Its settlement identification method for population distribution avoids exposure overprediction common in other population data and its high resolution can better capture the accurate location of settlements. Despite this, HRSL should not be considered a catchall dataset for flood exposure. Its high resolution may limit its use in certain situations due to computational restraints. Similarly, in studies of flood risk over time population data with multiple temporal epochs, such as GHS-POP or WorldPop, are better suited. The results we present in this section, and Figure 4.5, are intended to inform users of these population datasets about their appropriate use. In countries with high exposure disagreement, the choice of population dataset for flood exposure should be carefully considered, and further accuracy assessments of the population layers are recommended.

4.4.4 Relevance to Global Flood Models

The minimum size of river represented in GFMs varies (see Table 4.2), with minimum river size thresholds ranging between 50-5000 km^2 UDA, three orders of magnitude. River network size can be limited by the granularity of input data such as rainfall (Dottori et al., 2016c), or by the computational demand of modelling floods at the global scale.

Table 4.2 Global flood model river representation

Minimum river size (upstream drainage area)	Global flood model	River sizes modelled (P = partial)
50 km^2	Fathom (Sampson et al., 2015)	Stream (P), small, medium, medium-large, large, huge
500 km^2	ECMWF (Pappenberger et al., 2012) and U-Tokyo (Yamazaki et al., 2011)	Small (P), medium, medium-large, large, huge
1000 km^2	CIMA-UNEP (Rudari et al., 2015)	Medium, medium-large, large, huge
5000 km^2	JRC (Dottori et al., 2016c)	Medium (P), medium-large, large, huge

Differences in river network size between GFMs undoubtedly lead to differences in global flood exposure estimates. These differences can be even more pronounced at the national level, where GFMs have been used to inform disaster risk management (Ward et al., 2015). Flood exposure was calculated for the different GFM river thresholds using the GHS-POP layer. Globally, we found that exposure estimates between the river threshold which results in the largest river network (>50 km^2 UDA), and the river threshold which results in the smallest river network (>5000 km^2 UDA), differ by over a factor of 2. If the size of the river network was further increased by reducing the river threshold to 10 km^2 UDA (below current GFM representation), the exposed population captured increases by 13%.

At the national level, in countries such as Suriname, The Republic of Congo, and Egypt, the greatest proportion of flood risk is posed by rivers with a UDA of 5000 km^2 or greater. In these countries, GFMs could be used interchangeably. Understanding what size rivers pose a significant flood risk is key to accurately representing national flood risk. In Benin, for example, the estimated flood exposure when a 5000 km^2 UDA threshold is applied is 0.49 million people. When the threshold is reduced to 1000 km^2 UDA, the estimated exposure increases to 1.8 million people. Some countries do not have large rivers flowing through them, and the flood risk will result entirely from smaller rivers. Often these are island nations, such as in Jamaica or Trinidad and Tobago, where all flood risk is from rivers smaller than UDA 1000 km^2. However, in Andorra for example, a landlocked country, to capture any flood exposure, a 50 km^2 UDA threshold is needed.

To aid national level flood risk practitioners in their choice of GFM, we calculated the minimum river threshold required to capture a given percentage of the

largest river network's (>50 km^2 UDA) national exposure. Exposure percentages ranging from 10%-90% were calculated for each of the three population datasets used in this study and mapped for each nation, globally. All 27 maps are included in Figures B.15-B.17 in Appendix B. Figure 4.8, which shows the minimum river threshold required to capture at least 50% of possible GHS-POP exposure, illustrates these results. The map shows that while in some countries GFMs could be used interchangeably, in others, the size of the river network could significantly impact national flood exposure estimates.
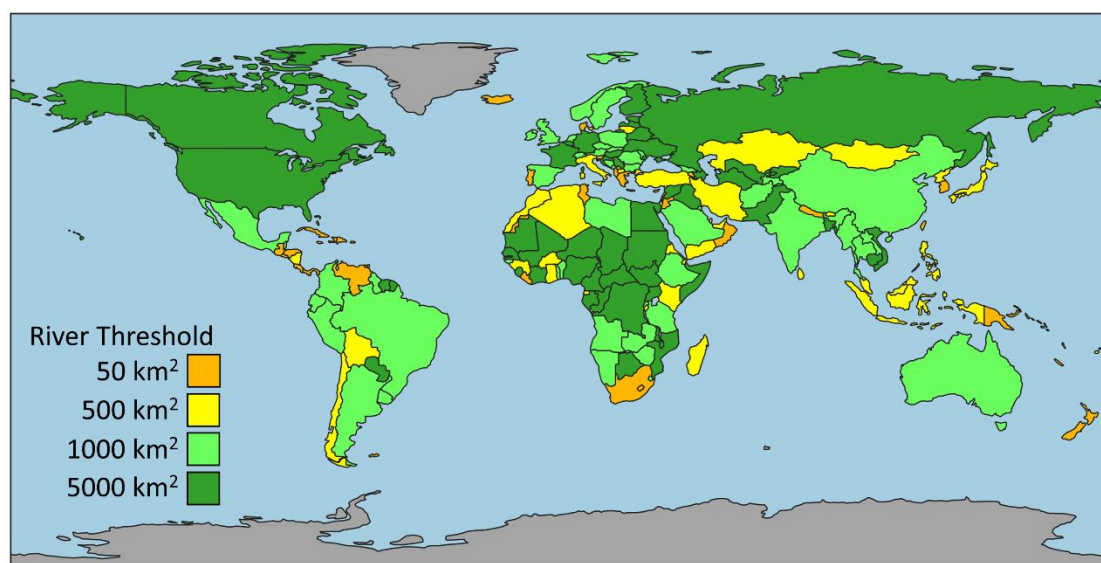
Figure 4.8 In which countries is the choice of river threshold important?

This map shows the global flood model (GFM) river upstream drainage area (UDA) threshold required to capture over half a country's total flood exposure. In dark green countries the choice of threshold is less important than in orange countries. Grey areas are no-data regions. The map was calculated using the Global Human Settlement Population (GHS-POP) layer. See Figures B15-B17 in Appendix B for maps calculated with the other two global population layers and for different percentages of total national exposure population.

It is difficult to exhaustively compare global flood exposure estimates from previous GFM studies as often exposure is expressed differently (e.g. expected annual exposure (EAE) vs. exposure to a return period flood) and sometimes global exposure is not reported at all. In the comparable studies, there is significant variation in global flood exposure estimates. In Ward et al. (2013) global EAE was calculated at 169 Million. This figure is almost triple the 58 Million calculated by

Dottori et al. (2018) and the 54 Million calculated by Alfieri et al. (2017). In studies reporting exposure to a 100-year flood, Hirabayashi et al. (2013) estimate 847 Million people exposed and Jongman et al. (2012) estimate 805 Million exposed.

The need for independent model comparison studies was met by Trigg et al. (2016b) and Aerts et al. (2020) who compared GFM output in Africa and China respectively. These studies compared the output of multiple GFMs, finding large disagreement between the modelled flood extents. Both studies also found large variations in calculated exposure. However, differences in exposure calculated by the GFMs were found to be influenced just as much by different model forcings and resolutions as by differences in river network size. Uncertainty in GFMs needs to be explored across the model cascade to identify where the models need to improve. Studies such as that of Zhou et al. (2020), which explores uncertainty in model forcing, and this study, which explores uncertainties in river network size, are important steps in directing future model development.

Granularity of input data is the main obstacle to increasing river network size in GFMs. The terrain data in all these models, which strongly influences their performance, is derived from the Shuttle Radar and Topography Mission (SRTM), a mission over two decades old (Farr et al., 2007). New, 1 arc second resolution (~ 30 m at the equator) global DEMs have recently been released by both the National and Aeronautics and Space Administration (NASA) and the European Space Agency (ESA). The ESA DEM is particularly important as its elevation is based on newer satellite data from TanDEM-X. A new method for deriving an elevation map from satellite images has also been developed by Google, capable of generating DEMs at 1 m resolution (Nevo, 2019). Whether it is terrain or climatology data, new and improved methods are constantly being developed and better datasets are being released. There is scope in the near future for increasing river network size in GFMs. This comes at a computational cost, however; whether it is the use of a higher-resolution DEM or the exponential increase in number of rivers to model when the threshold river size is reduced. Understanding where the representation of smaller rivers is needed most, namely in areas of high exposure, would streamline the future development of GFMs, targeting improvements in areas where flood risk is highest.

4.5 Conclusions

This study has presented the first global picture of flood exposure categorized by different sized rivers. We introduced a simple geomorphological approach to delineating a river's flood susceptibility, which is suitable for global-scale "first look" studies such as this and importantly, allows an assessment of river network size independent of global flood model structural and computational limitations. We find that over 75% of the global flood exposure is in Asia, with China and India making up a significant proportion of this total. Streams (UDA 10-100 km^2) and small rivers (UDA 100-1000 km^2) are responsible for over half of India's flood risk. At the global scale, these rivers contribute to 45% of total flood exposure, emphasizing the importance of the incorporation of these smaller rivers into global flood risk studies. We find that large increases and decreases in flood exposure over the last 40 years are a result of urbanisation, either inside the flood risk zone or outside of it. The effect that the choice of population dataset had on exposure calculations differed between countries. Globally, this effect was most pronounced on smaller rivers, suggesting future studies that incorporate these smaller rivers should be careful in their choice of population data. Global flood models, the current tools for examining global flood risk, differ significantly in the size of their river networks. We found that the global flood exposure estimates differed by more than a factor of 2 when calculated using the GFM river threshold that results in the largest river network (UDA >50 km^2) compared to the river threshold that results in the smallest river network (UDA >5000 km^2). These differences were often more pronounced at the national level.

The results of this study are intended to inform both the developers and users of global river flood models. Consideration of river network size and how this relates to exposure is imperative to having a comprehensive picture of flood risk. Increasing the size of the river network comes with both data and computational restraints. Doubling the resolution of the models (from 1 km to 90 m to 30 m) requires an order of magnitude increase in computing power. Finer-resolution grids are imperative for representing small streams accurately. This has big implications for models currently operating at coarse resolution. Modelling smaller rivers requires not only detailed high-resolution data, but also efficient modelling

structures capable of running at higher resolutions. Understanding where the representation of small rivers is needed most (areas of high exposure) can focus future model development. Similarly, accurate flood exposure estimates necessitate accurate population data. We have shown that the choice of population data used in exposure calculations can have an enormous impact on flood exposure estimates, and we have identified in which countries this disagreement is most extreme and have identified some of the reasons for this. Flood risk practitioners should use these results as guidance about which population layer is best suited for their locality and use. There is need for further research in this area, incorporating more population data as these layers play such an integral role in flood exposure calculations. In addition to more comparative analyses, there is also an urgent need for these population data to be validated at the global scale with actual data collected on the ground. Only then can definitive conclusions be drawn about the appropriate use of different population datasets. The selection of GFMs available to the end user is large and increasing. However, differences in the size of river networks between the models can have a significant impact on flood exposure estimates. While available GFMs could be used interchangeably in some countries, in others, discrepancies in river network size would lead to vastly different national flood exposure estimates. The results of this study should help to inform GFM users about the appropriate choice of GFM for their country of interest.

4.6 Acknowledgements

References

AERTS, J. P. M., UHLEMANN-ELMER, S., EILANDER, D. & WARD, P. J. 2020. Comparison of estimates of global flood models for flood hazard and exposed gross domestic product: a China case study. *Nat. Hazards Earth Syst. Sci.,* 20**,** 3245-3260.
ALFIERI, L., BISSELINK, B., DOTTORI, F., NAUMANN, G., DE ROO, A., SALAMON, P., WYSER, K. & FEYEN, L. 2017. Global projections of river flood risk in a warmer world. *Earths Future,* 5**,** 171-182.

ANNIS, A., NARDI, F., MORRISON, R. R. & CASTELLI, F. 2019. Investigating hydrogeomorphic floodplain mapping performance with varying DTM resolution and stream order. *Hydrological Sciences Journal,* 64**,** 525-538.

BAKRANIA, S. 2015. Urbanisation and urban growth in Nepal. *GSDRC Helpdesk Research Report 1294.* Birmingham, UK: GSDRC University of Birmingham.

BERNHOFEN, M. V., TRIGG, M. A., SLEIGH, P. A., SAMPSON, C. & SMITH, A. 2021. River Flood Susceptibility Map.

BERNHOFEN, M. V., WHYMAN, C., TRIGG, M. A., SLEIGH, P. A., SMITH, A., SAMPSON, C., YAMAZAKI, D., WARD, P., RUDARI, R., PAPPENBERGER, F., DOTTORI, F., SALAMON, P. & WINSEMIUS, H. C. 2018a. Analysis inputs for validation of six global flood models against observed flood events in Nigeria and Mozambique. Research Data Leeds Repository.

BERNHOFEN, M. V., WHYMAN, C., TRIGG, M. A., SLEIGH, P. A., SMITH, A. M., SAMPSON, C. C., YAMAZAKI, D., WARD, P. J., RUDARI, R., PAPPENBERGER, F., DOTTORI, F., SALAMON, P. & WINSEMIUS, H. C. 2018b. A first collective validation of global fluvial flood models for major floods in Nigeria and Mozambique. *Environmental Research Letters,* 13.

CENTER FOR INTERNATIONAL EARTH SCIENCE INFORMATION NETWORK - CIESIN - COLUMBIA UNIVERSITY 2016. Gridded Population of the World, Version 4 (GPWv4): Population Count. Palisades, NY: NASA Socioeconomic Data and Applications Center (SEDAC).

CEOLA, S., LAIO, F. & MONTANARI, A. 2014. Satellite nighttime lights reveal increasing human exposure to floods worldwide. *Geophysical Research Letters,* 41**,** 7184-7190.

CHEN, S.-A., MICHAELIDES, K., GRIEVE, S. W. D. & SINGER, M. B. 2019. Aridity is expressed in river topography globally. *Nature.*

CRED & UNDRR 2020. *The Human Cost of Natural Disasters - An overview of the last 20 years 2000-2019.*

DI BALDASSARRE, G., NARDI, F., ANNIS, A., ODONGO, V., RUSCA, M. & GRIMALDI, S. 2020. Brief communication: Comparing hydrological and hydrogeomorphic paradigms for global flood hazard mapping. *Nat. Hazards Earth Syst. Sci.,* 20**,** 1415-1419.

DODOV, B. A. & FOUFOULA-GEORGIOU, E. 2006. Floodplain morphometry extraction from a high-resolution digital elevation model: a simple algorithm for regional analysis studies. *IEEE Geoscience and Remote Sensing Letters,* 3**,** 410-413.

DOTTORI, F., ALFIERI, L., SALAMON, P., BIANCHI, A., FEYEN, L. & HIRPA, F. A. 2016a. Flood hazard map of the World - 100-year return period. *In:* EUROPEAN COMMISSION, J. R. C. J. (ed.).

DOTTORI, F., ALFIERI, L., SALAMON, P., BIANCHI, A., FEYEN, L. & LORINI, V. 2016b. Flood hazard map for Europe, 100-year return period. *In:* EUROPEAN COMMISSION, J. R. C. J. (ed.).

DOTTORI, F., SALAMON, P., BIANCHI, A., ALFIERI, L., HIRPA, F. A. & FEYEN, L. 2016c. Development and evaluation of a framework for global flood hazard mapping. *Advances in Water Resources,* 94**,** 87-102.

DOTTORI, F., SZEWCZYK, W., CISCAR, J. C., ZHAO, F., ALFIERI, L., HIRABAYASHI, Y., BIANCHI, A., MONGELLI, I., FRIELER, K.,

BETTS, R. A. & FEYEN, L. 2018. Increased human and economic losses from river flooding with anthropogenic warming. *Nature Climate Change,* 8**,** 781-+.

FACEBOOK. 2019. *Data for Good: Population Density Maps* [Online]. Available: https://dataforgood.fb.com/tools/population-density-maps/ [Accessed December 2020].

FACEBOOK & CIESIN 2016. High Resolution Settlement Layer (HRSL). *In:* UNIVERSITY, F. C. L. A. C. F. I. E. S. I. N.-C.-C. (ed.).

FARR, T. G., ROSEN, P. A., CARO, E., CRIPPEN, R., DUREN, R., HENSLEY, S., KOBRICK, M., PALLER, M., RODRIGUEZ, E., ROTH, L., SEAL, D., SHAFFER, S., SHIMADA, J., UMLAND, J., WERNER, M., OSKIN, M., BURBANK, D. & ALSDORF, D. 2007. The shuttle radar topography mission. *Reviews of Geophysics,* 45**,** 33.

FREIRE, S., KEMPER, T., PESARESI, M., FLORCZYK, A. & SYRRIS, V. Combining GHSL and GPW to improve global population mapping. 2015 IEEE International Geoscience and Remote Sensing Symposium (IGARSS), 26-31 July 2015 2015. 2541-2543.

FREIRE, S., MACMANUS, K., PESARESI, M., DOXSEY-WHITFIELD, E. & MILLS, J. 2016. *Development of new open and free multi-temporal global population grids at 250 m resolution*.

FREIRE, S., SCHIAVINA, M., FLORCZYK, A. J., MACMANUS, K., PESARESI, M., CORBANE, C., BORKOVSKA, O., MILLS, J., PISTOLESI, L., SQUIRES, J. & SLIUZAS, R. 2020. Enhanced data and methods for improving open and free global population grids: putting 'leaving no one behind' into practice. *International Journal of Digital Earth,* 13**,** 61-77.

HIRABAYASHI, Y., MAHENDRAN, R., KOIRALA, S., KONOSHIMA, L., YAMAZAKI, D., WATANABE, S., KIM, H. & KANAE, S. 2013. Global flood risk under climate change. *Nature Climate Change,* 3**,** 816-821.

JAFARZADEGAN, K., MERWADE, V. & SAKSENA, S. 2018. A geomorphic approach to 100-year floodplain mapping for the Conterminous United States. *Journal of Hydrology,* 561**,** 43-58.

JONGMAN, B., WARD, P. J. & AERTS, J. 2012. Global exposure to river and coastal flooding: Long term trends and changes. *Global Environmental Change-Human and Policy Dimensions,* 22**,** 823-835.

KUMMU, M., DE MOEL, H., WARD, P. J. & VARIS, O. 2011. How Close Do We Live to Water? A Global Analysis of Population Distance to Freshwater Bodies. *Plos One,* 6**,** 13.

LEHNER, B. & GRILL, G. 2013. Global river hydrography and network routing: baseline data and new approaches to study the world's large river systems. Hydrological Processes.

LEHNER, B., VERDIN, K. & JARVIS, A. 2008. New Global Hydrography Derived From Spaceborne Elevation Data. *Eos, Transactions American Geophysical Union,* 89**,** 93-94.

LEYK, S., GAUGHAN, A. E., ADAMO, S. B., DE SHERBININ, A., BALK, D., FREIRE, S., ROSE, A., STEVENS, F. R., BLANKESPOOR, B., FRYE, C., COMENETZ, J., SORICHETTA, A., MACMANUS, K., PISTOLESI, L., LEVY, M., TATEM, A. J. & PESARESI, M. 2019. The spatial allocation of population: a review of large-scale gridded population data products and their fitness for use. *Earth Syst. Sci. Data,* 11**,** 1385-1409.

LIU, F., WANG, S., XU, Y., YING, Q., YANG, F. & QIN, Y. 2020. Accuracy assessment of Global Human Settlement Layer (GHSL) built-up products over China. *PLOS ONE,* 15**,** e0233164.

LLOYD, C. T., CHAMBERLAIN, H., KERR, D., YETMAN, G., PISTOLESI, L., STEVENS, F. R., GAUGHAN, A. E., NIEVES, J. J., HORNBY, G., MACMANUS, K., SINHA, P., BONDARENKO, M., SORICHETTA, A. & TATEM, A. J. 2019. Global spatio-temporally harmonised datasets for producing high-resolution gridded population distribution datasets. *Big Earth Data,* 3**,** 108-139.

LUGERI, N., KUNDZEWICZ, Z. W., GENOVESE, E., HOCHRAINER, S. & RADZIEJEWSKI, M. 2010. River flood risk and adaptation in Europe—assessment of the present status. *Mitigation and Adaptation Strategies for Global Change,* 15**,** 621-639.

MANFREDA, S., NARDI, F., SAMELA, C., GRIMALDI, S., TARAMASSO, A. C., ROTH, G. & SOLE, A. 2014. Investigation on the use of geomorphic approaches for the delineation of flood prone areas. *Journal of Hydrology,* 517**,** 863-876.

MCCOOL, S. F., CLARK, R. N. & STANKEY, G. H. 2009. *Water and People: Challenges at the Interface of Symbolic and Utilitarian Values*, DIANE Publishing.

MONTGOMERY, D. R. & DIETRICH, W. E. 1988. Where do channels begin? 336**,** 232.

NARDI, F., ANNIS, A., DI BALDASSARRE, G., VIVONI, E. R. & GRIMALDI, S. 2019. GFPLAIN250m, a global high-resolution dataset of Earth's floodplains. *Scientific Data,* 6**,** 180309.

NARDI, F., VIVONI, E. R. & GRIMALDI, S. 2006. Investigating a floodplain scaling relation using a hydrogeomorphic delineation method. 42.

NEVO, S. 2019. An Inside Look at Flood Forecasting. *Google AI Blog* [Online]. Available from: https://ai.googleblog.com/2019/09/an-inside-look-at-flood-forecasting.html.

NOBRE, A. D., CUARTAS, L. A., HODNETT, M., RENNO, C. D., RODRIGUES, G., SILVEIRA, A., WATERLOO, M. & SALESKA, S. 2011. Height Above the Nearest Drainage - a hydrologically relevant new terrain model. *Journal of Hydrology,* 404**,** 13-29.

NOBRE, A. D., CUARTAS, L. A., MOMO, M. R., SEVERO, D. L., PINHEIRO, A. & NOBRE, C. A. 2016. HAND contour: a new proxy predictor of inundation extent. *Hydrological Processes,* 30**,** 320-333.

OCHA 2020. Sudan: Floods Flash Update No. 8. OCHA.

PALACIOS-LOPEZ, D., BACHOFER, F., ESCH, T., HELDENS, W., HIRNER, A., MARCONCINI, M., SORICHETTA, A., ZEIDLER, J., KUENZER, C., DECH, S., TATEM, A. J. & REINARTZ, P. 2019. New Perspectives for Mapping Global Population Distribution Using World Settlement Footprint Products. 11**,** 6056.

PAPPENBERGER, F., DUTRA, E., WETTERHALL, F. & CLOKE, H. L. 2012. Deriving global flood hazard maps of fluvial floods through a physical model cascade. *Hydrology and Earth System Sciences,* 16**,** 4143-4156.

RUDARI, R., SILVESTRO, F., CAMPO, L., REBORA, N., BONI, G. & HEROLD, C. 2015. IMPROVEMENT OF THE GLOBAL FLOOD MODEL FOR THE GAR 2015.

SAMELA, C., TROY, T. J. & MANFREDA, S. 2017. Geomorphic classifiers for flood-prone areas delineation for data-scarce environments. *Advances in Water Resources,* 102**,** 13-28.

SAMPSON, C. C., SMITH, A. M., BATES, P. B., NEAL, J. C., ALFIERI, L. & FREER, J. E. 2015. A high-resolution global flood hazard model. *Water Resources Research,* 51**,** 7358-7381.

SCHIAVINA, M. F., S.; MACMANUS, K 2019. GHS population grid multitemporal (1975, 1990, 2000, 2015). European Commission, Joint Research Centre (JRC).

SCUSSOLINI, P., AERTS, J., JONGMAN, B., BOUWER, L. M., WINSEMIUS, H. C., DE MOEL, H. & WARD, P. J. 2016. FLOPROS: an evolving global database of flood protection standards. *Natural Hazards and Earth System Sciences,* 16**,** 1049-1061.

SMITH, A., BATES, P. D., WING, O., SAMPSON, C., QUINN, N. & NEAL, J. 2019. New estimates of flood exposure in developing countries using high-resolution population data. *Nature Communications,* 10**,** 1814.

SMITH, A., SAMPSON, C. & BATES, P. 2015. Regional flood frequency analysis at the global scale. *Water Resources Research,* 51**,** 539-553.

STEVENS, F. R., GAUGHAN, A. E., LINARD, C. & TATEM, A. J. 2015. Disaggregating Census Data for Population Mapping Using Random Forests with Remotely-Sensed and Ancillary Data. *Plos One,* 10**,** 22.

STOKKOM, H., SMITS, A. & LEUVEN, R. S. E. W. 2005. Flood defense in The Netherlands: A New Era, A New Approach. *Water International - WATER INT,* 30**,** 76-87.

STRAHLER, A. N. 1957. Quantitative analysis of watershed geomorphology. *Eos, Transactions American Geophysical Union,* 38**,** 913-920.

TANOUE, M., HIRABAYASHI, Y. & IKEUCHI, H. 2016. Global-scale river flood vulnerability in the last 50 years. *Scientific Reports,* 6**,** 36021.

TARBOTON, D. G., BRAS, R. L. & RODRIGUEZ-ITURBE, I. J. H. P. 1991. On the extraction of channel networks from digital elevation data. 5**,** 81.

TIECKE, T. G. L., XIANMING ZHANG, AMY GROS, ANDREAS LI, NAN YETMAN, GREGORY KILIC, TALIP MURRAY, SIOBHAN BLANKESPOOR, BRIAN PRYDZ, ESPEN B. DANG, HAI-ANH H. 2017. *Mapping the World Population One Building at a Time*.

TRENDS 2020. Leaving no one off the map: a guide for gridded population data for sustainable development. Thematic Research Network on Data and Statistics.

TRIGG, M. A., BIRCH, C. E., NEAL, J., BATES, P., SMITH, A., SAMPSON, C., YAMAZAKI, D., HIRABAYASHI, Y., PAPPENBERGER, F., DUTRA, E., WARD, P. J., WINSEMIUS, H. C., SALAMON, P., DOTTORI, F., RUDARI, R., KAPPES, M. S., SIMPSON, A., HADZILACOS, G. & FEWTRELL, T. 2016a. Aggregated fluvial flood hazard output for six Global Flood Models for the African Continent. Research Data Leeds Repository.

TRIGG, M. A., BIRCH, C. E., NEAL, J. C., BATES, P. D., SMITH, A., SAMPSON, C. C., YAMAZAKI, D., HIRABAYASHI, Y., PAPPENBERGER, F., DUTRA, E., WARD, P. J., WINSEMIUS, H. C., SALAMON, P., DOTTORI, F., RUDARI, R., KAPPES, M. S., SIMPSON, A. L., HADZILACOS, G. & FEWTRELL, T. J. 2016b. The credibility challenge for global fluvial flood risk analysis. *Environmental Research Letters,* 11**,** 10.

WARD, P. J., BLAUHUT, V., BLOEMENDAAL, N., DANIELL, J. E., DE
        RUITER, M. C., DUNCAN, M. J., EMBERSON, R., JENKINS, S. F.,
        KIRSCHBAUM, D., KUNZ, M., MOHR, S., MUIS, S., RIDDELL, G. A.,
        SCHÄFER, A., STANLEY, T., VELDKAMP, T. I. E. & WINSEMIUS, H.
        C. 2020. Review article: Natural hazard risk assessments at the global scale.
        Nat. Hazards Earth Syst. Sci., 20**,** 1069-1096.
WARD, P. J., JONGMAN, B., SALAMON, P., SIMPSON, A., BATES, P., DE
        GROEVE, T., MUIS, S., DE PEREZ, E. C., RUDARI, R., TRIGG, M. A. &
        WINSEMIUS, H. C. 2015. Usefulness and limitations of global flood risk
        models. *Nature Climate Change,* 5**,** 712-715.
WARD, P. J., JONGMAN, B., WEILAND, F. S., BOUWMAN, A., VAN BEEK,
        R., BIERKENS, M. F. P., LIGTVOET, W. & WINSEMIUS, H. C. 2013.
        Assessing flood risk at the global scale: model setup, results, and sensitivity.
        Environmental Research Letters, 8**,** 10.
WARDROP, N. A., JOCHEM, W. C., BIRD, T. J., CHAMBERLAIN, H. R.,
        CLARKE, D., KERR, D., BENGTSSON, L., JURAN, S., SEAMAN, V. &
        TATEM, A. J. 2018. Spatially disaggregated population estimates in the
        absence of national population and housing census data. 115**,** 3529-3537.
WILKS, D. 2006. *Statistical Methods in the Atmospheric Sciences,* United States of
        America, Elsevier.
WING, O. E. J., BATES, P. D., SAMPSON, C. C., SMITH, A. M., JOHNSON, K.
        A. & ERICKSON, T. A. 2017. Validation of a 30 m resolution flood hazard
        model of the conterminous United States. *Water Resources Research,* 53**,**
        7968-7986.
WINSEMIUS, H. C., VAN BEEK, L. P. H., JONGMAN, B., WARD, P. J. &
        BOUWMAN, A. 2013. A framework for global river flood risk assessments.
        Hydrology and Earth System Sciences, 17**,** 1871-1892.
WORLDBANK 2018. United Nation's Population Division's World Urbanization
        Prospects: 2018 Revision. *In:* WORLDBANK (ed.).
WORLDBANK. 2019. *Over 350,000 Surinamese to Benifit from Flood Risk
        Management* [Online]. reliefweb. Available:
        https://reliefweb.int/report/suriname/over-350000-surinamese-benefit-flood-
        risk-management [Accessed].
YAMAZAKI, D., IKESHIMA, D., SOSA, J., BATES, P. D., ALLEN, G. H. &
        PAVELSKY, T. M. 2019. MERIT Hydro: A High-Resolution Global
        Hydrography Map Based on Latest Topography Dataset. *Water Resources
        Research,* 55**,** 5053-5073.
YAMAZAKI, D., IKESHIMA, D., TAWATARI, R., YAMAGUCHI, T.,
        O'LOUGHLIN, F., NEAL, J. C., SAMPSON, C. C., KANAE, S. & BATES,
        P. D. 2017. A high-accuracy map of global terrain elevations. *Geophysical
        Research Letters,* 44**,** 5844-5853.
YAMAZAKI, D., KANAE, S., KIM, H. & OKI, T. 2011. A physically based
        description of floodplain inundation dynamics in a global river routing
        model. *Water Resources Research,* 47**,** 21.
ZHOU, X., MA, W., ECHIZENYA, W. & YAMAZAKI, D. 2020. Uncertainty in
        flood frequency analysis of hydrodynamic model simulations. *Nat. Hazards
        Earth Syst. Sci. Discuss.,* 2020**,** 1-31.

Chapter 5

The role of global datasets for flood risk management at national scales

5.1 Abstract

Over the last two decades, several datasets have been developed to assess flood risk at the global scale. In recent years, some of these datasets have become detailed enough to be informative at national scales. The use of these datasets nationally could have enormous benefits in areas lacking existing flood risk information and allow better flood management decisions and disaster response. In this study, we evaluate the usefulness of global data for assessing flood risk in five countries: Colombia, England, Ethiopia, India, and Malaysia. National flood risk assessments are carried out for each of the five countries using global datasets and methodologies. We also conduct interviews with key water experts in each country to explore what capacity there is to use these global datasets nationally. To assess national flood risk, we use 6 datasets of global flood hazard, 7 datasets of global population, and 3 different methods for calculating vulnerability that have been used in previous global studies of flood risk. We find that the datasets differ substantially at the national level, and this is reflected in the national flood risk estimates. While some global datasets could be of significant value for national flood risk management, others are either not detailed enough, or too outdated to be relevant at this scale. For the relevant global datasets to be used most effectively for national flood risk management, a country needs a functioning, institutional framework with capability to support their use and implementation.

5.2 Introduction

Flooding is a global problem that affects most regions in the world. In the last twenty years, over 1.65 Billion people were affected by flooding (UNDRR, 2020), while estimated losses as a result of flood events exceeded 1 Trillion US Dollars over the last forty years (MunichRE). The impacts of flooding can be reduced through good flood risk management (FRM). For FRM measures to be most

effective, they need to be implemented in areas of high flood risk, which are identified through flood risk assessments. These assessments follow the conceptual framework that flood risk is a product of hazard (the flooding), exposure (who or what is exposed to the flooding), and vulnerability (the susceptibility of the exposure to damages) (UNISDR, 2015).

The objectives and data required for flood risk assessments change with the spatial scale of the analysis (de Moel et al., 2015). At the city or basin scale, flood risk assessments are carried out using locally calibrated models and data. The results of assessments at this scale are used to inform local flood management strategies and the design of flood mitigation infrastructure. National scale flood risk assessments either combine regionally derived flood information into a national picture of flood risk, such as with the National Flood Insurance Program (NFIP) in the US (Burby, 2001) and the National Flood Risk Assessment (NaFRA) in the UK (Environment Agency, 2009), or risk is mapped nationally in its entirety (Hall et al., 2003, Hall et al., 2005). The objectives of national flood risk assessments are to inform joined up strategic FRM, allowing for prioritized evidence-based interventions. They also provide nationally consistent data for planning. For flood risk assessments at these scales, there is a bias in the evidence base towards contexts with greater research and monitoring capability. Since the mid-2000s, efforts have been made to assess flood risk at the global scale using globally available data (Hall, 2014, Ward et al., 2020a). Global flood risk assessments are a multi-national equivalent of the national approach. International agencies and stakeholders want consistent data and approaches to make strategic investments at the global scale. Early global assessments used simple coarse resolution flood risk data, necessary at the time to assess flood risk at such large spatial scales (Dilley et al., 2005, Hirabayashi et al., 2008). Recent advances in global flood risk data, both in resolution and accuracy, have expanded their potential usefulness beyond global studies of flood risk to include more local applications, filling data gaps that had previously precluded flood risk assessments in data and institutional capability constrained regions. Some global data are now detailed enough to be relevant at national and catchment scales. This could, in theory, have potential benefits in areas lacking existing flood risk information and allow better flood management decisions and disaster response. Whilst the list of global datasets is large and growing

(Lindersson et al., 2020), not all global datasets are created equally. There is an urgent need to evaluate available global flood risk datasets for use at the national scale.

There are two approaches to representing flood hazard globally: either through remote sensing (RS) of historical flood events or through global flood models (GFMs). The two are often considered complimentary (Hawker et al., 2020), as RS data is used to validate the global models (Bernhofen et al., 2018, Mester et al., 2021). GFMs use global datasets, automated methods, and simplified hydraulic equations to simulate flood hazard globally (Trigg et al., 2020). These models, which began as research experiments, are now being used for disaster response (Emerton et al., 2020), to inform policy decisions (Ward et al., 2015), to assess business risks (Ward et al., 2020b), and recently their modelling frameworks have incorporated detailed national level data to assess national flood risk (Wing et al., 2017, Wing et al., 2018, Bates et al., 2021). Several GFMs have been developed in academia (Yamazaki et al., 2011, Ward et al., 2013), by research institutions (Dottori et al., 2016, Rudari et al., 2015), and by commercial companies (Sampson et al., 2015). Their differing approaches to global flood hazard mapping result in flood extent disagreement (Trigg et al., 2016, Aerts et al., 2020) and varied performance (Bernhofen et al., 2018), suggesting no single model is uniformly fit for purpose.

Similarly, global population maps, necessary for calculating exposure, adopt equally divergent approaches to mapping human population. These range in complexity from simply distributing census data across administrative boundaries to statistically estimating population distribution and density from auxiliary datasets that relate to human presence (Leyk et al., 2019). Recent studies by Smith et al. (2019) and Bernhofen et al. (2021) found that flood exposure estimates are significantly impacted by the population dataset used. As these datasets become increasingly locally relevant, there is an urgent need to investigate their fitness-for-use in flood risk assessments at these scales.

A key component of flood risk assessments, frequently absent from global studies, is vulnerability (Ward et al., 2020a). Vulnerability is multifaceted; it can be assessed through societal, economic, environmental, or physical means (Birkmann et al., 2006). The most visible, and most commonly assessed, aspect of vulnerability is

direct damages (Meyer et al., 2013). Direct damages are typically calculated using some form of vulnerability curve, which translates a component of the modelled flood hazard (often depth) into a degree of damage. Depth-damage curves are derived from data collected from historical flood events or expert judgement; or a combination of the two (van Westen, 2014). As a result, vulnerability functions are globally disparate. In countries with a wealth of historical data, such as the UK (Penning-Rowsell et al., 2013), the Netherlands (Kok, 2004), and the US (Davis and Skaggs, 1992) there are detailed vulnerability functions, whereas in other countries there are none at all. These data gaps were addressed by Huizinga et al. (2017) who developed a global database of depth-damage functions for multiple land-use classes. Significant uncertainties remain, however, both in the datasets used to identify assets at risk in the vulnerability calculations and in the assumptions made about the land-use classes.

A cross-disciplinary approach needs to be taken when evaluating global datasets for FRM at national scales (Morrison et al., 2018). The physical science (global data) needs to be understood in the context of the social science. There needs to be a focus on the capabilities of regional and local governance in interpreting and using this data to inform and address flood risk. Governing bodies require datasets to be accessible, unambiguous, and easy to use; however, variability between datasets poses risks for effective policy and decision-making, for example the different conceptualizations of vulnerability may not translate to actual administrative and political structures. Also integral is the capacity of organizations and other governance structures to use the data. Human, technical, and financial resources of services are often lacking. Failures in coordination and communication between related departments and other relevant stakeholders over other scales may result in the incorrect use of data. For example, the dissemination of data to the local scale can be complicated and challenged by local priorities, alternative perceptions, elite capture, and language. Data also has the potential to be manipulated and/or abused in power struggles or for political motives (Wissman-Weber and Levy, 2018, Venot et al., 2021).

The UK Research and Innovation (UKRI) Global Challenges Research Fund (GCRF) Water Security and Sustainable Development Hub project (https://www.watersecurityhub.org/) connects water experts in five different

countries, spanning four continents. This project provides a unique opportunity to test the global datasets for use at these scales in countries with vastly different histories of flooding and flood management structures and allows us to explore the commonality and variability of global data used locally. In this paper, we use global datasets and methods from previously published studies of global flood risk to carry out flood risk assessments in five countries: Colombia, England, Ethiopia, India, and Malaysia. We calculate national flood risk using a 20-year catalogue of historical flooding, five GFMs, seven global population datasets, and three approaches to calculating vulnerability. We then assess the credibility of this data for use at the national scale considering the variability of the flood risk estimates and exploring the implications this has on their usefulness. We also examine the capacity to use this data for FRM in each country.

5.3   National Flood Risk Management Approaches, Study Countries, and the Role of Global Data

5.3.1   National Flood Risk Management Approaches

There are two distinctive approaches to FRM, as laid out by Morrison et al. (2018): the resistance approach and the adaptive approach. The resistance, or standard, approach to FRM consists of mitigating flood risks through infrastructure or laws and regulations. The adaptive approach focusses less on preventing flooding and places greater emphasis on increasing resilience in high risk areas (Schelfaut et al., 2011). The approaches are complimentary, and successful examples of FRM often consist of a marriage of the two (van Wesenbeeck et al., 2014).

The implementation of FRM strategies typically falls on the government. The level of government responsible for executing FRM strategies is dependent on the country and the strategy being implemented (Merz et al., 2010). Governance strategies to FRM vary, as countries prioritize certain approaches over others (Driessen et al., 2018). Governance strategies can be hierarchical, consisting of a traditional 'top down' decision making structure (Alexander et al., 2016a); they can be decentralized, where policy decisions are made at the local level with a greater emphasis placed on stakeholder engagement (Driessen et al., 2012); they can be polycentric, where policy power is shared between different levels of government and non-government stakeholders (Loeschner et al., 2019, Garvey and Paavola,

2021); or they can be panarchy, which is an adaptive approach to governance that consists of a nested set of adaptive cycles (Gunderson and S, 2002, Alexander et al., 2016a), where certain conditions can trigger 'bottom up' changes in the system (Garmestani and Benson, 2013).

To evaluate global flood risk data for use at the national scale it is important to understand a country's approach to national FRM. Where, and how, the data will be used will depend on the national FRM strategy and who is responsible for implementing it. Taking a multi-country approach, as we are doing, enables us to pick apart the differences and commonalities in national strategies and how these influence the applicability of global flood risk data in a national flood risk context.

5.3.2 Study Countries

We evaluate the global data for use at the national level in five countries: Colombia, England, Ethiopia, India, and Malaysia. These five countries bring together local communities and 46 different stakeholder partners that work together to address water security issues in the Global Challenges Research Fund (GCRF) funded Water Security and Sustainable Development Hub (https://www.watersecurityhub.org/). Below, we briefly summarize flood risk in each country and how it is managed.

5.3.2.1 Colombia

Colombia is particularly susceptible to extreme weather events such as hurricanes, storms, and flooding due to its hydro-climatology that emerges from Colombia being located in the Intertropical Convergence Zone (ITCZ). The ITCZ is a place where both warm and humid winds from Northern and Southern latitudes converge, creating a belt of clouds. This situation generates constant provision of wind and humidity that, when interacting with topography, defines the rainy and dry seasons. The hydro-climatology is further influenced by El Niño–Southern Oscillation (ENSO). The cold phase of ENSO, otherwise known as La Niña, increases rainfall which leads to increased river flow and flooding. For example, in 2011 four million people were affected by a strong La Niña event, causing losses of $7.8 billion through damage to economic infrastructure, flooding of agricultural land, and the issuing of government subsidies (Hoyos et al., 2013). Climate change is also projected to increase rainfall by 2.5% by 2050 which will further increase

incidences of flooding (Ramirez-Villegas et al., 2012). Colombia manages flood risk alongside other risks posed by volcanos, landslides, and earthquakes under their National Disaster Risk Management System (UNGRD in Spanish). Policy, legislation, and regulations under this system are decentralized over the global, national, regional, and local levels to directly include public entities, non-profit entities and communities within the policy's remit and subsequent activities. Colombia takes an ex-post approach to FRM through a reaction to flood events which occur.

5.3.2.2 England

Flooding has been recognized by the UK government as one of the most serious threats facing the country. The National Flood Risk Assessment (NaFRA) estimate that one in six commercial and residential properties are at risk from surface water, fluvial, and coastal flooding. These risks are exacerbated by factors such as population growth, deteriorating drainage infrastructure, land use change and natural erosive processes, and will worsen with climate change (Alexander et al., 2016b). Extreme flood events have become more frequent in recent years, for example, Kendon et al. (2019) report that in 2019 England and Wales had its fifth wettest autumn since 1766 resulting in severe flooding in Yorkshire, Nottinghamshire, Derbyshire, and Lincolnshire; the most severe flood event to occur in the UK since 2015. Governed by the Department for Environment, Food and Rural Affairs (DEFRA), current flood risk policy centres on resilience to manage flood and climate change risk and to protect economic growth and infrastructure. It recognizes the importance of public participation over a decentralized structure to nurture long term and flexible approaches; to enable life to continue alongside water rather than keeping water out (Forrest et al., 2017). This entails community groups working alongside other flood related agencies to come up with long term solutions.

5.3.2.3 Ethiopia

Ethiopia is exposed to a wide range of disasters associated with the country's diverse geo-climatic and socio-economic conditions, but floods and droughts represent major challenges to communities and livelihoods. Flooding has become one of the most common, frequent, and severe natural disasters in Ethiopia affecting lowlands, highland, and urban areas; displacing thousands and causing loss of property and livelihoods. Increased rainfall variability and extreme events have

increased the likelihood of flooding, while risk is exacerbated by rapid population growth and urbanization, particularly in Addis Ababa the capital (Haile et al., 2013a, Beshir and Song, 2021). Environmental degradation, poverty and conflict further aggravate the risks and reduce the coping capacity and resilience of communities. For example, Haile et al. (2013b), illustrate how resettlement programs by the Ethiopian Government between 1983 and 1996 in the lowland region Gambela and consequent land use change resulted in increased flood events that affected up to a third of the population in some woredas. FRM in Ethiopia is governed by the National Disaster Risk Management Commission (NDRMC), established in 2015, to coordinate an integrated approach with all hazards to streamline their disaster risk management approach over multiple administrative scales to including an early warning and response system across all government sectors. The Government of Ethiopia (GOE) has a long institutional history of addressing disaster risk management (DRM), starting with the establishment of the Relief and Rehabilitation Commission (RRC) following the 1974 famines. Since then, the country has taken several steps to shift to a more proactive approach to DRM. This includes updating the National Policy and Strategy on DRM (2013) and developing a DRM Strategic Program and Investment Framework (SPIF) for government and donor interventions in 2014 (DRMFSS, 2014).

5.3.2.4 India

Flood risk in India differs across the country due to the various geomorphological locations and different atmospheric circulations. The Indian Summer Monsoon through several transient atmospheric conditions brings rain to different parts of the country via different monsoonal phases as onset and advance (mid-May to mid-July), peak rainfall (July to August) and withdrawal (mid-September to mid-October). Rainfall intensity and extreme flood events have increased in intensity between 1951 and 2015 (Vinnarasi and Dhanya, 2016, Ray et al., 2019). Flood risk is particularly severe for urban settlements in India due to the huge populations who reside in mega-cities (population of over 1 million). The number of mega-cities has risen exponentially to 52 cities over the last two decades due to migration from rural areas (De et al., 2013). Flooding and water-logging have become common occurrences due to the reduction of green spaces and aging storm drains which struggle to cope, especially during the monsoon seasons, leading to

loss of income and increased disease risk (Ali et al., 2021). In the capital, Delhi, 24,840 hectares of the city is built on floodplains, 68% of which are the low-lying Yamuna floodplains. The apex organization for flood management schemes of India is the Central Water Commission (CWC). However, FRM in India is always state-led, with the federal government only assisting when relief measures (e.g., through National Disaster Response Force (NDRF), State Disaster Response Fund (SDRF) etc.) are required. Many States, especially the ones which are flood-prone, have established Flood Control Boards, organized by the respective Irrigation Departments (majorly), to assess the flood problems and evaluate the flood schemes. For example, the Irrigation and Flood Control Department leads FRM in Delhi. The city is demarcated into six drainage zones, and twelve municipal zones manage the storm run-off between them for the whole city. This approach reflects the structural approach of policy to flood risk which focuses on mainly infrastructural measures to control flooding. Different structural/administrative measures have been adopted by these organizations to reduce the flood losses and protect the flood plains across India. In addition to the several laws enacted by the Central Government (e.g., Inter-state River Disputes Act 1956, The River Boards Act of 1956, Damodar Valley Corporation Act, 1948, Betwa River Board Act, 1976, Brahmaputra Board Act, 1980, The Land Acquisition Act, 1894 etc.), a few States have also enacted laws to deal with disputes related to flood control works (CWC, 2018).

5.3.2.5 Malaysia

Malaysia is severely affected by flooding. Eighty-five of Malaysia's 189 river basins are prone to recurrent flooding, all of which flow into the South China Sea (Saifulsyahira et al., 2016). Rainfall intensity in Malaysia is high all year round, with most of the flooding occurring between November and February during the Northeast Monsoon. For example, in January 2021, six people died and 50,000 were displaced during the monsoon on the east coast (Al Jazeera, 2021). Flash floods have also become more common with increased urbanization, infrastructure development alongside rivers, and the poor maintenance of drains and waterways (Yusoff et al., 2018, Mabahwi et al., 2020). FRM in Malaysia is driven by the federal government and characterized by a mostly technocratic approach. The Department of Irrigation and Drainage Malaysia (DID) is the main entity involved with flood management which includes the management of hydrological data, planning and development of flood defences, planning and development of flood

mitigation, management of national river resources, and coordination of other relevant agencies over federal, state and district administrative levels (Mabahwi et al., 2020).

5.3.3   The Role of Global Data

The use of global datasets to assess national flood risk is dependent on the extent to which countries have the capacity, institutions, and governance structures to use and interpret the information. Many countries, especially those in the Global South, frequently lack the resources, expertise and strong institutional frameworks needed to access, collect, interpret, and analyse available datasets to implement effective FRM. For example, in Colombia, the gap between policy, the political will, and capacity to act on flooding influences FRM; also the country's ex-post approach to FRM may limit the usefulness of these datasets (Key Informant Interview, Universidad del Valle, 2021). In Malaysia, efforts to manage flood disasters are hampered by a lack of legislative guidance on the management of flooding within the National Disaster Management Agency (NADMA), the federal agency in charge of disaster risk management, despite the NADMA's close association with flooding management agencies. Obstructive bureaucracy over administrative scales and between agencies and limited authority in decision making also restrains the ability to manage flood risk in Malaysia (Mabahwi et al., 2020). Effective use of global flood risk data by these countries also entails corroboration with local data collected concerning flood risk, however local data may be limited, unavailable, or incompatible with global datasets due to poor data management, lack of resources systems, and unreserved, restricted access to data.

5.4   Global Data

The number of global datasets for calculating climate risks is large and growing (Lindersson et al., 2020). In this study, we use global datasets that have been used in previously published studies of global flood risk. The datasets we use are free and can be easily obtained by the end-user, either by directly downloading them online or by contacting the developer of the datasets. In total, we use 6 global datasets of flood hazard, 7 global datasets of human population, and 3 global

approaches to calculating vulnerability. These datasets are detailed in the sections below and in Tables 5.1 and 5.2.

5.4.1 Global Flood Hazard Data

We use both models and satellite observed flood events to represent hazard. We use five GFMs that have been used in previous studies of global flood risk. The models are CaMa-UT (Zhou et al., 2020, Yamazaki et al., 2011), CIMA-UNEP (Rudari et al., 2015), Fathom (Sampson et al., 2015), GLOFRIS (Ward et al., 2020b, Ward et al., 2013, Winsemius et al., 2013), and JRC (Dottori et al., 2016) These models represent the state-of-the-art in publicly available global flood hazard maps. They produce spatially continuous flood maps, meaning that the return period simulated is assumed constant across the modelled domain. The five models can be categorized into two distinct structures: cascade model structure and gauged flow data model structure (Trigg et al., 2016). Cascade models use global climate precipitation data to force land surface models which predict extreme flows across the river network. Gauged flow data models use global gauge data and regional flood frequency analysis to estimate extreme flows in ungauged basins globally. Previous intercomparison studies found large differences between these models in Africa (Trigg et al., 2016) and China (Aerts et al., 2020). Validation of the same models against observed flooding in Nigeria and Mozambique found that the best models performed favourably compared with historical flood events (Bernhofen et al., 2018). Some, but not all, of the GFMs have incorporated flood defences into their modelling frameworks. Similarly, some models have introduced different types of flooding, such as pluvial and coastal. To maintain consistency between the GFMs we use only the fluvial undefended flood hazard maps. The 100-year return period, or 1% annual probability flood, is used for our calculations. In England, we use Fathom-UK flood extents, which utilizes the same modelling framework as their global model but makes use of more detailed national data. In addition to globally modelled flood extents, we use satellite derived flood extents from the Global Flood Database (GFD), a 20-year catalogue of observed flood events (Tellman et al., 2021). The global flood hazard datasets are outlined in Table 5.1. Detailed descriptions of the datasets and how to access them, as well as previous flood risk studies they have been used in are included in Appendix C.

Table 5.1 Global Flood Hazard Data Summary Table

			Flood Models			
Name	Model Structure	Rivers Modelled	Inundation Solver	Elevation Data	Downscaling Procedure	Output Resolution
CaMa-UT	Cascade	Catchments >0.25° grid cell (~600 km^2) some inundation captured on rivers as small as 50 km^2 during downscaling	2D inertial wave	SRTM (MERIT)	Flood depth down-scaled from 0.25°	3 arcsecond
CIMA-UNEP	Gauged flow	Rivers >1000 km^2 drainage area	1D Manning's	SRTM (Hydro-SHEDS)	None	3 arcsecond
Fathom Global 2.0	Gauged flow	Rivers >50 km^2 drainage area	2D inertial wave	SRTM (MERIT)	None	3 arcsecond
Fathom-UK		All rivers		LiDAR		1 arcsecond
GLOFRIS	Cascade	Rivers ≥ Strahler order 6	2D kinematic wave	SRTM (Hydro-SHEDS)	Volume redistributed from 0.5°	30 arcsecond
JRC	Cascade	Rivers > 5000 km^2 drainage area	2D inertial wave	SRTM (Hydro-SHEDS)	None	30 arcsecond
			Observed Data			
Name	Image Source	Type of Flooding	Image Type	Observed Period	Total Events	Resolution
Global Flood Database (GFD)	MODIS	Heavy rain, storm surge, snowmelt, dam break	Optical	2000-2018	913	250 m

5.4.2 Global Population Data

To identify who is exposed to flooding it is essential to understand where people live. Gridded population datasets, which distribute census information over spatial data, are the tools commonly used to calculate flood exposure at the global scale. The methods applied to distribute census data differ in complexity. These methods, their development, and their wide-ranging applications are reviewed in detail by Leyk et al. (2019). To summarize the different methods briefly, census data can be distributed across a grid by areal weighting or by dasymetric weighting. The areal weighting approach distributes census data evenly across an area. The dasymetric weighting approach uses ancillary datasets to weight the distribution of

census data. This can vary in complexity from binary weighting (settlement or no settlement) to statistical weighting approaches based on multiple ancillary datasets. Another way to distinguish the population datasets is whether they are constrained or unconstrained. The constrained approach masks out all non-settled areas as uninhabited, while the unconstrained approach assumes that not all settlements can be accurately mapped globally and residual census data is distributed across non-settled area to account for any unmapped settlements (Thomson et al., 2021)

The use, and limitations, of gridded population data in flood exposure studies specifically, are addressed in the studies of Smith et al. (2019) and Bernhofen et al. (2021). The two studies collectively consider four different global population datasets, however, many more have been used in previous studies of global flood risk. In Table 5.2, we identify and summarize seven different global population datasets which we use to calculate flood exposure: GPW4 (Doxsey-Whitfield et al., 2015), GHS-POP (Freire et al., 2016), GRUMP (Balk et al., 2005), HRSL (Tiecke, 2017), HYDE (Klein Goldewijk et al., 2010, Klein Goldewijk et al., 2017), Landscan, and Worldpop (Stevens et al., 2015). These datasets have all been used in previous studies of global flood risk. In our analysis, we use the most up-to-date epoch for each population dataset, which are then scaled to 2020 national population totals for exposure comparison. Detailed descriptions of each population datasets and how to access them, as well as previous global flood risk studies they have been used in are included in Appendix C.

Table 5.2 Global Population Data Summary Table

Name	Census Data	Daytime / Nighttime	Years	Census Distribution Method	Constrained or Unconstrained	Resolution
GPW4	subnational census data (and UNDP adjustments)	Nighttime	2000, 2005, 2015, 2020	Areal weighting across administrative units	Unconstrained	30 arcsecond
GHS-POP	GPW4	Nighttime	1975, 1990, 2000, 2015	Dasymetric weighting based on Landsat data	Constrained	9 arcsecond
GRUMP	GPW3	Nighttime	1990, 1995, 2000	Dasymetric weighting based on night-time lights	Unconstrained	30 arcsecond
HRSL	GPW4	Nighttime	2018	Binary dasymetric weighting	Constrained	1 arcsecond

HYDE	UN world prospects and literature (pre-1950)	Nighttime	10,000 BC - 2015	based on settlements from DigitalGlobe (~0.5 m resolution) imagery Multi-variable dasymetric weighting based on a number of input datasets	Constrained	30 arcsecond
Landscan	subnational census data (and U.S. Census Bureau adjustments)	Daytime	Annually 2000-2019	Statistical dasymetric weighting based on a number of input datasets	Constrained	30 arcsecond
WorldPop	GPW4	Nighttime	Annually 2000-2020	Statistical dasymetric weighting based on a number of input datasets	Unconstrained	3 arcsecond

5.4.3 Global Vulnerability Approaches

Vulnerability is the susceptibility of a community or system to experience losses from a hazardous event (UNISDR, 2004). It is a complex, multifaceted concept that can be experienced directly or indirectly across human, physical, economic, and environmental spheres (van Westen, 2014). Vulnerability has received less attention at the global scale than hazard and exposure (Ward et al., 2020a). Below, we identify and summarize three intercomparable methods for calculating vulnerability that have been used in previous studies of global flood risk. The three methods calculate direct economic damages using land cover maps to identify assets at risk and depth-damage curves to determine the degree of damage experienced by the asset. We name the three vulnerability approaches based on the global land cover map used to represent assets at risk.

5.4.3.1 GHSL

The approach to calculating vulnerability in the Aqueduct Floods project (Ward et al., 2020b) is based on the global depth-damage function database developed by Huizinga et al. (2017). Only urban damages are considered. The urban area is split into three classes: residential, commercial, and industrial. Because

current global land cover datasets do not differentiate between urban classes, assumptions are made about the fractional split of urban classes globally. Based on the spatial distribution of urban classes in Europe derived from the Corine Land Cover dataset and the findings of a report by the Buildings Performance Institute Europe (Economidou et al., 2011) the global fractional split of urban areas used in Ward et al. (2020b) is 75 percent residential, 15 percent commercial, and 10 percent industrial. Urban areas are defined as cells in the 1 km resolution Global Human Settlement Layer (GHSL) dataset (Corbane et al., 2019) that correspond to a percentage of built-up area of 50 percent or greater (Ward et al., 2020b).

5.4.3.2 GlobCover

The same global depth-damage function database (Huizinga et al., 2017) was used alongside the 10 arcsecond resolution (~300 m at the equator) GlobCover (v2.3) land cover map (Bontemps et al., 2011) to calculate vulnerability in a number of other studies of global flood risk (Alfieri et al., 2017, Alfieri et al., 2018, Dottori et al., 2018). In these studies, five land use classes were considered in the vulnerability assessment: four urban classes (residential, commercial, industrial, and infrastructure) and agriculture. This is the only approach of the three that considers any non-urban (agricultural) damages. While the GlobCover dataset explicitly represents agriculture area, it makes no distinction between urban land-use classes, which are represented as 'artificial areas'. These 'artificial areas' are split into the four urban land-use classes using globally consistent ratios, derived from studies of land-use occupation in cities across different continents (Dottori et al., 2018). The urban land-use ratios used are 56 percent residential, 20 percent commercial, 16 percent industrial, and 8 percent infrastructure (L. Alfieri, personal communication, December 1, 2020).

5.4.3.3 HYDE

In Ward et al. (2013) a single depth damage function, derived by averaging the high and low urban density land class functions in the Damagescanner tool (Klijn et al., 2007), is used to calculate vulnerability globally. Maximum damage values are calculated for each country following the approach of Jongman et al. (2012) which uses a country's GDP to normalize maximum damages obtained from the Damagescanner tool. Damages are calculated exclusively for urban areas which are derived from the HYDE (Klein Goldewijk et al., 2010) fractional urban

landcover dataset at 5 arcminute resolution (~10 km at the equator). It should be noted that the limitations of using a single depth-damage function globally are outlined in Ward et al. (2013) and subsequent studies have incorporated spatially variable functions (Ward et al., 2020b).

5.5 Methods

5.5.1 GFM and Population Agreement Calculations

The datasets are aggregated following the approach of Trigg et al. (2016) and Aerts et al. (2020). GFM output is aggregated by first resampling the five GFMs to the finest GFM resolution (1 arcsecond in England and 3 arcsecond in the remaining countries) using the nearest-neighbor approach, which ensures depths of the resampled flood map are the same as the native resolution flood map. The GFM flood depth maps are converted to binary wet/dry rasters for any non-zero flood depth and then summed to produce the aggregated GFM map. Permanent water bodies are masked out using the G3WBM permanent water body mask (Yamazaki et al., 2015). Values in the aggregated GFM map range from 5 (highest agreement) to 1 (lowest agreement). Similarly, to produce the aggregated population map the seven global population datasets are resampled to the finest population resolution (1 arcsecond). The population maps are then converted to binary populated area maps where any cell with a non-zero population is defined as a populated cell. It should be noted that this approach just represents the agreement between the population data in terms of populated area and does not account for variations in population density. Values in the aggregated population map range from 7 (highest agreement) to 1 (lowest agreement).

Agreement between the datasets is calculated using the Model Agreement Index (MAI) first introduced by Trigg et al. (2016) and three variations of this index. The MAI is calculated using the aggregated GFM map. For each model agreement level, the total flooded area is multiplied by the fractional level of agreement. These values are summed for all agreement levels and then divided by the total flooded area to give a fraction of model agreement, which ranges from 0 (no agreement) to 1 (total agreement).

$$MAI = \frac{\sum_{i=2}^{n} \frac{i}{n} \cdot a_{fi}}{A_f} \qquad (5.1)$$

where A_f is the total flooded area in the aggregated GFM map, i is the agreement level, n is the total number of models, and a_{fi} is the flooded area at the agreement level i. The Population Agreement Index (PAI) is calculated in the same way that the MAI is calculated. The only difference is that the aggregated population map rather than the aggregated GFM map is used in the calculations.

$$PAI = \frac{\sum_{i=2}^{n} \frac{i}{n} \cdot a_{pi}}{A_p} \qquad (5.2)$$

where A_p is the total populated area in the aggregated population map and a_{pi} is the total populated area at agreement level i. Values for the PAI range from 0 (no populated area agreement) to 1 (total populated area agreement). The Exposure Agreement Index (EAI) is another variation of the MAI. Similar to the exposure weighted metrics used in Pappenberger et al. (2007) and Wing et al. (2019), the EAI uses exposed population, rather than flooded area, to calculate agreement. EAI is calculated for each of the seven population datasets.

$$EAI = \frac{\sum_{i=2}^{n} \frac{i}{n} \cdot e_i}{E} \qquad (5.3)$$

where E is the total population exposed to the entire aggregated GFM map and e_i is the population exposed at agreement level i. The EAI ranges from 0 (no model exposure agreement) to 1 (total model exposure agreement) and is an indicator of the level of agreement between the models when used for exposure calculations. The final agreement index is the Volume Agreement Index (VAI). While the MAI calculates agreement between the models in two dimensions, the VAI calculates model agreement in three dimensions by incorporating flood depth. The VAI needs to be calculated using the aggregated GFM map alongside all the GFM flood depth maps.

$$VAI = \frac{\sum_{i=2}^{n} \frac{i}{n} \cdot v_i}{V_{max}} \qquad (5.4)$$

where V_{max} is the maximum volume possible for the aggregated flood extent and v_i is the volume of models in agreement at agreement level i (in three dimensions). The VAI ranges from 0 (no agreement) to 1 (total agreement).

5.5.2 Flood Exposure Calculations

Flood exposure is calculated for each country using observational flood data, five GFMs, and seven population datasets outlined in Section 5.4. Observational flood data for the last 20 years is collated from the GFD and merged into one 20-year flood map. We remove any observed flood events caused by storm surges or by dams. In total, 237 events are merged across the five countries. There are two resolutions at which exposure calculations are carried out: 1 arcsecond and 3 arcsecond. Exposure calculations for the HRSL population map are carried out at 1 arcsecond resolution (the native resolution of HRSL). Similarly, in England exposure calculations are all carried out at 1 arcsecond resolution (the native resolution of the Fathom-UK flood map). The remaining exposure calculations are carried out at 3 arcsecond resolution. The six flood hazard datasets are resampled to 3 arcseconds resolution (if not already native at 3 arcseconds) and 1 arcsecond resolution using the nearest neighbor approach. Global population datasets coarser in resolution than 3 arcseconds (GHS-POP, GPW4, GRUMP, HYDE and LandScan) are resampled and the population is evenly distributed to a 3 arcsecond resolution grid (or 1 arcsecond in England). Flood exposure is calculated by intersecting a flood map with a global population dataset. Permanent water bodies are masked out using the G3WBM water body map (Yamazaki et al., 2015). To account for any differences in total national populations between the seven global population datasets (and because not all population data is in the same epoch), each dataset's total national population is scaled to match the WorldPop 2020 national population totals.

5.5.3 Flood Damage Calculations

Flood damages are calculated in each country using the five GFMs and three vulnerability methods outlined in Section 5.4. Observational data is not used for the vulnerability calculations as the maps contain no information about flood depth. Because the depth-damage curves are in units of metres, depths for the CIMA-UNEP GFM are first converted from centimetres to metres. Each vulnerability

method uses a different landcover map (GlobCover, GHSL, and HYDE). These maps are resampled to the analysis resolution (1 arcsecond in England, 3 arcseconds in the rest) using the nearest neighbor approach. Permanent water bodies are masked out in the GFMs with the G3WBM water body map (Yamazaki et al., 2015)

For the GlobCover vulnerability method, the approach follows that of Alfieri et al. (2017) and Dottori et al. (2018). Damages are calculated across five different sectors: agriculture, commercial, industrial, infrastructure, and residential, the latter four making up the urban class. Those areas defined as "Artificial" in the GlobCover landcover map are classified as urban areas. Because the GlobCover map does not distinguish between urban sectors, we use constant urban ratios of 56% residential, 20% commercial, 16% industrial, and 8% infrastructure that have been used in the aforementioned studies. When defining agricultural areas, we use the GlobCover "Cropland" class. Where a range of potential cropland area is given in the GlobCover documentation we use the average value (e.g. for 20-50% coverage we use 35%). Damage curves and maximum damages for each sector in each country are taken from the Huizinga et al. (2017) global database of depth damage functions.

For the GHSL vulnerability method, we follow the Aqueuduct approach (Ward et al., 2020b). Damages are calculated for three urban sectors: residential, commercial, and industrial. Urban areas are defined as those cells in the GHSL dataset with a built-up area greater than 50%. Constant ratios of 75% residential, 15% commercial, and 10% industrial are used for the urban sector split. The same Huizinga et al. (2017) database is used to determine maximum damage values and damage curves per sector in each country.

For the HYDE vulnerability method, we follow the approach outlined in Ward et al. (2013). Maximum damages for each country are calculated using a GDP normalization equation from Jongman et al. (2012) applied to a maximum damage value from the Damagescanner model (Klijn et al., 2007). To convert the maximum damage values from 2005 USD into 2010 EUR (to ensure consistency with the Huizinga et al. (2017) database), we use the average annual inflation from 2005 to 2010 and the average USD to EUR exchange rate for 2010. Urban areas are calculated using the HYDE urban land cover dataset for the year 2015, which shows the percentage urban coverage per grid cell. This percentage urban coverage is converted to an urban area, to which we assign the calculated country-specific

maximum damage value. A single depth-damage function is used, which is the average of the functions for the high and low urban density classes in the Damagescanner model.

Damages are calculated for each of the three approaches by intersecting a GFM flood hazard map with depths with the relevant land use dataset. Where the flooding and the land use data intersect, percentage damage is calculated for the specific land use type using the flood depth at that location and the specific depth-damage curve for that sector. Damages are calculated by multiplying the percentage damage by the maximum damage value for that land-use type. Damages are reported in 2010 Euros.

5.5.4 Institutional Capacity of Flood Risk Management

Qualitative interviews are conducted among key water experts of the five countries to explore the extent and capacity to which they access and use these global datasets. Data from these interviews were used to illustrate the national context of FRM, as outlined in Section 5.3.2, and feed into the discussion in Section 5.7.

5.6 Results

5.6.1 Global Flood Hazard and Population Data Agreement

Aggregated maps of GFM hazard extent (Figure 5.1) were used to evaluate model agreement (see agreement scores in Table 5.3). In Colombia, the country with the best MAI score (0.363), the models showed the highest levels of agreement to the north of the country on the Magdalena river. In India, the country with the second highest MAI score (0.322), the areas of highest GFM agreement were in the north-east of the country, along the Ganges and the Brahmaputra rivers. This was a trend seen across the five countries: the models tended to agree more on larger rivers and disagree more on smaller rivers. This is evident in the Orinoquia region in central Colombia where only one of the five models predicts significant inundation. Most of the rivers here have an upstream drainage area less than 500 km^2. Of the five GFMs, Fathom is the only one that models rivers this small (rivers with an upstream drainage area greater than 50 km^2). The impact of river thresholds was most marked in England, here Fathom-UK has ingested higher accuracy national

elevation and gauge data to model flooding on all rivers. By comparison, JRC only models flooding on six rivers in England. The models also disagree in low-lying coastal areas and deltas, such as the western Ganges delta and the Godavari delta in India, the Sarawak's Rajang River Delta in Malaysia, and the Fens in eastern England near The Wash. In these low-lying areas, the flood extent is more sensitive to differences in modelled flood depth leading to lower model agreement. To further disseminate model agreement, we split the countries into drainage basins from level 4 - level 6 according to the HydroAtlas (Linke et al., 2019) classification. Maps of basin level agreement scores can be found in Appendix C. When examining the relationship in level 6 basins between the catchment area upstream of the basin and the MAI score within the basin, we found a positive normative association between the two (Spearman's rank coefficient, $\rho = 0.429$), evidence that GFM agreement improves as the size of river modelled increases. Comparing MAI scores between coastal level 6 basins and inland level 6 basins we found that the mean inland MAI score (0.293) was 38% larger than the mean MAI score for coastal basins (0.212). The same trends were found when examining the relationships at basin levels 4 and 5 (results included in Appendix C).
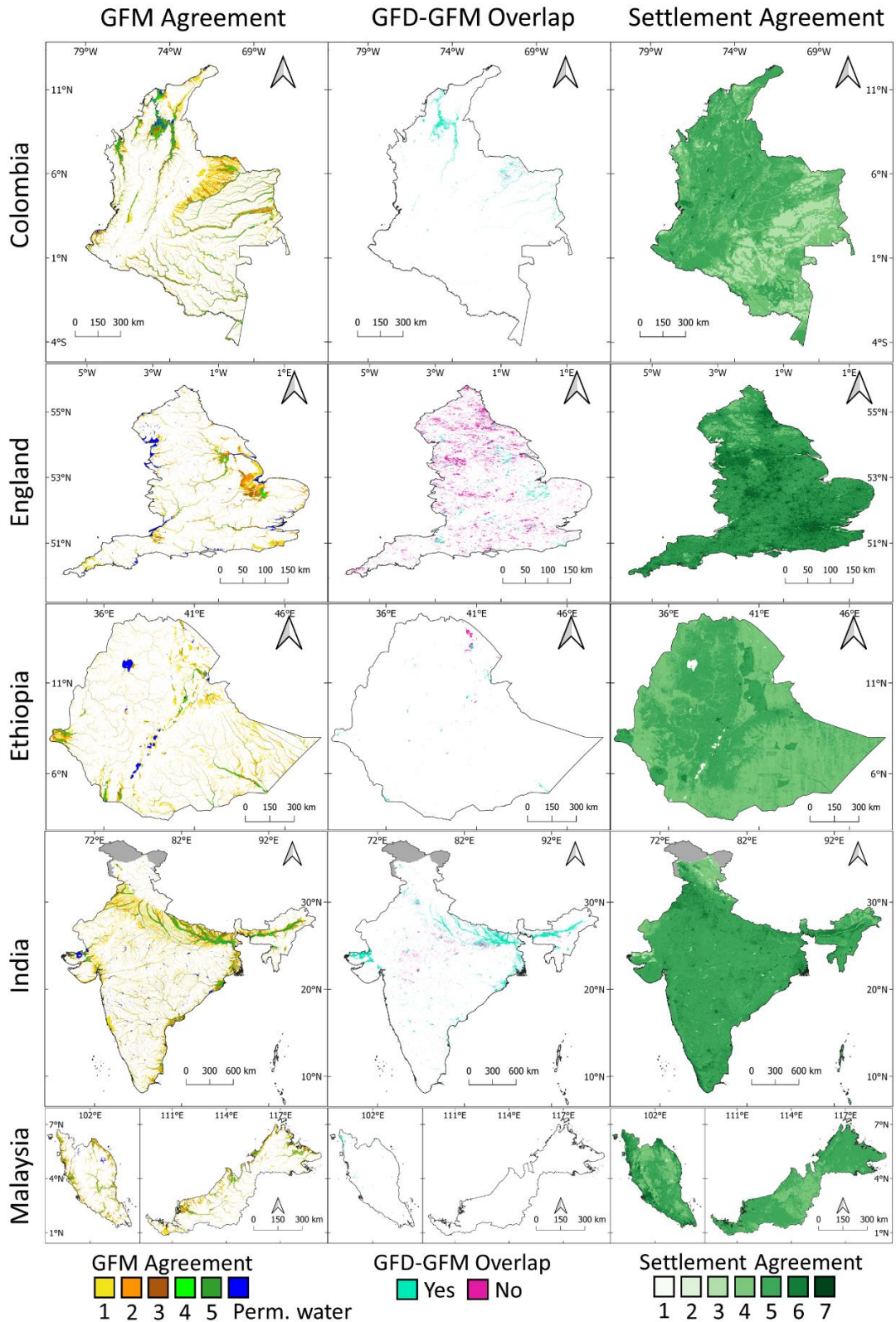
Figure 5.1 Maps of Global Flood Model (GFM) agreement, GFM and Global Flood Database (GFD) observed flooding overlap, and global population data settlement agreement.

Grey areas indicate no-data regions.

The preceding section considered agreement between the modelled flood extents in two dimensions. Agreement was also measured in three dimensions using the VAI score, which incorporates modelled flood depth in the calculation. In general, VAI scores showed similar trends to MAI scores: scores were higher in basins with larger rivers and lower in coastal basins compared to inland basins. At the national level, Colombia and India remained the two highest scoring countries with VAI scores of 0.217 and 0.183, respectively. Interestingly, Ethiopia had the third highest VAI score (0.169) despite having the lowest MAI score, suggesting there was greater agreement between the modelled flood depths in Ethiopia than in Malaysia or England.

To evaluate GFM agreement in a risk context, exposure agreement when intersected with a population map was calculated using the EAI score. EAI scores were calculated for each of the seven population maps (see Table 5.3). The lower a population map's EAI score the greater the proportion of exposure that falls within the low agreement zones of the aggregated flood map. As the EAI score decreases the effect the choice of GFM has on calculated flood exposure increases. For example, in Colombia the choice of GFM has a greater impact on exposure estimates calculated with Landscan (EAI of 0.232) than with HYDE (0.358). The implications of using different datasets for exposure calculations are explored in greater detail in section 5.6.2.

Comparing the maximum aggregated GFM extent with 20 years of observational flooding from GFD (see Figure 5.1) we find that in Colombia the GFMs capture over 92% of the historical flooding. Almost 40% of the captured flooding is in the high agreement zone of the aggregated map (5 models agree), likely because a large proportion of the observed flooding occurred in the north of the country where the models showed higher levels of agreement. In India, much of the observed flooding on the Ganges and Brahmaputra rivers is captured by the models. However, there are large areas of observed flooding missed by the models in central India in the state of Madhya Pradesh. In England the 20-year observed flood extent (10,938 km^2) is almost as large as the maximum aggregated 100-year return period GFM flood extent (13,608 km^2), but with little overlap. Much of this observed flooding can be attributed to commission errors from cloud cover.

Table 5.3 Country level Model Agreement Index (MAI), Volume Agreement Index (VAI), Exposure Agreement Index (EAI), and Population Agreement Index (PAI) scores.

				EAI						
Country	MAI	VAI	GPW4	GHS-POP	GRUMP	HRSL	HYDE	Landscan	WorldPop	PAI
Colombia	0.363	0.217	0.346	0.235	0.321	0.247	0.358	0.232	0.298	0.624
England	0.258	0.132	0.244	0.223	0.264	0.214	0.275	0.241	0.224	0.782
Ethiopia	0.240	0.169	0.196	0.240	0.185	0.191	0.194	0.160	0.213	0.644
India	0.322	0.183	0.365	0.292	0.358	0.280	0.354	0.305	0.341	0.719
Malaysia	0.299	0.160	0.253	0.229	0.272	0.223	0.283	0.237	0.236	0.679

When assessing population map agreement, we consider only binary populated or unpopulated areas; we do not consider variations in population density. England's PAI score (0.782) (see Table 5.3) is much higher than the other four countries. This can also be seen visually in Figure 5.1, where the aggregated population map for England has more dark green areas relative to the other countries. Population disagreement stems largely from the differing approaches to modelling rural / low populated areas. Unconstrained population datasets (which spread residual census data across uninhabited areas) are responsible for the large areas of low population agreement in Colombia and Ethiopia in Figure 5.1 and contributes to their comparatively low PAI scores. Another contributing factor to population disagreement is the difference in dataset resolution. The finest (HRSL, 1 arcsecond) resolution dataset is detailed enough to identify individual buildings while the coarsest (HYDE, 5 arcminute) resolution dataset is detailed enough to identify only cities.

5.6.2 Flood Exposure

National flood exposure estimates calculated for each country using 35 different combinations of GFM and global population dataset are shown in Figure 5.2. No single GFM consistently predicted the most or least exposure across the five countries. The same is true for the global population datasets. In Colombia, Fathom predicted more than double the average exposure than any of the other GFMs. Here, Fathom's flood extent (152,304 km^2) was significantly larger relative to the other GFMs (the next largest extent is JRC at 87,961 km^2). In Malaysia, the model with the highest exposure was GLOFRIS. This was because it predicted far more exposure on the Malaysian coast than the other GFMs. This was a trend seen across the five countries, GLOFRIS predicted far more coastal inundation than any other GFM. Flooding in level 6 coastal basins accounted for 21.5% of the total GLOFRIS

flood extent, compared with 10.2% (CaMa-UT), 7.7% (Fathom), 7.2% (CIMA), and 6.8% (JRC). In each of the five countries, the average exposure calculated using Fathom was consistently above the 35-dataset exposure average, while exposure calculated using CaMa-UT and CIMA was consistently below the 35-dataset average.

The choice of global population dataset used also had a significant effect on exposure estimates. In Ethiopia, when LandScan and HRSL population maps were used, national flood exposure estimates were far lower across all the GFMs. In Colombia, flood exposure estimate disagreement in the Rio Negro basin to the south-east of the country was a result of the use of different population datasets rather than the use different GFMs. In this basin, average HRSL (47 thousand) and GHS-POP (39 thousand) exposures were far greater than Landscan (17 thousand), HYDE (9 thousand), WorldPop (8 thousand), GPW4 (4 thousand), and GRUMP (2 thousand) exposures. Much of this exposure disagreement in this basin came from the town of Mitú (see Figure C.14 in Appendix C). Here, the GPW4 and GRUMP datasets did not even represent a town (populations below 100), WorldPop and HYDE picked up some population (below 4,000), only Landscan, GHS-POP, and HRSL represented population totals over 10,000 (2018 Mitú population estimate was 29,850 (DANE, 2019)). The difficulty in accurately representing rural towns and populations is one of the major contributing factors to exposure disagreement, especially if the population is exposed to a river as in Mitú. The population datasets agreed better in large urban areas. This is especially evident in Figure 5.2 when examining the spread of the population exposure estimates for the JRC GFM in England. The majority (65%) of JRC's national exposure came from the Thames river in Greater London. Because the population datasets show greater agreement in dense urban areas, the differences in exposure estimates here are lower.
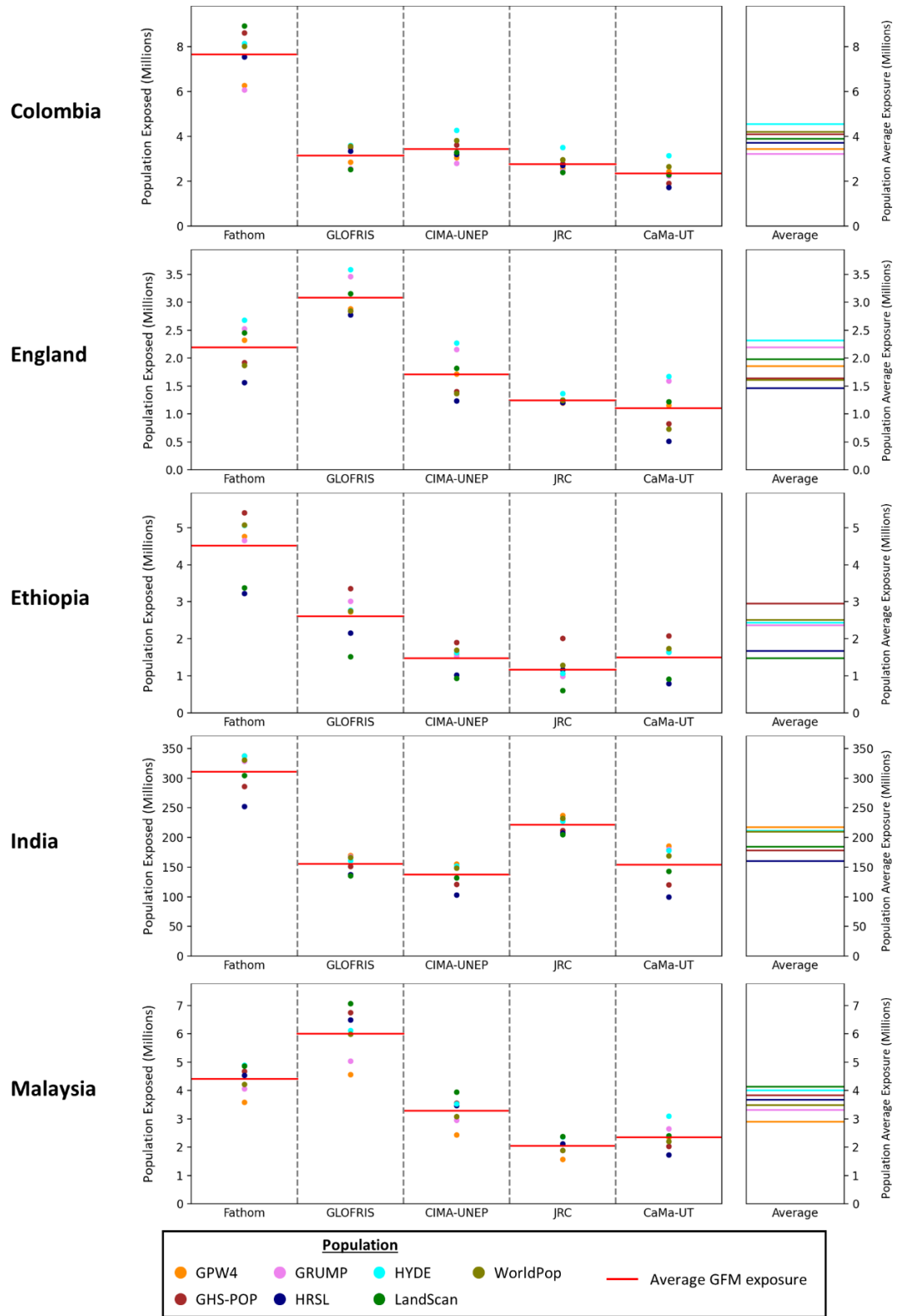
Figure 5.2 National flood exposure dot plots.

35 national flood exposure estimates calculated using five global flood models and seven global population datasets. Column on the right shows the average national flood exposure estimate calculated with each population dataset

Across the five countries, the only population dataset whose average exposure showed a consistent trend above or below the 35-dataset average was HYDE, suggesting there are less cross-national trends in exposure estimates for global population data than there are for GFMs. The HYDE dataset maps population distribution at a resolution of nearly 9 km at the equator, which is between ten and three hundred times coarser than the other population datasets and between ten and one hundred times coarser than the GFMs. At such a coarse resolution, HYDE represents the interaction between the inundation and the exposure with significantly less precision, therefore, the resulting HYDE exposure estimates are influenced more by the modelled inundated area than the location of the population exposed. Conversely, HRSL exposure estimates were typically lower than the average (except for Malaysia). This is because the detailed representation of individual buildings in the HRSL dataset better captures the population's avoidance of obvious floodplains.
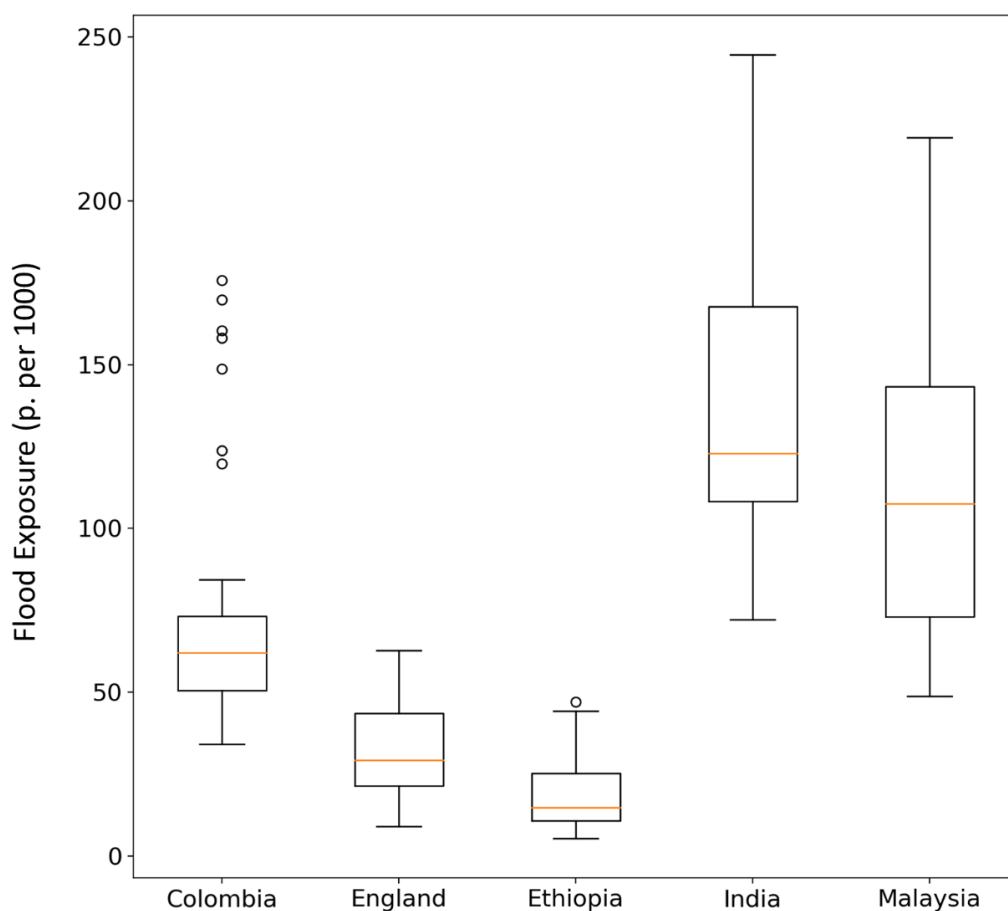
Figure 5.3 Box and whisker plots of normalized national flood exposure estimates for all five countries

The spread of average GFM exposure is larger than the spread of average global population exposure in each of the five countries, suggesting that the choice

of GFM used has a greater impact on exposure estimates than the choice of global population dataset used. To explore this further at the basin level, we compare the average coefficient of variation of flood exposure estimates when the choice of GFM is held constant to the average coefficient of variation when the choice of global population dataset is held constant. Across the five countries, we find that the choice of GFM had a greater influence on exposure estimates than the choice of population dataset in 90% of level 4 basins, 80% of level 5 basins, and 78% of level 6 basins. Figure C.15 in Appendix C illustrates these basins.

In Figure 5.3, exposure results are normalized and combined to produce box and whisker plots for cross-country comparison. The distribution of national flood exposure estimates is comparatively smaller in England and Ethiopia than it is in Colombia, India, or Malaysia. The range of potential normalized national flood exposures calculated using global data in these three countries is substantial. In Colombia, normalized national exposure ranges between 34 and 175 people exposed per 1000; in India, it ranges between 72 and 244 people exposed per 1000; and in Malaysia, it ranges between 50 and 219 people exposed per 1000.

Table 5.4 Maximum combined Global Flood Model (Max GFM) and observed Global Flood Database (GFD) flood exposure comparison (exposed people per 1000)

Country	Flood Data	GPW4	GHS-POP	GRUMP	HRSL	HYDE	LandScan	WorldPop
	Max GFM	154.4	229	150.6	202	199.8	216.7	206.6
Colombia	GFD	11.4	12.1	11.3	9.9	13.5	16.7	13.6
	Overlap	9.5	6.2	9.5	5.3	10.7	7.8	9.9
	Max GFM	92.1	84.7	104.7	77.1	108.3	99	83.3
England	GFD	200.7	211.8	145.1	218.2	150.9	196.9	218.1
	Overlap	21	20.2	19.8	19.5	20.8	21.9	20.7
	Max GFM	63.5	71.3	65.2	44.9	65.4	42.7	64.7
Ethiopia	GFD	1.1	1.4	1.7	0.4	1.3	0.4	1.3
	Overlap	0.6	1.1	0.7	0.2	0.7	0.2	0.8
	Max GFM	351.1	330.2	346.7	304.1	348.8	332.8	354.3
India	GFD	88.1	54.4	82.3	50	81.5	65	80.7
	Overlap	76.4	42.7	71.1	39.5	69.3	51.8	68
	Max GFM	252.6	347.5	278.6	337.9	327.5	369.6	311.9
Malaysia	GFD	10.8	7	11.9	6.8	12.1	9.2	9
	Overlap	8.1	3.5	9.8	3.3	9.7	6.3	5.6

We also calculate population exposure to 20 years of historical flood events from the GFD. These exposure results are listed in Table 5.4 along with exposure to

the maximum combined GFM extent and exposure where the two datasets overlapped. The population dataset used to calculate exposure has an equally significant impact on observed flood exposure estimates as it does on modelled flood exposure estimates. For example in India, observed flood exposure calculated using HRSL (50 people per 1000) is 43% smaller than observed flood exposure calculated GPW4 (81.1 people per 1000). This is significant as often these datasets are used in immediate disaster response to estimate those exposed to flood events.

5.6.3 Flood Damages

Direct economic damages for the five countries were calculated using five GFMs and three different vulnerability approaches. The total economic damages and the GDP normalized economic damages for each country are shown in Figure 5.4. Total flood damages were largest in India: ranging from 29.7 billion EUR (39.4 billion USD) to 109 billion EUR (145 billion USD) depending on the GFM and vulnerability approach used. Damages were most acute in Malaysia, where normalized damages made up between 2.2% and 29% of national GDP. Flood damages were comparatively small in Ethiopia, never exceeding 0.5% of national GDP. Here, when the GlobCover vulnerability approach was used, agricultural damages accounted for the majority of total damages (between 83% - 100%). Only two of the five GFMs (Fathom and CaMa-UT) calculated any urban GlobCover damages in Ethiopia. This is because the rivers running through the two cities where urban damages were calculated (Addis Ababa and Dawa) are too small to be modelled by three of the five GFMs.

In each of the five countries, the choice of vulnerability approach used had a greater impact on direct damage estimates than the choice of GFM. In Colombia, the average total damages calculated using the GlobCover approach was 650 million EUR (862 million USD) compared to 3.5 billion EUR (4.6 billion USD) and 9.9 billion EUR (13.1 billion USD) when GHSL and HYDE approaches were used, respectively. No vulnerability approach consistently predicted the most or least damages. In Colombia, England, and Malaysia the HYDE method predicted the most damages, while in Ethiopia and India the GlobCover approach predicted the most damages. Differences in direct damages between the three approaches are a function of the land cover dataset used, and the assumptions made during the calculations. Apart from GlobCover, which also considers agriculture, damages are

only calculated for urban areas. The three landcover datasets differ in their classification of urban areas. In Colombia, the total urban area defined by GlobCover was just 99 km^2, for GHSL it was 946 km^2, and for HYDE it was 2436 km^2. The differences in damages calculated in Colombia reflect these differences in urban area. This trend was similar in Malaysia, where urban areas were 1178 km^2, 1929 km^2, and 4929 km^2 for GlobCover, GHSL, and HYDE respectively. The three approaches make different assumptions about the categorization of damages. Inclusion of agricultural damages is significant in Ethiopia, but not in the other four countries. Infrastructure damages, which are only considered in the GlobCover approach, make up less than 2% of total damages in each of the five countries.
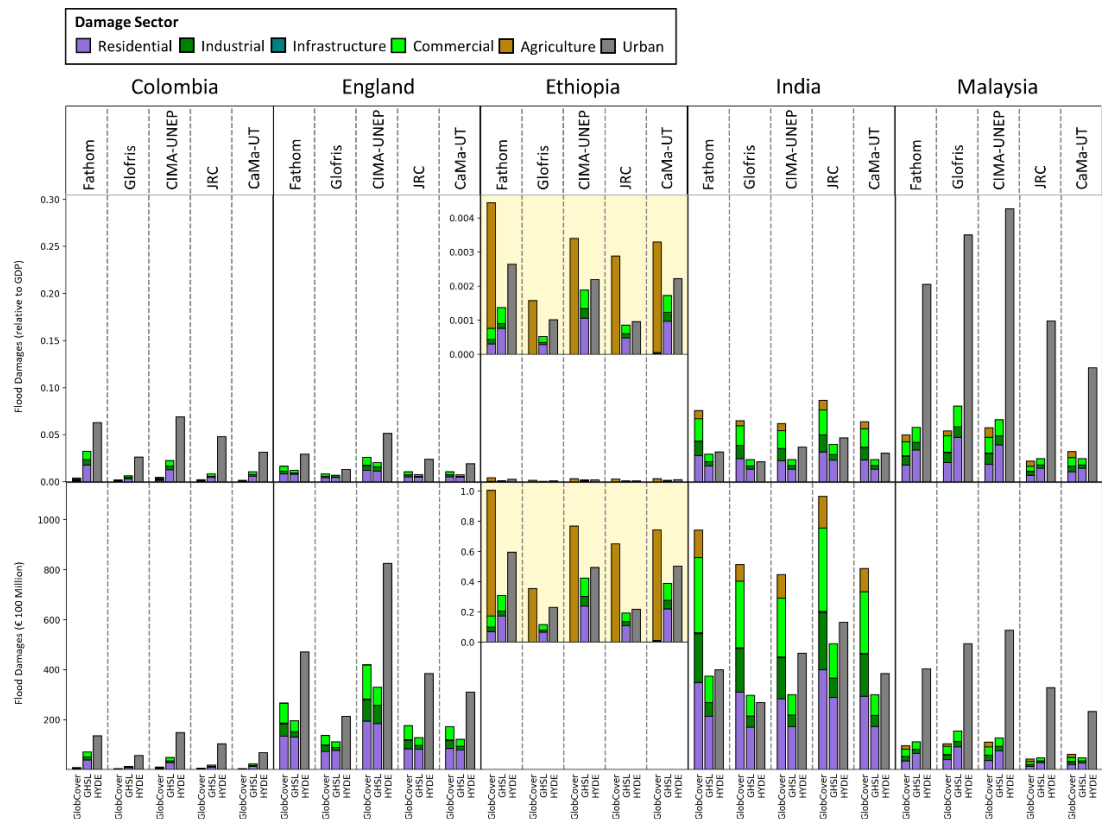
Figure 5.4 National flood damages calculated using five global flood models and three vulnerability approaches.

(Top row) Normalized national flood damages (relative to national GDP).
(Bottom row) Total national flood damages. Damages in 2010 Euros.

5.7 Discussion

5.7.1 Global Data Used Nationally

We identify 16 different global flood risk datasets and methods that have been used in previous studies of global flood risk and use them to calculate national flood risk in five countries: Colombia, England, Ethiopia, India, and Malaysia. These datasets, which have been instrumental in improving our understanding of global flood risk over the past two decades, are becoming increasingly relevant at the national scale. However, as Ward et al. (2015) postulated about GFMs, "there is often a mismatch between their actual ability and the envisaged use by practitioners". We have shown that there is also mismatch between the different global datasets, which is reflected in what they tell us about national flood risk.

Disagreement between the GFMs is substantial, and this is reflected in their MAI scores. The scores, which range from 0.24-0.363, are in line with the scores of the intercomparison of the first generation of GFMs in Africa (Trigg et al., 2016). As the models develop, you would expect convergence in their modelled output. However, these models are not being developed at the same rate. Only three of the five GFMs tested in this study (Fathom, CaMa-UT, GLOFRIS) have updated their model outputs since the first Trigg et al. (2016) intercomparison. Fundamental differences between the models remain; most notably the thresholds set on the size of river modelled (Bernhofen et al., 2021). These thresholds impact estimates of flood risk at the national scale, as seen with the large Fathom risk estimates relative to the other models (especially in Colombia and Ethiopia); and risk estimates at the basin and city scale, such as in the capital of Ethiopia, Addis Ababa, where only two of the five GFMs estimated any flood risk. Beyond differences in modelled domain, the models differ in their very structure. Although there are limits to the conclusions that can be drawn by a comparison of raw modelled output alone, results suggests differing levels of hydrodynamic representation and coastal boundary conditions contribute to disagreement in low-lying and coastal areas. This is evident across the five countries, but especially in England and Malaysia., the two countries with higher coast to area ratios. In these countries, GLOFRIS (a volume spreading model) predicts far higher coastal exposure, and subsequent national exposure, relative to the other (more hydrodynamic) models. The final resolution of the modelled flood extent should also be considered. The detail lost when using a 30 m or 90 m

resolution flood map compared with a 1 km resolution flood map is not insignificant.

Equally important to globally modelled flood data is global observational flood data. Although the limits to this data have been shown in England, Ethiopia, and Malaysia. The incorrect classification of flooding from satellite imagery due to cloud or terrain shadows, as is apparent in England, can lead to significant over prediction of flooding and lead to potentially misclassified exposure (Revilla-Romero et al., 2015). In Ethiopia and Malaysia, the limited 20-year timeframe of the satellite observed data is evident, as the area of the country which is flooded is a small fraction of the 100-year return period GFM flooded area. Rather than used in isolation, global flood observations and GFM data should be used to complement each other (Hawker et al., 2020).

Population disagreement was almost as significant as GFM disagreement. This was most notable in rural areas, such as in south-east Colombia, where the town of Mitú was captured by only some of the population datasets. Global population data were classified in Leyk et al. (2019) by the complexity of modelled population distribution. Unmodelled population datasets, such as GPW4, evenly distribute population data over census enumerated areas. This means the detail at which population is represented is entirely dependent on the size of the enumerated areas; something which is highly variable across countries. In Colombia, where the size of the average census enumerated area is 1021 km^2, GPW4 calculated exposure is a lot less accurate than in England, where the size of the average census enumerated area is 0.76 km^2 (CIESIN, 2018). Indeed, it's surprising that GPW4 is still so widely used in studies of flood exposure, as it does not capture the population distribution at any detail finer than the census unit. The discrepancy in detail between national census data is something that needs to be considered for all population datasets that use GPW data as input (GHS-POP, GRUMP, HRSL, WorldPop), although the impact this has on final population estimates is smaller due to the additional population distribution modelling carried out by these datasets. The resolution of the population data is equally important to consider. The most resolved of the population datasets, HRSL, identifies individual dwellings at 30 m resolution. Highly resolved population data was shown in the studies of Smith et al. (2019) and Bernhofen et al. (2021) to be of significant importance in accurately representing the

avoidance of flood prone areas. Indeed, the low HRSL flood exposure estimates in four of the five countries examined in this study would support this finding. There are obvious limits to the conclusions that can be drawn with coarse resolution population data. Those datasets with a resolution of 1 km (GPW4, GRUMP, LandScan) will struggle to accurately model exposure on anything but the largest rivers. Even GHS-POP, which has a resolution of 250 m, was shown in Bernhofen et al. (2021) to be too coarse to accurately represent exposure on some smaller rivers. Certain population data, such as GRUMP and HYDE, are not relevant at the national scale. GRUMP, which has not been updated since 2000, is obsolete for flood risk analysis under current conditions. The HYDE data, at a resolution of roughly 9 km, is far too coarse to draw any meaningful conclusions at the national level. It was the only population dataset that consistently overpredicted exposure across the five countries examined. Population data should be chosen with the intended use in mind. Previous studies have highlighted the benefits of HRSL (Smith et al., 2019, Bernhofen et al., 2021), however, HRSL population estimates are limited to 2018. If consistent population estimates across time are required, datasets such as GHS-POP or WorldPop would be better suited. Similarly, if you want to calculate exposed day-time population rather than night-time population, Landscan is the only dataset you can use.

The range of low national VAI scores (0.132-0.217), which consider both extent and depth disagreement between the models, would suggest that the choice of GFM has a large effect on calculated national damages. What we found, was that the choice of vulnerability approach has a far greater effect on national damages than the choice of GFM. This was largely due to how the three different land cover maps used in the vulnerability calculations identified urban areas. Across the five countries, the size of urban area defined by each dataset was reflected in the national damage estimates. Equally important, but less reflected in the national flood damage estimates, was how the GlobCover and GHSL approaches split urban sector damages. Each approach applied constant global ratios of urban sector split, which were based on studies of either global or European cities (Dottori et al., 2018, Ward et al., 2020b). Sector level damages were directly impacted by these constant global ratios, meaning GHSL residential damages always made up a larger proportion of urban damages than GlobCover residential damages. The lack of a ceteris paribus comparison between vulnerability approaches limits the definite conclusions that

can be drawn about the impact different aspects of the vulnerability calculation had on disagreement. Previous work by de Moel and Aerts (2011) found that the valuation of assets and the choice of damage curve had the greatest impact on damage uncertainty in the Dutch basin they were investigating. Similarly, when examining loss data in the US from the National Flood Insurance Program Wing et al. (2020) found that claims data does not fit the monotonic shape of traditional damage curves. It's well established that the vulnerability component of any flood risk assessment carries the most uncertainty at any scale. The assumptions and uncertainties associated with the three global vulnerability approaches tested in this study do not translate well into the national context.

5.7.2 Uncertainty and Decision Making

Exploring the hazard, vulnerability and exposure components of flood risk using different models and datasets provides a useful basis for discussing uncertainty across all three components. Often quantifiable uncertainties are understood as risks, while unquantifiable uncertainties are understood as uncertainties. Some of these uncertainties are amenable to quantitative or qualitative evaluation, while some cannot be evaluated (Riesch, 2013). Key sources of modelling related uncertainty include; context and framing, input, model structure, parameter, and model technical uncertainty (Refsgaard et al., 2007). GFMs are not always developed for answering questions associated with context and framing, such as social, environmental, economic, technological, and infrastructural characteristics at the local scale. The extent to which these characteristics (often not accounted for) affect uncertainties differs from location to location and involves complex interactions. These characteristics may not always be captured in the calibration and validation process and does not always include all streamflow observation stations (Hirpa et al., 2021, Wing et al., 2021). This means that model parameterization is not always sensitive to local characteristics. Input data across GFMs suggests that there are commonalities (e.g. the DEM), interdependences, and differences making it difficult to isolate the impact of different factors on uncertainty. Substantial model structure, parameterization, and technical differences also mean that without a significantly complex sensitivity analysis it would be difficult to ascertain how and to what extent they individually or collectively affect uncertainty (Hoch and Trigg, 2019). As a consequence, while we use multiple models and datasets to illustrate

uncertainties, the contribution of different sources of uncertainty is difficult to ascertain quantitatively or qualitatively.

With cascading uncertainty as GFM information is combined with exposure and vulnerability information from different datasets, there is an expansion of the uncertainty space. Flood risk assessments, based on the three components, would involve a further increase in uncertainty. Furthermore, the flood risk information may not always account for smaller scale flood prevention interventions or be relevant at hyperlocal scales where other socio-economic factors may affect flood risk. Further scrutiny may also reveal that there are important differences between extreme flood magnitudes (not explored in this study), as demonstrated in Africa (Trigg et al., 2016) and the conterminous United States (Devitt et al., 2021). There may also be other models, datasets, and even factors affecting risk that need to be accounted for to better understand risks. This suggests that although this study brings together multiple variants of the contributors to flood risk assessment, the uncertainty space is unclear and the contribution of different factors to exposure, damage and risk is not well characterized. This makes it challenging to interpret results in a way that can aid decision making at local scales. For instance, we discuss disagreement in typically flood prone areas like low-lying deltas and low relief coastal areas, and higher agreement in larger river basins. This could affect the salience and credibility of the information for local to national level decision makers, some of whom may have primary knowledge and experience of dealing with flooding in such areas. Such information may be relevant to decision makers who are interested in hotspots and may focus on areas with greater agreement, or on areas where populations also face other hazards. An alternative way could be for decision makers to think of these different combinations (exposure, damage and risk) as scenarios that are plausible, but do not necessarily capture the full range of possibilities. Decision makers, who are often used to dealing with uncertainty, may find that a structured decision making under uncertainty approach (Bhave et al., 2016) may help assess the value of the information and make more informed flood management decisions.

5.7.3 National Capacity to Use Global Data

The inconsistencies and variation between these global datasets may call into question their 'usefulness' for evaluating flood risk, especially for some countries

who experience limited institutional capacity and policy in FRM. The corroboration of global data with data collected locally may potentially ensure accuracy and consistency. However, the quality and availability of data in countries in the Global South is frequently very poor. For example, spatio-temporal time series are often not complete and bureaucratic, administrative barriers or political motivation can prevent access to data. These global datasets can hold exceptional value in areas that are data poor; for example, planetary level datasets have been used to detect long-term meteorological changes in Pakistan, India and Inner Mongolia (Lindersson et al., 2020).

Evaluations at the national scale may have limited impact on the most vulnerable of which usually inhabit agriculturally dependent rural areas, especially if population datasets are not resolved enough for these areas, or due to narrow or misaligned interpretations of vulnerability. For example, calculation of economic damage reflects inequality; hence it becomes important in relation to how something like agricultural damages are accounted for, given the centrality of agriculture in the livelihoods of many. whilst not economically catastrophic in GDP terms, this is potentially devastating on a local, livelihoods scale.

Effective FRM and the ability to use these global flood risk datasets requires policy and institutions that recognize the interconnected and interdependent systems that are inevitable, not only with technical interventions and infrastructure but also the socio-political networks that provide expertise and coordination (Jonkman and Dawson, 2012). However, the resources and agency to achieve this is frequently lacking, for example, some countries do not have specific FRM policies and with other disaster management areas taking priority, such as drought in Ethiopia and earthquakes in Colombia resulting in lack of agency regarding FRM.

5.8 Conclusions

As global flood risk data develops and becomes increasingly relevant at national scales there is an urgent need to evaluate its credibility in a national flood risk context. By carrying out national flood risk assessments using global data in five different countries we explore the commonality and variability of global data used nationally. Global datasets vary significantly at the national level, and this is

reflected in the national flood risk estimates. We find that the choice of GFM has a larger effect on exposure estimates than the choice of population dataset, while the choice of vulnerability approach has the greatest influence on national flood damage estimates. The detail of the datasets becomes increasingly important at the national scale. GFMs that do not model the flooding of small rivers are leaving a substantial amount of national flood risk unaccounted for. Similarly, coarse resolution global data limits the detail at which risk can be evaluated and diminishes the usefulness of certain datasets at this scale. Global approaches to calculating vulnerability are limited both by the uncertainty of global land cover datasets and the assumptions made to calculate damages at the global scale.

Further to these challenges and inconsistencies but just as significant is whether countries have the capacity to access and use these datasets. These datasets can only be effective if a country has a functioning, institutional framework with capability to support their use and implementation. This can include informed and proactive policies which both monitor and plan for future flood risk. Additionally, strong institutions that effectively implement these policies, which encourage expertise and assist the consultation and coordination between a diverse range of key stakeholders (Jonkman and Dawson, 2012). Technical and financial capital is significant in introducing and maintaining the infrastructure needed to monitor and assess flood-risk; as is the availability of good quality, compatible data to complement and use alongside these global datasets. Variation in the methods of conceptualizing population and vulnerability could be particularly problematic for compatibility.

5.9 Recommendations and Future Work

Global flood risk datasets were evaluated in this study by quantifying the uncertainty when used interchangeably for flood risk assessments at the national scale. Further work should incorporate locally sourced data and locally calibrated models to test the global datasets. Only then could one definitively conclude which data is 'best' for a given locality or use. These datasets could have considerable potential for assisting and furthering FRM in countries who have limited capacity to access local data, however further investigation is needed to reveal the extent to which countries find these datasets useful and have the capacity to use these

datasets. Further work should examine in greater detail the institutional capability of national and local FRM to access and apply such datasets. The variation between these datasets also requires technical understanding of the nature of limitations of the data. Further, the application of such datasets as evidence for decision making entails choices over the allocation of resources. Future work should seek to examine the types of policy and resource allocations that result from the application of such datasets to FRM.

5.10 Acknowledgements

References

AERTS, J. P. M., UHLEMANN-ELMER, S., EILANDER, D. & WARD, P. J. 2020. Comparison of estimates of global flood models for flood hazard and exposed gross domestic product: a China case study. *Nat. Hazards Earth Syst. Sci.,* 20**,** 3245-3260.

AL JAZEERA. 2021. *Six dead, nearly 50,000 evacuated in Malaysia floods* [Online]. aljazeera.com: Al Jazeera. Available: https://www.aljazeera.com/news/2021/1/9/six-dead-nearly-50000-evacuated-in-malaysia-floods [Accessed 20 October 2021].

ALEXANDER, M., PRIEST, S. & MEES, H. 2016a. A framework for evaluating flood risk governance. *Environmental Science & Policy,* 64**,** 38-47.

ALEXANDER, M., PRIEST, S. J., MICOU, P., TAPSELL, S. M., GREEN, C. H., PARKER, D. J. & HOMEWOOD, S. 2016b. Analysing and evaluating flood risk governance in England–enhancing societal resilience through comprehensive and aligned flood risk governance arrangements.

ALFIERI, L., BISSELINK, B., DOTTORI, F., NAUMANN, G., DE ROO, A., SALAMON, P., WYSER, K. & FEYEN, L. 2017. Global projections of river flood risk in a warmer world. *Earths Future,* 5**,** 171-182.

ALFIERI, L., DOTTORI, F., BETTS, R., SALAMON, P. & FEYEN, L. 2018. Multi-Model Projections of River Flood Risk in Europe under Global Warming. 6**,** 6.

ALI, Q. S. W., PANDEY, S., CHAUDHURI, R. R., BEHERA, S. & JEYAKUMAR, L. 2021. Development of rainfall-infiltration measurement system and recharge strategies for urban flooding areas: a case study of Delhi, India. *Modeling Earth Systems and Environment,* 7**,** 2719-2731.

BALK, D., POZZI, F., YETMAN, G., DEICHMANN, U. & NELSONC, A. 2005. The distribution of people and the dimension of place: Methodologies to improve the global estimation of urban extents. *International Society for Photogrammetry and Remote Sensing, Proceedings of the Urban Remote Sensing Conference*.

BATES, P. D., QUINN, N., SAMPSON, C., SMITH, A., WING, O., SOSA, J., SAVAGE, J., OLCESE, G., NEAL, J., SCHUMANN, G., GIUSTARINI, L., COXON, G., PORTER, J. R., AMODEO, M. F., CHU, Z., LEWIS-GRUSS, S., FREEMAN, N. B., HOUSER, T., DELGADO, M., HAMIDI, A., BOLLIGER, I., E. MCCUSKER, K., EMANUEL, K., FERREIRA, C. M., KHALID, A., HAIGH, I. D., COUASNON, A., E. KOPP, R., HSIANG, S. & KRAJEWSKI, W. F. 2021. Combined Modeling of US Fluvial, Pluvial, and Coastal Flood Hazard Under Current and Future Climates. *Water Resources Research,* 57**,** e2020WR028673.

BERNHOFEN, M. V., TRIGG, M. A., SLEIGH, P. A., SAMPSON, C. C. & SMITH, A. M. 2021. Global Flood Exposure from Different Sized Rivers. *Nat. Hazards Earth Syst. Sci. Discuss.,* 2021**,** 1-25.

BERNHOFEN, M. V., WHYMAN, C., TRIGG, M. A., SLEIGH, P. A., SMITH, A. M., SAMPSON, C. C., YAMAZAKI, D., WARD, P. J., RUDARI, R., PAPPENBERGER, F., DOTTORI, F., SALAMON, P. & WINSEMIUS, H. C. 2018. A first collective validation of global fluvial flood models for major floods in Nigeria and Mozambique. *Environmental Research Letters,* 13.

BESHIR, A. A. & SONG, J. 2021. Urbanization and its impact on flood hazard: the case of Addis Ababa, Ethiopia. *Natural Hazards: Journal of the International Society for the Prevention and Mitigation of Natural Hazards,* 109**,** 1167-1190.

BHAVE, A. G., CONWAY, D., DESSAI, S. & STAINFORTH, D. A. 2016. Barriers and opportunities for robust decision making approaches to support climate change adaptation in the developing world. *Climate Risk Management,* 14**,** 1-10.

BIRKMANN, J., DECH, S., HIRZINGER, G., KLEIN, R., KLÜPFEL, H., LEHMANN, F., MOTT, C., NAGEL, K., SCHLURMANN, T., SETIADI, N., SIEGERT, F. & STRUNZ, G. Measuring vulnerability to promote disaster-resilient societies: Conceptual frameworks and definitions. 2006.

BONTEMPS, S., DEFOURNY, P., VAN BOGAERT, E., ARINO, O., KALOGIROU, V. & RAMOS PEREZ, J. 2011. GLOBCOVER 2009: Products Description and Validation Report. UCLouvain & ESA Team.

BURBY, R. J. 2001. Flood insurance and floodplain management: the US experience. *Global Environmental Change Part B: Environmental Hazards,* 3**,** 111-122.

CIESIN 2018. Gridded Population of the World, Version 4 (GPWv4): Administrative Unit Center Points with Population Estimates, Revision 11. Palisades, NY: NASA Socioeconomic Data and Applications Center (SEDAC).

CORBANE, C., PESARESI, M., KEMPER, T., POLITIS, P., FLORCZYK, A. J., SYRRIS, V., MELCHIORRI, M., SABO, F. & SOILLE, P. 2019. Automated global delineation of human settlements from 40 years of Landsat satellite data archives. *Big Earth Data,* 3**,** 140-169.

CWC, C. W. C. 2018. Comprehensive flood management in India.

DANE 2019. Informacion Capital. Colombia: Departamento Administrativo Nacional de Estadistica (DANE).

DAVIS, S. A. & SKAGGS, L. L. 1992. Catalog of residential depth-damage functions used by the army corps of engineers in flood damage estimation. ARMY ENGINEER INST FOR WATER RESOURCES ALEXANDRIA VA.

DE MOEL, H. & AERTS, J. C. J. H. 2011. Effect of uncertainty in land use, damage models and inundation depth on flood damage estimates. *Natural Hazards,* 58**,** 407-425.

DE MOEL, H., JONGMAN, B., KREIBICH, H., MERZ, B., PENNING-ROWSELL, E. & WARD, P. J. 2015. Flood risk assessments at different spatial scales. *Mitigation and Adaptation Strategies for Global Change,* 20**,** 865-890.

DE, U., SINGH, G. & RASE, D. J. J. I. G. U. 2013. Urban flooding in recent decades in four mega cities of India. 17**,** 153-165.

DEVITT, L., NEAL, J., WAGENER, T. & COXON, G. 2021. Uncertainty in the extreme flood magnitude estimates of large-scale flood hazard models. *Environmental Research Letters,* 16**,** 064013.

DILLEY, M., CHEN, R. S., DEICHMANN, U., L., L.-L. A. & ARNOLD, M. 2005. *Natural Disaster Hotsposts: A Global Risk Analysis,* Washington, DC, Wolrd Bank.

DOTTORI, F., SALAMON, P., BIANCHI, A., ALFIERI, L., HIRPA, F. A. & FEYEN, L. 2016. Development and evaluation of a framework for global flood hazard mapping. *Advances in Water Resources,* 94**,** 87-102.

DOTTORI, F., SZEWCZYK, W., CISCAR, J. C., ZHAO, F., ALFIERI, L., HIRABAYASHI, Y., BIANCHI, A., MONGELLI, I., FRIELER, K., BETTS, R. A. & FEYEN, L. 2018. Increased human and economic losses from river flooding with anthropogenic warming. *Nature Climate Change,* 8**,** 781-+.

DOXSEY-WHITFIELD, E., MACMANUS, K., ADAMO, S. B., PISTOLESI, L., SQUIRES, J., BORKOVSKA, O. & BAPTISTA, S. R. 2015. Taking Advantage of the Improved Availability of Census Data: A First Look at the Gridded Population of the World, Version 4. *Papers in Applied Geography,* 1**,** 226-234.

DRIESSEN, P. P. J., DIEPERINK, C., VAN LAERHOVEN, F., RUNHAAR, H. A. C. & VERMEULEN, W. J. V. 2012. Towards a Conceptual Framework for The Study of Shifts in Modes of Environmental Governance – Experiences From The Netherlands. *Environmental Policy and Governance,* 22**,** 143-160.

DRIESSEN, P. P. J., HEGGER, D. L. T., KUNDZEWICZ, Z. W., VAN RIJSWICK, H. F. M. W., CRABBÉ, A., LARRUE, C., MATCZAK, P., PETTERSSON, M., PRIEST, S., SUYKENS, C., RAADGEVER, G. T. & WIERING, M. 2018. Governance Strategies for Improving Flood Resilience in the Face of Climate Change. 10**,** 1595.

DRMFSS 2014. Disaster Risk Management Strategic Program and Investment Framework. Addis Ababa, Ethiopia: Ministry of Agriculture.

ECONOMIDOU, M., ATANASIU, B., STANIASZEK, D., MAIO, J., NOLTE, I., RAPF, O., LAUSTSEN, J., RUYSSEVELT, P., STRONG, D. & ZINETTI, S. 2011. *Europe's buildings under the microscope. A country-by-country review of the energy performance of buildings.*

EMERTON, R., CLOKE, H., FICCHI, A., HAWKER, L., DE WIT, S., SPEIGHT, L., PRUDHOMME, C., RUNDELL, P., WEST, R., NEAL, J., CUNA, J., HARRIGAN, S., TITLEY, H., MAGNUSSON, L., PAPPENBERGER, F., KLINGAMAN, N. & STEPHENS, E. 2020. Emergency flood bulletins for Cyclones Idai and Kenneth: A critical evaluation of the use of global flood forecasts for international humanitarian preparedness and response. *International Journal of Disaster Risk Reduction,* 50**,** 101811.

ENVIRONMENT AGENCY 2009. Flooding in England: A National Assessment of Flood Risk. Bristol: Environment Agency.

FORREST, S., TRELL, E.-M. & WOLTJER, J. 2017. Flood Groups in England: Governance arrangements and contribution to flood resilience.

FREIRE, S., MACMANUS, K., PESARESI, M., DOXSEY-WHITFIELD, E. & MILLS, J. 2016. *Development of new open and free multi-temporal global population grids at 250 m resolution.*

GARMESTANI, A. S. & BENSON, M. H. 2013. A Framework for Resilience-based Governance of Social-Ecological Systems. *Ecology and Society,* 18.

GARVEY, A. & PAAVOLA, J. 2021. Community action on natural flood management and the governance of a catchment-based approach in the UK. n/a.

GUNDERSON, L. H. & S, H. C. 2002. *Panarchy: understanding transformations in human and natural systems,* Washington DC, USA, Island Press.

HAILE, A. T., HABIB, E. & RIENTJES, T. 2013a. Evaluation of the climate prediction center (CPC) morphing technique (CMORPH) rainfall product on hourly time scales over the source of the Blue Nile River. 27**,** 1829-1839.

HAILE, A. T., KUSTERS, K. & WAGESHO, N. 2013b. Loss and damage from flooding in the Gambela region, Ethiopia. *International Journal of Global Warming,* 5**,** 483-497.

HALL, J. W. 2014. Editorial: steps towards global flood risk modelling. *Journal of Flood Risk Management,* 7**,** 193-194.

HALL, J. W., DAWSON, R. J., SAYERS, P. B., ROSU, C., CHATTERTON, J. B. & DEAKIN, R. 2003. A methodology for national-scale flood risk assessment. 156**,** 235-247.

HALL, J. W., SAYERS, P. B. & DAWSON, R. J. 2005. National-scale Assessment of Current and Future Flood Risk in England and Wales. *Natural Hazards,* 36**,** 147-164.

HAWKER, L., NEAL, J., TELLMAN, B., LIANG, J., SCHUMANN, G., DOYLE, C., SULLIVAN, J. A., SAVAGE, J. & TSHIMANGA, R. 2020. Comparing earth observation and inundation models to map flood hazards. *Environmental Research Letters,* 15**,** 124032.

HIRABAYASHI, Y., KANAE, S., EMORI, S., OKI, T. & KIMOTO, M. 2008. Global projections of changing risks of floods and droughts in a changing climate. Hydrological Sciences Journal.

HIRPA, F. A., LORINI, V., DADSON, S. J. & SALAMON, P. 2021. Calibration of Global Flood Models. *Global Drought and Flood.*

HOCH, J. M. & TRIGG, M. A. 2019. Advancing global flood hazard simulations by improving comparability, benchmarking, and integration of global flood models. *Environmental Research Letters,* 14**,** 034001.

HOYOS, N., ESCOBAR, J., RESTREPO, J. C., ARANGO, A. M. & ORTIZ, J. C. 2013. Impact of the 2010–2011 La Niña phenomenon in Colombia, South America: The human toll of an extreme weather event. *Applied Geography,* 39**,** 16-25.

HUIZINGA, K., DE MOEL, H. & SZEWCZYK, W. 2017. Global flood depth-damage functions. Methodology and the database with guidelines. JRC Technical Reports.

JONGMAN, B., WARD, P. J. & AERTS, J. 2012. Global exposure to river and coastal flooding: Long term trends and changes. *Global Environmental Change-Human and Policy Dimensions,* 22**,** 823-835.

JONKMAN, S. N. & DAWSON, R. J. 2012. Issues and Challenges in Flood Risk Management *Editorial for the Special Issue on Flood Risk Management,* 4**,** 785-792.

KENDON, M., MCCARTHY, M., JEVREJEVA, S., MATTHEWS, A. & LEGG, T. 2019. State of the UK climate 2018. 39**,** 1-55.

KLEIN GOLDEWIJK, K., BEUSEN, A., DOELMAN, J. & STEHFEST, E. 2017. Anthropogenic land use estimates for the Holocene – HYDE 3.2. *Earth Syst. Sci. Data,* 9**,** 927-953.

KLEIN GOLDEWIJK, K., BEUSEN, A. & JANSSEN, P. 2010. Long-term dynamic modeling of global population and built-up area in a spatially explicit way: HYDE 3.1. 20**,** 565-573.

KLIJN, F., BAAN, P., DE BRUIJN, K., KWADIJK, J. & VAN BUREN, R. 2007. Overstromingsrisico's in Nederland in een veranderend klimaat: Verwachtingen, schattingen en berekeningen voor het project Nederland Later.

KOK, M. 2004. *Standaardmethode 2004: Schade en slachtoffers als gevolg van overstromingen*, Ministerie van Verkeer en Waterstaat, Rijkswaterstaat.

LEYK, S., GAUGHAN, A. E., ADAMO, S. B., DE SHERBININ, A., BALK, D., FREIRE, S., ROSE, A., STEVENS, F. R., BLANKESPOOR, B., FRYE, C., COMENETZ, J., SORICHETTA, A., MACMANUS, K., PISTOLESI, L., LEVY, M., TATEM, A. J. & PESARESI, M. 2019. The spatial allocation of population: a review of large-scale gridded population data products and their fitness for use. *Earth Syst. Sci. Data,* 11**,** 1385-1409.

LINDERSSON, S., BRANDIMARTE, L., MÅRD, J. & DI BALDASSARRE, G. 2020. A review of freely accessible global datasets for the study of floods, droughts and their interactions with human societies. *WIREs Water,* 7**,** e1424.

LINKE, S., LEHNER, B., OUELLET DALLAIRE, C., ARIWI, J., GRILL, G., ANAND, M., BEAMES, P., BURCHARD-LEVINE, V., MAXWELL, S., MOIDU, H., TAN, F. & THIEME, M. 2019. Global hydro-environmental sub-basin and river reach characteristics at high spatial resolution. *Scientific Data,* 6**,** 283.

LOESCHNER, L., NORDBECK, R., SCHINDLEGGER, A. & SEHER, W. 2019. COMPENSATING FLOOD RETENTION ON PRIVATE LAND IN AUSTRIA: TOWARDS POLYCENTRIC GOVERNANCE IN FLOOD RISK MANAGEMENT? 7**,** 32-45.

MABAHWI, N. A., NAKAMURA, H. & BHATTACHARYA, Y. 2020. Flood Risk Management in Malaysia: The current hindrances for flood related agencies. *Asian Journal of Behavioural Studies,* 5**,** 11-24.

MERZ, B., HALL, J., DISSE, M. & SCHUMANN, A. 2010. Fluvial flood risk management in a changing world. *Nat. Hazards Earth Syst. Sci.,* 10**,** 509-527.

MESTER, B., WILLNER, S. N., FRIELER, K. & SCHEWE, J. 2021. Evaluation of river flood extent simulated with multiple global hydrological models and climate forcings. *Environmental Research Letters,* 16**,** 094010.

MEYER, V., BECKER, N., MARKANTONIS, V., SCHWARZE, R., VAN DEN BERGH, J. C. J. M., BOUWER, L. M., BUBECK, P., CIAVOLA, P., GENOVESE, E., GREEN, C., HALLEGATTE, S., KREIBICH, H., LEQUEUX, Q., LOGAR, I., PAPYRAKIS, E., PFURTSCHELLER, C., POUSSIN, J., PRZYLUSKI, V., THIEKEN, A. H. & VIAVATTENE, C. 2013. Review article: Assessing the costs of natural hazards – state of the art and knowledge gaps. *Nat. Hazards Earth Syst. Sci.,* 13**,** 1351-1373.

MORRISON, A., WESTBROOK, C. J. & NOBLE, B. F. 2018. A review of the flood risk management governance and resilience literature. *Journal of Flood Risk Management,* 11**,** 291-304.

MUNICHRE. *Risks from floods, storm surges and flash floods* [Online]. Available: https://www.munichre.com/en/risks/natural-disasters-losses-are-trending-upwards/floods-and-flash-floods-underestimated-natural-hazards.html [Accessed May 5 2021].

PAPPENBERGER, F., BEVEN, K., FRODSHAM, K., ROMANOWICZ, R. & MATGEN, P. 2007. Grasping the unavoidable subjectivity in calibration of flood inundation models: A vulnerability weighted approach. *Journal of Hydrology,* 333**,** 275-287.

PENNING-ROWSELL, E. C., PRIEST, S. J., PARKER, D. J., MORRIS, J., TUNSTALL, S. M. V., VIAVATTENE, C., CHATTERTON, J. & OWEN, D. 2013. *Flood and coastal erosion risk management: a manual for economic appraisal,* London, U.K., Routledge, Taylor & Francis.

RAMIREZ-VILLEGAS, J., SALAZAR, M., JARVIS, A. & NAVARRO-RACINES, C. E. 2012. A way forward on adaptation to climate change in Colombian agriculture: perspectives towards 2050. *Climatic Change,* 115**,** 611-628.

RAY, K., PANDEY, P., PANDEY, C., DIMRI, A. P. & KISHORE, K. 2019. On the Recent Floods in India. *Current science,* 117.

REFSGAARD, J. C., VAN DER SLUIJS, J. P., HØJBERG, A. L. & VANROLLEGHEM, P. A. 2007. Uncertainty in the environmental modelling process – A framework and guidance. *Environmental Modelling & Software,* 22**,** 1543-1556.

REVILLA-ROMERO, B., HIRPA, F. A., POZO, J. T.-D., SALAMON, P., BRAKENRIDGE, R., PAPPENBERGER, F. & DE GROEVE, T. 2015. On the Use of Global Flood Forecasts and Satellite-Derived Inundation Maps for Flood Monitoring in Data-Sparse Regions. 7**,** 15702-15728.

RIESCH, H. 2013. Levels of Uncertainty. *In:* ROESER, S., HILLERBRAND, R., SANDIN, P. & PETERSON, M. (eds.) *Essentials of Risk Theory.* Dordrecht: Springer Netherlands.

RUDARI, R., SILVESTRO, F., CAMPO, L., REBORA, N., BONI, G. & HEROLD, C. 2015. IMPROVEMENT OF THE GLOBAL FLOOD MODEL FOR THE GAR 2015.

SAIFULSYAHIRA, J., EDRE, M., AF, A. F., JUNI, M. H. J. I. J. O. P. H. & SCIENCES, C. 2016. Governance of flood disaster management: Malaysian case study. 3**,** 17-30.

SAMPSON, C. C., SMITH, A. M., BATES, P. B., NEAL, J. C., ALFIERI, L. & FREER, J. E. 2015. A high-resolution global flood hazard model. *Water Resources Research,* 51**,** 7358-7381.

SCHELFAUT, K., PANNEMANS, B., VAN DER CRAATS, I., KRYWKOW, J., MYSIAK, J. & COOLS, J. 2011. Bringing flood resilience into practice: the FREEMAN project. *Environmental Science & Policy,* 14**,** 825-833.

SMITH, A., BATES, P. D., WING, O., SAMPSON, C., QUINN, N. & NEAL, J. 2019. New estimates of flood exposure in developing countries using high-resolution population data. *Nature Communications,* 10**,** 1814.

STEVENS, F. R., GAUGHAN, A. E., LINARD, C. & TATEM, A. J. 2015. Disaggregating Census Data for Population Mapping Using Random Forests with Remotely-Sensed and Ancillary Data. *Plos One,* 10**,** 22.

TELLMAN, B., SULLIVAN, J. A., KUHN, C., KETTNER, A. J., DOYLE, C. S., BRAKENRIDGE, G. R., ERICKSON, T. A. & SLAYBACK, D. A. 2021. Satellite imaging reveals increased proportion of population exposed to floods. *Nature,* 596**,** 80-86.

THOMSON, D. R., GAUGHAN, A. E., STEVENS, F. R., YETMAN, G., ELIAS, P. & CHEN, R. 2021. Evaluating the Accuracy of Gridded Population Estimates in Slums: A Case Study in Nigeria and Kenya. 5**,** 48.

TIECKE, T. G. L., XIANMING ZHANG, AMY GROS, ANDREAS LI, NAN YETMAN, GREGORY KILIC, TALIP MURRAY, SIOBHAN BLANKESPOOR, BRIAN PRYDZ, ESPEN B. DANG, HAI-ANH H. 2017. *Mapping the World Population One Building at a Time*.

TRIGG, M. A., BERNHOFEN, M. V., MARECHAL, D., ALFIERI, L., DOTTORI, F., HOCH, J. M., HORRITT, M. S., SAMPSON, C., SMITH, A., YAMAZAKI, D. & LI, H. Y. 2020. Global Flood Models. *American Geophysical Union Monograph: Global drought and flood.* Wiley.

TRIGG, M. A., BIRCH, C. E., NEAL, J. C., BATES, P. D., SMITH, A., SAMPSON, C. C., YAMAZAKI, D., HIRABAYASHI, Y., PAPPENBERGER, F., DUTRA, E., WARD, P. J., WINSEMIUS, H. C., SALAMON, P., DOTTORI, F., RUDARI, R., KAPPES, M. S., SIMPSON, A. L., HADZILACOS, G. & FEWTRELL, T. J. 2016. The credibility challenge for global fluvial flood risk analysis. *Environmental Research Letters,* 11**,** 10.

UNDRR 2020. *Human Cost of Disasters: An overview of the last 20 years 2000-2019*, United Nations.

UNISDR 2004. Living with risk: a global review of disaster reduction initiatives. United Nations for Disaster Risk Reduction (UNISDR).

UNISDR 2015. Sendai Framework for Disaster Risk Reduction 2015-2030. United Nations - Headquarters (UN).

VAN WESENBEECK, B. K., MULDER, J. P. M., MARCHAND, M., REED, D. J., DE VRIES, M. B., DE VRIEND, H. J. & HERMAN, P. M. J. 2014. Damming deltas: A practice of the past? Towards nature-based flood defenses. *Estuarine, Coastal and Shelf Science,* 140**,** 1-6.

VAN WESTEN, C. J. 2014. Vulnerability. *Caribbean Handbook on Risk Management: Methodology Book.* Carribean Disaster Emergency Managment Agency.

VENOT, J.-P., BOWERS, S., BROCKINGTON, D., KOMAKECH, H., RYAN, C. M., VELDWISCH, G. J. & WOODHOUSE, P. J. W. A. 2021. Below the

Radar: Data, Narratives and the Politics of Irrigation in Sub-Saharan Africa. 14**,** 546-572.

VINNARASI, R. & DHANYA, C. T. 2016. Changing characteristics of extreme wet and dry spells of Indian monsoon rainfall. 121**,** 2146-2160.

WARD, P. J., BLAUHUT, V., BLOEMENDAAL, N., DANIELL, J. E., DE RUITER, M. C., DUNCAN, M. J., EMBERSON, R., JENKINS, S. F., KIRSCHBAUM, D., KUNZ, M., MOHR, S., MUIS, S., RIDDELL, G. A., SCHÄFER, A., STANLEY, T., VELDKAMP, T. I. E. & WINSEMIUS, H. C. 2020a. Review article: Natural hazard risk assessments at the global scale. *Nat. Hazards Earth Syst. Sci.,* 20**,** 1069-1096.

WARD, P. J., JONGMAN, B., SALAMON, P., SIMPSON, A., BATES, P., DE GROEVE, T., MUIS, S., DE PEREZ, E. C., RUDARI, R., TRIGG, M. A. & WINSEMIUS, H. C. 2015. Usefulness and limitations of global flood risk models. *Nature Climate Change,* 5**,** 712-715.

WARD, P. J., JONGMAN, B., WEILAND, F. S., BOUWMAN, A., VAN BEEK, R., BIERKENS, M. F. P., LIGTVOET, W. & WINSEMIUS, H. C. 2013. Assessing flood risk at the global scale: model setup, results, and sensitivity. *Environmental Research Letters,* 8**,** 10.

WARD, P. J., WINSEMIUS, H. C., KUZMA, S., BIERKENS, M. F. P., BOUWMAN, A., DE MOEL, H., DÍAZ LOAIZA, A., EILANDER, D., ENGLHARDT, J., ERKENS, G., TAFETE GEBTEMEDHIN, E., ICELAND, C., KOOI, H., LIGTVOET, W., MUIS, S., SCUSSOLINI, P., SUTANUDJAJA, E. H., VAN BEEK, R., VAN BEMMEL, B., VAN HUIJSTEE, J., VAN RIJN, F., VAN WESENBEECK, B., VATVANI, D., VERLAAN, M., TIGGELOVEN, T. & LUO, T. 2020b. Aqueduct Floods Methodology. Wasington D.C.: World Resources Institute.

WING, O. E. J., BATES, P. D., NEAL, J. C., SAMPSON, C. C., SMITH, A. M., QUINN, N., SHUSTIKOVA, I., DOMENEGHETTI, A., GILLES, D. W., GOSKA, R. & KRAJEWSKI, W. F. 2019. A New Automated Method for Improved Flood Defense Representation in Large-Scale Hydraulic Models. *Water Resources Research,* 55**,** 11007-11034.

WING, O. E. J., BATES, P. D., SAMPSON, C. C., SMITH, A. M., JOHNSON, K. A. & ERICKSON, T. A. 2017. Validation of a 30 m resolution flood hazard model of the conterminous United States. *Water Resources Research,* 53**,** 7968-7986.

WING, O. E. J., BATES, P. D., SMITH, A. M., SAMPSON, C. C., JOHNSON, K. A., FARGIONE, J. & MOREFIELD, P. 2018. Estimates of present and future flood risk in the conterminous United States. *Environmental Research Letters,* 13**,** 7.

WING, O. E. J., PINTER, N., BATES, P. D. & KOUSKY, C. 2020. New insights into US flood vulnerability revealed from flood insurance big data. *Nature Communications,* 11**,** 1444.

WING, O. E. J., SMITH, A. M., MARSTON, M. L., PORTER, J. R., AMODEO, M. F., SAMPSON, C. C. & BATES, P. D. 2021. Simulating historical flood events at the continental scale: observational validation of a large-scale hydrodynamic model. *Nat. Hazards Earth Syst. Sci.,* 21**,** 559-575.

WINSEMIUS, H. C., VAN BEEK, L. P. H., JONGMAN, B., WARD, P. J. & BOUWMAN, A. 2013. A framework for global river flood risk assessments. *Hydrology and Earth System Sciences,* 17**,** 1871-1892.

WISSMAN-WEBER, N. K. & LEVY, D. L. 2018. Climate adaptation in the Anthropocene: Constructing and contesting urban risk regimes. *Organization,* 25**,** 491-516.

YAMAZAKI, D., KANAE, S., KIM, H. & OKI, T. 2011. A physically based description of floodplain inundation dynamics in a global river routing model. *Water Resources Research,* 47**,** 21.

YAMAZAKI, D., TRIGG, M. A. & IKESHIMA, D. 2015. Development of a global similar to 90 m water body map using multi-temporal Landsat images. *Remote Sensing of Environment,* 171**,** 337-351.

YUSOFF, I. M., RAMLI, A., ALKASIRAH, N. A. M., NASIR, N. A. A. M. J. G. M. J. O. S. & SPACE 2018. Exploring the managing of flood disaster: A Malaysian perspective. 14**,** 24-36.

ZHOU, X., MA, W., ECHIZENYA, W. & YAMAZAKI, D. 2020. Uncertainty in flood frequency analysis of hydrodynamic model simulations. *Nat. Hazards Earth Syst. Sci. Discuss.,* 2020**,** 1-31.

Chapter 6

Discussion and Conclusions

The aim of this thesis was to further the evaluation of global flood risk datasets to inform their appropriate application and continued development. Global flood models were reviewed in **Chapter 2**, providing users of these datasets with a source that details the different global flood model structures and applications. In **Chapter 3**, the global flood models were collectively validated for the first time against flood events in Nigeria and Mozambique. This collective evaluation identified model components that affected performance and showed that while there was significant variation between the global flood models, the best performing models showed an acceptable level of performance on the large rivers examined. However, global flood models don't all model flooding on the same rivers. In **Chapter 4**, flood exposure to different sized rivers was examined globally and nationally using a geomorphological flood susceptibility map. Flood exposure estimates were significantly impacted by both the size of the flood map's river network and the choice of global population dataset used in the exposure calculation. In **Chapter 5**, global datasets comprising all components of flood risk (hazard, exposure, and vulnerability) were evaluated for flood risk management at the national scale in Colombia, England, Ethiopia, India, and Malaysia. There was significant variation in the national flood risk estimates calculated using global data and constraints related to the institutional capacity required to use this data nationally were identified. While some global flood risk data could be useful at national scales, further corroboration with local data is necessary.

In this chapter, the key outcomes and findings from this thesis will be summarized and discussed with reference to the wider literature. Future research directions building on the work of this thesis will then be identified. This chapter (and thesis) will finish with some concluding remarks.

6.1   Key Outcomes and Findings

6.1.1   A comprehensive review of global flood risk models

One of the common objectives throughout this thesis was to produce useful information for end-users of global flood risk datasets. Articles (Teng et al., 2017) and desktop studies (Neelz and Pender, 2009) reviewing hydraulic modelling methods and packages are useful starting (and reference) points for prospective modellers. Existing studies reviewing global flood risk models had either been short commentaries (Ward et al., 2015) or focussed on individual models (Bates et al., 2018). **Chapter 2** presented the first detailed review of all existing global flood models. This chapter introduced a development timeline of global flood models, highlighting the release of key datasets and scientific meetings which furthered the science of global flood risk. The structural similarities and differences between the global flood models were also discussed, providing potential users of the model with information pertinent to the selection of the appropriate model. The important work of Hoch and Trigg (2019) was built upon in **Chapter 2** and a map was produced illustrating where these models had been validated globally, and thus where they could be used with more confidence. Global flood models are rarely used in isolation and are often used to represent a single component of risk (hazard) in global flood risk studies. In **Chapter 5**, global datasets and approaches comprising the three components of risk (hazard, exposure, and vulnerability) were reviewed and applied nationally in five countries. Global population data — the most common datasets for calculating global flood exposure — had recently been reviewed in detail by Leyk et al. (2019). **Chapter 5** was the first time the entire catalogue of previously used global population datasets had been reviewed and assessed in the context of flood exposure; similarly, this was the first time different global vulnerability approaches had been reviewed and compared. In addition to informing end-users where to access global flood risk data, **Chapter 5** detailed how national flood risk assessments could be carried out with global data and highlighted potential limits to their use.

6.1.2   Collective validation of global flood models is essential

The global flood models had all been subject to internal validation studies. However, due to different validation approaches, data, and locations (illustrated in Figure 2.3) these results were incomparable between studies. Global flood model intercomparison studies in Africa (Trigg et al., 2016b) and China (Aerts et al., 2020) had shown large discrepancies in modelled output, but relative performance could not be assessed due to the lack of validation data. In **Chapter 3** the first collective validation of global flood models was carried out and the benefits of such a study were realized. Collective evaluation meant the model components contributing to performance could be identified with greater confidence. In Trigg et al. (2016b) it was hypothesized that poor representation of precipitation in reanalysis data led to comparatively large flood extents for the ECMWF model in Africa relative to the rest. In **Chapter 3,** there was further evidence to support this hypothesis as all the models forced by reanalysis data showed less return period accuracy than the models forced by gauged data. The collective validation also showed that hydrodynamic global flood models were better able to replicate the validation data compared with global flood models with cruder representations of fluid flow. The spatial resolution of the models was found to have no impact on performance, contrary to the findings of previous research (Horritt and Bates, 2001, Savage et al., 2016). This was likely due to the large size of the rivers examined and the comparatively greater impact of other model characteristics on performance.

Whilst the primary purpose of **Chapter 3** was to demonstrate the value of collective validation, a secondary goal of the study was to encourage future model evaluation studies to use the data (and share theirs) so model results could be easily compared across studies. In **Chapter 4**, the benefits of shared validation data were shown as the developed geomorphological flood susceptibility map was validated against this data, allowing its performance to be evaluated relative to existing global flood models. Further evidence highlighting the value of sharing validation data can be found in the study of Mester et al. (2021) who, in their evaluation of multiple global hydrological models, used the validation data published in **Chapter 3**.

No approach to validation is without its limitations. In **Chapter 3**, optical satellite images were used to delineate reference flood extents in Nigeria and Mozambique and then used as validation data. There are two key limitations to such

a validation approach. Firstly, global flood models simulate floods with spatially uniform return periods, such behaviour is uncharacteristic of an actual flood event. To accurately validate a flood model against historical flood events Wing et al. (2021) proposed a methodology which consists of first simulating the historical events with a model and then validating the model with observed data. While such an approach would certainly result in more accurate validation, the application of such a methodology is limited to regions with the necessary data (river or rain gauge) to simulate the historical events. Additionally, applied in the context of global flood model validation intercomparison it would require the models being compared to be re-run for each event, which could pose a problem for the global flood models due to the discrepancy of inputs required to run each model. The validation regions in **Chapter 3** were purposely restricted to areas containing major flood extents (rather than examining the entire basin) to reduce spatial variations in the extremity of the validation data and allow for a more representative validation of the homogenous return period global flood maps. The second key limitation relates to the accuracy of the optical imagery used as validation data. This is an established issue in model evaluation and several workarounds have been proposed including treating the observed data probabilistically (Stephens et al., 2012) and explicitly accounting for known sources of observational uncertainty (Hawker et al., 2020). Observational uncertainty was accounted for in a more qualitative manner in **Chapter 3**, as the optical images were manually checked for errors.

6.1.3   The varied representativeness of global flood models

One of the considerations when choosing the validation locations and events in **Chapter 3** was that flooding needed to have occurred on rivers large enough to be represented by all the global flood models because they don't all model flooding on the same rivers. Indeed, the best performing global flood model in **Chapter 3** (JRC) was also one of the most restrictive in terms of rivers modelled — only modelling rivers with an upstream drainage area of 5,000 km^2 or greater. Flooding from different sized rivers is something that has received little attention in the literature. In Wing et al. (2017), a continental model of the US was validated against existing national flood maps and performance metrics were reported for different river size categories, with notable performance increases on larger rivers. At the global scale, Kummu et al. (2011) explored population distance to different sized rivers, however,

this study was concerned with fresh water access rather than the flood risk posed by different sized rivers. In **Chapter 4**, global flood exposure to different sized rivers was explored for the first time. Using a geomorphological flood susceptibility map, rivers classified as streams (upstream drainage area 10-100 km^2) and small rivers (upstream drainage area 100 km^2 - 1,000 km^2) were found to be responsible for nearly 40% of global flood exposure. When specific global flood model river size thresholds were applied, global flood exposure estimates differed by over a factor of 2 between the most representative river size threshold (upstream drainage area > 50 km^2) and the least representative river size threshold (upstream drainage area > 5000 km^2). The impact of river size thresholds on exposure estimates was often more extreme at the national level. This was especially evident in **Chapter 5**, where national flood exposure estimates in Colombia and Ethiopia calculated using the most representative model (Fathom) were roughly double the national flood exposure estimates calculated using the remaining four models. The findings of **Chapter 4** and **Chapter 5** highlighted the impact different global flood model river threshold sizes can have on model outputs. This impact is certainly not trivial and can be of several orders of magnitude — especially at the national scale — and should therefore be an important consideration in the both the choice of global flood model and in the interpretation of global flood model outputs. The river flood susceptibility map developed in **Chapter 4** was published openly with the intention of allowing users to carry out a first order analysis with the dataset to determine their required global flood model representativeness.

6.1.4 The impact of population data on exposure estimates

Global population maps are vital datasets for translating flood hazard into flood exposure. Approaches to mapping global population differ significantly (Leyk et al., 2019), which results in global population maps with different spatial distributions of population (Thomson et al., 2021). Although they have been used extensively in studies of global flood exposure, the implication of using different global population maps in estimates of flood exposure has only recently been addressed. A study by Smith et al. (2019) found flood exposure estimates in 18 developing countries were reduced when using new high-resolution population maps (HRSL) compared with two existing, widely used, population maps (WorldPop and Landscan). To build on this work, **Chapter 4**, explored the impact of using three different global population datasets (HRSL, GHS-POP, and WorldPop) on flood

exposure estimates globally. The comparison with HRSL was also extended from 18 countries (Smith et al., 2019) to include 168 different countries globally. The findings of **Chapter 4** correspond with those of Smith et al. (2019) in that flood exposure estimates calculated using HRSL were typically lower than exposure estimates calculated with existing global population maps. The results of **Chapter 4** do not, however, correspond with the results of Lindersson et al. (2021) who compared the same population datasets and found different relative impacts on national flood exposure estimates in the 26 countries examined. The result differed because the Lindersson et al. (2021) study did not scale national population totals equally between datasets, thus making national population estimates the driving factor in exposure disagreement. The population datasets compared in **Chapter 4** and in the studies of Smith et al. (2019) and Lindersson et al. (2021) still did not encompass all the global population maps used in previous studies of global flood exposure. In **Chapter 5**, all such datasets were identified and compared. In total, 7 different global population maps were used to calculate flood exposure in Colombia, England, Ethiopia, India, and Malaysia. This work demonstrated that national flood exposure estimates could be significantly altered by the choice of global population map and showed that some previously used population datasets result in questionable exposure estimates, suggesting they may not be appropriate for use in flood exposure studies.

6.1.5 Limitations to global vulnerability approaches

Vulnerability is the component of flood risk most frequently absent from global studies (Ward et al., 2020); however, it is arguably the risk component most important to communicating flood impacts. Global studies reporting vulnerability rely on global approaches and datasets with significant limitations; consequently they must make quite strong assumptions. Three global approaches for calculating the direct economic damages of flooding were compared for the first time in **Chapter 5.** The choice of vulnerability approach was found to have a huge impact on national flood damage estimates. The most notable difference between the three approaches was how they identified assets at risk. Urban areas were defined three ways: artificial areas in a global land cover map, cells in a settlement map above a certain built-up area threshold, or through a map of fractional urban land cover. These three urban definitions led to urban areas which differed by up to a factor 25

and was the reason for the stark differences in national damages between the three vulnerability approaches. The influence of other vulnerability inputs such as asset valuation and damage curves, which had been the primary sources of uncertainty in the evaluation of different regional damage models (de Moel and Aerts, 2011), were negligible in the face of such variations in the quantification of assets at risk. Similarly, the impact different assumptions of urban sector land-use had on national flood damage estimates paled in comparison to the impact of different urban areas.

The comparison of vulnerability approaches in **Chapter 5** merely scratched the surface of the different uncertainties associated with these global vulnerability methods. A more detailed sensitivity analysis of the different vulnerability inputs and assumptions could have been carried out to better quantify uncertainties. However, this was deemed outside the scope of the work, as the goal of the study was to compare "off-the-shelf" global approaches for each component of flood risk. Vulnerability was certainly the most uncertain component of global flood risk and the one which translated least well nationally.

6.1.6 Advocating a multi-dataset approach

In **Chapter 3,** the performance of an aggregated global flood model (Trigg et al., 2016a) was found to be similar to the best performing model and an ensemble of the three best performing models. The use of multiple models was proposed in regions where it is not possible to determine the best performing model through validation. Advocating a multi-dataset approach has been a common theme throughout this thesis. In **Chapter 4**, three global population datasets commonly used to calculate flood exposure were compared and found to vary significantly, especially at the national level. Similarly, in **Chapter 5**, when 16 global datasets of flood hazard, population, and vulnerability were used to calculate national flood risk in five countries there was significant variation in the resultant risk estimates. The discrepancies between the global datasets and approaches used to calculate flood risk raised some questions about the validity of the flood risk estimates in previous studies where only a single model or dataset had been used. Flood modelling is rife with uncertainties (Dottori et al., 2013), and these are exacerbated at the global scale. Where model uncertainty cannot be represented probabilistically (Neal et al., 2013, Savage et al., 2016) and evaluation is not possible due to the lack of validation

data, the use of multiple datasets can be a useful starting point for determining the confidence in flood risk estimates.

6.1.7 Local capacity considerations when using global data nationally

One of the most promising applications of global flood risk data is to fill data gaps in regions lacking any existing flood risk information. However, simply producing and sharing these datasets does not mean they will have any useful practical application. The usefulness of global flood risk data depends on its intended use, the context and locality in which it is used, and the expectations of end-users (Ward et al., 2015). These considerations have often been absent from studies exploring the practical application of global flood risk data. In Emerton et al. (2020) these considerations were addressed in the context of flood forecasting and disaster impact assessments for cyclones Idai and Kenneth in Mozambique. Timelines of when, how, and by whom global data were used were presented for both disasters as well as how these datasets were used in the context of Mozambique's existing disaster risk management structure. In **Chapter 5**, the use of global datasets for flood risk management was explored in five countries: Colombia, England, Ethiopia, India, and Malaysia. The flood risk management structure of each country was outlined and issues related to the capacity of each country to use this data for national flood risk management were identified through literature review and interviews with local water experts. **Chapter 5** emphasized that considering local context and capacity is equally as important as evaluating the quality of global data when considering its use nationally. For example, global flood models may be of little use in Colombia, irrespective of data quality, due to the country's ex-post approach to flood risk management. The work in **Chapter 5** started a dialogue on using global data for flood risk management, highlighting the challenges and potential pitfalls to its effective application nationally.

6.2 Contributions to Science

This thesis has contributed to the science of global flood risk in a number of ways. In **Chapter 2**, all global flood risk models were reviewed for the first time, providing users of the data with a single reference that details different model structures and applications. In **Chapter 3**, six global flood models were collectively

validated, shedding light on the comparative performance of global flood models, which had not been possible in previous intercomparison work. The validation data used in **Chapter 3** was published openly and further model evaluation studies have incorporated this data into their testing frameworks. In **Chapter 4**, flood exposure to different sized rivers was quantified globally, demonstrating that global flood model river size thresholds have enormous impacts on exposure estimates. The geomorphological river flood susceptibility map developed in **Chapter 4** was published openly to allow prospective global flood model users to carry out a first order analysis to determine the appropriate level of river representation required for their needs. **Chapter 4** was also the first study to compare population datasets globally in the context of flood exposure, showing that the choice of global population data can have significant impacts on flood exposure estimates. In **Chapter 5**, the entire catalogue of previously used, openly available, global datasets of flood hazard, exposure, and vulnerability were assessed for national flood risk management in five countries, identifying global data characteristics that would limit their use nationally. In addition to being the first intercomparison of global datasets comprising the three components of flood risk, **Chapter 5** also explored the national applicability of global data from a local capacity perspective, which had not been done before in the context of flood risk management.

6.3 Future Work

There are numerous avenues to continue and build upon the research in this thesis. Arguably the most pressing future research direction, which could build on the work of **Chapter 3**, is the global evaluation of global flood models. Recently published large datasets of observed flood events (Tellman et al., 2021) could be the starting point for developing a global catalogue of validation data through which new and updated models could be tested and performance results compared. Incorporating new approaches to account for observational uncertainty (Hawker et al., 2020) and methods to estimate the return periods of observed flood events (Kettner et al., 2021) would certainly make any global validation more robust. Local and national flood maps could also be incorporated as additional validation data sets where available. In regions lacking any validation data the intercomparison of global flood maps could be a useful indicator about where the models are confident in their flood predictions (where they agree) and where they are not. Indeed, an

intercomparison of global flood models globally would be a useful starting point for any global evaluation of these models. Further expanding this intercomparison to look at future estimates of flooding would be a timely addition, as industry users of these models are increasingly needing to assess future climate risks (Fiedler et al., 2021).

Several resources have been published over the last few years which have been invaluable to users of global population maps (Leyk et al., 2019, TReNDS, 2020). These studies detail the different available datasets, their approaches, limitations, and intended use. However, there has been no quantification of how these global population datasets differ globally, meaning users have to rely on qualitative judgments in choosing which global population map to use. Approaches for comparing population maps were explored in **Chapter 5**, where agreement between populated cells was measured between datasets. There were limits to the conclusions that could be drawn from such an approach, because differences in population density were not compared. Quantitative global comparison of population maps will require novel techniques and approaches, which may have to be tailored to the context in which the data will be used. Further to the intercomparison of global population maps is the need to validate these maps; something that became evident in **Chapter 4**, where no single population dataset could be definitively recommended without reference data to gauge relative performance. The validation of population maps is more data and time intensive than the validation of flood models, often requiring locally collected and geo-referenced data (Tiecke, 2017, Thomson et al., 2021). Despite these challenges, there are a number of potential opportunities for research in this space, especially as these population datasets continue to improve through the development of new remote sensing products and the growth of community mapping projects such as Open Street Map.

Two interesting further research directions related to the practical application of global flood risk data have been identified. The first relates to how and what these global datasets can be used for, what the limits are to their application, and how locally available data can complement global data to expand their usefulness. **Chapter 5** showed how global vulnerability approaches were limited by global land cover maps. However, these vulnerability approaches could easily incorporate local

land use and land value data to significantly improve the accuracy and local relevance of damage estimates. The incorporation of local data could improve all components of global flood risk. Potentially useful from a user perspective would be a framework that demonstrates flood risk assessment best practice and how to effectively incorporate locally available data with global data. The second future research direction builds on the work started in **Chapter 5**, and relates to the institutional capacity to use global flood risk data nationally. Some institutional capacity constraints were realized and identified in **Chapter 5.** Further work should examine these capacity considerations in greater detail and dig deeper into the structure of national flood risk management to identify where, and if, these global datasets could be useful.

6.4 Concluding Remarks

Global flood risk models have progressed enormously over the last decade and will continue to do so over the coming years as new approaches and datasets are developed. The continued refinement of these models will see them applied across a wide variety of use cases. As their applicability increases, it is important that the evaluation of these models progresses in a similar fashion. This thesis introduced the first collective validation of global flood models and highlighted the benefits of such an approach. Future model evaluation studies should build on this framework, which allows end-users to easily compare model performance and allows model developers to discern where certain modelling approaches work best and where they don't. Also addressed in this thesis were issues of global flood model representativeness: thresholds applied to the size of rivers modelled were shown to have enormous implications on estimates of flooding. Translating global flood hazard into risk requires additional global datasets of exposure and vulnerability, which this thesis showed leads to cascading uncertainty in flood risk estimates, especially at the national level. If these datasets are to be used effectively for national flood risk management, this uncertainty needs to be considered alongside the local capacity to use these datasets.

The work in this thesis has highlighted and addressed numerous challenges related to the evaluation and effective application of global flood risk data. These

findings should inform both users and developers of these global flood risk datasets while also providing a starting point for further avenues of research.

References

AERTS, J. P. M., UHLEMANN-ELMER, S., EILANDER, D. & WARD, P. J. 2020. Comparison of estimates of global flood models for flood hazard and exposed gross domestic product: a China case study. *Nat. Hazards Earth Syst. Sci.,* 20**,** 3245-3260.

BATES, P. D., NEAL, J., SAMPSON, C., SMITH, A. & TRIGG, M. 2018. Chapter 9 - Progress Toward Hyperresolution Models of Global Flood Hazard. *In:* MICHEL, G. (ed.) *Risk Modeling for Hazards and Disasters.* Elsevier.

DE MOEL, H. & AERTS, J. C. J. H. 2011. Effect of uncertainty in land use, damage models and inundation depth on flood damage estimates. *Natural Hazards,* 58**,** 407-425.

DOTTORI, F., DI BALDASSARRE, G. & TODINI, E. 2013. Detailed data is welcome, but with a pinch of salt: Accuracy, precision, and uncertainty in flood inundation modeling. 49**,** 6079-6085.

EMERTON, R., CLOKE, H., FICCHI, A., HAWKER, L., DE WIT, S., SPEIGHT, L., PRUDHOMME, C., RUNDELL, P., WEST, R., NEAL, J., CUNA, J., HARRIGAN, S., TITLEY, H., MAGNUSSON, L., PAPPENBERGER, F., KLINGAMAN, N. & STEPHENS, E. 2020. Emergency flood bulletins for Cyclones Idai and Kenneth: A critical evaluation of the use of global flood forecasts for international humanitarian preparedness and response. *International Journal of Disaster Risk Reduction,* 50**,** 101811.

FIEDLER, T., PITMAN, A. J., MACKENZIE, K., WOOD, N., JAKOB, C. & PERKINS-KIRKPATRICK, S. E. 2021. Business risk and the emergence of climate analytics. *Nature Climate Change,* 11**,** 87-94.

HAWKER, L., NEAL, J., TELLMAN, B., LIANG, J., SCHUMANN, G., DOYLE, C., SULLIVAN, J. A., SAVAGE, J. & TSHIMANGA, R. 2020. Comparing earth observation and inundation models to map flood hazards. *Environmental Research Letters,* 15**,** 124032.

HOCH, J. M. & TRIGG, M. A. 2019. Advancing global flood hazard simulations by improving comparability, benchmarking, and integration of global flood models. *Environmental Research Letters,* 14**,** 034001.

HORRITT, M. S. & BATES, P. D. 2001. Effects of spatial resolution on a raster based model of flood flow. *Journal of Hydrology,* 253**,** 239-249.

KETTNER, A. J., BRAKENRIDGE, G. R. & COHEN, S. 2021. Analyzing flood frequency using multi-sensor satellite data: a global approach. *American Geophysical Union.* New Orleans, LA.

KUMMU, M., DE MOEL, H., WARD, P. J. & VARIS, O. 2011. How Close Do We Live to Water? A Global Analysis of Population Distance to Freshwater Bodies. *Plos One,* 6**,** 13.

LEYK, S., GAUGHAN, A. E., ADAMO, S. B., DE SHERBININ, A., BALK, D., FREIRE, S., ROSE, A., STEVENS, F. R., BLANKESPOOR, B., FRYE, C., COMENETZ, J., SORICHETTA, A., MACMANUS, K., PISTOLESI, L., LEVY, M., TATEM, A. J. & PESARESI, M. 2019. The spatial allocation of

population: a review of large-scale gridded population data products and their fitness for use. *Earth Syst. Sci. Data,* 11**,** 1385-1409.

LINDERSSON, S., BRANDIMARTE, L., MÅRD, J. & DI BALDASSARRE, G. 2021. Global riverine flood risk – how do hydrogeomorphic floodplain maps compare to flood hazard maps? *Nat. Hazards Earth Syst. Sci.,* 21**,** 2921-2948.

MESTER, B., WILLNER, S. N., FRIELER, K. & SCHEWE, J. 2021. Evaluation of river flood extent simulated with multiple global hydrological models and climate forcings. *Environmental Research Letters,* 16**,** 094010.

NEAL, J., KEEF, C., BATES, P., BEVEN, K. & LEEDAL, D. 2013. Probabilistic flood risk mapping including spatial dependence. *Hydrological Processes,* 27**,** 1349-1363.

NEELZ, S. & PENDER, G. 2009. Desktop review of 2D hydraulic modelling packages. Bristol, UK: Environment Agency.

SAVAGE, J. T. S., BATES, P., FREER, J., NEAL, J. & ARONICA, G. 2016. When does spatial resolution become spurious in probabilistic flood inundation predictions? *Hydrological Processes,* 30**,** 2014-2032.

SMITH, A., BATES, P. D., WING, O., SAMPSON, C., QUINN, N. & NEAL, J. 2019. New estimates of flood exposure in developing countries using high-resolution population data. *Nature Communications,* 10**,** 1814.

STEPHENS, E. M., BATES, P. D., FREER, J. E. & MASON, D. C. 2012. The impact of uncertainty in satellite data on the assessment of flood inundation models. *Journal of Hydrology,* 414-415**,** 162-173.

TELLMAN, B., SULLIVAN, J. A., KUHN, C., KETTNER, A. J., DOYLE, C. S., BRAKENRIDGE, G. R., ERICKSON, T. A. & SLAYBACK, D. A. 2021. Satellite imaging reveals increased proportion of population exposed to floods. *Nature,* 596**,** 80-86.

TENG, J., JAKEMAN, A. J., VAZE, J., CROKE, B. F. W., DUTTA, D. & KIM, S. 2017. Flood inundation modelling: A review of methods, recent advances and uncertainty analysis. *Environmental Modelling & Software,* 90**,** 201-216.

THOMSON, D. R., GAUGHAN, A. E., STEVENS, F. R., YETMAN, G., ELIAS, P. & CHEN, R. 2021. Evaluating the Accuracy of Gridded Population Estimates in Slums: A Case Study in Nigeria and Kenya. 5**,** 48.

TIECKE, T. G. L., XIANMING ZHANG, AMY GROS, ANDREAS LI, NAN YETMAN, GREGORY KILIC, TALIP MURRAY, SIOBHAN BLANKESPOOR, BRIAN PRYDZ, ESPEN B. DANG, HAI-ANH H. 2017. *Mapping the World Population One Building at a Time*.

TRENDS 2020. Leaving no one off the map: a guide for gridded population data for sustainable development. Thematic Research Network on Data and Statistics.

TRIGG, M. A., BIRCH, C. E., NEAL, J., BATES, P., SMITH, A., SAMPSON, C., YAMAZAKI, D., HIRABAYASHI, Y., PAPPENBERGER, F., DUTRA, E., WARD, P. J., WINSEMIUS, H. C., SALAMON, P., DOTTORI, F., RUDARI, R., KAPPES, M. S., SIMPSON, A., HADZILACOS, G. & FEWTRELL, T. 2016a. Aggregated fluvial flood hazard output for six Global Flood Models for the African Continent. Research Data Leeds Repository.

TRIGG, M. A., BIRCH, C. E., NEAL, J. C., BATES, P. D., SMITH, A., SAMPSON, C. C., YAMAZAKI, D., HIRABAYASHI, Y., PAPPENBERGER, F., DUTRA, E., WARD, P. J., WINSEMIUS, H. C., SALAMON, P., DOTTORI, F., RUDARI, R., KAPPES, M. S., SIMPSON, A. L., HADZILACOS, G. & FEWTRELL, T. J. 2016b. The credibility

challenge for global fluvial flood risk analysis. *Environmental Research Letters,* 11, 10.

WARD, P. J., BLAUHUT, V., BLOEMENDAAL, N., DANIELL, J. E., DE RUITER, M. C., DUNCAN, M. J., EMBERSON, R., JENKINS, S. F., KIRSCHBAUM, D., KUNZ, M., MOHR, S., MUIS, S., RIDDELL, G. A., SCHÄFER, A., STANLEY, T., VELDKAMP, T. I. E. & WINSEMIUS, H. C. 2020. Review article: Natural hazard risk assessments at the global scale. *Nat. Hazards Earth Syst. Sci.,* 20, 1069-1096.

WARD, P. J., JONGMAN, B., SALAMON, P., SIMPSON, A., BATES, P., DE GROEVE, T., MUIS, S., DE PEREZ, E. C., RUDARI, R., TRIGG, M. A. & WINSEMIUS, H. C. 2015. Usefulness and limitations of global flood risk models. *Nature Climate Change,* 5, 712-715.

WING, O. E. J., BATES, P. D., SAMPSON, C. C., SMITH, A. M., JOHNSON, K. A. & ERICKSON, T. A. 2017. Validation of a 30 m resolution flood hazard model of the conterminous United States. *Water Resources Research,* 53, 7968-7986.

WING, O. E. J., SMITH, A. M., MARSTON, M. L., PORTER, J. R., AMODEO, M. F., SAMPSON, C. C. & BATES, P. D. 2021. Simulating historical flood events at the continental scale: observational validation of a large-scale hydrodynamic model. *Nat. Hazards Earth Syst. Sci.,* 21, 559-575.

Appendix A

Supplementary Material to Chapter 3

Appendix A consists of the supplementary material that accompanied the manuscript on which **Chapter 3** is based.

A.1 Description of DFO JPEG to GeoTiff conversion

The 2007 flood event vector data was not available from the Dartmouth Flood Observatory (DFO) website and instead the JPEG of the observed event (Figure A.1) had to be georeferenced in QGIS (v2.18) for analysis. The QGIS 'Raster Georeferencer' tool was used to add latitudinal and longitudinal information to a raster image. As the DFO image in Figure A.1 displays latitude and longitude on a simple grid, it was possible to input the exact coordinates of the four grid intersections in the Georeferencer tool. Coordinates were input as WGS84 as stated on the DFO event header (Figure A.1).

The DFO inundation map in Figure 1 maps observed flooding in different shades of red depending on the recorded date of inundation. To allow for analysis, the range of colours representing flooded areas needed to be condensed into one common 'wet' type. To do this the 'RGB to PCT' tool in QGIS was used which creates a classified raster by grouping colours by similarity. Through trial and error, the optimal number of colour classes to use was found to be 150. This is compared with the original 25,000 colour classes present before. The various colour values of red were merged into one 'flooded' value using the GRASS GIS 'r.reclass' tool in QGIS. All remaining colours were redefined as zero.

An issue that was encountered when georeferencing the DFO image was the town names and markers which overlap onto the river and the observed flood extents. A zoomed in image of this issue can be seen in Figure A.2. Determining whether the pixels behind the text in the map were flooded or not was found to be a highly subjective exercise. To prevent any user bias these regions were reclassified as 'no data' regions, thereby excluding these areas from further analysis.

Figure A.1 Dartmouth Flood Observatory JPEG image of observed flooding in
2007 in Mozambique.

Source: Anderson and Brakenridge (2007)
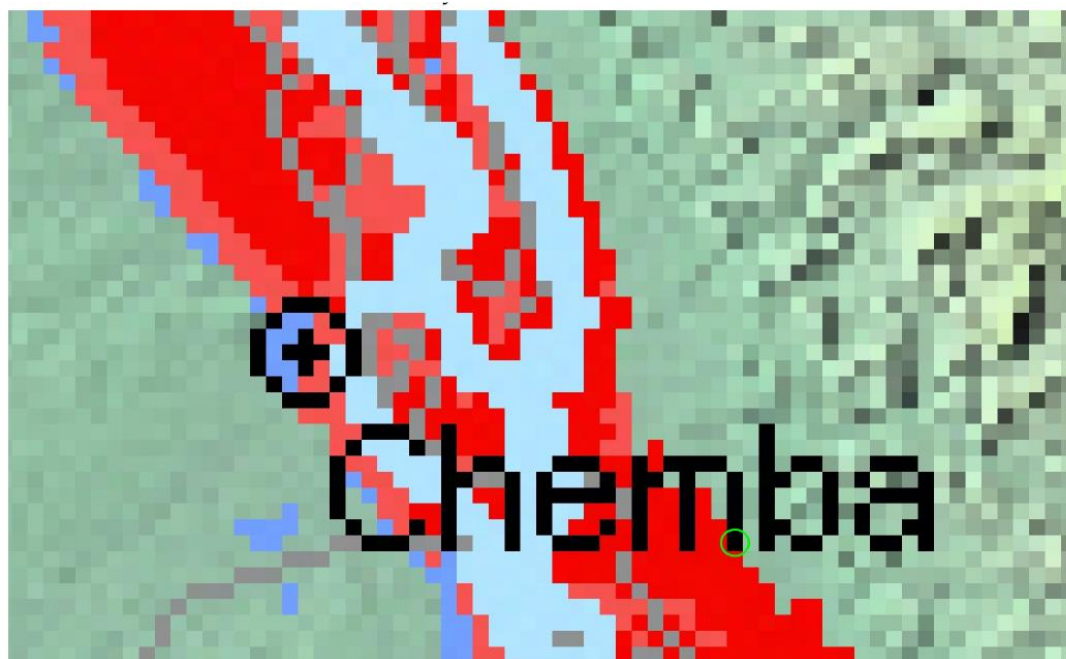
Figure A.2 Zoomed in example of the issue caused with town names and markers. The green circle indicates a particularly difficult pixel to identify as either 'flooded' or 'not flooded'.

A.2 Individual Global Flood Model Details

Table A.1 was taken from the supplementary material of the Trigg et al. (2016) global flood model intercomparison paper as it provides key model structure information that is useful to the reader of the validation study

Table A.1 Model Details.

Reproduced from Trigg et al. (2016). © IOP Publishing. CC BY 3.0

MODEL	Climate Forcing	Land Surface Model	River Routing	Floodplain	Flood Frequency	Down-scaling	Output Data Resolution	Smallest River size or upstream catchment area considered
GLOFRIS	EU-Watch reanalysis 1960-1999	Hydrological model PCR-GLOBWB 0.5 degree	Kinematic 0.5 deg	30 arc sec SRTM model	Flood volume Gumbel distribution for 1960 to 1999	Volume redistribution on 30 arcsec SRTM model	30 arc sec ~900m	Strahler order >=6 only
CaMa-Flood	JRA-25 Reanalysis 1979-2010 +GPCP rain gauge correction	MARSIRO=GW Energy and Water Balance (1 degree)	Inertia 0.25 deg	Sub-grid topo. Upscaled from 3 arc sec HydroSHEDS & SRTM	Water Level Gumbel distribution for 1979 to 2010	Flood depth downscaled onto 18 arc sec DEM	18 arc sec ~540m	Drainage area > 0.25 degree grid box (Approximately ~500km^2)
ECMWF	ERAInterim reanalysis 1979-2014	HTESSEL, T255 (~80km)	3 methods Kinematic, Inertia (x2) 0.25 deg	Sub-grid topo. Upscaled from 3 arc sec HydroSHEDS & SRTM	Flood depth GEV distribution for 1979 to 2014	Depth downscaled onto 19 arc sec DEM	18 arc sec ~540m	~500 km^2
JRC	GloFAS, ERA-Interim reanalysis 1980-2013	HTESSEL	LISFLOOD-Global (0.1 deg) + Inertia (30 arc sec)	Sub-grid topo. Upscaled from 3 arc sec HydroSHEDS & SRTM	Gumbel distribution for 1980 to 2013	N/A	30 arc sec ~900m	5000 km^2
SSBN	Regional Flood Frequency Analysis (FFA) from global gauge data	N/A	Inertia 30 arc sec	HydroSHEDS & SRTM 30 arc sec	From FFA	Depth downscaled onto 3 arc sec DEM	3 arc sec ~90m	~50 km^2
CIMA-UNEP	Regional FFA from global gauge data + ECEarth bias corrected	Continuum Model to improve FFA	Manning's at multiple points	Reconditioned HydroSHEDS & SRTM	From FFA, GEV fitting	Native at 3 arc sec	3 arc sec ~90m	~1000 km^2

A.3 Comparison of DFO extents and new database's extents

A.3.1 Lokoja
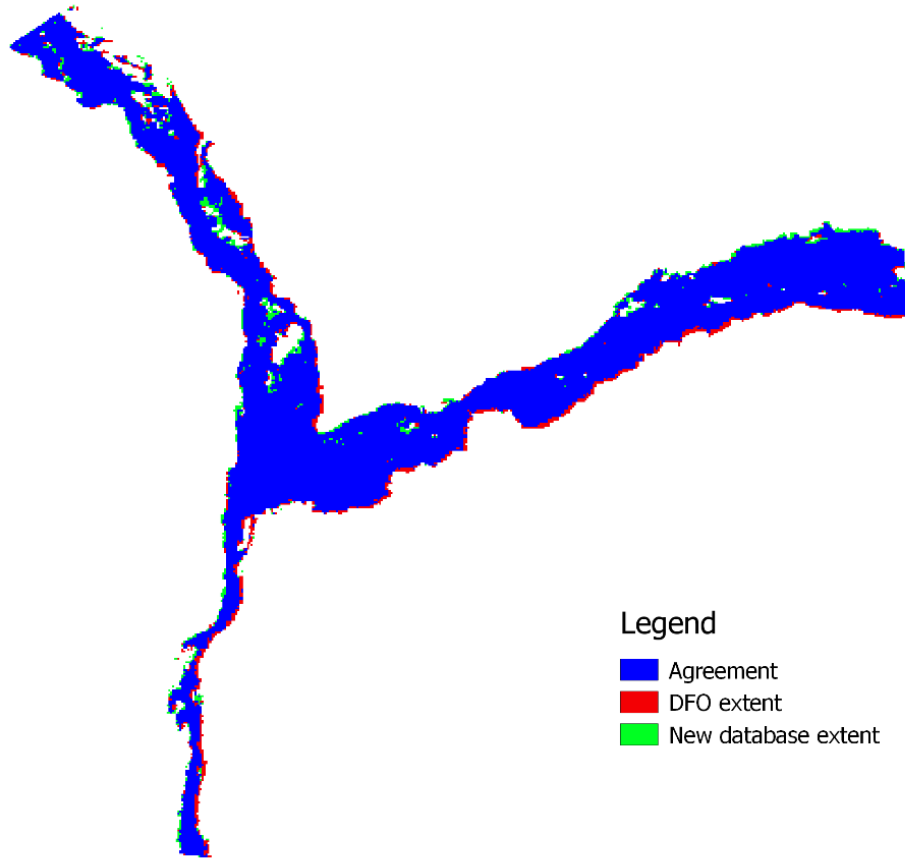
Figure A.3 Overlap of DFO observed extent and new database observed extent for Lokoja

A.3.2 Idah
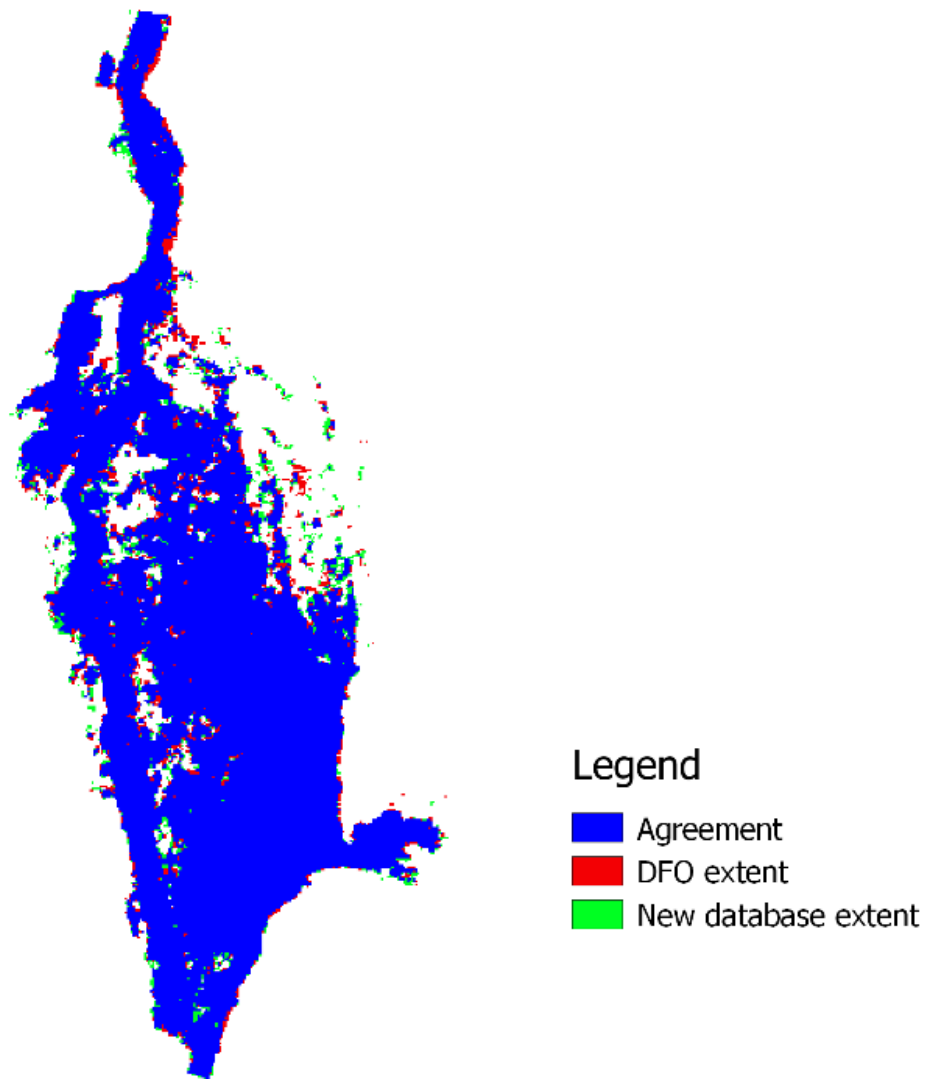
Figure A.4 Overlap of DFO observed extent and new database observed extent for
     Idah

A.3.3 Chemba
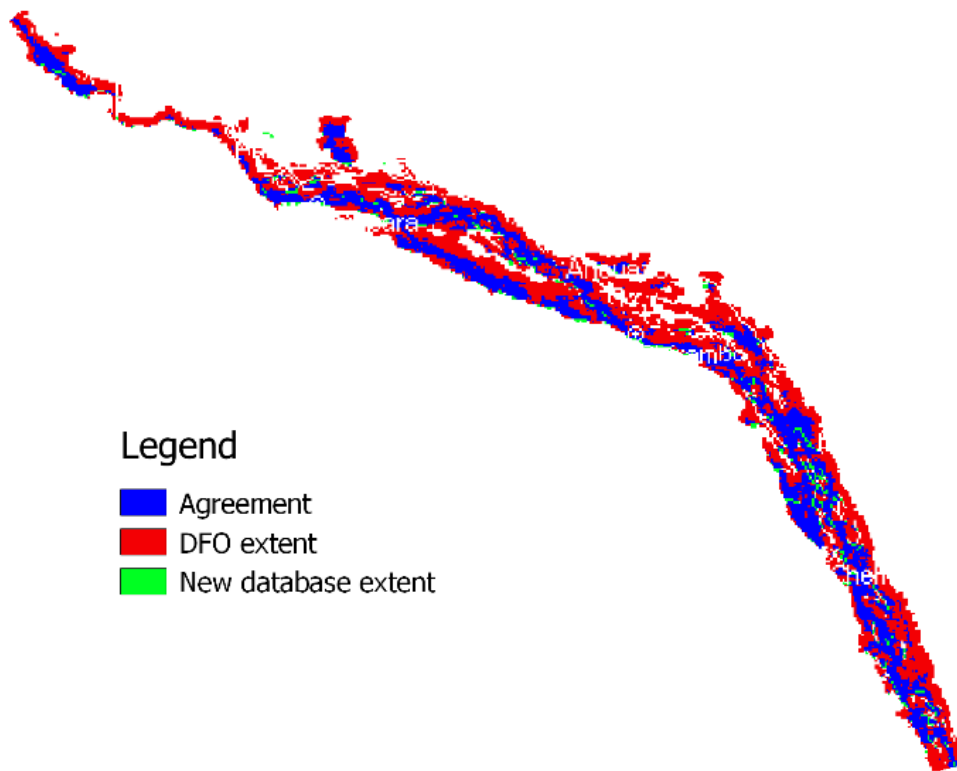
Figure A.5 Overlap of DFO observed extent and new database observed extent for Chemba

References

ANDERSON, E. & BRAKENRIDGE, G. R. 2007. DFO Event #2007-003 -
        Zambezi and Shire Rivers - Mozambique and Malawi - Rapid Response
        Inundation Map 1. Dartmouth Flood Observatory.
TRIGG, M. A., BIRCH, C. E., NEAL, J. C., BATES, P. D., SMITH, A.,
        SAMPSON, C. C., YAMAZAKI, D., HIRABAYASHI, Y.,
        PAPPENBERGER, F., DUTRA, E., WARD, P. J., WINSEMIUS, H. C.,
        SALAMON, P., DOTTORI, F., RUDARI, R., KAPPES, M. S., SIMPSON,
        A. L., HADZILACOS, G. & FEWTRELL, T. J. 2016. The credibility
        challenge for global fluvial flood risk analysis. *Environmental Research
        Letters,* 11**,** 10.

Appendix B

Supplementary Material to Chapter 4

Appendix B consists of the supplementary material that accompanied the manuscript on which **Chapter 4** is based.

B.1 Model Calibration

The globe was split into five simplified climate zones. The 30 Köppen-Geiger climate classifications (Beck et al., 2018) were categorized into five climate zones as follows: **Tropical** (Af – Tropical, rainforest; Am – Tropical, monsoon; Aw – Tropical, savannah), **Arid** (BWh – Arid, desert, hot; BWk – Arid, desert, cold; BSh – Arid, steppe, hot; BSk – Arid, steppe, cold), **Temperate** (Csa – Temperate, dry summer, hot summer; Csb – Temperate, dry summer, warm summer; Csc – Temperate, dry summer, cold summer; Cwa – Temperate, dry winter, hot summer; Cwb – Temperate, dry winter, warm summer; Cwc – Temperate, dry winter, cold summer; Cfa – Temperate, no dry season, hot summer; Cfb – Temperate, no dry season, warm summer; Cfc – Temperate, no dry season, cold summer), **Continental** (Dsa – Cold, dry summer, hot summer; Dsb – Cold, dry summer, warm summer; Dsc – Cold, dry summer, cold summer; Dsd – Cold, dry summer, very cold winter; Dwa – Cold, dry winter, hot summer; Dwb – Cold, dry winter, warm summer; Dwc – Cold, dry winter, cold summer; Dwd – Cold, dry winter, very cold winter; Dfa – Cold, no dry season, hot summer; Dfb – Cold, no dry season, warm summer; Dfc – Cold, no dry season, cold summer; Dfd – Cold, no dry season, very cold winter), **Polar** (ET – Polar, tundra; EF – Polar, frost).

Our River Flood Susceptibility Model (RFSM) was calibrated against reference flood maps in 19 different calibration basins globally. These calibration basins span all climate zones (except Polar regions). The aim in choosing the calibration basins was to ensure that for each climate zone we had reference flood maps for rivers of all Strahler stream orders. We use 4 different reference flood maps: FEMA's 100 year national flood hazard layer (https://www.fema.gov/flood-maps/tools-resources/flood-map-products/national-flood-hazard-layer), The Environment Agency's 100 year flood map for planning (http://apps.environment-

agency.gov.uk/wiyby/cy/151263.aspx), JRC's 100 year flood map for Europe (Dottori et al., 2016b), and JRC's Global 100 year flood map (Dottori et al., 2016a). The 100-year return period was chosen as it was the only return period consistent across all the datasets. Table B.1 summarizes information about each of the calibration basins and the reference flood map used. Figure B.1 shows maps of each of the calibration basins and visualizes the reference flood maps within the basins.

Table B.1 Calibration Basin Information

#	Basin Name	Climate Zone	Reference Flood Map	Basin Area (km^2)	Elevation Range (m)	Mean Slope (%)	Strahler Orders
1	Puerto Rico	Tropical	FEMA 100 YR	8,970	0 - 1,310	13.4	1-5
2	Central Amazon	Tropical	JRC GLOBAL 100 YR	388,824	0 - 1,121	6.7	6-8, 11
3	Lower Congo	Tropical	JRC GLOBAL 100 YR	720,639	275 - 872	3.7	5-10
4	Lower Mekong	Tropical	JRC GLOBAL 100 YR	709,538	0 - 2,810	10.8	6-10
5	Lower Gila	Arid	FEMA 100 YR	19,444	41 - 2,360	7.5	1-6, 9-10
6	Upper Pecos	Arid	FEMA 100 YR	60,948	0 - 3,943	7.8	1-7
7	Jucar	Arid	JRC EU 100 YR	21,920	0 - 1,853	10.6	4-7
8	Upper Nile	Arid	JRC GLOBAL 100 YR	794,843	-59 - 1,862	2.7	6-10
9	Lower Lena	Arid	JRC GLOBAL 100 YR	315,790	-27 - 640	1.2	6-9, 11
10	Lower Mississippi	Temperate	FEMA 100 YR	88,261	0 - 265	1.6	1-10
11	Alabama	Temperate	FEMA 100 YR	58,896	0 - 1,274	5.7	1-7
12	Thames	Temperate	EA 100 YR	16,201	0 - 327	4.1	1-6
13	Loire	Temperate	JRC EU 100 YR	117,034	0 - 1,846	5.7	4-9
14	Po	Temperate	JRC EU 100 YR	100,182	0 - 4,786	27.2	4-8
15	Muskingum	Continental	FEMA 100 YR	20,849	0 - 463	7.4	1-7
16	Rock	Continental	FEMA 100 YR	28,276	0 - 522	3.1	1-7
17	Susquehanna	Continental	FEMA 100 YR	42,036	0 - 956	13	1-8
18	Oder	Continental	JRC EU 100 YR	119,243	0 - 1,559	3.3	4-9
19	Central Lena	Continental	JRC GLOBAL 100 YR	213,826	0 - 382	2.8	6-7, 10-11
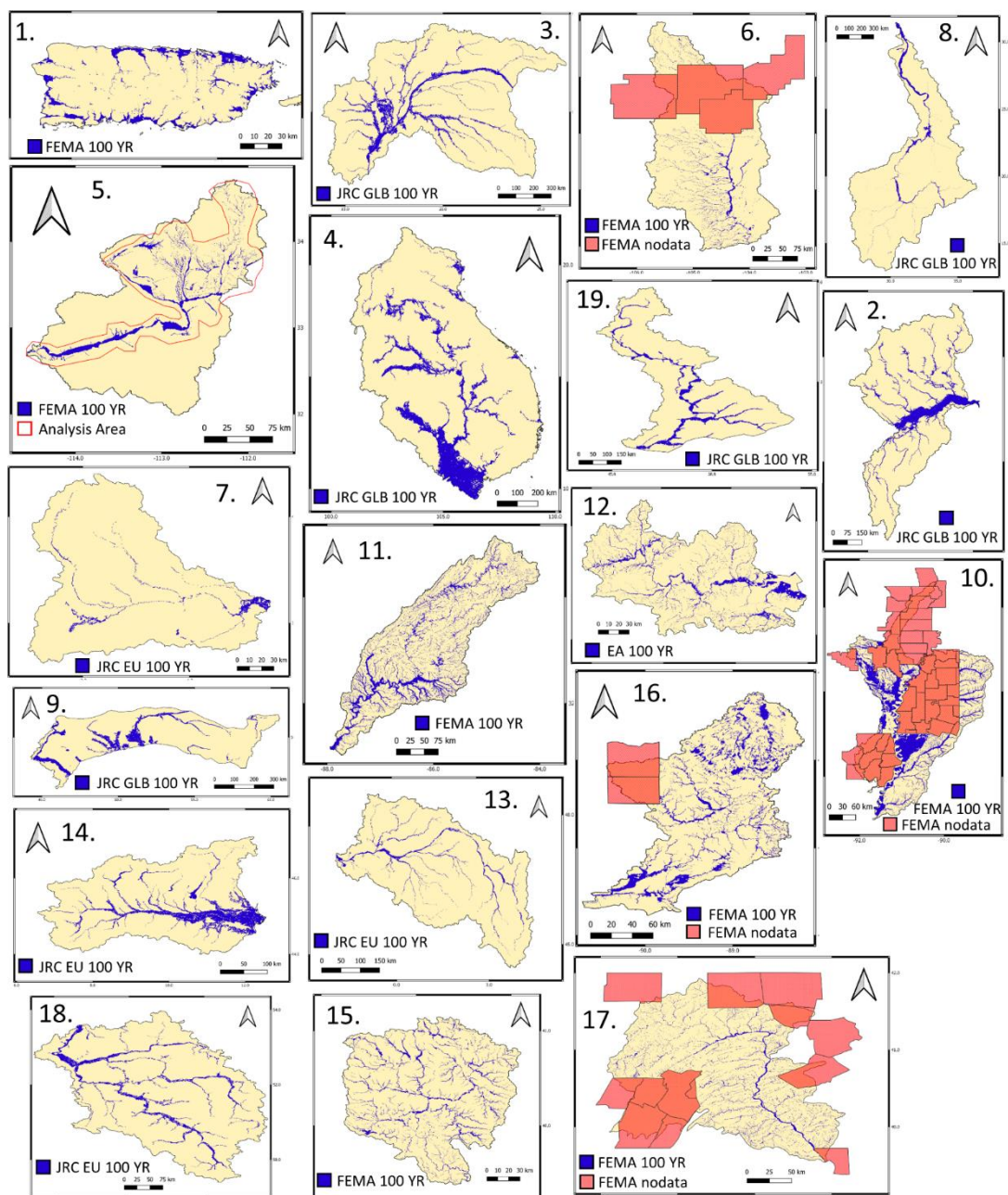
Figure B.1 Visualization of the reference flood maps used for calibration in each of the calibration basins.

Calibration basins are as follows: 1. Puerto Rico, 2. Central Amazon, 3. Lower Congo, 4. Lower Mekong, 5. Lower Gila, 6. Upper Pecos, 7. Jucar, 8. Upper Nile, 9. Lower Lena, 10. Lower Mississippi, 11. Alabama, 12. Thames, 13. Loire, 14. Po, 15. Muskingum, 16. Rock, 17. Susquehanna, 18. Oder, 19. Central Lena

Table B.2 Performance Score Contingency Table

		Model	
		Wet	Dry
Reference	Wet	**A** – wet agreement	**C** – model underpredict
	Dry	**B** – model overpredict	**D** – dry agreement

Our method of model calibration aims to find the optimum maximum relative elevation difference to the nearest draining channel, H_n, for each Strahler stream order river that results in the best fit with the reference flood map. We use three different 'fit' statistics, derived from a contingency table (*Table S2*). The first score is the critical success index (CSI):

$$CSI = \frac{A}{A + B + C} \qquad (B5)$$

CSI scores range from 1 (best) to 0 (worst). The second score is the hit rate (HR):

$$HR = \frac{A}{A + C} \qquad (B2)$$

HR ranges from 1 (entire reference flood map captured) to 0 (none of the reference flood map captured). The third score is Bias:

$$Bias = \frac{A + B}{A + C} \qquad (B3)$$

Bias scores <1 and >1 indicate a bias towards underprediction and overprediction, respectively.

Calibration was split into two stages. In the first stage, each river in the calibration basin was split by Strahler stream order and each order was processed individually. A range of permissible H_n values (typically the 5 H_n values resulting in bias scores close to 1) was found for each stream order. In the second calibration stage, the H_n ranges for each stream order were combined to produce maps with several different H_n combinations. Each of these combinations was then tested against the reference flood maps to find the optimal H_n combination for each climate zone.

In the first calibration stage, the river network was split into separate Strahler stream orders. Potential H_n values ranging from 0-20 m were tested for each Strahler

stream order in each basin. H_n values that produced Bias scores closest to 1 (unbiased), hereafter referred to as u-H_n, were identified for each Strahler stream order. The u-H_n values were then used as the basis for producing the permissible H_n ranges for each order. Ranges were initially chosen as u-H_n ± 2. Some of the ranges were widened to match the ranges of the other calibration basins in the same climate zone. The final H_n ranges taken into part 2 of the calibration are listed in Table B.3.

In the second calibration stage, flood maps were produced in each basin for all possible combinations of H_n within the pre-specified ranges. The only rule for H_n combinations was that a higher order stream's H_n couldn't be smaller than a lower order stream's H_n ($H_{n-1} \leq H_n$). The number of different H_n combinations (or flood maps) tested varied between each basin and was dependent on how many Strahler stream orders were present in the basin. The total combinations tested for each basin are listed in Table S3. The Jucar river basin (ID 7) had the fewest combinations (758) while the Mississippi basin (ID 10) had the most (868,915). Scores were calculated to capture the level of fit between each flood map iteration and the reference flood map. CSI was the main score used for determining the best level of fit between the model and the reference map. Because only one H_n combination can be used to define the flood map in each climate zone, the optimal H_n combination across all calibration basins within the same climate zones were determined by iteratively applying CSI thresholds to each basin. From the small selection of H_n combinations remaining after this iterative process, the final combination chosen was the one that resulted in the highest average CSI across the basins. Final H_n values for each climate zone are presented in Table B.4.

Table B.3 H_n ranges for Calibration Stage 2 for each basin in each climate zone. Basin IDs correspond with Table B.1

	Basin ID									
Order	**1**	**2**	**3**	**4**	**5**	**6**	**7**	**8**	**9**	**10**
1	0-4 m				0-4 m	0-4 m				0-2 m
2	0-5 m				0-4 m	0-4 m				0-3 m
3	0-5 m				0-4 m	0-4 m				0-6 m
4	3-8 m				0-5 m	0-5 m	0-5 m			0-9 m
5	2-13 m		2-13 m		0-7 m	0-7 m	0-7 m			2-11 m
6		3-13 m	3-13 m	3-13 m	1-8 m	1-8 m	1-8 m	1-8 m	1-8 m	3-12 m
7		3-13 m	3-13 m	3-13 m		2-10 m	2-10 m	2-10 m	2-10 m	5-13 m
8		3-13 m	3-13 m	3-13 m				2-10 m	2-10 m	7-13 m
9			7-17 m	7-17 m	2-14 m			2-14 m	2-14 m	7-13 m
10			7-17 m	7-17 m	5-15 m			5-15 m		9-14 m
11		7-17 m							9-15 m	
Combinations	2220	1890	38756	9426	84504	7726	758	7899	7088	868915

	Basin ID									
Order	**11**	**12**	**13**	**14**	**15**	**16**	**17**	**18**	**19**	
1	0-2 m	0-2 m			0-2 m	0-2 m	0-2 m			
2	0-3 m	0-3 m			0-2 m	0-2 m	0-2 m			**Climate Key**
3	0-6 m	0-6 m			0-5 m	0-5 m	0-5 m			Tropical
4	0-9 m	0-9 m	0-9 m	0-9 m	2-7 m	2-7 m	2-7 m	2-7 m		Arid
5	2-11 m	2-11 m	2-11 m	2-11 m	2-10 m	2-10 m	2-10 m	2-10 m		Temperate
6	3-12 m	3-12 m	3-12 m	3-12 m	4-13 m	4-13 m	4-13 m	4-13 m	4-13 m	Continental
7	5-13 m		5-13 m	5-13 m	5-14 m	5-14 m	5-14 m	5-14 m	5-14 m	
8			7-13 m	7-13 m			6-16 m	6-16 m		
9			7-13 m					7-16 m		
10									8-16 m	
11									8-16 m	
Combinations	33576	7733	17172	6283	26728	26728	148340	29443	1280	

Table B.4 Final H_n Values for RFSM

Order	Maximum Height Above Nearest Drainage (H_n)			
	Tropical	Arid	Temperate	Continental
1	1 m	0 m	0 m	0 m
2	2 m	0 m	1 m	0 m
3	4 m	0 m	2 m	2 m
4	6 m	1 m	4 m	4 m
5	8 m	3 m	5 m	5 m
6	8 m	3 m	7 m	6 m
7	9 m	5 m	9 m	8 m
8	10 m	5 m	10 m	9 m
9	10 m	12 m	10 m	10 m
10	10 m	13 m	13 m	11 m
11	13 m	14 m	-	12 m

B.2 Model Validation

Validation of the RFSM was split into two stages. The first stage compared the RFSM to existing global flood model (GFM) outputs in Africa. The performance of the RFSM with respect to these existing GFMs was compared with the performance of another global geomorphological floodplain map: GFPLAIN250 (Nardi et al., 2019). The second stage involved validating the RFSM output against historical observed flood events. The performance of the RFSM at capturing these historical events was compared with the performance of existing GFMs.

B.2.1 Validation Against Existing Models

The output of 6 GFMs was compared in Africa by Trigg et al. (2016b) in the first GFM intercomparison study. One of the outputs of the study was an aggregated map (Trigg et al., 2016a) of flood hazard for Africa that showed the number of models (1-6) that agreed it would flood in a given location (see Figure B.2). We use this aggregated map to validate our RFSM. We also validate another geomorphological flood map, GFPLAIN250 (Nardi et al., 2019), against the aggregated GFM map. We then compare the results to see how our approach

compares to geomorphological approaches. We use the 100-year return period aggregated GFM map for our validation.
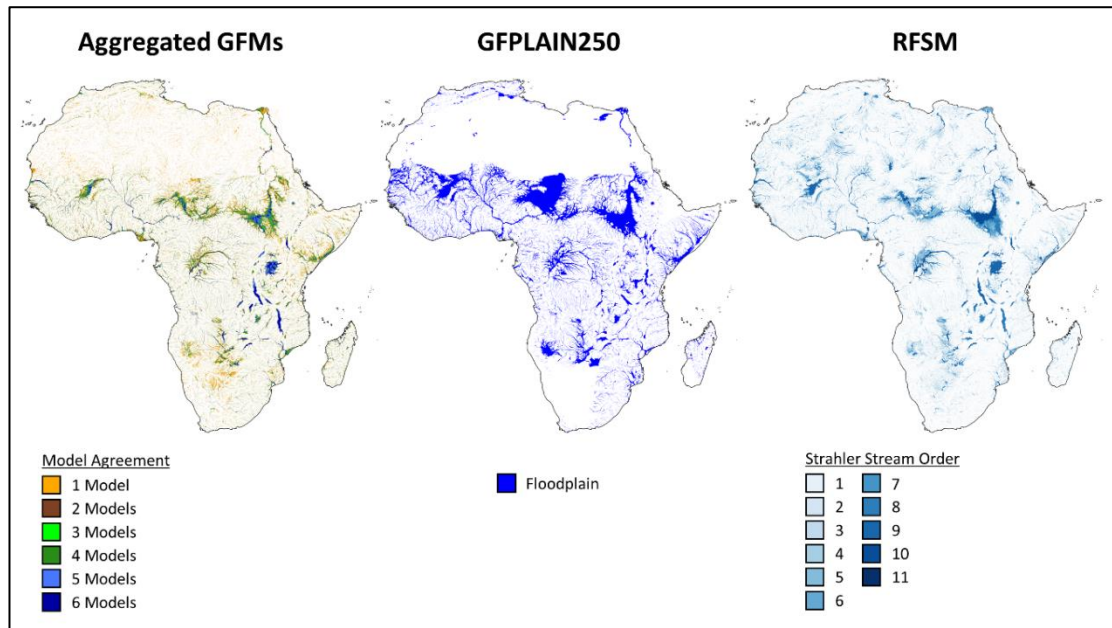
Figure B.2 Datasets used in the validation.

(From left to right) 100-year return period aggregated global flood model output for Africa (Trigg et al., 2016a). GFPLAIN250 geomorphological floodplain map for Africa (Nardi et al., 2019). RFSM map with rivers split by their Strahler stream orders.

Comparison of the RFSM map with the aggregated GFM map is split into three parts. In the first part, we split the RFSM map into Strahler stream orders. We then overlay the entire aggregated GFM map (any level of agreement) with the RFSM map and calculated the percentage of each Strahler stream order's extent that is overpredicting flooding with respect to the aggregated GFM map:

$$\% \, OP_{order} = \frac{RFSM_{order} - (RFSM_{order} \cap AGG)}{RFSM_{order}} x100 \qquad (B4)$$

where $RFSM_{order} \cap AGG$ is the intersection of the RFSM map (of a given order) and the aggregated GFM map, and $RFSM_{order}$ is the total extent of the RFSM map at that order.

In the second part of the analysis, we split the aggregated GFM map into its different levels of agreement, ranging from 1-6. We then calculate, for each level of agreement, the percentage of the aggregated GFM map that is captured by both the RFSM map and the GFPLAIN250 map:

$$\% \ Captured_{agg \ level} = \frac{GFM_{agg \ level} \cap FM}{GFM_{agg \ level}} x100 \qquad (B5)$$

where $GFM_{agg \ level} \cap FM$ is the intersection of the aggregated GFM map (at the specified agreement level) and the flood map (either RFSM or GFPLAIN250) and $GFM_{agg \ level}$ is the total aggregated GFM extent for the specified agreement level.

In the third part of the analysis, the RFSM map and GFPLAIN250 maps were scored using the performance scores outlined in the calibration section (equations S1-S3). To make the comparison between the RFSM map and the GFPLAIN250 as fair as possible an upstream drainage area (UDA) threshold of 1000 km^2 was applied to the RFSM map. This is because GFPLAIN250 does not map rivers below this threshold (Nardi et al., 2019). Performance scores were calculated by intersecting the GFPLAIN250 and RFSM maps with the aggregated GFM map, with 6 different thresholds of agreement applied to the aggregated GFM map. These thresholds of agreement ranged from ≥1 model (where any model predicts flooding) to 6 models (where all 6 models agree it will flood).

The African continent was split into major drainage basins for this first stage of validation. We use the HydroBasins dataset (Lehner and Grill, 2013) at the level 2 categorization as our validation basins. The basin split for the continent of Africa can be seen in Figure B.3, alongside basin names and HydroBasin specific numeric codes. For the continent of Africa there are a total of 8 level 2 basins. The three parts of the validation analysis outlined above were carried out in each of the 8 basins. Results for validation parts 1-3 are recorded in Tables B.5 - B.9. Figures B.4-B.11 visualize the overlap between both the RFSM and GFPLAIN250 maps and the aggregated GFM map for each of the 8 level 2 basins.
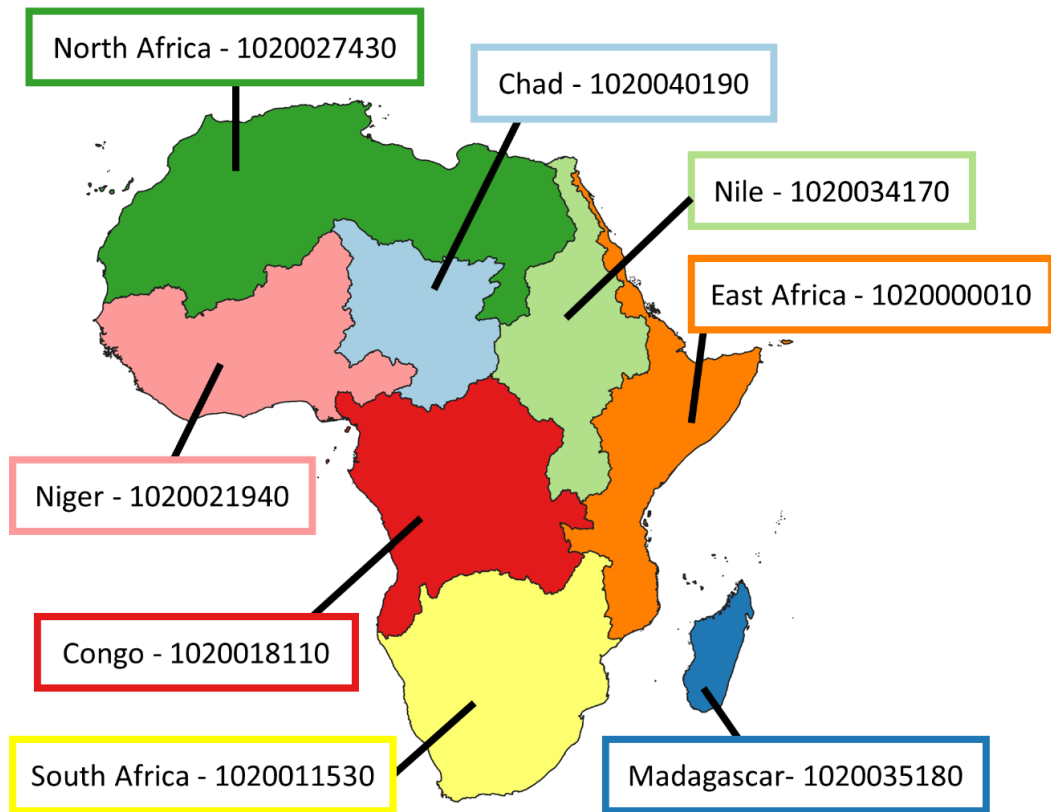
Figure B.3 The level 2 HydroBasins used for validation

   Basin names listed alongside HydroBasin specific numeric codes

Table B.5 Validation Part 1 Results - RFSM Percentage Overprediction per Stream
   Order

Basin	Strahler Stream Order										
	1	**2**	**3**	**4**	**5**	**6**	**7**	**8**	**9**	**10**	**11**
East Africa - 1020000010	83	80	69	49	31	14	11	5	4	14	X
South Africa - 1020011530	86	83	74	55	37	19	13	6	2	16	X
Congo - 1020018810	91	91	74	49	32	16	11	9	4	4	7
Niger - 1020021940	81	91	77	64	32	14	23	16	10	2	X
North Africa - 1020027430	94	96	93	88	77	65	62	61	68	X	X
Nile - 1020034170	84	80	71	55	40	29	20	13	2	5	X
Madagascar - 1020035180	83	85	68	45	22	6	3	1	X	X	X
Chad - 1020040190	86	82	77	61	48	34	31	19	33	1	X

Throughout Africa, the RFSM follows the general trend that as the Strahler stream order of the river increases, the degree of overprediction decreases (Table B.5). Low orders (1, 2 and 3) have high degrees of overprediction. This is because the RFSM has a smaller minimum UDA threshold (10 km^2) than any of the other GFMs (between 50-5000 km^2) and a lot of the rivers in these categories fall below the minimum upstream drainage area threshold of any GFM. Intermediate orders (4-6) still show some levels of overprediction as a lot of these rivers will be modelled by some, but not all, of the GFMs. The levels of overprediction decrease for higher order rivers (>7) for which there is complete coverage across the GFMs.

Table B.6 Validation Part 2 Results - Percentage Flooding Captured per GFM
        Agreement Level

Basin	Flood Map	GFM Agreement Level					
		1	2	3	4	5	6
East Africa - 1020000010	RFSM	34	52	67	78	87	94
	GFPLAIN250	25	51	66	76	79	73
South Africa - 1020011530	RFSM	43	59	73	83	93	98
	GFPLAIN250	20	43	58	71	74	63
Congo - 1020018110	RFSM	50	58	73	84	93	98
	GFPLAIN250	33	58	72	79	77	68
Niger - 1020021940	RFSM	52	69	83	91	96	98
	GFPLAIN250	44	69	85	93	97	97
North Africa - 1020027430	RFSM	46	62	74	82	90	93
	GFPLAIN250	16	27	46	62	80	92
Nile - 1020034170	RFSM	61	78	88	94	98	99
	GFPLAIN250	49	73	84	83	65	55
Madagascar - 1020035180	RFSM	38	42	63	80	91	96
	GFPLAIN250	12	31	48	60	74	80
Chad - 1020040190	RFSM	56	73	84	89	92	95
	GFPLAIN250	60	76	86	93	97	99

In *Part 2* of the validation, we look at the different levels of GFM agreement in the aggregated GFM map and examine the percentage of each agreement level that is captured by the RFSM and GFPLAIN250 maps (Table B.6). The higher the GFM agreement level, the greater the confidence that it will flood in a given location. As such, it is especially important that the models being tested correctly capture these areas of high agreement. For the two highest GFM agreement levels (5

models agree, and 6 models agree) the RFSM has a *% captured* value of above 90% in each basin in Africa. This shows that the RFSM map is correctly capturing these areas of high confidence of flooding. Comparing the *% captured* results of the RFSM with the GFPLAIN250 map, the RFSM has higher *% captured* results in each basin except the Chad basin (where both maps still score highly). This shows that the RFSM captures more of aggregated GFM extent than the GFPLAIN250 map.

Table B.7 Validation Part 3 Results - Critical Success Index Scores for each GFM Agreement Threshold

		GFM Agreement Threshold					
Basin	**Flood Map**	**≥1**	**≥2**	**≥3**	**≥4**	**≥5**	**6**
East Africa - 1020000010	RFSM	0.31	0.46	0.47	0.41	0.31	0.14
	GFPLAIN250	0.35	0.36	0.29	0.21	0.14	0.07
South Africa - 1020011530	RFSM	0.35	0.5	0.49	0.43	0.34	0.22
	GFPLAIN250	0.33	0.36	0.31	0.24	0.17	0.1
Congo - 1020018110	RFSM	0.44	0.56	0.56	0.49	0.38	0.22
	GFPLAIN250	0.45	0.44	0.36	0.28	0.19	0.1
Niger - 1020021940	RFSM	0.47	0.54	0.5	0.39	0.27	0.14
	GFPLAIN250	0.48	0.43	0.33	0.24	0.15	0.08
North Africa - 1020027430	RFSM	0.21	0.13	0.06	0.03	0.01	0.003
	GFPLAIN250	0.15	0.12	0.07	0.04	0.02	0.01
Nile - 1020034170	RFSM	0.59	0.61	0.54	0.44	0.31	0.13
	GFPLAIN250	0.52	0.45	0.35	0.24	0.15	0.06
Madagascar - 1020035180	RFSM	0.27	0.42	0.51	0.5	0.37	0.19
	GFPLAIN250	0.32	0.42	0.41	0.34	0.24	0.12
Chad - 1020040190	RFSM	0.4	0.39	0.31	0.21	0.13	0.06
	GFPLAIN250	0.41	0.29	0.19	0.12	0.07	0.03

Table B.8 Validation Part 3 Results - Hit Rate Scores for each GFM Agreement
Threshold

Basin	Flood Map	GFM Agreement Threshold					
		≥1	≥2	≥3	≥4	≥5	6
East Africa - 1020000010	RFSM	0.32	0.54	0.68	0.78	0.85	0.9
	GFPLAIN250	0.45	0.65	0.73	0.76	0.76	0.73
South Africa - 1020011530	RFSM	0.37	0.62	0.76	0.87	0.93	0.97
	GFPLAIN250	0.39	0.58	0.65	0.69	0.67	0.63
Congo - 1020018110	RFSM	0.47	0.67	0.79	0.88	0.94	0.97
	GFPLAIN250	0.55	0.69	0.73	0.74	0.72	0.68
Niger - 1020021940	RFSM	0.51	0.71	0.83	0.9	0.95	0.97
	GFPLAIN250	0.68	0.84	0.92	0.96	0.97	0.97
North Africa - 1020027430	RFSM	0.36	0.53	0.67	0.76	0.82	0.85
	GFPLAIN250	0.22	0.37	0.56	0.7	0.83	0.92
Nile - 1020034170	RFSM	0.65	0.8	0.89	0.94	0.97	0.98
	GFPLAIN250	0.65	0.73	0.72	0.68	061	0.55
Madagascar - 1020035180	RFSM	0.28	0.45	0.61	0.74	0.85	0.91
	GFPLAIN250	0.34	0.51	0.62	0.7	0.77	0.8
Chad - 1020040190	RFSM	0.49	0.64	0.73	0.79	0.83	0.86
	GFPLAIN250	0.74	0.85	0.92	0.95	0.98	0.99

Table B.9 Validation Part 3 Results - Bias Scores for each GFM Agreement
    Threshold

Basin	Flood Map	GFM Agreement Threshold					
		≥1	≥2	≥3	≥4	≥5	6
East Africa - 1020000010	RFSM	0.36	0.72	1.1	1.66	2.65	5.35
	GFPLAIN250	0.73	1.46	2.24	3.34	5.36	10.94
South Africa - 1020011530	RFSM	0.42	0.86	1.29	1.87	2.68	4.4
	GFPLAIN250	0.58	1.19	1.78	2.58	3.69	6.06
Congo - 1020018110	RFSM	0.52	0.86	1.2	1.66	2.42	4.32
	GFPLAIN250	0.76	1.25	1.75	2.42	3.53	6.3
Niger - 1020021940	RFSM	0.6	1.1	1.5	2.21	3.46	7.06
	GFPLAIN250	1.09	1.83	2.71	4	6.27	12.79
North Africa - 1020027430	RFSM	1.03	3.51	10.03	25.6	69.3	266.4
	GFPLAIN250	0.71	2.45	7	17.87	48.36	185.89
Nile - 1020034170	RFSM	0.75	1.13	1.53	2.09	3.08	3.63
	GFPLAIN250	0.89	1.33	1.81	2.47	7.66	9.05
Madagascar - 1020035180	RFSM	0.29	0.52	0.81	1.24	2.13	2.96
	GFPLAIN250	0.41	0.72	1.13	1.73	4.82	6.71
Chad - 1020040190	RFSM	0.71	1.3	2.14	3.54	6.24	14.2
	GFPLAIN250	1.55	2.83	4.66	7.73	13.63	31

In the Part 3 of the validation the same UDA threshold as the GFPLAIN250 map (1000 km^2) was applied to the RFSM map. Three different performance scores were then calculated for both of these maps in each basin in Africa. In terms of CSI (Table B.7), the RFSM map outperformed the GFPLAIN250 map in almost all the basins in Africa. The bias scores (Table B.9) for the GFPLAIN250 map were also higher than the RFSM map's bias scores, suggesting that GFPLAIN250 overpredicts the 100-year flood to a greater degree than the RFSM map.

It should be noted that the GFPLAIN250 map was not intended to map the '100-year' flood, but rather to identify floodplain boundaries (Nardi et al., 2019). Additionally, in the North Africa basin, which contains the majority of the Sahara Desert, GFPLAIN250 and a few of the global flood models apply masks that exclude these areas from the analysis. This explains the low validation scores in this basin with respect to the other basins in Africa. We chose not to apply any mask in these areas for two reasons. Firstly, there is little to no population in these areas, so

applying / not applying a mask would have little impact on the final results. Secondly, applying a mask could mistakenly remove areas that do contain rivers. This is evident in the Nile Basin in Figure B.9. The mask applied to the GFPLAIN250 removes a portion of the Nile River in Northern Sudan.

We have shown, in our validation of the RFSM against the aggregated output of six GFMs, that the RFSM does a good job at capturing areas where there is high agreement between the GFMs. It also does a better job at predicting the 100-year flood extent than existing global geomorphological floodplain datasets.
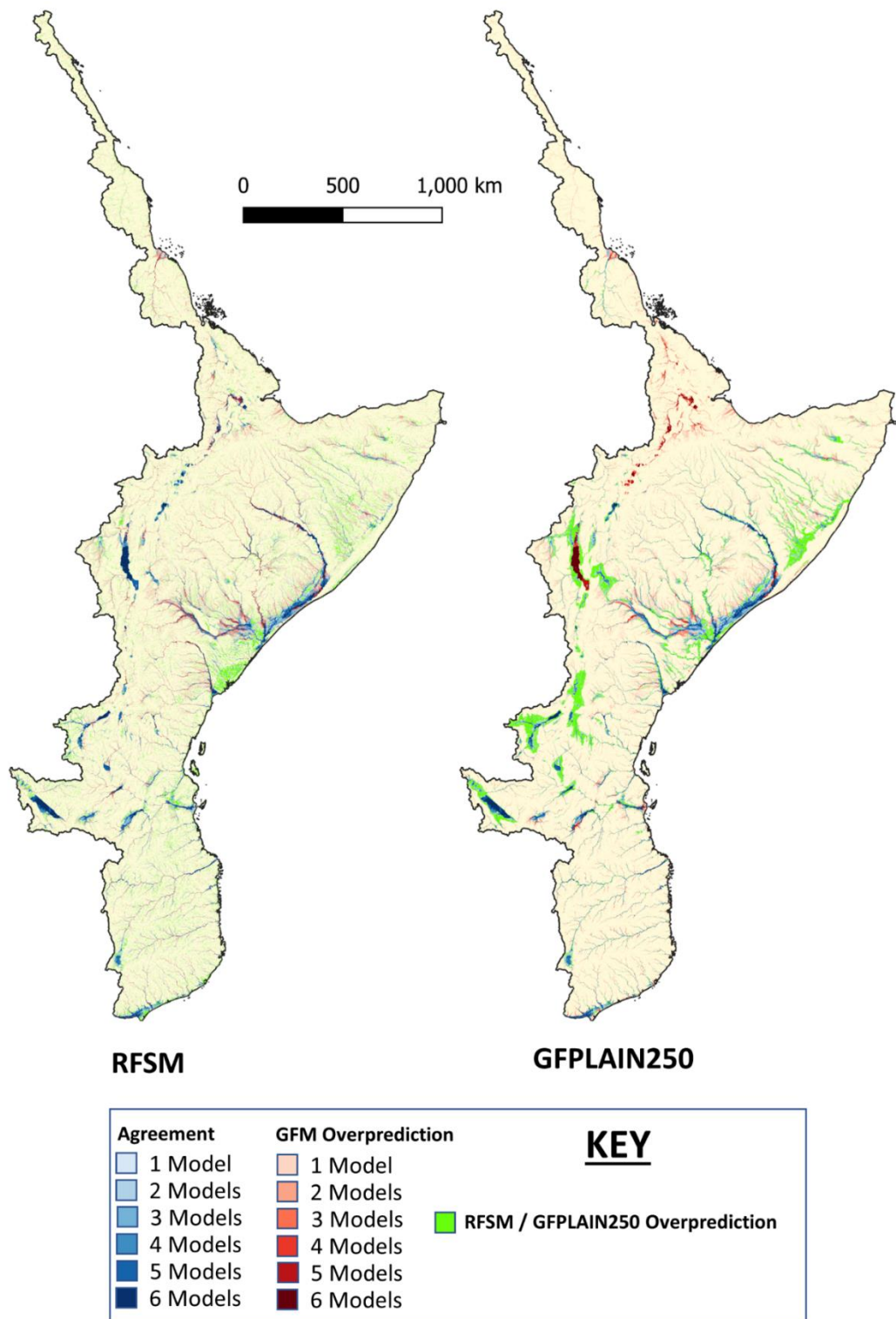
Figure B.4 Overlap of the RFSM and GFPLAIN250 maps with the 100-year return period aggregated global flood map (Trigg et al., 2016a) in the East Africa Basin (1020000010)

Figure B.5 Overlap of the RFSM and GFPLAIN250 maps with the 100-year return period aggregated global flood map (Trigg et al., 2016a) in the South Africa Basin (1020011530)
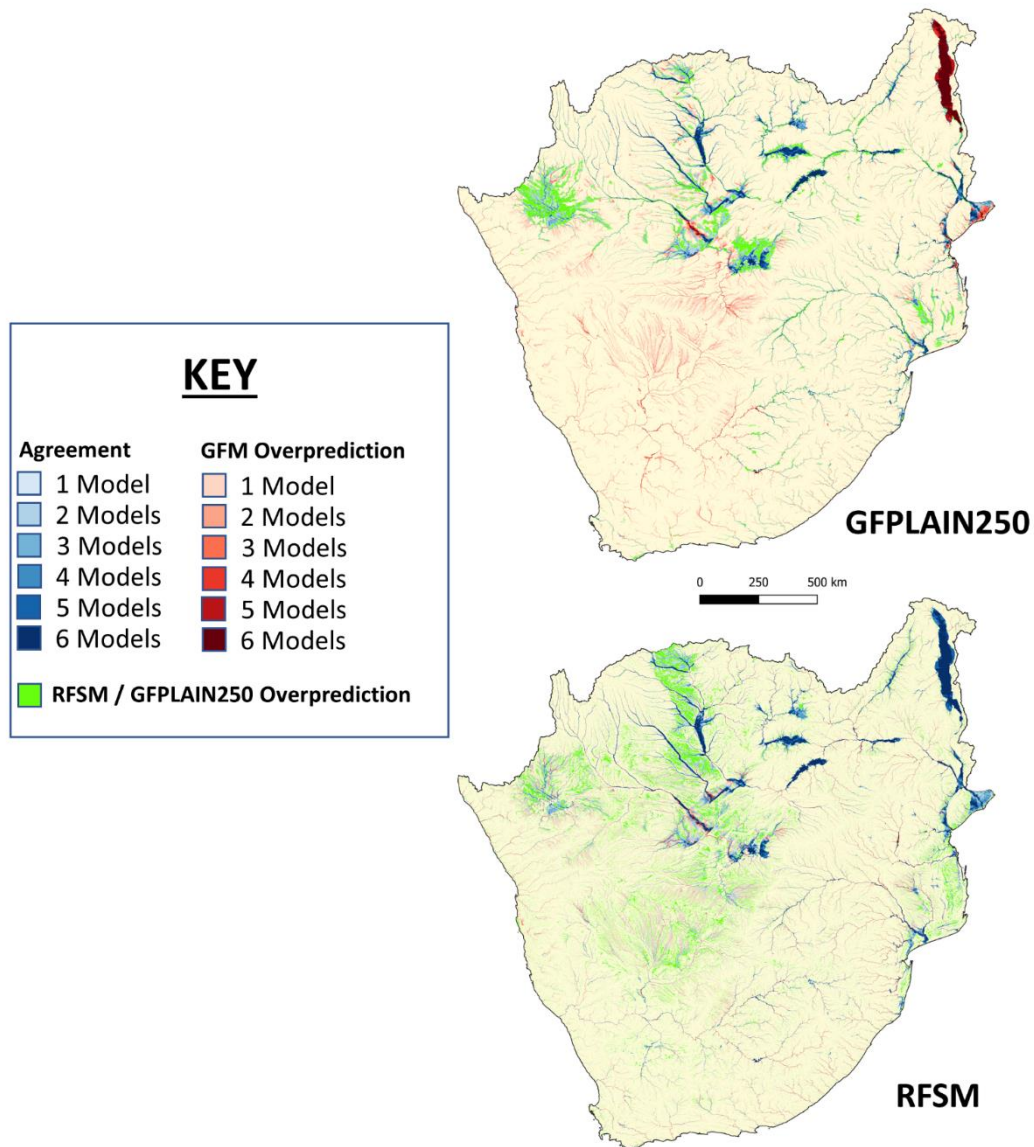
Figure B.6 Overlap of the RFSM and GFPLAIN250 maps with the 100-year return period aggregated global flood map (Trigg et al., 2016a) in the Congo Basin (1020018110)

Figure B.7 Overlap of the RFSM and GFPLAIN250 maps with the 100-year return period aggregated global flood map (Trigg et al., 2016a) in the Niger Basin (1020021940)

Figure B.8 Overlap of the RFSM and GFPLAIN250 maps with the 100-year return period aggregated global flood map (Trigg et al., 2016a) in the North Africa Basin (1020027430)
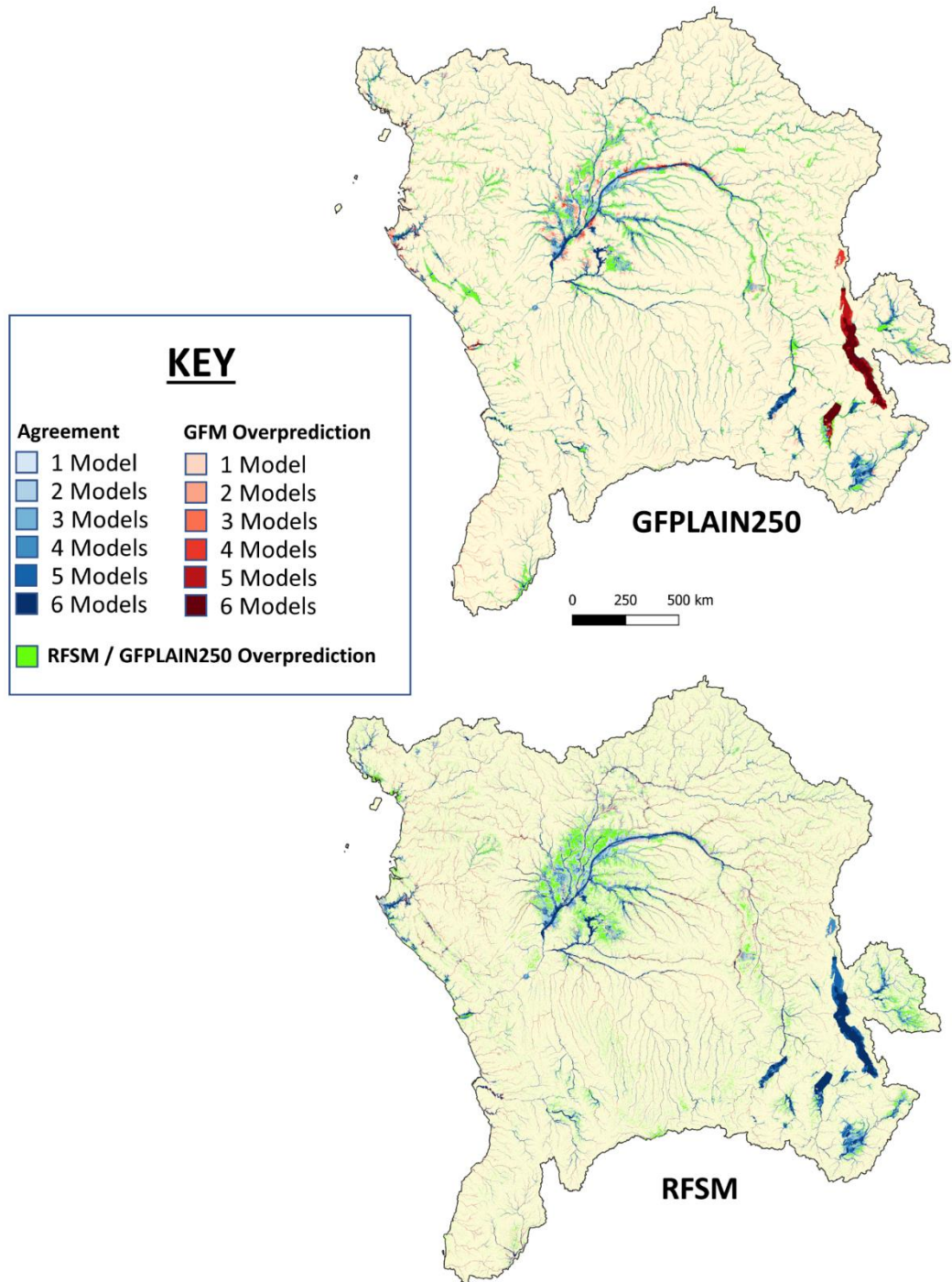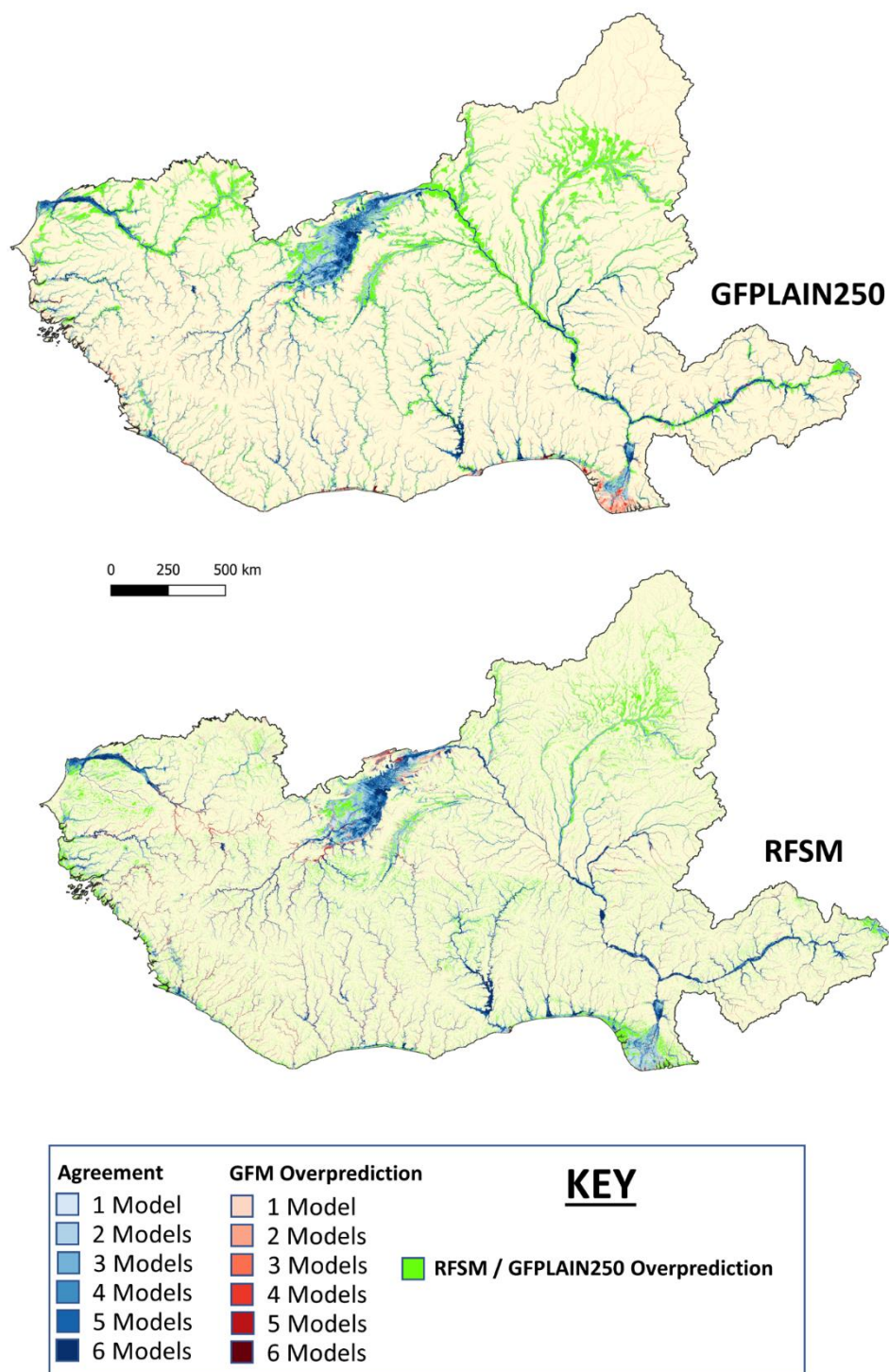
Figure B.9 Overlap of the RFSM and GFPLAIN250 maps with the 100-year return period aggregated global flood map (Trigg et al., 2016a) in the Nile Basin (1020034170)

GFPLAIN250   **RFSM**

Agreement	GFM Overprediction	KEY
1 Model	1 Model	
2 Models	2 Models	
3 Models	3 Models	RFSM / GFPLAIN250 Overprediction
4 Models	4 Models	
5 Models	5 Models	
6 Models	6 Models	

Figure B.10 Overlap of the RFSM and GFPLAIN250 maps with the 100-year
    return period aggregated global flood map (Trigg et al., 2016a) in the
    Madagascar Basin (1020035180)

Figure B.11 Overlap of the RFSM and GFPLAIN250 maps with the 100-year
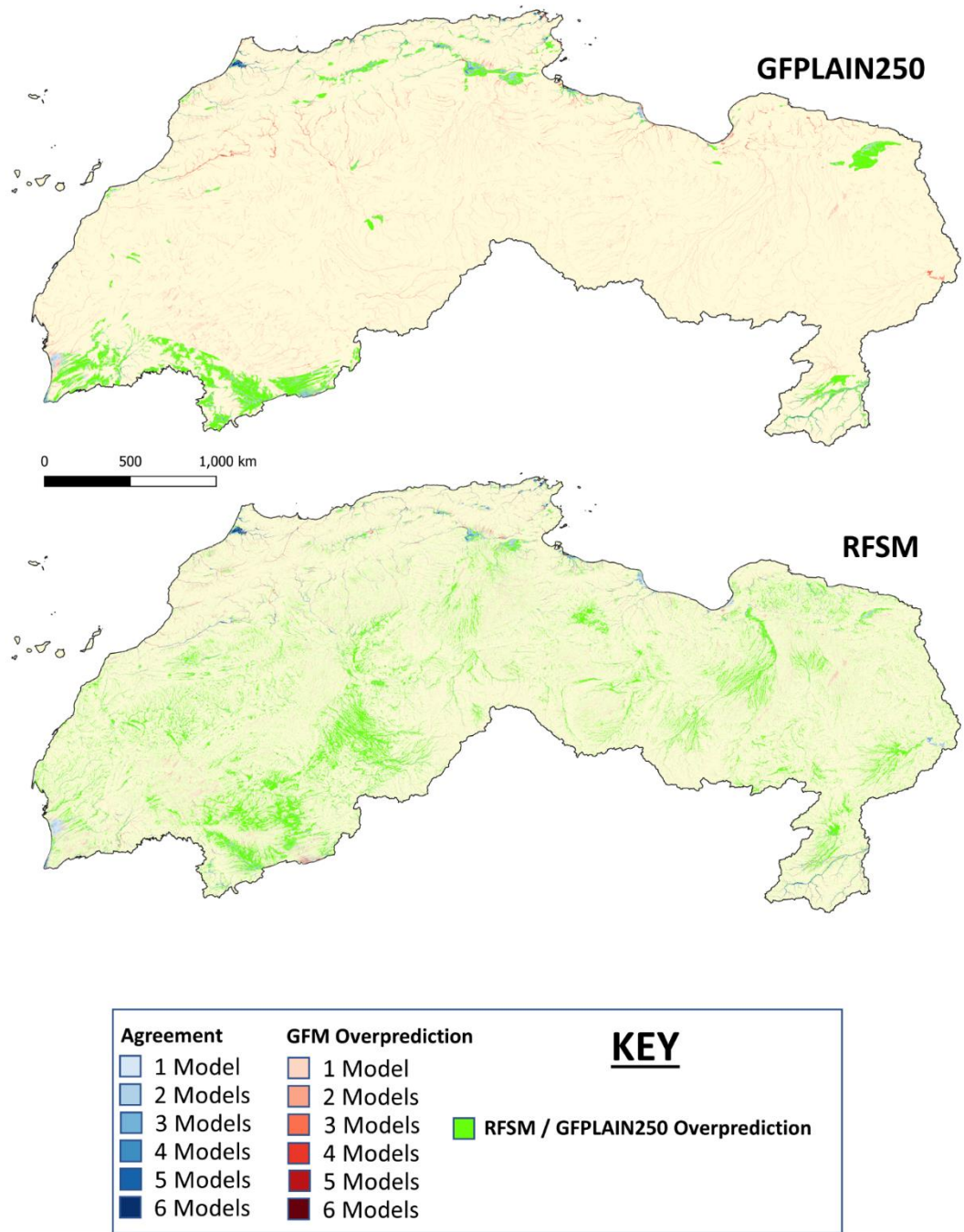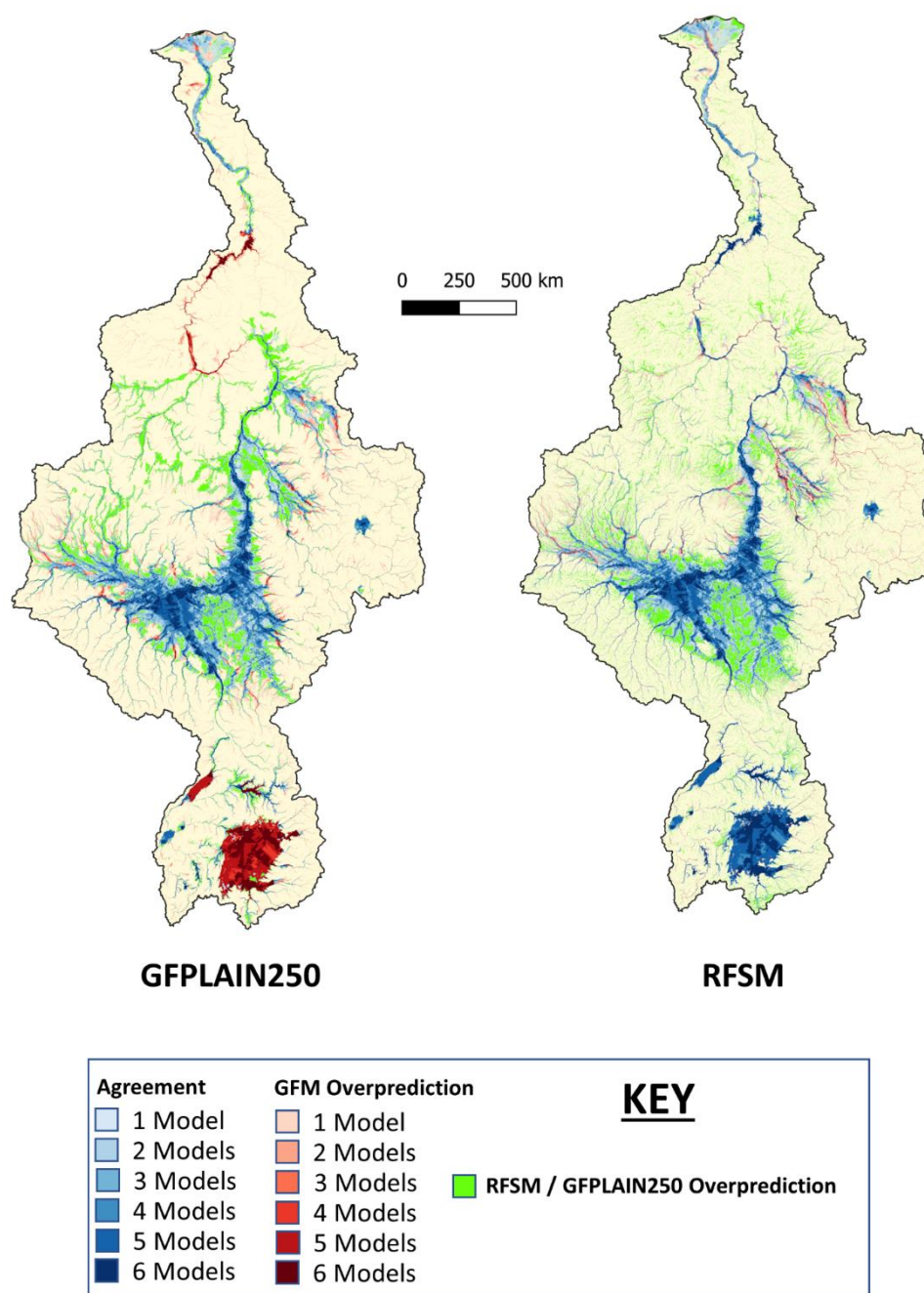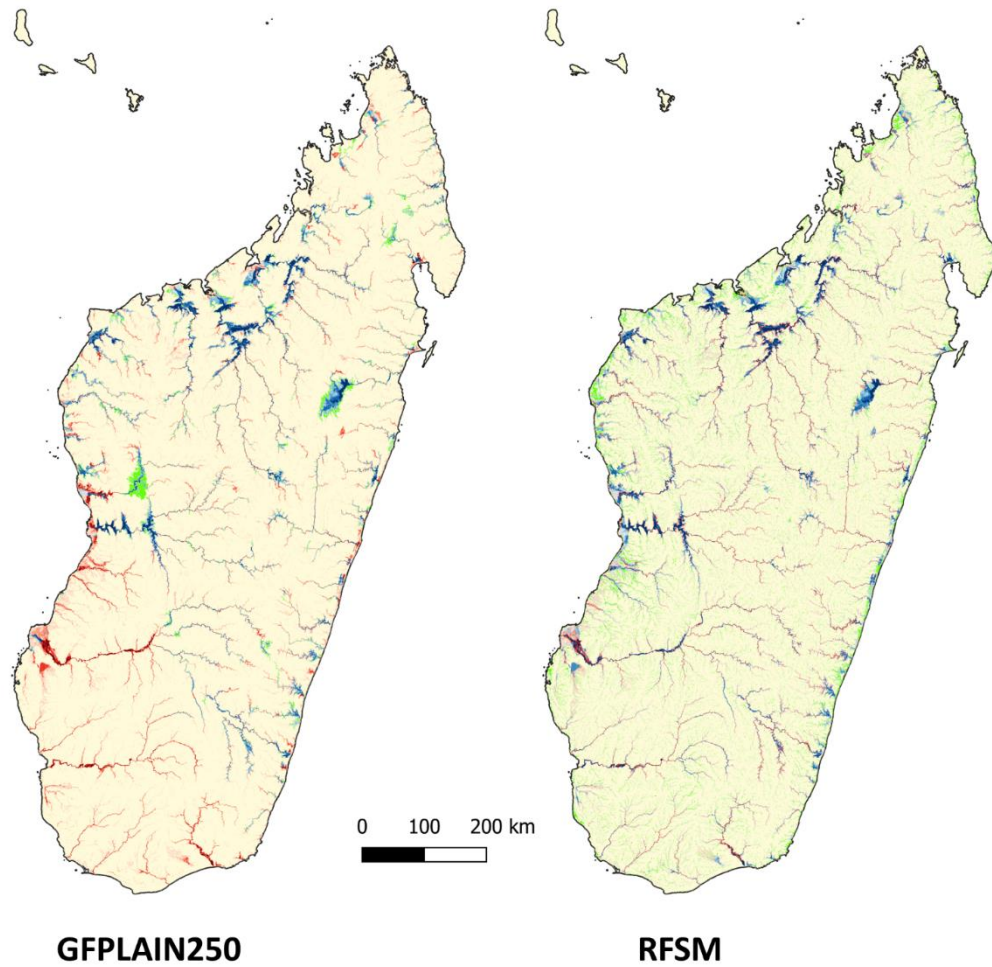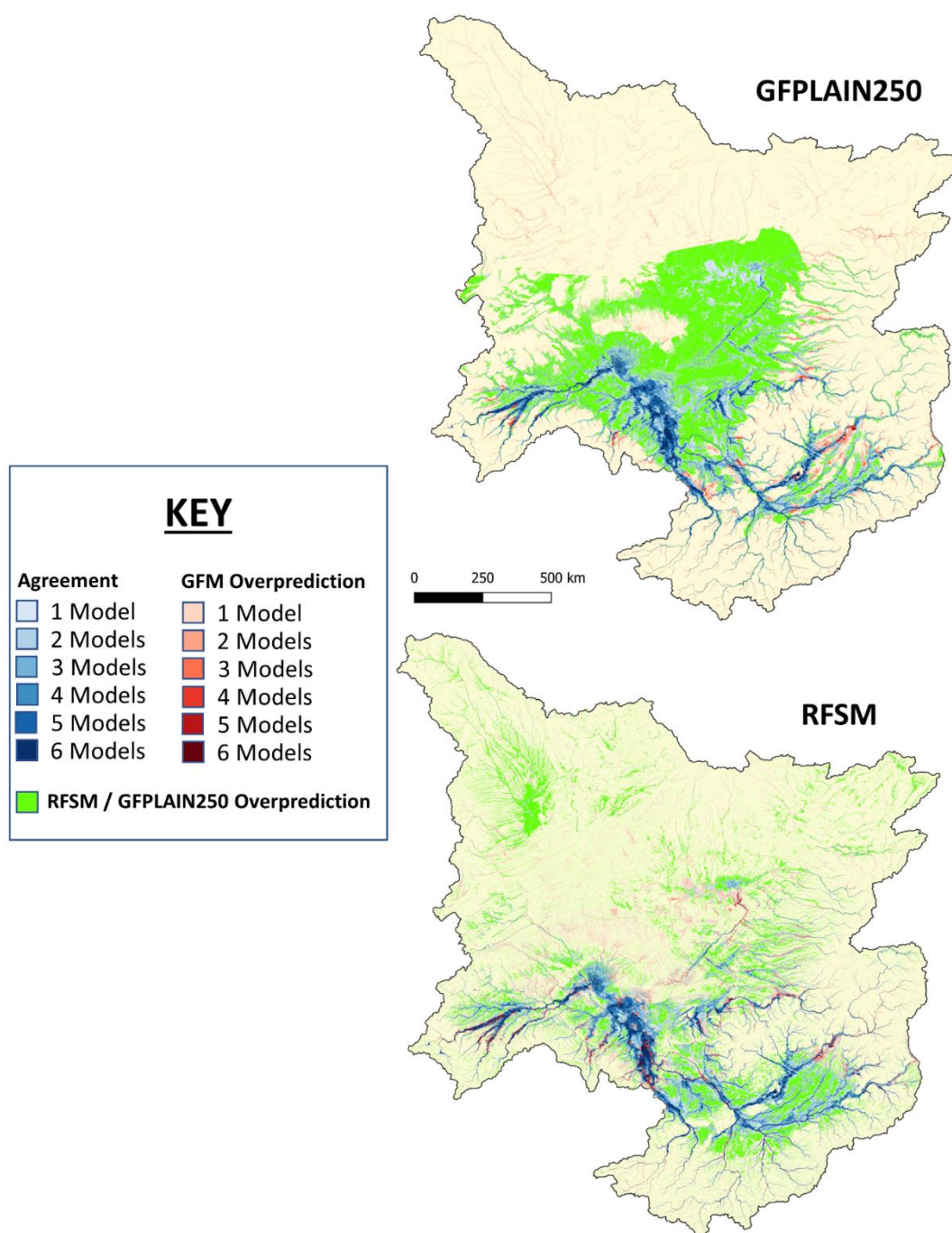return period aggregated global flood map (Trigg et al., 2016a) in the Chad
Basin (1020040190)

B.2.2 Validation Against Observed Events

In a follow up study to the Trigg et al. (2016b) GFM intercomparison study, Bernhofen et al. (2018b) did a comparative validation of 6 GFMs against observed flood events in Nigeria and Mozambique. The two flood events used for validation were the 2012 floods in Nigeria and the 2007 floods in Mozambique. Validation was split into three hydraulically diverse analysis regions: two in Nigeria and one in Mozambique. The analysis areas in Nigeria were Lokoja, which is a narrow, confined floodplain that sits at the confluence of the Niger and Benue rivers; and Idah, which sits downstream of Lokoja and is a flat extensive floodplain. The analysis area in Mozambique is Chemba, which is a multichannel portion of the lower Zambezi river. Six global flood models were tested in total, GLOFRIS (Winsemius et al., 2013), JRC (Dottori et al., 2016c), U-Tokyo (Winsemius et al., 2013), ECMWF (Pappenberger et al., 2012), CIMA-UNEP (Rudari et al., 2015), and Fathom (Sampson et al., 2015). The study found varied performance between the GFMs, with some models scoring very well and others not very well (Bernhofen et al., 2018b).

Here, we use the validation outputs from Bernhofen et al. (2018a) to see how the RFSM map compares when validated against the same observed flood events as six other GFMs. We use the three performance scores outlined in the Calibration section (equations B.1-B.3). These are the same scores used in the Bernhofen et al. (2018b) study. We use the 100-year return period extents for each of the six GFMs for our validation. The overlap between the models and the observed events can be visualized in Figure B.12a and the performance scores for each of the models can be visualized graphically in Figure B.12b.

Across the three study regions, the RFSM consistently scores amongst the best GFMs in terms of CSI. In Chemba, the RFSM CSI score is the higher than any of the GFMs. In both basins in Nigeria, the RFSM has the second highest Bias score. The low river initiation threshold of the RFSM map (10 km^2 UDA) contributes to this overprediction. You can see in Figure B.12a that a number of tributaries are included in Lokoja on which there is no flooding. Similarly, in Idah several floodplain channels not modelled by the other GFMs are represented in the RFSM, resulting in a larger flood extent and higher overprediction within the floodplain.

We've shown that the RFSM map performs similarly to the best performing GFMs when validated against historical flood events in three regions in Nigeria and Mozambique. This indicates that the RFSM does a good job of mapping the flood susceptibility of rivers and is appropriate for use in this study.
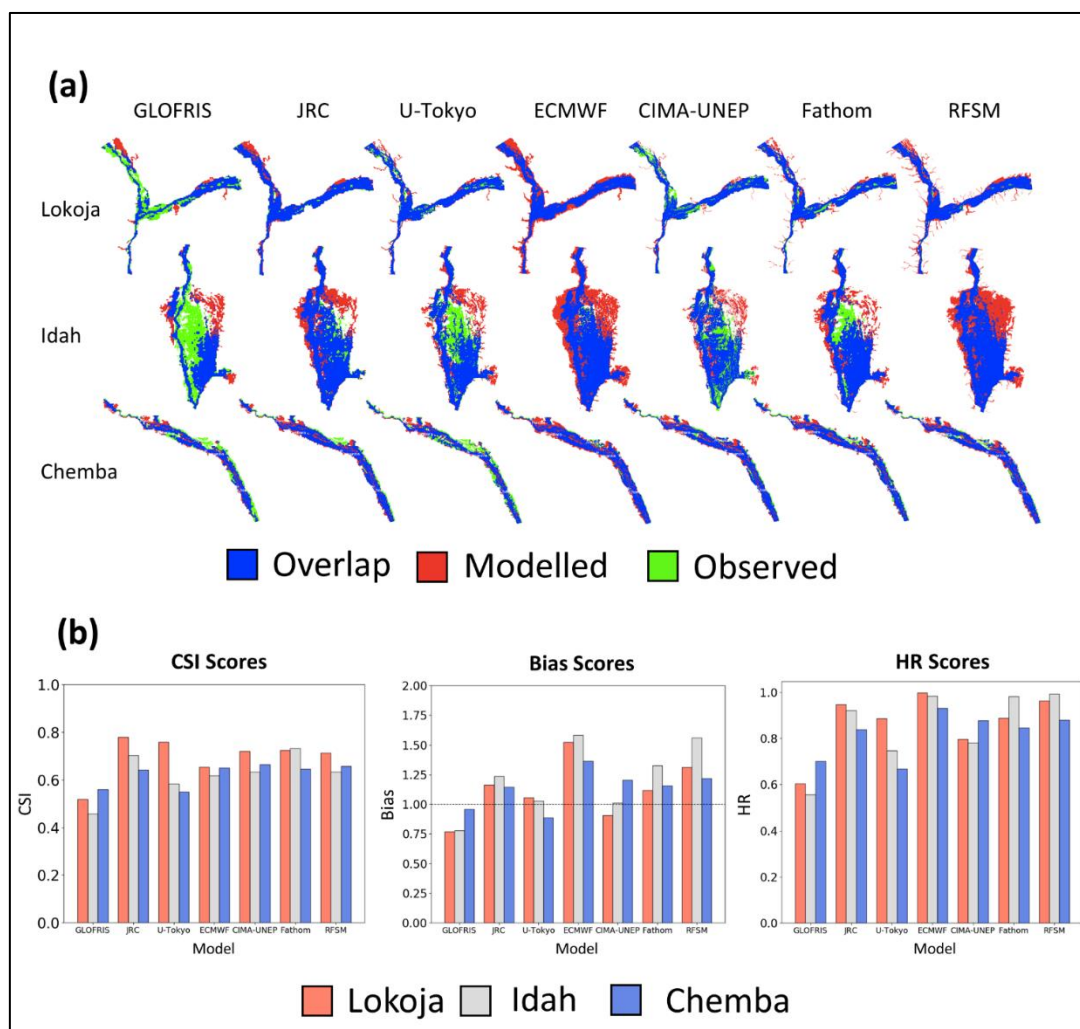
Figure B.12 (a) Overlap of modelled 100-year flood extent and observed flood events in the three validation regions for 6 global flood models and the RFSM. (b) Performance scores for 6 global flood models and the RFSM in the three validation regions.

Figure adjusted from (Bernhofen et al., 2018b)

B.3 Top 50 Countries Exposure

River Class	UDA range (km²)	Colour
Stream	10-100	
Small	100-1,000	
Medium	1,000-10,000	
Medium-Large	10,000-100,000	
Large	100,000-1,000,000	
Huge	>1,000,000	

Figure B.13 WorldPop calculated flood exposure.

(a) Top 50 most exposed countries in terms of total flood exposure. (b) Top 50 most exposed countries in terms of normalized flood exposure (normalized to country's total population)

Figure B.14 HRSL calculated flood exposure.

(a) Top 50 most exposed countries in terms of total flood exposure. (b) Top 50 most exposed countries in terms of normalized flood exposure (normalized to country's total population). Note: flood exposure is calculate only for the 168 countries where HRSL is available. For countries missing from this analysis see Table B.11

B.4 GHS-POP Exposure Change 1975-1990-2000-2015
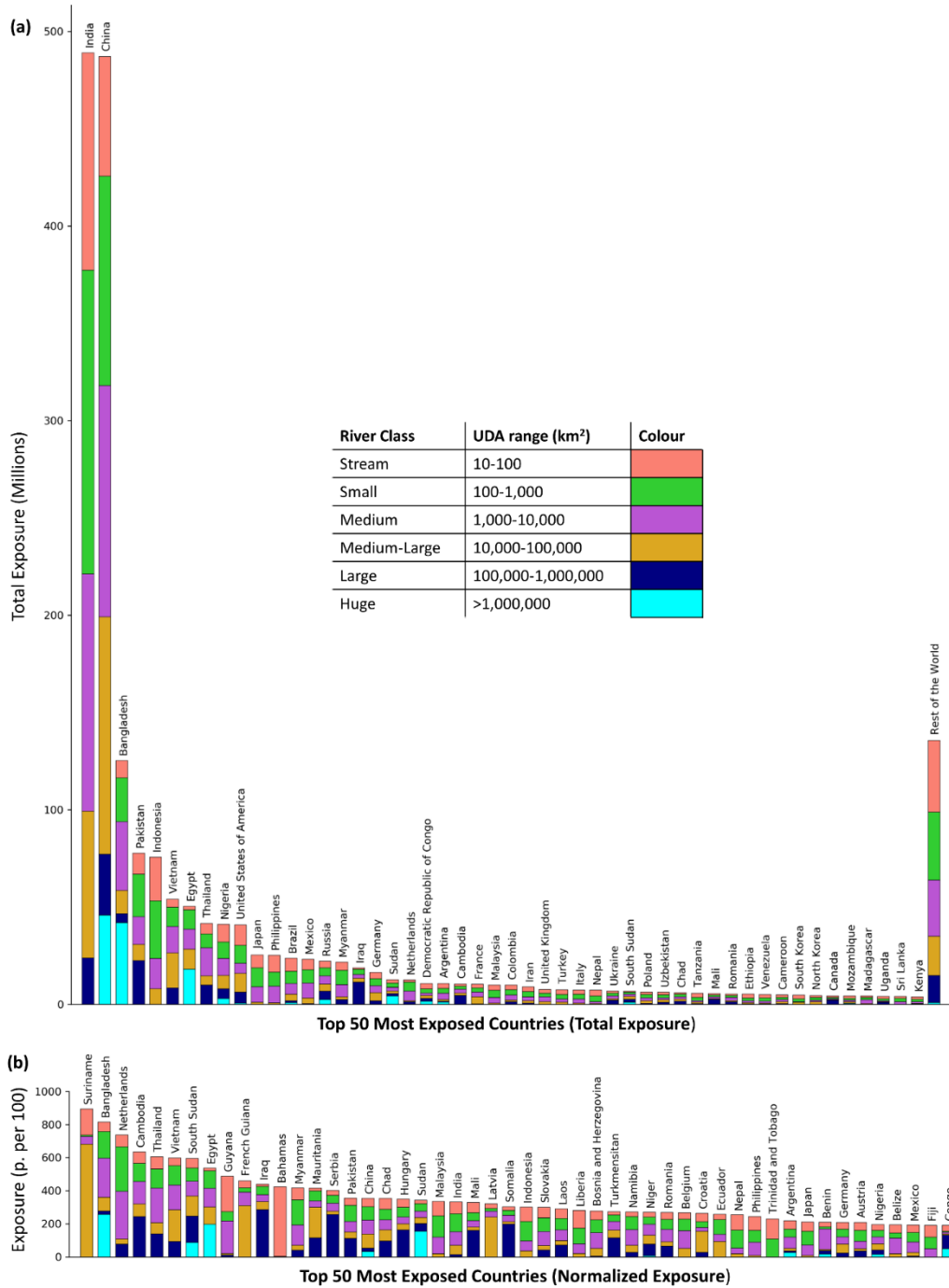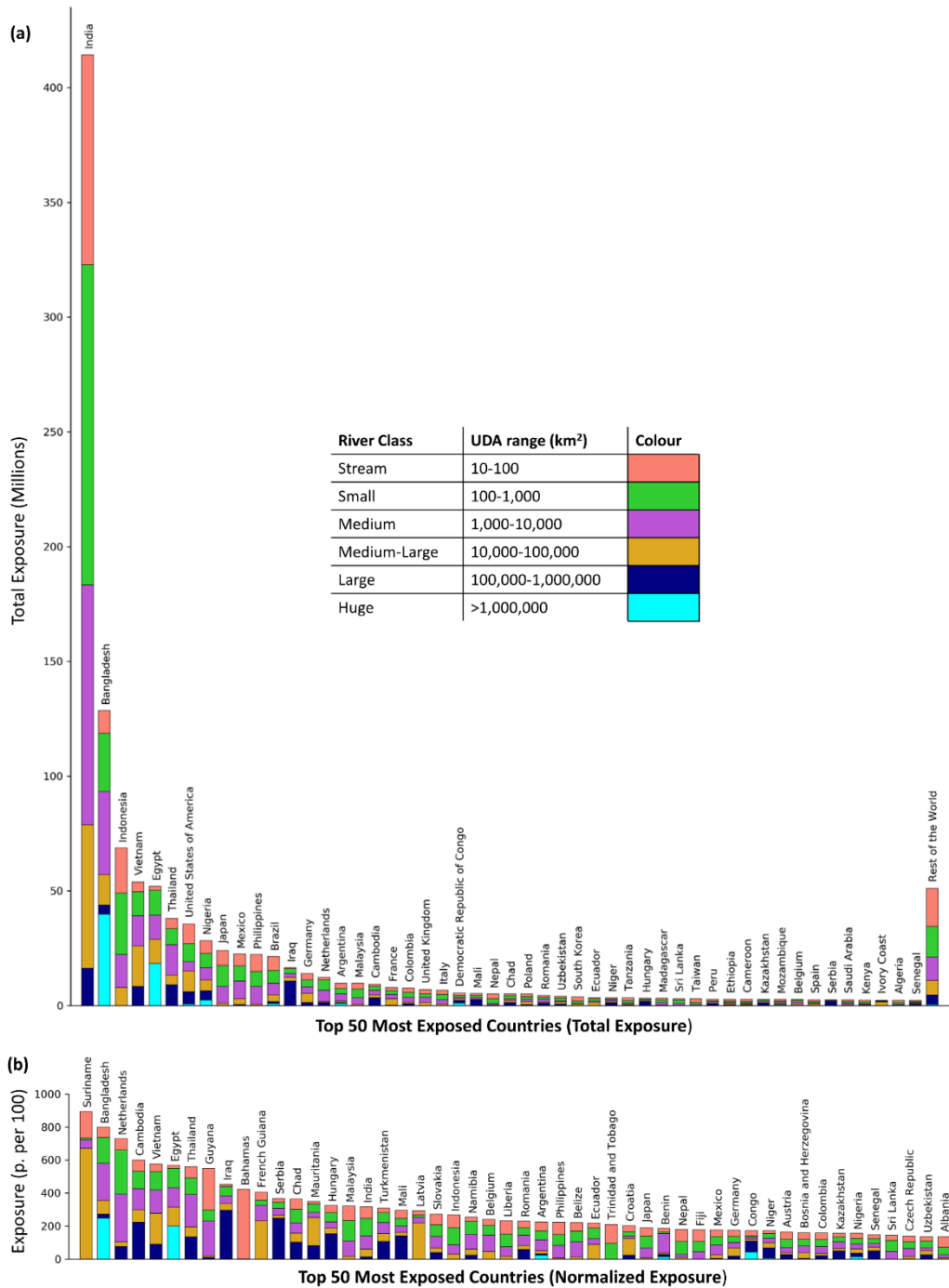
Table B.10 Normalized GHS-POP Total Flood Exposure 1975-1990-2000-2015 (people exposed per 1000)

Country	1975	1990	2000	2015
Aaland Islands	4.58	4.49	4.51	5.87
Afghanistan	149.25	157.55	156.43	156.53
Albania	138.18	163.11	165.59	168.56
Algeria	91.02	74.67	71.28	72.57
Andorra	223.04	207.99	188.52	167.90
Angola	28.15	39.71	49.25	57
Anguilla	15.36	14.02	8.75	8.55
Argentina	215.72	215.93	218.78	218.09
Armenia	64.98	65.51	65.14	65.43
Aruba	0.94	1.00	0.98	0.96
Australia	85.94	85.46	85.18	85.34
Austria	208.18	207.20	206.05	207.24
Azerbaijan	96.10	89.78	92.32	89.98
Bahamas	423.73	426.20	422.18	423.41
Bahrain	30.38	26.71	23.68	20.84
Bangladesh	835.97	828.39	823.49	815.49
Barbados	32.18	32.01	33.45	33.89
Belarus	91.65	91.36	92.88	99.44
Belgium	268.15	266.87	266.33	266.26
Belize	195.68	193.03	194.93	194.06
Benin	241.05	219.47	209.06	208.44
Bhutan	50.01	59.50	72.97	84.52
Bolivia	115.71	113.76	122.79	129.47
Bonaire Saint Eustatius and Saba	4.48	4.48	4.29	4.38
Bosnia and Herzegovina	330.71	299.24	288.51	276.69
Botswana	101.62	100.21	101.39	108.46
Brazil	113.70	114.50	115.73	117.56
British Virgin Islands	0	0	0	0
Brunei	372.20	382.18	371.09	357.00
Bulgaria	189.84	179.45	176.52	174.82
Burkina Faso	147.92	135.42	125.61	117.56

Burundi	55.95	50.74	53.23	60.87
Cambodia	688.96	667.62	662.91	634.40
Cameroon	116.84	123.93	133.34	143.56
Canada	145.92	141.22	138.09	134.19
Cayman Islands	9.16	5.76	4.52	3.49
Central African Republic	130	132.02	138.97	146.09
Chad	375.95	358.47	358.47	353.06
Chile	96.46	95.97	95.85	97.95
China	344.07	344.99	348.70	353.79
Colombia	162.37	169.69	172.73	176.27
Comoros	14.32	14.57	14.73	12.73
Congo	113.22	109.52	113.43	190.56
Costa Rica	102.21	104.94	104.46	105.55
Croatia	269.66	265.10	263.76	263.55
Cuba	133.04	136.48	138.25	142.10
Curacao	3.66	3.62	3.41	3.06
Cyprus	42.00	41.41	40.58	39.64
Czech Republic	176.36	169.78	167.36	163.10
Democratic Republic of Congo	95.47	96.24	95.8	96.07
Denmark	82.51	82.72	82.44	82.21
Djibouti	30.04	35.41	34.24	35.75
Dominica	58.49	60.19	62.76	66.66
Dominican Republic	291.21	125.18	112.04	113.18
Ecuador	264.38	264.19	262.56	257.03
Egypt	542.36	533.38	535.79	536.38
El Salvador	73.30	71.84	73.22	78.69
Equatorial Guinea	124.83	116.14	117.28	121.67
Eritrea	34.02	32.91	51.75	58.93
Estonia	30.86	66.66	98.35	103.27
Ethiopia	53.14	49.38	48.09	52.08
Falkland Islands	1.63	2.38	2.82	3.32
Faroe Islands	5.98	6.56	6.82	6.98
Fiji	182.86	183.96	184.69	190.78
Finland	200.64	178.71	171.11	166.69
France	178.09	171.63	167.68	163.66
French Guiana	259.45	317.51	372.09	459.89
Gabon	134.63	125.4	123.76	122.25

Gambia	133.95	132.72	129.06	122.93
Georgia	111.40	100.95	97.14	93.63
Germany	205.31	204.25	205.37	207.91
Ghana	103.45	105.9	104.71	107.09
Gibraltar	0	0	0	0
Greece	62.87	62.91	64.34	65.84
Grenada	11.31	11.50	11.92	11.38
Guadeloupe	68.11	63.94	60.60	56.35
Guatemala	77.21	79.22	81.35	87.18
Guam	26.11	27.31	27.97	28.60
Guernsey	0	0	0	0
Guinea	94.49	101.89	109.36	121.24
Guinea Bissau	96.64	98.65	99.63	104.44
Guyana	490.06	488.23	487.58	487.22
Haiti	60.72	149.72	157.31	156.11
Honduras	127.87	128.20	128.68	130.16
Hong Kong	35.17	39.60	42.09	46.65
Hungary	346.48	346.95	347.18	348.72
Iceland	35.10	34.81	40.46	42.78
India	303.04	307.43	317.00	331.29
Indonesia	333.65	317.91	310.11	300.44
Iran	51.12	89.76	97.82	96.68
Iraq	450.51	421.74	432.13	439.50
Ireland	121.15	115.23	113.80	115.38
Isle of Man	48.54	49.25	50.46	51.56
Israel	70.13	65.78	64.09	64.33
Italy	120.68	124.39	126.98	130.81
Ivory Coast	127.71	128.02	127.59	126.48
Jamaica	127.35	127.54	126.41	125.51
Japan	216.51	212.56	211.06	210.11
Jersey	19.88	20.90	21.58	22.60
Jordan	42.35	25.03	22.71	22.61
Kazakhstan	148.52	147.56	150.10	154.68
Kenya	74.79	77.29	77.17	81.91
Kiribati	0	0	0	0
Kosovo	169.53	162.07	155.75	151.41

Kuwait	54.80	48.01	51.08	54.09
Kyrgyzstan	62.01	62.56	62.05	62.38
Laos	233.60	267.83	280.07	290.38
Latvia	323.73	320.94	319.35	320.82
Lebanon	26.19	23.94	26.32	24.42
Lesotho	56.89	46.38	45.63	48.93
Liberia	229.25	248.73	259.36	280.51
Libya	151.56	142.65	142.32	144.43
Liechtenstein	127.40	128.90	134.36	137.72
Lithuania	92.01	91.49	91.14	92.30
Luxembourg	131.32	124.89	119.51	114.45
Macao	37.42	38.20	36.71	32.57
Macedonia	142.71	136.14	133.96	136.82
Madagascar	152.53	166.61	181.61	183.90
Malawi	126.97	129.02	128.21	126.02
Malaysia	383.19	365.57	350.96	334.21
Mali	374.23	355.15	343.98	329.31
Malta	23.57	21.18	21.05	20.86
Marshall Islands	0	0	0	0
Martinique	57.88	55.12	52.60	50.02
Mauritania	378.34	395.32	391.08	415.86
Mayotte	9.46	9.67	9.70	10.02
Mexico	215.58	204.55	198.85	191.50
Micronesia	3.81	5.01	5.57	5.84
Moldova	112.21	99.21	95.98	94.57
Monaco	0	0	0	0
Mongolia	124.52	125.12	129.14	128.39
Montenegro	155.39	143.23	140.12	137.74
Montserrat	2.20	2.20	3.91	4.63
Morocco	93.58	92.85	94.59	96.15
Mozambique	152.54	151.09	145.63	147.36
Myanmar	477.15	441.42	417.63	417.30
Namibia	324.82	309.36	296.99	271.60
Nauru	0	0	0	0
Nepal	52.83	129.49	195.13	253.94
Netherlands	699.35	712.36	724.71	738.06
New Caledonia	132.82	93.10	75.80	60.41

New Zealand	131.65	125.18	120.56	113.60
Nicaragua	99.59	105.12	111.04	122.93
Niger	317.70	291.97	276.43	269.06
Nigeria	174.89	175.57	184.34	194.97
Norfolk Island	0	0	0	0
Northern Mariana Islands	3.26	3.24	3.22	4.03
North Korea	172.42	173.71	178.76	184.87
Norway	101.69	94.11	86.99	77.54
Oman	79.61	78.64	76.25	75.83
Pakistan	300.87	309.20	332.03	354.45
Palau	11.99	11.55	10.49	7.33
Palestine	17.63	19.04	19.90	21.64
Panama	90.42	92.93	101.34	109.05
Papa New Guinea	85.30	101.89	100.14	98.45
Paraguay	68.03	64.10	64.41	70.51
Peru	83.60	89.44	93.26	98.15
Philippines	262.80	251.42	247.09	243.54
Poland	153.75	152.49	152.82	155.60
Portugal	31.91	31.80	31.67	31.56
Puerto Rico	124.80	121.67	119.84	116.85
Qatar	82.98	79.97	83.98	88.26
Romania	240.42	238.53	240.44	268.43
Russia	132.63	132.32	133.47	139.27
Rwanda	62.28	57.63	52.28	51.87
Saint Barthelemy	0	0	0	0
Saint Martin (French)	46.02	65.01	75.58	78.05
Saint Lucia	34.92	36.71	37.62	38.28
Saint Pierre and Miquelon	0	0	0	0
Saint Vincent and the Grenadines	23.05	22.70	22.26	21.54
San Marino	20.05	18.86	18.67	18.90
Saudi Arabia	84.28	71.62	71.04	73.02
Sao Tome and Principe	48.69	48.66	48.64	45.00
Senegal	177.88	172.26	176.42	177.40
Serbia	397.30	396.53	397.18	401.71
Seychelles	0	0	0	0

Sierra Leone	147.18	144.95	140.83	141.10
Singapore	52.45	50.29	48.86	47.90
Sint Maarten (Dutch)	28.50	30.69	26.89	26.65
Slovakia	304.02	300.32	298.66	299.67
Slovenia	158.07	156.71	156.36	157.28
Solomon Islands	51.68	55.26	55.97	65.89
Somalia	313.39	310.90	309.76	303.01
South Africa	38.07	36.68	36.14	36.20
South Korea	109.07	103.01	100.59	99.33
South Sudan	765.72	716.32	687.14	593.82
Spain	80.60	79.35	77.93	76.24
Sri Lanka	183.00	188.09	187.47	188.22
Sudan	346.81	346.50	349.60	343.28
Suriname	885.55	887.18	888.74	893.98
Swaziland	131.30	141.66	122.49	109.67
Sweden	153.84	145.08	141.13	136.23
Switzerland	143.04	139.86	138.97	138.37
Syria	130.56	117.98	117.66	119.01
Taiwan	159.93	153.82	152.50	147.31
Tajikistan	75.61	75.60	76.87	77.85
Tanzania	114.47	104.10	104.11	110.51
Timor-Leste	144.38	149.69	143.17	141.17
Thailand	530.14	550.91	567.44	605.17
Togo	118.84	111.79	109.13	120.18
Trinidad and Tobago	218.92	224.22	227.41	229.96
Tunisia	77.45	74.98	78.03	85.57
Turkey	108.09	104.32	101.51	99.78
Turkmenistan	272.90	269.52	271.73	272.14
Turks and Caicos Islands	3.48	4.03	3.85	3.72
Tuvalu	0	0	0	0
Uganda	95.10	85.57	77.93	77.75
Ukraine	136.61	133.58	135.49	139.96
United Arab Emirates	103.30	94.26	92.10	91.63
United Kingdom	114.54	117.13	119.02	121.97
United States of America	130.15	131.61	132.46	130.59
United States Virgin Islands	8.77	9.12	8.93	8.77
Uruguay	42.41	38.74	39.64	39.71

Uzbekistan	139.01	139.01	141.24	142.49
Vanuatu	37.06	39.91	41.79	45.11
Vatican City	0	0	0	0
Venezuela	151.66	152.30	153.58	159.67
Vietnam	622.03	629.97	619.10	597.67
Western Sahara	74.64	67.14	61.52	55.35
Yemen	46.44	47.64	50.51	55.95
Zambia	190.44	104.17	101.80	113.21
Zimbabwe	136.45	125.30	120.25	114.46
Global	**256.5**	**259.29**	**262.82**	**264.85**

B.5 HRSL Missing Countries

Table B.11 Countries not mapped by HRSL (at time of writing). These countries
were not represented in any of the results calculated using the HRSL dataset.

Aaland Islands	Gibraltar	Pakistan
Afghanistan	Guernsey	Palestine
Antarctica	Iran	Russia
Andorra	Isle of Man	Saint Pierre and Miquelon
Armenia	Israel	Saint-Barthelemy
Azerbaijan	Jersey	Saint-Martin (French)
Bhutan	Kosovo	Sint Maarten (Dutch)
Brunei	Kuwait	Somalia
Canada	Laos	South Sudan
China	Lebanon	Sudan
Cuba	Luxembourg	Sweden
Curacao	Martinique	Sweden
Cyprus	Montserrat	Syria
Denmark	Morocco	Turkey
Falkland Islands	Myanmar	Ukraine
Faroe Islands	Norfolk Island	Vatican City
Finland	North Korea	Venezuela
Georgia	Norway	Yemen

B.6 GFM Coverage Maps
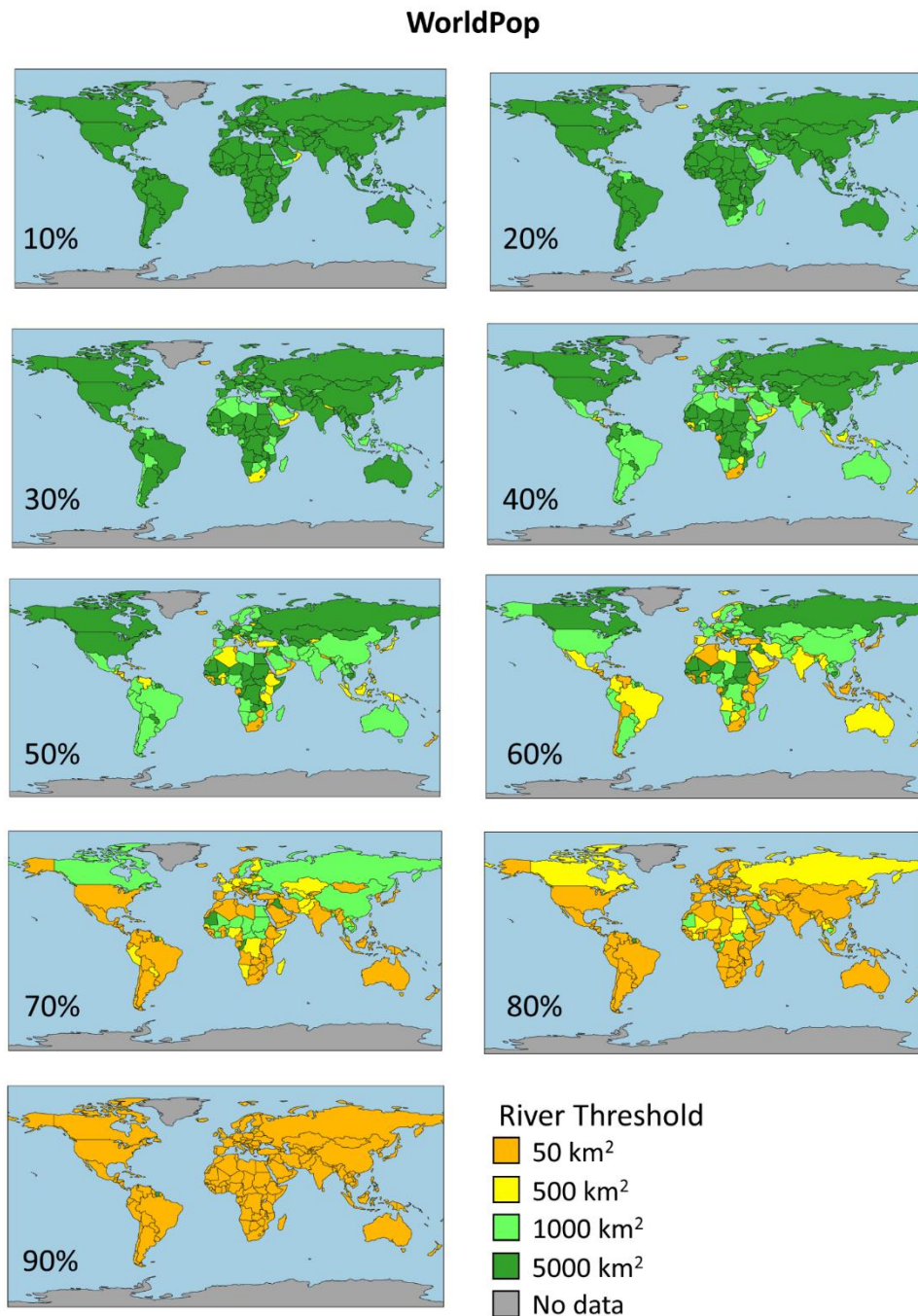
Figure B.15 What size GFM river initiation threshold is required to capture _% of a country's total GFM flood (>50 km2) exposure calculated with WorldPop. Each map is a different target percentage.

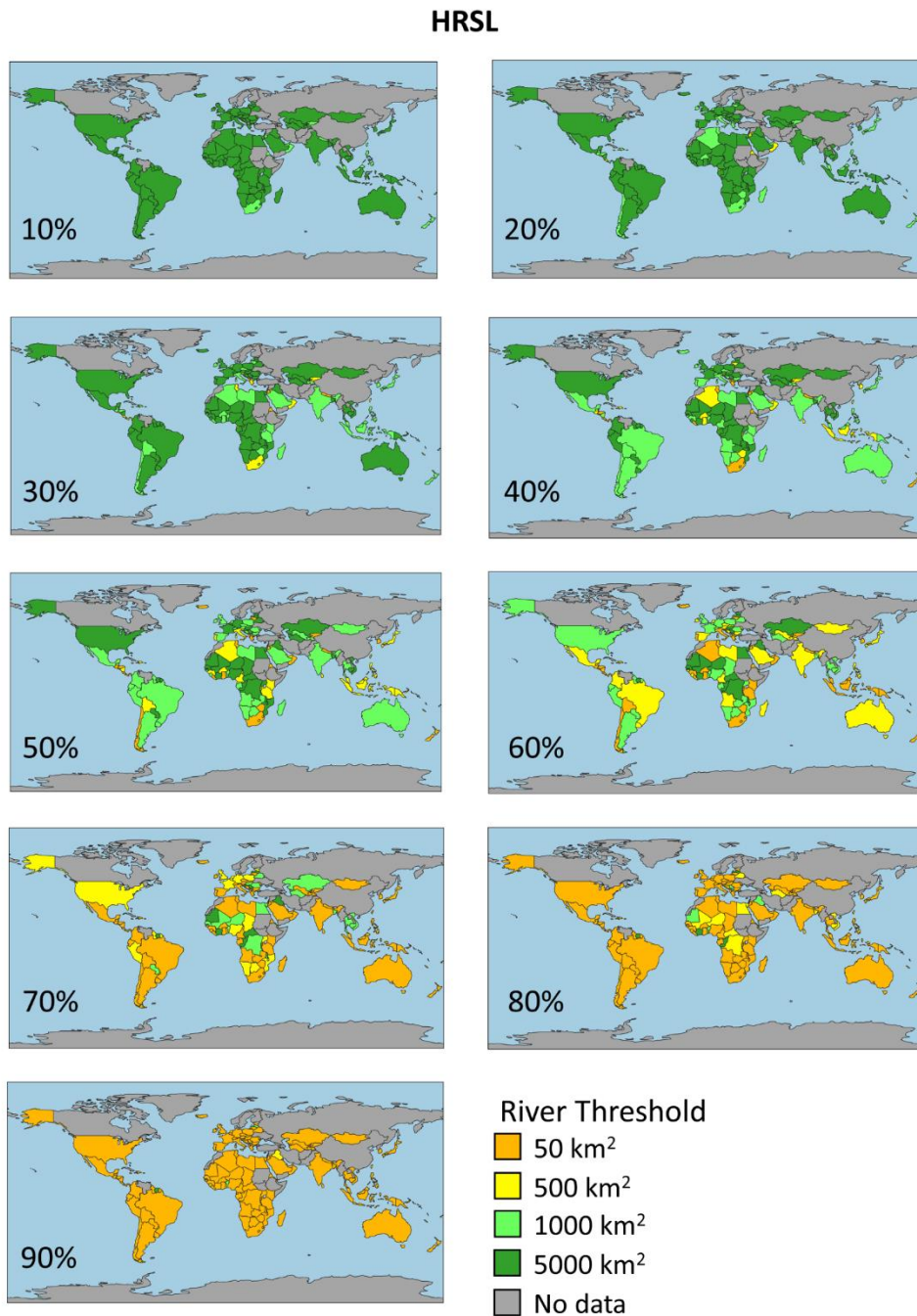This map is intended to inform users of GFMs about the appropriate GFM to use in a given country.

GHSL
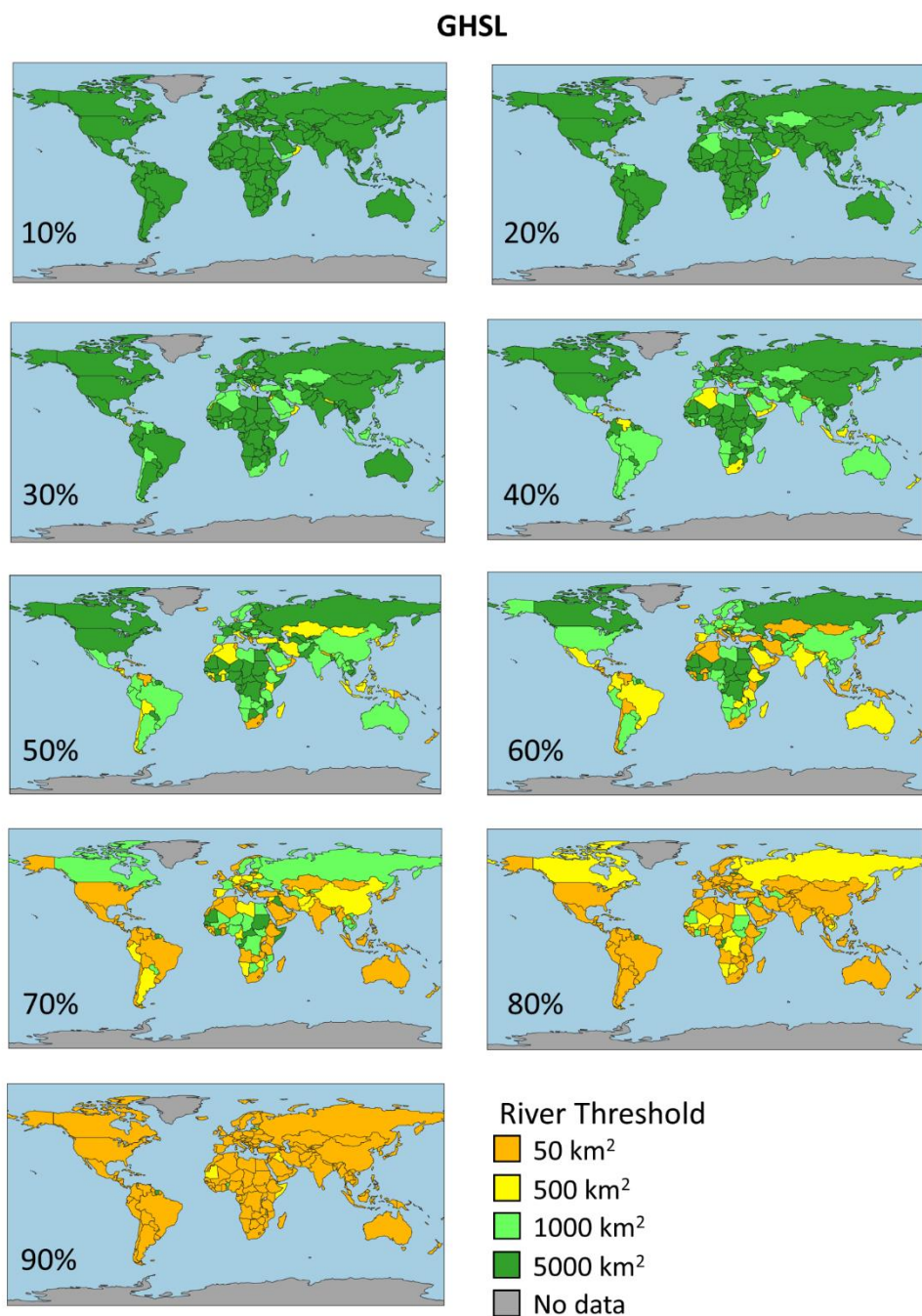
Figure B.16 What size GFM river initiation threshold is required to capture _% of a
country's total GFM flood (>50 km2) exposure calculated with GHS-POP.
Each map is a different target percentage.

This map is intended to inform users of GFMs about the appropriate GFM to
use in a given country.

HRSL

Figure B.17 What size GFM river initiation threshold is required to capture _% of a country's total GFM flood (>50 km2) exposure calculated with HRSL. Each map is a different target percentage.

This map is intended to inform users of GFMs about the appropriate GFM to use in a given country.

References

BECK, H. E., ZIMMERMANN, N. E., MCVICAR, T. R., VERGOPOLAN, N., BERG, A. & WOOD, E. F. 2018. Present and future Köppen-Geiger climate classification maps at 1-km resolution. *Scientific Data,* 5**,** 180214.

BERNHOFEN, M. V., WHYMAN, C., TRIGG, M. A., SLEIGH, P. A., SMITH, A., SAMPSON, C., YAMAZAKI, D., WARD, P., RUDARI, R., PAPPENBERGER, F., DOTTORI, F., SALAMON, P. & WINSEMIUS, H. C. 2018a. Analysis inputs for validation of six global flood models against observed flood events in Nigeria and Mozambique. Research Data Leeds Repository.

BERNHOFEN, M. V., WHYMAN, C., TRIGG, M. A., SLEIGH, P. A., SMITH, A. M., SAMPSON, C. C., YAMAZAKI, D., WARD, P. J., RUDARI, R., PAPPENBERGER, F., DOTTORI, F., SALAMON, P. & WINSEMIUS, H. C. 2018b. A first collective validation of global fluvial flood models for major floods in Nigeria and Mozambique. *Environmental Research Letters,* 13.

DOTTORI, F., ALFIERI, L., SALAMON, P., BIANCHI, A., FEYEN, L. & HIRPA, F. A. 2016a. Flood hazard map of the World - 100-year return period. *In:* EUROPEAN COMMISSION, J. R. C. J. (ed.).

DOTTORI, F., ALFIERI, L., SALAMON, P., BIANCHI, A., FEYEN, L. & LORINI, V. 2016b. Flood hazard map for Europe, 100-year return period. *In:* EUROPEAN COMMISSION, J. R. C. J. (ed.).

DOTTORI, F., SALAMON, P., BIANCHI, A., ALFIERI, L., HIRPA, F. A. & FEYEN, L. 2016c. Development and evaluation of a framework for global flood hazard mapping. *Advances in Water Resources,* 94**,** 87-102.

LEHNER, B. & GRILL, G. 2013. Global river hydrography and network routing: baseline data and new approaches to study the world's large river systems. Hydrological Processes.

NARDI, F., ANNIS, A., DI BALDASSARRE, G., VIVONI, E. R. & GRIMALDI, S. 2019. GFPLAIN250m, a global high-resolution dataset of Earth's floodplains. *Scientific Data,* 6**,** 180309.

PAPPENBERGER, F., DUTRA, E., WETTERHALL, F. & CLOKE, H. L. 2012. Deriving global flood hazard maps of fluvial floods through a physical model cascade. *Hydrology and Earth System Sciences,* 16**,** 4143-4156.

RUDARI, R., SILVESTRO, F., CAMPO, L., REBORA, N., BONI, G. & HEROLD, C. 2015. IMPROVEMENT OF THE GLOBAL FLOOD MODEL FOR THE GAR 2015.

SAMPSON, C. C., SMITH, A. M., BATES, P. B., NEAL, J. C., ALFIERI, L. & FREER, J. E. 2015. A high-resolution global flood hazard model. *Water Resources Research,* 51**,** 7358-7381.

TRIGG, M. A., BIRCH, C. E., NEAL, J., BATES, P., SMITH, A., SAMPSON, C., YAMAZAKI, D., HIRABAYASHI, Y., PAPPENBERGER, F., DUTRA, E., WARD, P. J., WINSEMIUS, H. C., SALAMON, P., DOTTORI, F., RUDARI, R., KAPPES, M. S., SIMPSON, A., HADZILACOS, G. & FEWTRELL, T. 2016a. Aggregated fluvial flood hazard output for six Global Flood Models for the African Continent. Research Data Leeds Repository.

TRIGG, M. A., BIRCH, C. E., NEAL, J. C., BATES, P. D., SMITH, A., SAMPSON, C. C., YAMAZAKI, D., HIRABAYASHI, Y., PAPPENBERGER, F., DUTRA, E., WARD, P. J., WINSEMIUS, H. C.,

SALAMON, P., DOTTORI, F., RUDARI, R., KAPPES, M. S., SIMPSON, A. L., HADZILACOS, G. & FEWTRELL, T. J. 2016b. The credibility challenge for global fluvial flood risk analysis. *Environmental Research Letters,* 11**,** 10.

WINSEMIUS, H. C., VAN BEEK, L. P. H., JONGMAN, B., WARD, P. J. & BOUWMAN, A. 2013. A framework for global river flood risk assessments. *Hydrology and Earth System Sciences,* 17**,** 1871-1892.

Appendix C

Supplementary Material to Chapter 5

Appendix C consists of the supplementary material that accompanied the manuscript on which **Chapter 5** is based.

C.1 Global Flood Hazard Dataset Details

C.1.1 CaMa-UT

Developed at the University of Tokyo, the CaMa-UT global flood model (GFM) uses the global hydrodynamic river routing model CaMa-Flood (Catchment-based Macro-scale Floodplain model) (Yamazaki et al., 2011) to simulate inundation using runoff inputs from a global hydrological model and global forcing data. River discharge is calculated in CaMa-Flood using the local inertial formulation of the shallow water equations (Yamazaki et al., 2013) with explicit representation of channel bifurcations (Yamazaki et al., 2014). Floodplain inundation is simulated using a floodplain storage elevation relationship and sub-grid topographic information (Yamazaki et al., 2011). The flood maps used in this study, described in detail in Zhou et al. (2020), are run using CaMa-Flood v4 forced by e2o_ecmwf runoff data from the eartH2OObserve (e2o) project (Schellekens et al., 2017). The runoff data is forced by the WATCH Forcing Data methodology applied to ERA-Interim data for the years 1980 to 2014 (Weedon et al., 2014) and return periods are determined using the generalized extreme value (GEV) fitting function. Storage volumes are calculated globally at 0.25° resolution and then downscaled to the native output resolution of 3 arc seconds (~90 m at the equator) using the Multi-Error-Removed Improved-Terrain (MERIT) Digital Elevation Model (DEM) (Yamazaki et al., 2017) and MERIT derived hydrography (MERIT Hydro) (Yamazaki et al., 2019). The downscaling approach follows the assumption that the water surface is flat within the unit catchment and areas of lowest elevation are inundated first until the total water volume of the unit catchment matches the computed storage volume (Zhou et al., 2020). Catchments smaller than a 0.25° resolution grid box (~ 600 km^2 at the equator) are not explicitly modelled, however,

some rivers below this catchment threshold are inundated in the downscaling procedure.

C.1.2 CIMA-UNEP

The CIMA-UNEP GFM was produced as an input for the 2015 Global Assessment Report (GAR) on Disaster Risk Reduction (UNDRR, 2015). It is the only GFM which simulates flooding in one dimension. Cross sections are generated along sections of a river network derived from HydroSHEDS (Lehner and Grill, 2013) and Manning's equation is used to derive stage-discharge functions at each section. Flooded area along each cross section is then simulated for each return period and merged into a flood hazard map using a reconditioned SRTM3 DEM (Rudari et al., 2015). Flood flows are estimated using a regionalized flood frequency approach using data from over 8000 gauging stations globally. Regression techniques were used to estimate extreme flows in ungauged basins using geomorphological and climatological variables. This regionalized flood frequency approach was improved in areas with insufficient gauge observations by a global hydrological model, Continuum GHM (Silvestro et al., 2013), forced by version 3 of the EC-Earth Global Climatic Model (Hazeleger et al., 2012) for the time period 1960-2012. The CIMA-UNEP GFM models flooding on all rivers with an upstream drainage area of 1000 km^2. Simulations are performed at 3 arcsecond resolution (~90 m at the equator) with no downscaling. There are two available resolutions of CIMA-UNEP. The native 3 arc second resolution global flood hazard maps and aggregated 32 arc second maps (~1 km at the equator). We use the native 3 arcsecond global flood hazard maps in this study.

C.1.3 Fathom

Fathom Global is the only GFM used in this study that is an 'industry' model. But their model can be used free-of-charge for research purposes. The Fathom model uses a regionalized flood frequency approach to simulate extreme flows (Sampson et al., 2015). The catchment characteristics of well gauged basins are used to extrapolate extreme flows from data-rich catchments to data-poor catchments that share similar catchment characteristics. This regionalized flood frequency approach is described in detail in Smith et al. (2015). Flooding is simulated using the sub-grid channel version (Neal et al., 2012) of the two-

dimensional hydrodynamic model LISFLOOD-FP, which solves the local inertia approximation of the shallow water equations (Bates et al., 2010). Hydraulic simulations are carried out at the native model output resolution (3 arcsecond globally, 1 arcsecond nationally). The Fathom Global 2.0 GFM improves on Fathom Global 1.0 by incorporating new terrain: MERIT DEM (Yamazaki et al., 2017), and hydrography data: MERIT Hydro (Yamazaki et al., 2019), as well as improving the representation of river channels (Neal et al., 2021). The Fathom Global modelling framework has been applied in both the US (Wing et al., 2017) and the UK to produce higher accuracy flood maps by ingesting higher accuracy local terrain and gauge data. Fathom-UK incorporates the latest LiDAR data and gauge data to produce flood maps at 1 arcsecond resolution (~10 m in the UK). We use both the Fathom Global 2.0 flood maps and the Fathom-UK flood maps in this study. In Colombia, Ethiopia, India, and Malaysia we use Fathom Global 2.0 flood hazard maps at 3 arcsecond resolution (~90 m at the equator) on rivers with an upstream drainage area of 50 km^2 or greater. In England, we use the Fathom-UK model which simulates flood hazard on all rivers to produce flood hazard maps at 1 arcsecond resolution (~10 m in England, ~30 m at the equator). In this study, we use only the fluvial undefended Fathom flood maps. Flood defenses, as well as pluvial and coastal flooding, are not considered.

C.1.4 GLOFRIS

The Global Flood Risk with IMAGE Scenarios (GLOFRIS) model simulates fluvial flood hazard for the Aqueduct Flood Platform (https://www.wri.org/applications/aqueduct/floods/). To simulate flooding under current climate conditions, the European Union Water and Global Change (EUWATCH) (Weedon et al., 2011) forcing data is used for the years 1960 to 1999 (Ward et al., 2020). Hydrological simulations were run using the PCRaster Global Water Balance (PCR-GLOBWB) (Sutanudjaja et al., 2018) hydrological model, which simulates flood levels and discharge using the kinematic wave approximation of the Saint-Venant Equation (van Beek et al., 2011) at 5 arcmin resolution (~9 km at the equator). Extreme value statistics are then used to calculate floodplain volumes in each grid cell for different return periods. Floodplain volumes are downscaled from 5 arcmin resolution onto a 30 arcseconds (~900 m at the equator) HydroSHEDS DEM (Lehner et al., 2008) using a volume redistribution approach outlined in Winsemius et al. (2013). The final global flood hazard maps represent

flooding at 30 arcsecond resolution on rivers with a Strahler stream order of 6 or greater. Flood maps under different climate conditions are available on the Aqueduct floods platform. In this study, we use the fluvial flood maps under current climate conditions.

C.1.5 JRC

The GFM developed by the European Union Joint Research Centre (JRC) uses ERA-Interim forcing data (Dee et al., 2011, Balsamo et al., 2015) for the years 1980-2013 to feed hydrological simulations using the Global Flood Awareness System (GloFAS) (Alfieri et al., 2013) modelling framework. GloFAS uses the land surface model HTESSEL (Balsamo et al., 2009) to simulate surface and sub-surface runoff and LISFLOOD Global to simulate streamflow across the river network at 0.1 degree resolution (~11 km at the equator) (Alfieri et al., 2013). Return period streamflows are calculated for each point along the GloFAS river network using a Gumbel distribution (Dottori et al., 2016). The streamflow information is downscaled from 0.1 degree resolution (~11 km at the equator) to 30 arcseconds resolution (~900 m at the equator) onto a river network derived from the HydroSHEDs DEM (Lehner et al., 2008). Flood maps are then simulated at 30 arcsecond resolution using the 2D hydrodynamic model CAD2D, which solves the semi-inertial formulation of the shallow water equations (Dottori and Todini, 2011). The final flood hazard maps represent flooding at 30 arcseconds resolution for rivers with an upstream drainage area of 5000 km^2 or greater.

C.1.6 GFD

The Global Flood Database (GFD) is a catalogue of 913 satellite observed large flood events captured between 2000-2018 (Tellman et al., 2021). The dates and locations of historic flood events are taken from the Dartmouth Flood Observatory (DFO) archive of large flood events (Kettner et al., 2021). Inundation is detected from optical MODIS satellite imagery at 250 m resolution using an algorithm that detects the surface reflectance of water. Of the total 3,054 flood events listed in the DFO archive, 913 events are found to have sufficient cloud-free MODIS images for inundation detection (Tellman et al., 2021). Flood events are categorized by the type of flood: dam breaks, heavy rain, snow or ice melt, and tropical storms and surges. In this study, we use flood data from snow or ice melt

and heavy rain events only. The total number of observed flood events used for each country are as follows: Colombia (29), England (12), Ethiopia (28), India (147), and Malaysia (21).

C.2 Global Population Dataset Details

C.2.1 GPW4

The Gridded Population of the World (GPW) dataset, which is currently in version 4 (GPW4), uses sub-national census data and uniformly distributes it over an area of land. GPW4 improves on previous iterations of GPW in that it incorporates the latest census data and the size of administrative areas are reduced in 87 countries (Doxsey-Whitfield et al., 2015). The accuracy of GPW's approach of uniformly distributing population over an area, known as areal weighting, is highly dependent on the size of these administrative areas; smaller administrative areas result in more precise grid cell population estimates. This means that the appropriate scale for analysis differs in countries with detailed census and administrative units compared to countries with coarser input data (Leyk et al., 2019). Despite these drawbacks, the areal weighting approach to population distribution ensures that the census data retains its fidelity (Doxsey-Whitfield et al., 2015) and GPW data can be used as the population input for a number of other global population maps (Freire et al., 2016, Tiecke, 2017, Lloyd et al., 2019). GPW4 reports data on population density and population counts as well as demographics and data quality across five epochs: 2000, 2005, 2010, 2015, and 2020. The output resolution of the gridded data is 30 arcseconds (~900 m at the equator). In this study, we use the GPW v4.11 population counts for the year 2020, adjusted to match United Nation's World Population Prospects.

C.2.2 GHS-POP

Developed by the European Union JRC, the Global Human Settlement Population Grid (GHS-POP) (Freire et al., 2016) uses the built-up area grids defined by the Global Human Settlement Layer (GHSL) project (Pesaresi et al., 2013) to distribute census data over built up areas. Built up areas are identified in the GHSL project using Landsat imagery across four epochs: 1975, 1990, 2000, and 2014. Over 30,000 Landsat scenes (resolution ~30 m) were processed to identify structures and produce grids of proportion of built-up area at 250 m resolution globally

(Pesaresi et al., 2016). The GHS-POP dataset uses the GHSL built-up area grid and population estimates from GPW4 to distribute population over a census area by proportionally allocating population to gridded cells according to the ratio of built-up area in each cell as defined by GHSL (Freire et al., 2015, Freire et al., 2020). In areas where no built-up area is detected by GHSL, but where census data indicates there is population, the population data is disaggregated across the census area using areal weighting (Freire et al., 2016). GHS-POP data is available globally at 9 arcseconds resolution (~250 m at the equator) across four epochs: 1975, 1990, 2000, 2015. In this study, we use the R2019a revision of GHS-POP for the population year 2015.

C.2.3 GRUMP

The Global Rural-Urban Mapping Project (GRUMP) uses a similar allocation approach to GPW but attempts to explicitly identify the population of urban areas (Balk et al., 2005). GRUMP uses night-time light data to determine the footprints of major cities (Elvidge et al., 1997). Population totals derived from both urban center estimates and GPW census unit estimates are proportionally allocated across the identified urban footprints (Balk et al., 2006). The nighttime lights' data used to determine the urban footprint in GRUMP has been shown to overestimate urban areas (Balk et al., 2006). GRUMP is available globally at 30 arcsecond (~900 m at the equator) resolution across three epochs: 1990, 1995, 2000. The GRUMP dataset is no longer being updated but is still being used today (Arnell and Gosling, 2016, Tanoue et al., 2016). In this study, we use the GRUMP population count grid v1 for the year 2000.

C.2.4 HRSL

The High Resolution Settlement Layer (HRSL) developed by Facebook in collaboration with Columbia University's Centre for International Earth Science Information Network (CIESIN) uses Convolutional Neural Networks (CNN) to identify individual buildings from ultra-high resolution DigitalGlobe (now Maxar) satellite data (0.5 m resolution) to produce maps of human settlements at 1 arcsecond (~30 m at the equator) resolution (Tiecke, 2017). GPW4 census data is proportionally allocated across these settlements to produce maps of both total

population and population demographics. We use the latest iteration of the HRSL, which gives population estimates for the years 2018-2019.

C.2.5 HYDE

The History Database of the Global Environment (HYDE) maps global population totals, urban/rural population, population density, and fractions of built-up area as well as land use changes for the years 10,000 BC to 2015 AD (Klein Goldewijk et al., 2010, Klein Goldewijk et al., 2017). Population estimates for the years 1950-2015 are based on the United Nations Population Prospects (2008 Revision). Pre-1950 population estimates are taken from a number of previous studies and historical population sources outlined in Klein Goldewijk et al. (2010). Population is distributed across the grid using weights determined by auxiliary datasets such as slope, soil suitability, distance to water, as well as a number of historical case studies (Klein Goldewijk et al., 2017). The HYDE population maps estimate global population at 5 arc minute resolution (~10 km at the equator). In this study, we use the HYDE 3.2 population estimates for the year 2015.

C.2.6 LandScan

Developed by the Oak Ridge National Laboratory, LandScan has produced annual global population maps since 1998. In contrast to other global population maps, where the use of census data results in estimates of night-time population, LandScan estimates the ambient global population (a combination of where people work and live) (TReNDS, 2020). The LandScan population modelling method uses Digital Global (now Maxar) satellite imagery and a number of ancillary datasets such as roads, landcover, water bodies, and urban and environmental data to calculate the likelihood that a gridded cell is populated during the day. These likelihood coefficients are then used to weight the distribution of subnational census data across the gridded area (Leyk et al., 2019). LandScan maps are available globally at 30 arcseconds resolution (~900 m at the equator) and are open access for academic research and for humanitarian projects. In this study, we use Landscan global population maps for the year 2019.

C.2.7 WorldPop

WorldPop uses a Random Forest model and a number of ancillary datasets to weight the distribution of GPW4 census data across a gridded area (Stevens et al.,

2015). Ancillary datasets include land cover, roads, nighttime lights, water bodies, OpenStreetMap data and images from a number of satellite sources such as Landsat and TerrSAR-x. These datasets, and others used by WorldPop, are all summarized in Lloyd et al. (2019). WorldPop produces global population estimates at 3 arcseconds (~90 m at the equator) resolution annually for the years 2000-2020. Because GPW4 data is used as input, these population maps also include the same demogprahic breakdowns as GPW4. In this study, we use the 3 arcsecond (~90 m at the equator) resolution WorldPop UN adjusted unconstrained population counts for the year 2020.

Table C.1 Global flood hazard data access

Dataset	Availability	Access
CaMa-UT	Available on request from developer	Maps can be obtained from developer http://hydro.iis.u-tokyo.ac.jp/~yamadai/
CIMA-UNEP	Online / available on request from developer	Aggregated 1 km maps available from https://preview.grid.unep.ch 3 arcsecond maps available on request from developer
Fathom	Available on request from developer (free for research purposes)	Maps can be requested from developer website https://www.fathom.global/
GLOFRIS	Online	https://www.wri.org/applications/aqueduct/floods/
JRC	Online	https://data.jrc.ec.europa.eu/collection/id-0054
GFD	Online	https://global-flood-database.cloudtostreet.ai/

Table C.2 Non-exhaustive list of previous studies using global flood hazard data
Yellow highlighted studies use multiple datasets

Dataset	Study
CaMa-UT	Yamazaki et al. (2011), Hirabayashi et al. (2013), Trigg et al. (2016), Tanoue et al. (2016), Aerts et al. (2020), Zhou et al. (2020), Hirabayashi et al. (2021)
CIMA-UNEP	Rudari et al. (2015), Trigg et al. (2016), Aerts et al. (2020), Lindersson et al. (2021)
Fathom	Sampson et al. (2015), Trigg et al. (2016), Smith et al. (2019), Aerts et al. (2020), Rentschler and Salhab (2020)
GLOFRIS	Ward et al. (2013), Winsemius et al. (2016), Trigg et al. (2016), Ward et al. (2017), Aerts et al. (2020)
JRC	Dottori et al. (2016), Trigg et al. (2016), Alfieri et al. (2017), Dottori et al. (2018), Aerts et al. (2020), Zischg and Bermúdez (2020), Lindersson et al. (2021)
GFD	Tellman et al. (2021)

Table C.3 Global population data access

Dataset	Availability	Access
GPW4	Online	https://doi.org/10.7927/H4PN93PB
GHS-POP	Online	https://doi.org/10.2905/42E8BE89-54FF-464E-BE7B-BF9E64DA5218
GRUMP	Online	https://doi.org/10.7927/H4VT1Q1H
HRSL	Online	https://data.humdata.org/organization/facebook search 'population density'
HYDE	Online	https://dataportaal.pbl.nl/downloads/HYDE/
LandScan	Online (free for research purposes)	https://landscan.ornl.gov/landscan-datasets need to register to download
WorldPop	Online	https://www.worldpop.org/geodata/listing?id=69

Table C.4 Non-exhaustive list of previous studies using global population data
Yellow highlighted studies use multiple datasets

Dataset	Study
GPW4	Willner et al. (2018), Zischg and Bermúdez (2020), Gu et al. (2020)
GHS-POP	Alfieri et al. (2017), Dottori et al. (2018) Rentschler and Salhab (2020), Tellman et al. (2021), Bernhofen et al. (2021), Lindersson et al. (2021)
GRUMP	Arnell and Gosling (2016), Tanoue et al. (2016)
HRSL	Smith et al. (2019), Tellman et al. (2021), Bernhofen et al. (2021) Lindersson et al. (2021)
HYDE	Jongman et al. (2012), Tanoue et al. (2016)
LandScan	Ward et al. (2013), Winsemius et al. (2013), Smith et al. (2019)
WorldPop	Trigg et al. (2016), Smith et al. (2019), Eilander et al. (2020), Dryden et al. (2021), Bernhofen et al. (2021), Lindersson et al. (2021)
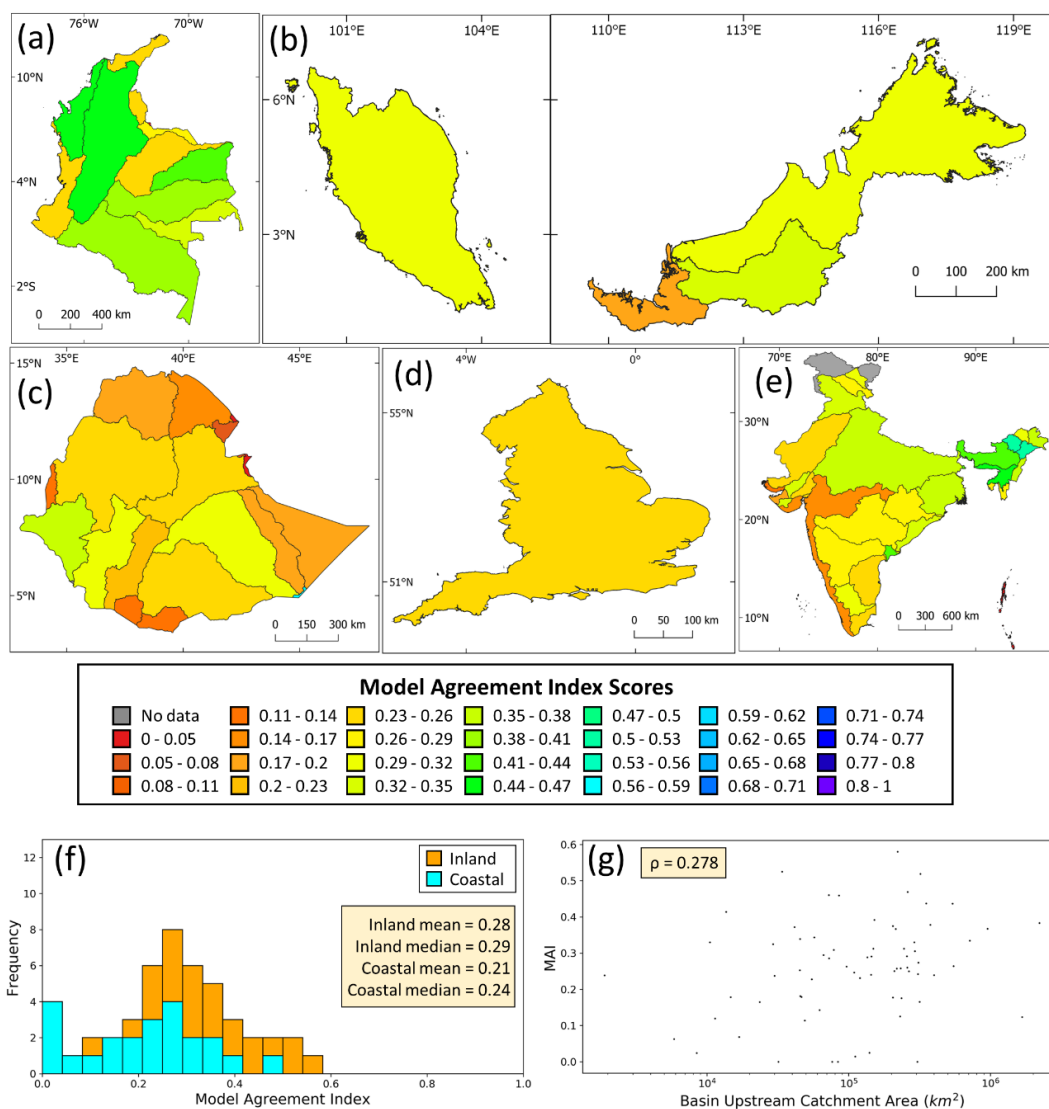
Figure C.1 HydroAtlas Basin Level 4 Model Agreement Index (MAI) scores for (a) Colombia (b) Malaysia (c) Ethiopia (d) England (e) India. (f) Histogram of coastal and inland basin Model Agreement (g) Scatterplot of MAI scores vs. catchment area upstream of the basin with calculated Spearman's Rank coefficient (ρ)
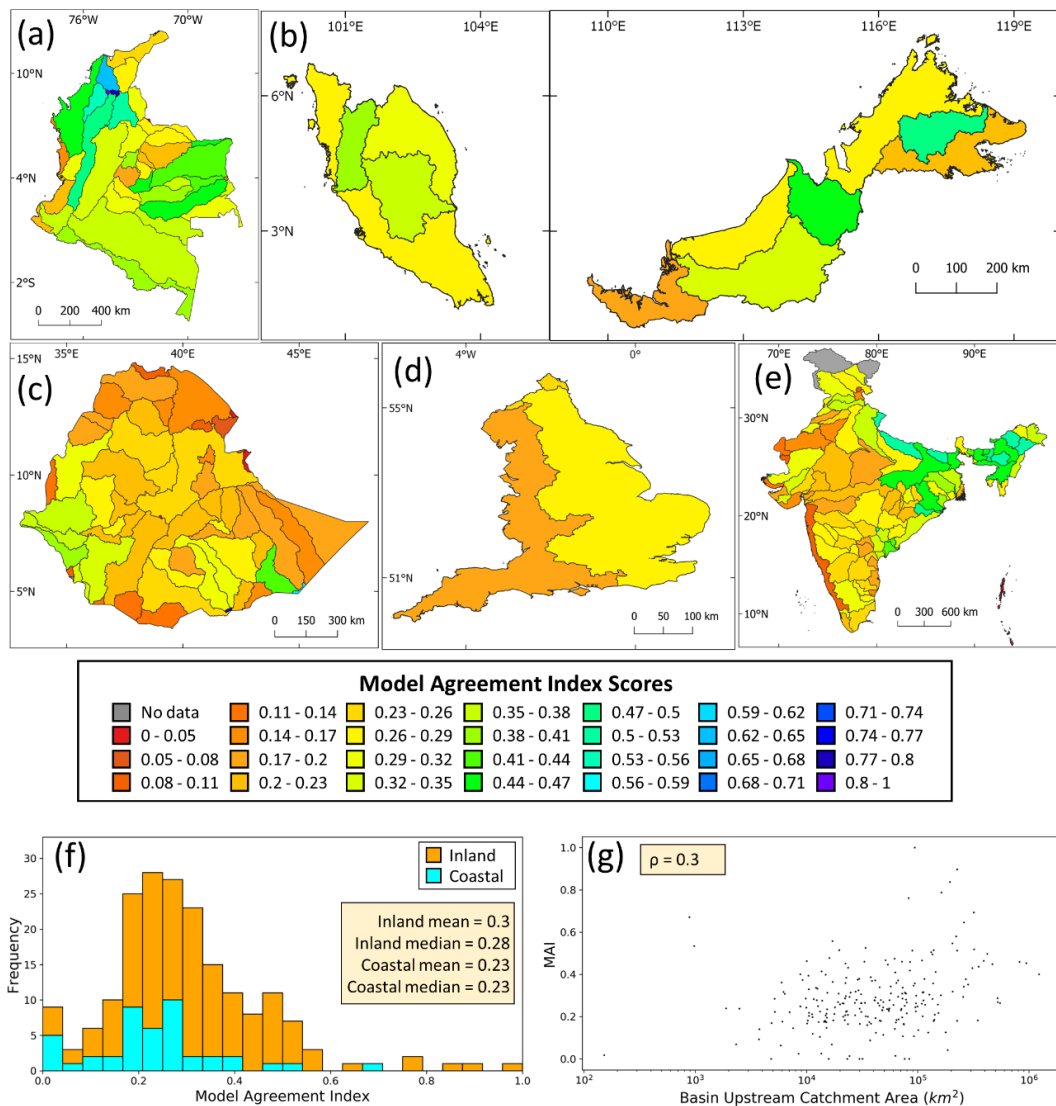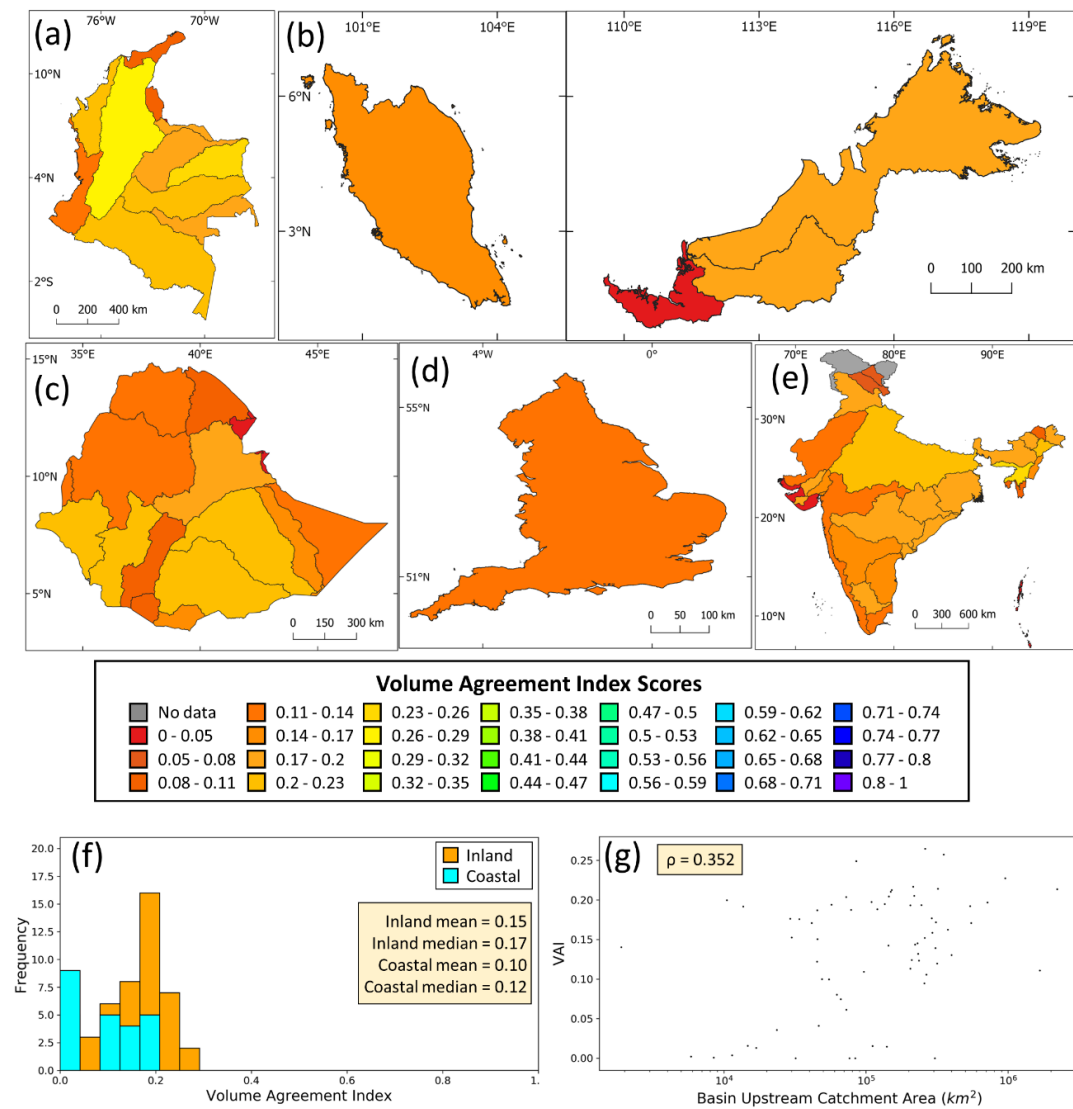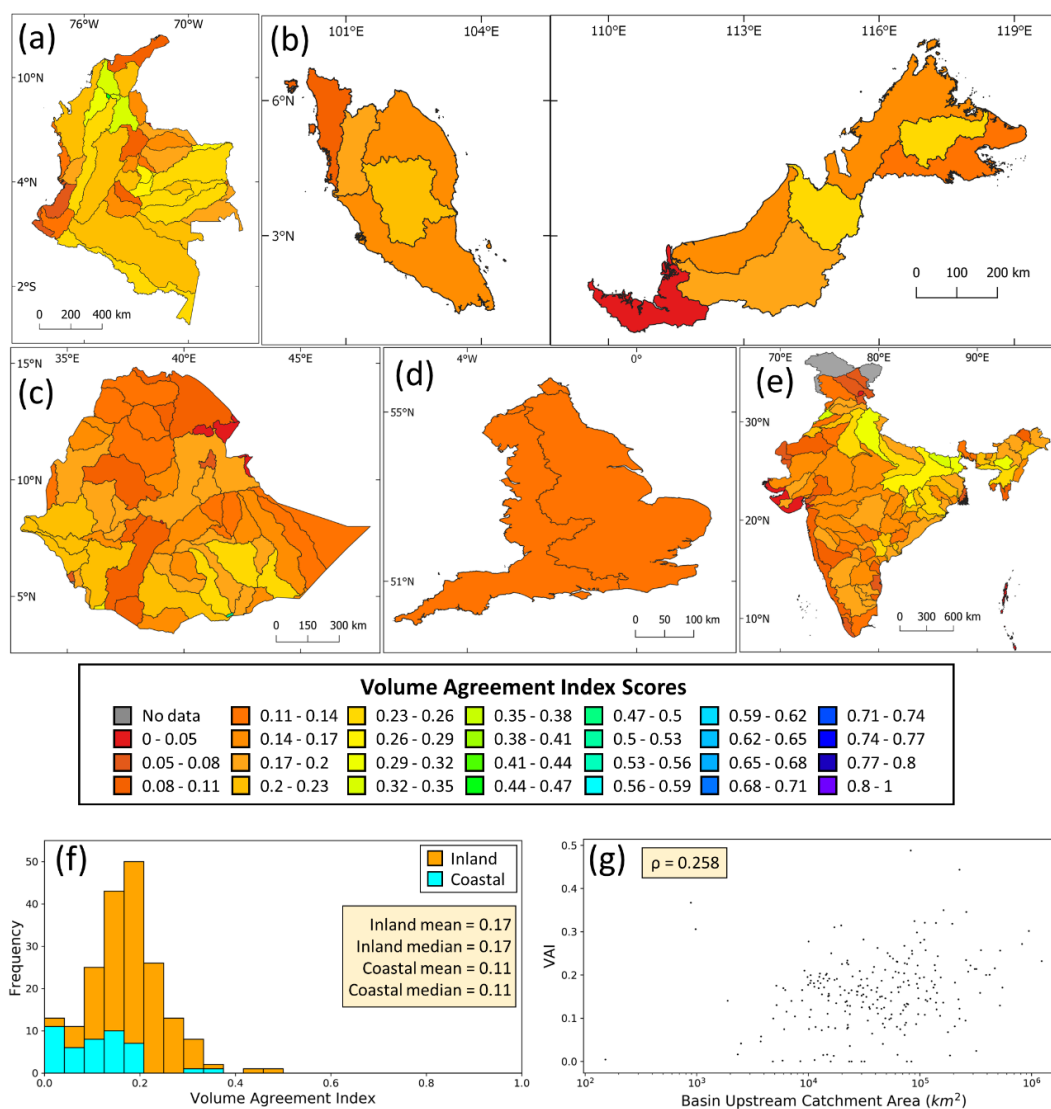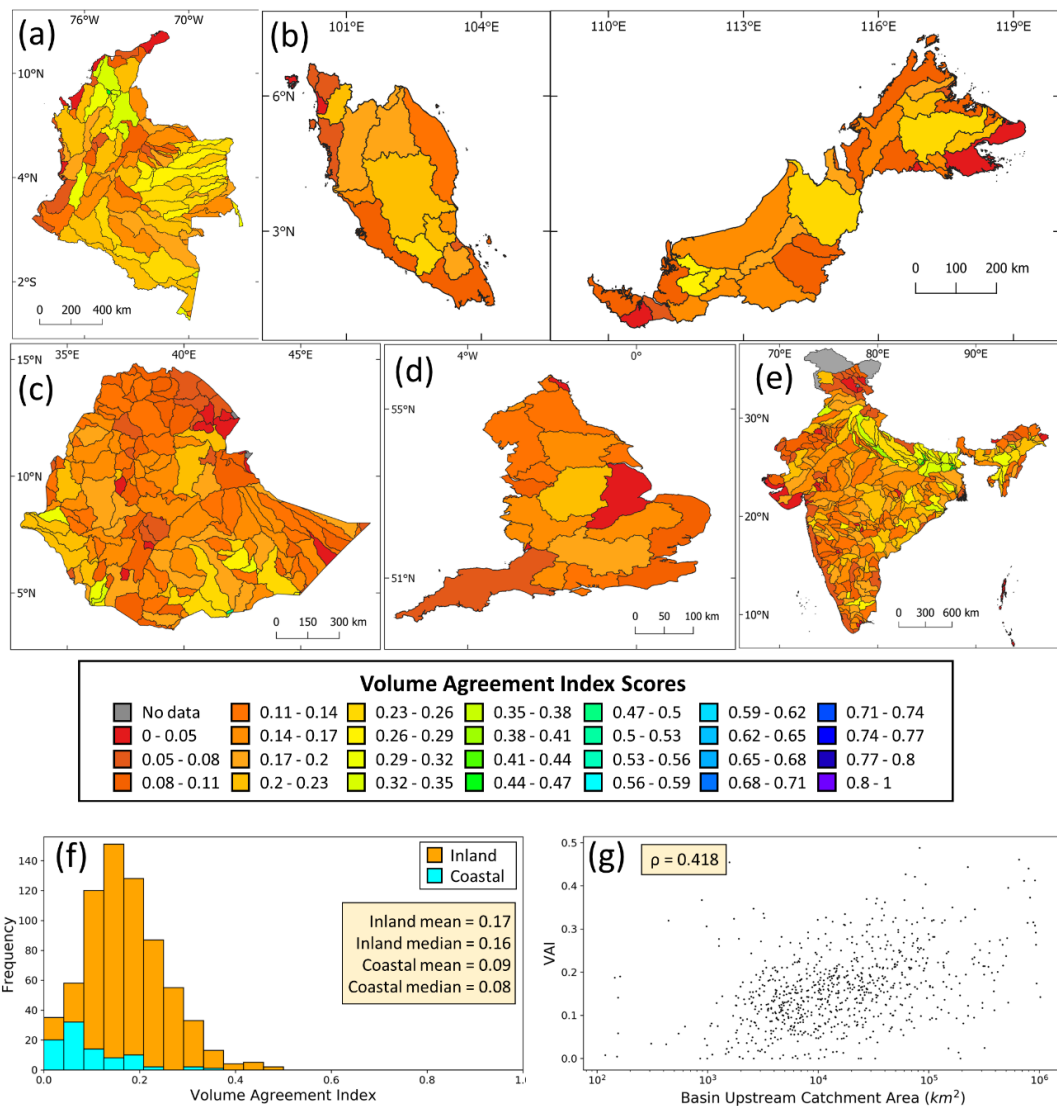
Figure C.2 HydroAtlas Basin Level 5 Model Agreement Index (MAI) scores for (a) Colombia (b) Malaysia (c) Ethiopia (d) England (e) India. (f) Histogram of coastal and inland basin Model Agreement (g) Scatterplot of MAI scores vs. catchment area upstream of the basin with calculated Spearman's Rank coefficient (ρ)
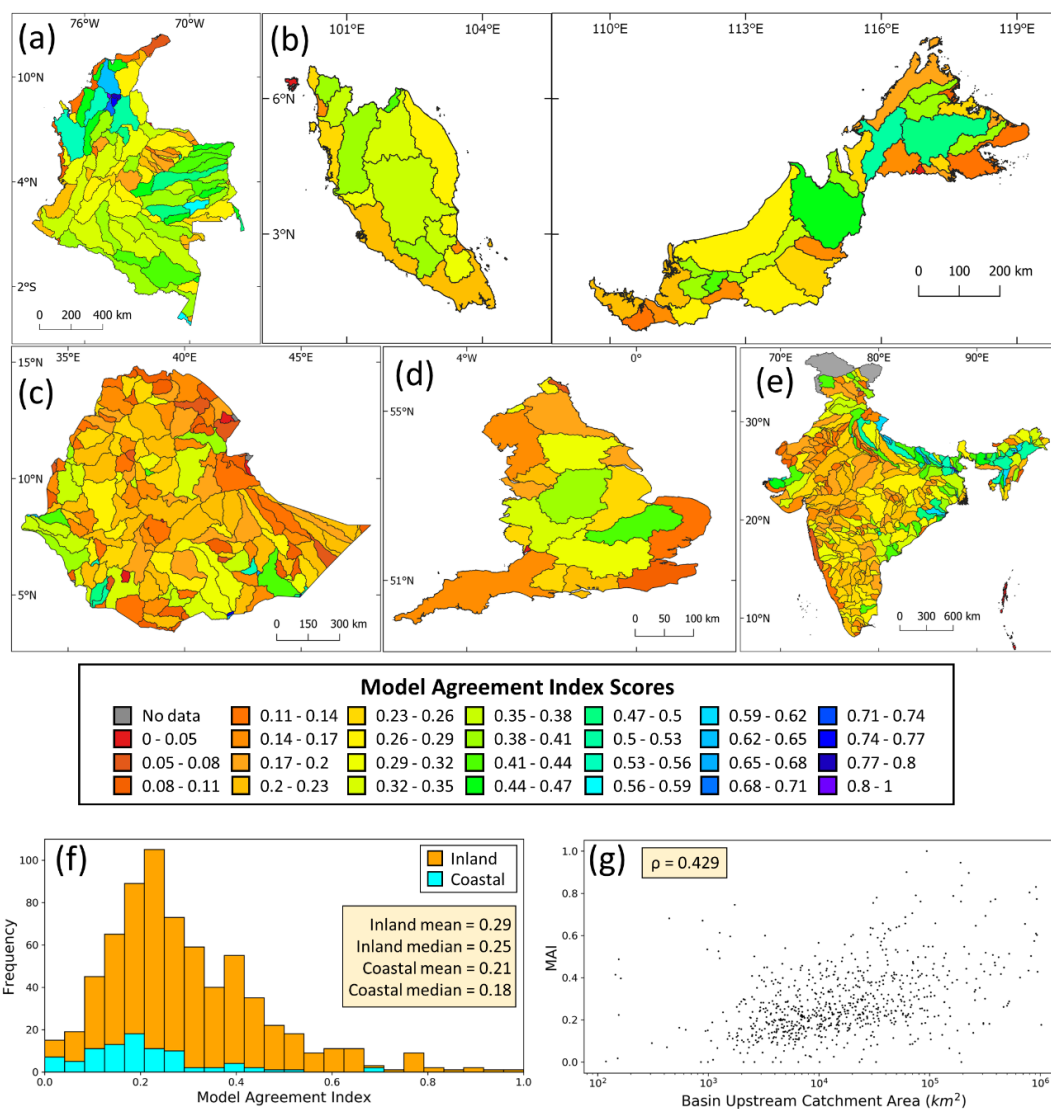
Figure C.3 HydroAtlas Basin Level 6 Model Agreement Index (MAI) scores for (a)
Colombia (b) Malaysia (c) Ethiopia (d) England (e) India. (f) Histogram of
coastal and inland basin Model Agreement (g) Scatterplot of MAI scores vs.
catchment area upstream of the basin with calculated Spearman's Rank
coefficient (ρ)

Figure C.4 HydroAtlas Basin Level 4 Volume Agreement Index (VAI) scores for (a) Colombia (b) Malaysia (c) Ethiopia (d) England (e) India. (f) Histogram of coastal and inland basin Model Agreement (g) Scatterplot of VAI scores vs. catchment area upstream of the basin with calculated Spearman's Rank coefficient (ρ)

Figure C.5 HydroAtlas Basin Level 5 Volume Agreement Index (VAI) scores for
(a) Colombia (b) Malaysia (c) Ethiopia (d) England (e) India. (f) Histogram of
coastal and inland basin Model Agreement (g) Scatterplot of VAI scores vs.
catchment area upstream of the basin with calculated Spearman's Rank
coefficient (ρ)

Figure C.6 HydroAtlas Basin Level 6 Volume Agreement Index (VAI) scores for (a) Colombia (b) Malaysia (c) Ethiopia (d) England (e) India. (f) Histogram of coastal and inland basin Model Agreement (g) Scatterplot of VAI scores vs. catchment area upstream of the basin with calculated Spearman's Rank coefficient (ρ)
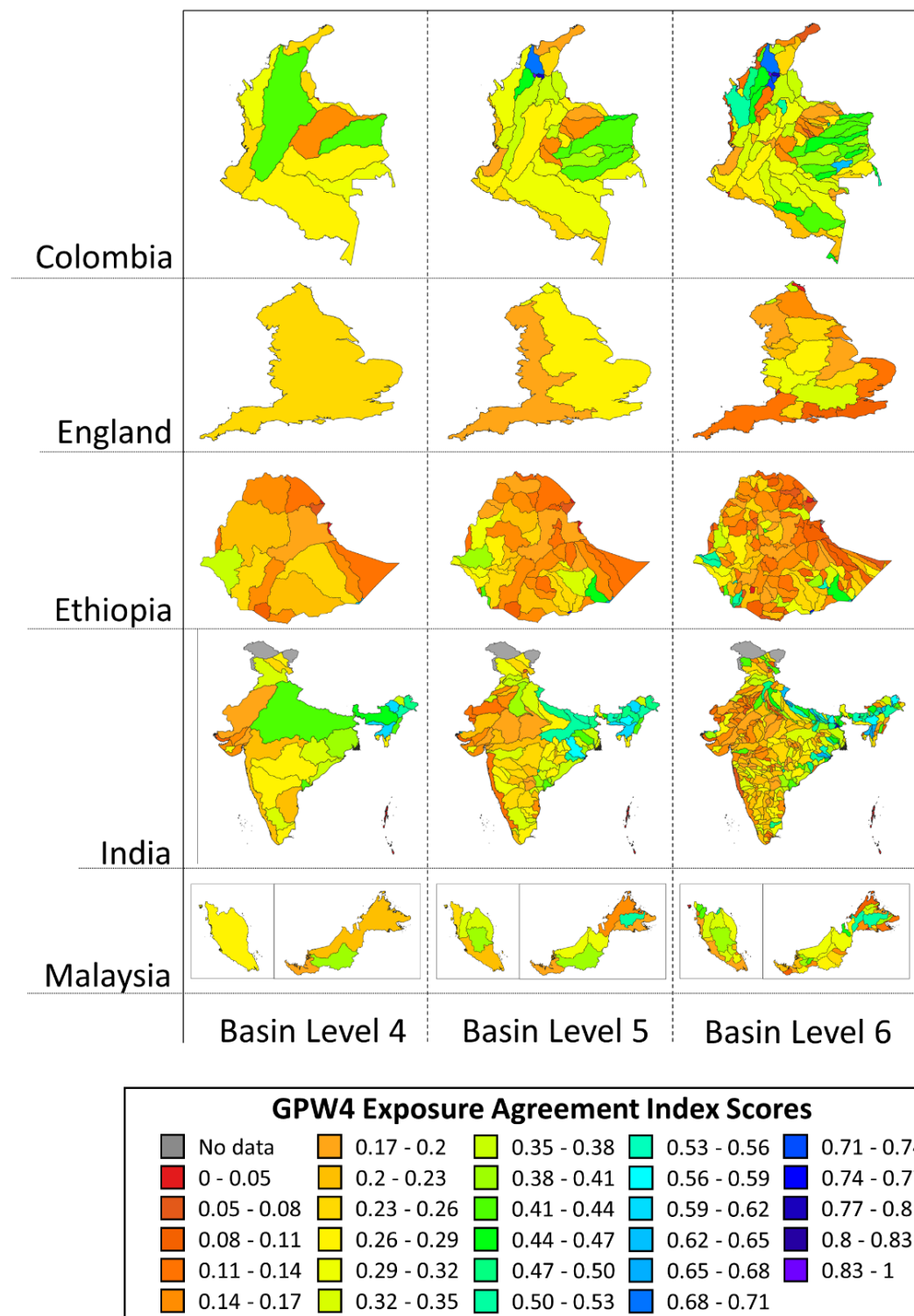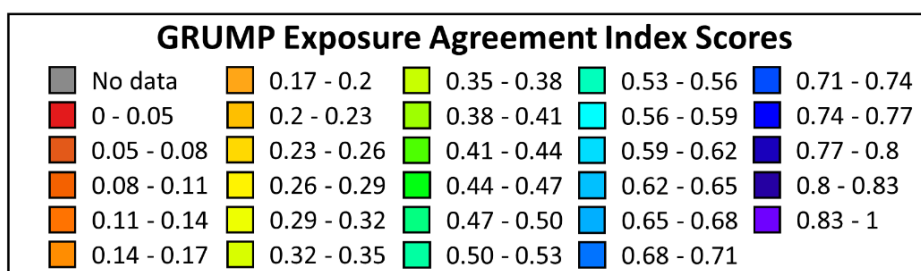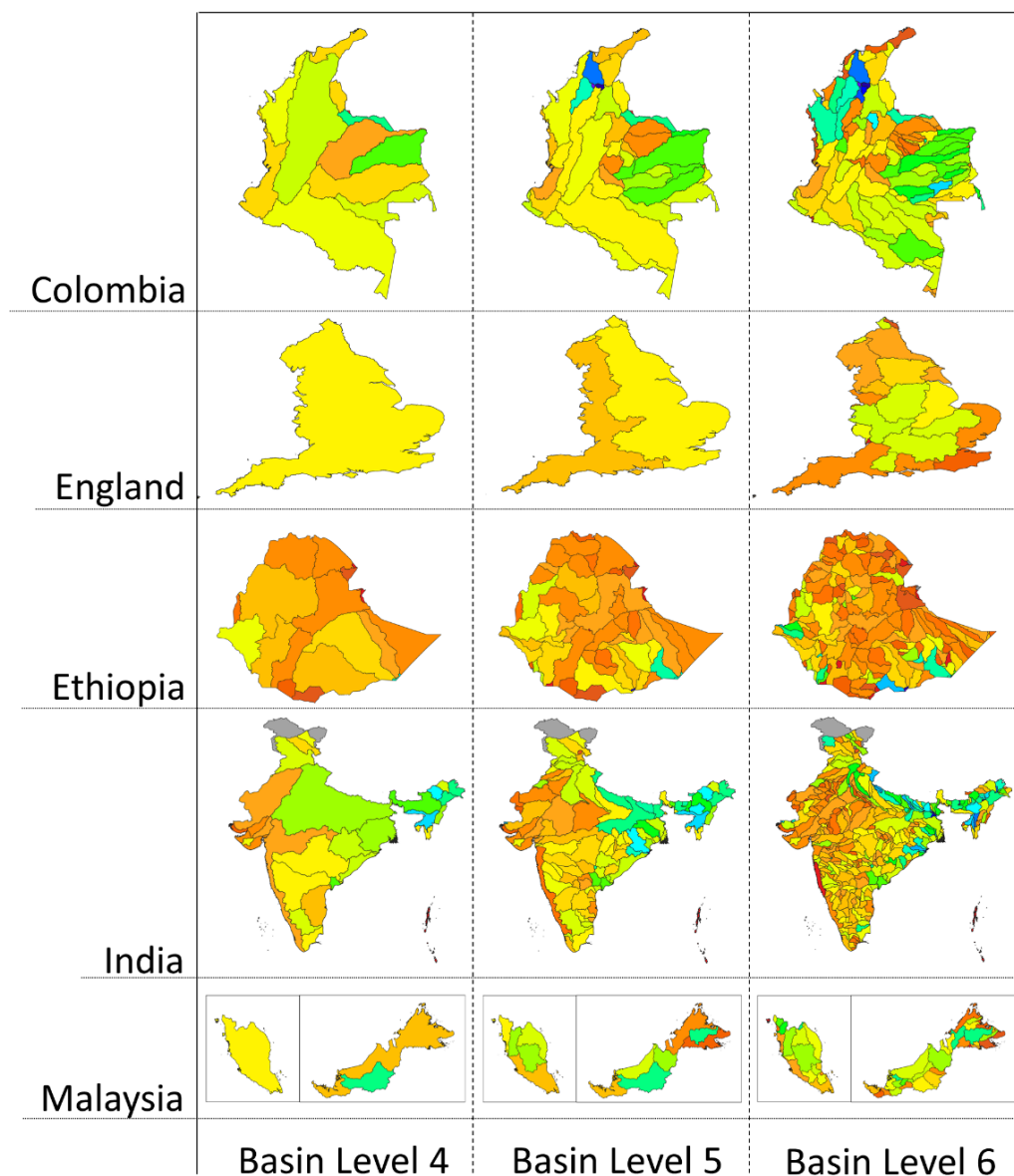
Figure C.7 Basin level GPW4 exposure agreement index scores for HydroAtlas
     basin levels 4-6.
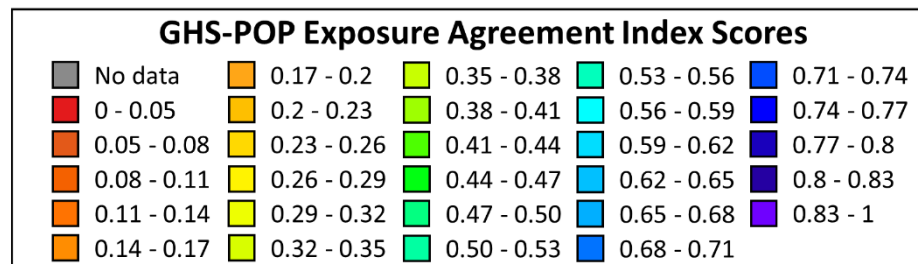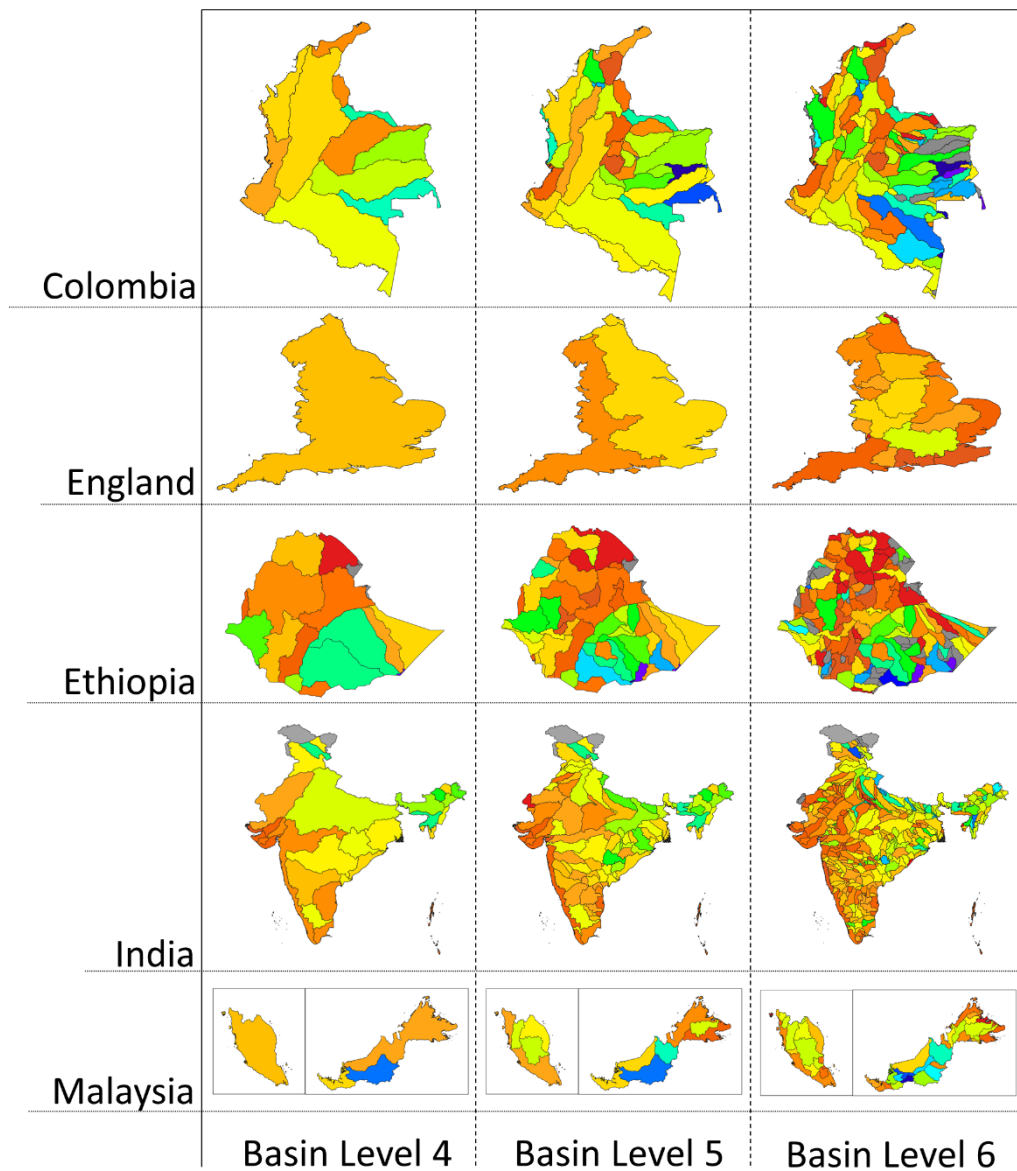
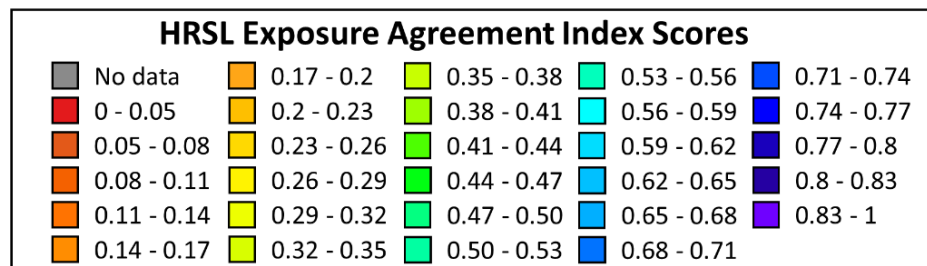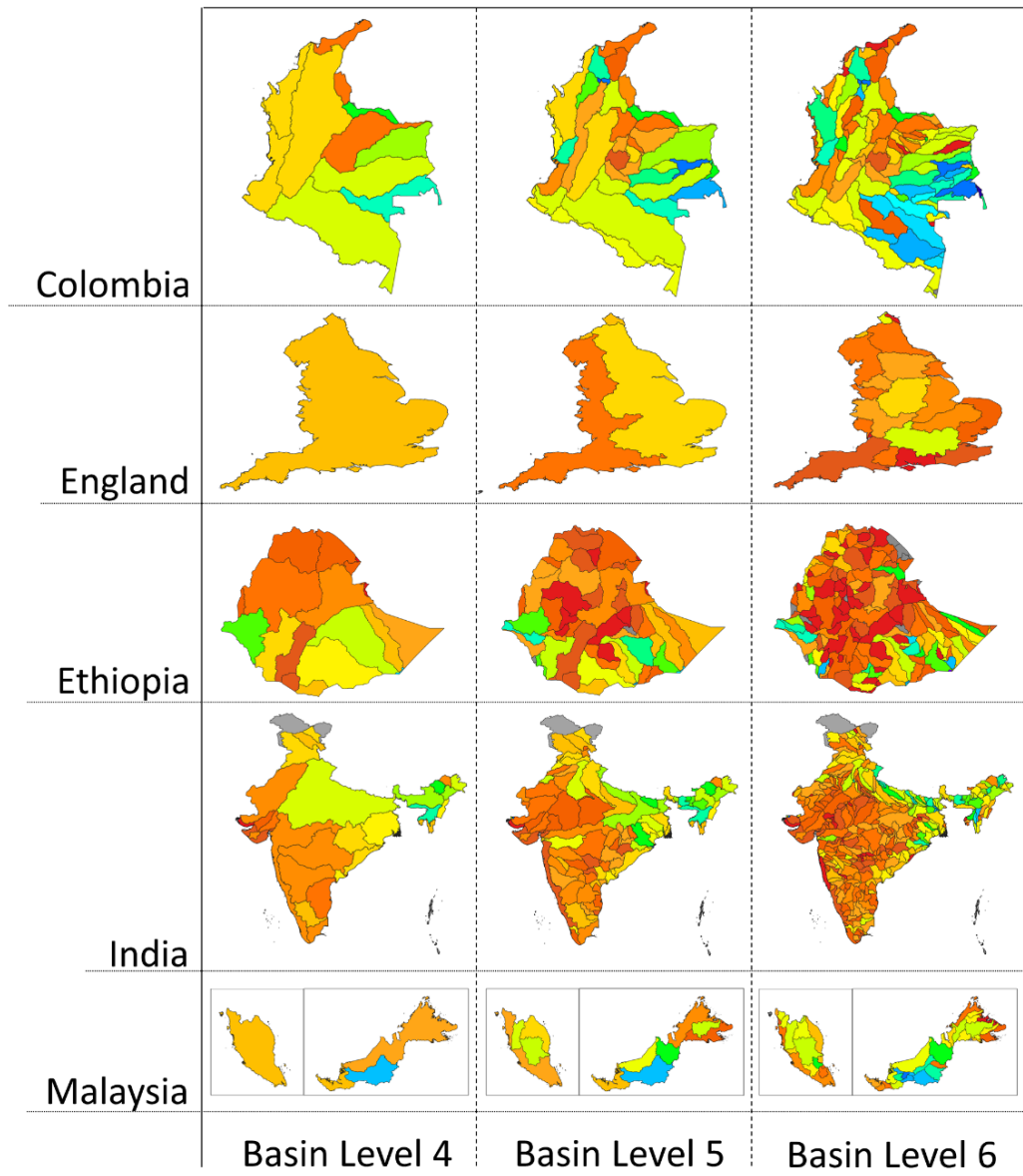**Figure C.8** Basin level GHS-POP exposure agreement index scores for HydroAtlas basin levels 4-6.

GRUMP Exposure Agreement Index Scores

No data	0.17 - 0.2	0.35 - 0.38	0.53 - 0.56	0.71 - 0.74
0 - 0.05	0.2 - 0.23	0.38 - 0.41	0.56 - 0.59	0.74 - 0.77
0.05 - 0.08	0.23 - 0.26	0.41 - 0.44	0.59 - 0.62	0.77 - 0.8
0.08 - 0.11	0.26 - 0.29	0.44 - 0.47	0.62 - 0.65	0.8 - 0.83
0.11 - 0.14	0.29 - 0.32	0.47 - 0.50	0.65 - 0.68	0.83 - 1
0.14 - 0.17	0.32 - 0.35	0.50 - 0.53	0.68 - 0.71	

Figure C.9 Basin level GRUMP exposure agreement index scores for HydroAtlas basin levels 4-6.

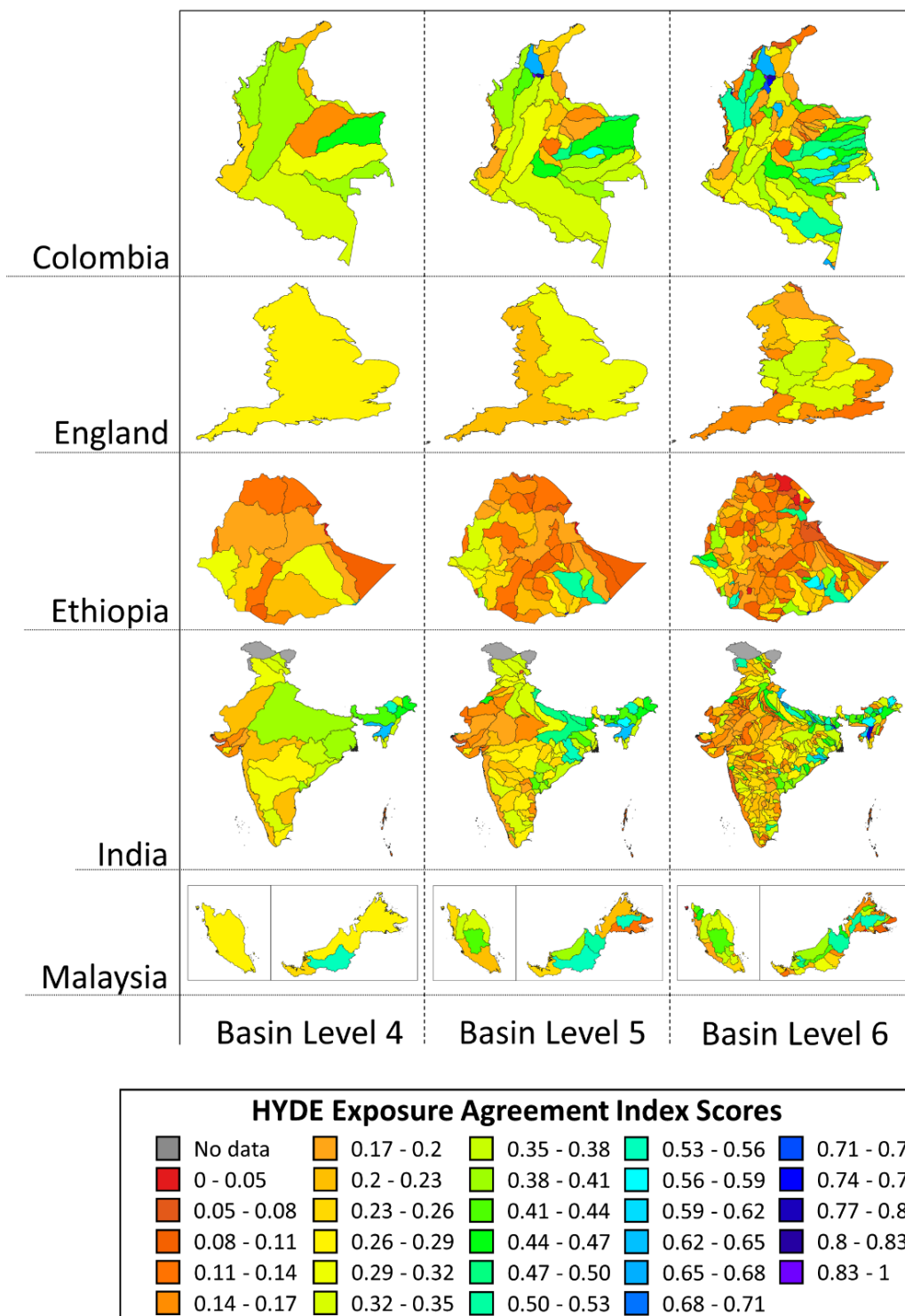**Figure C.10** Basin level HRSL exposure agreement index scores for HydroAtlas basin levels 4-6.

Figure C.11 Basin level HYDE exposure agreement index scores for HydroAtlas basin levels 4-6.
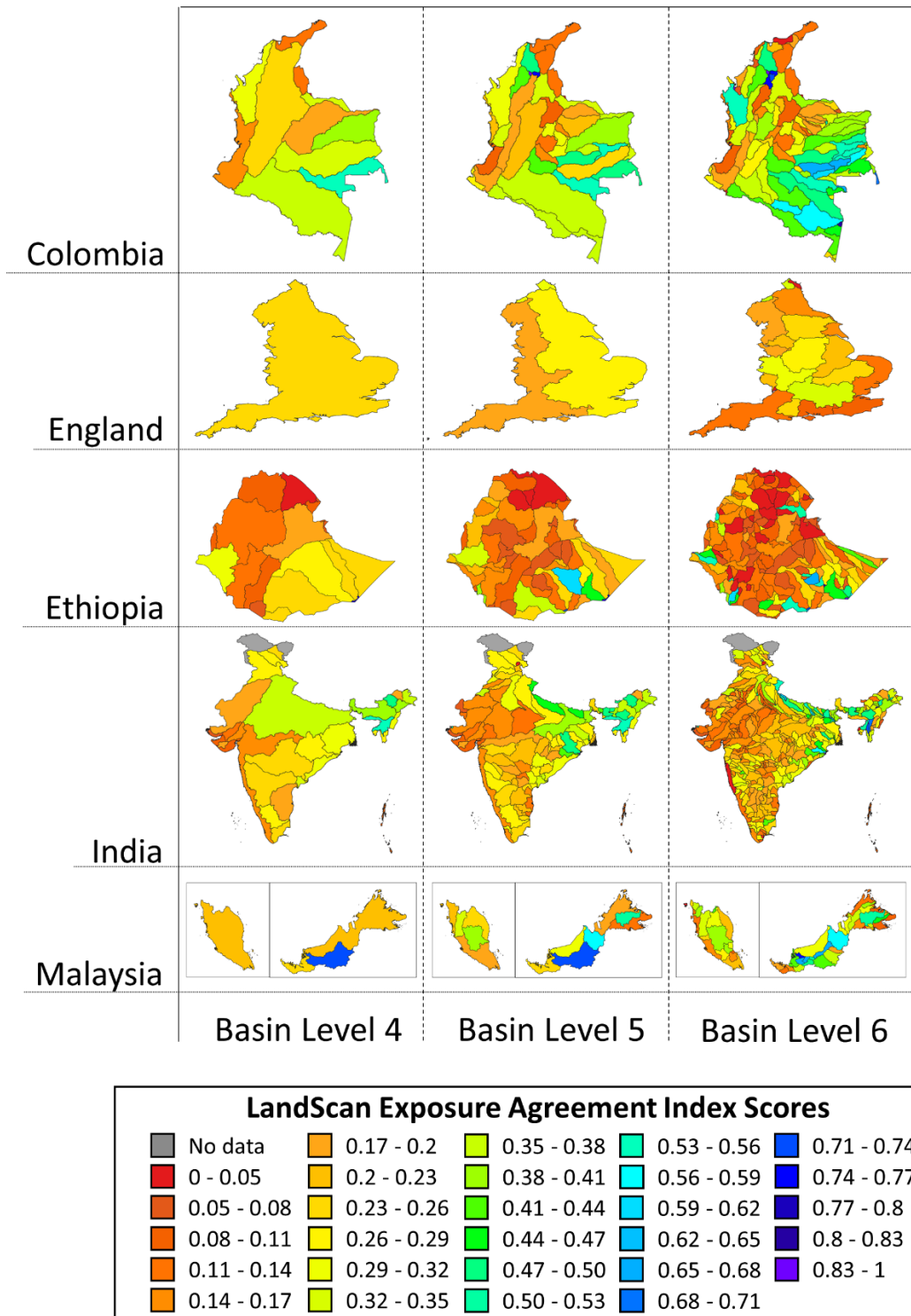
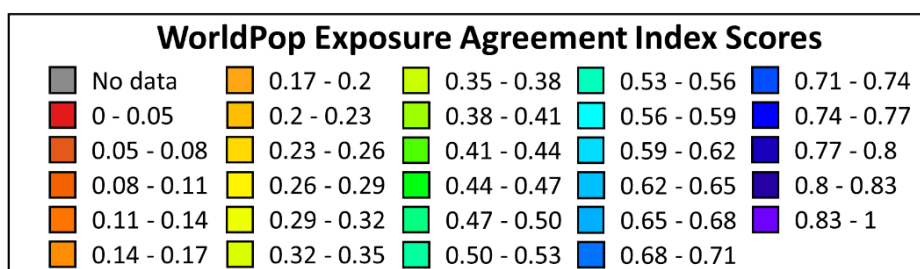**Figure C.12** Basin level LandScan exposure agreement index scores for HydroAtlas basin levels 4-6.
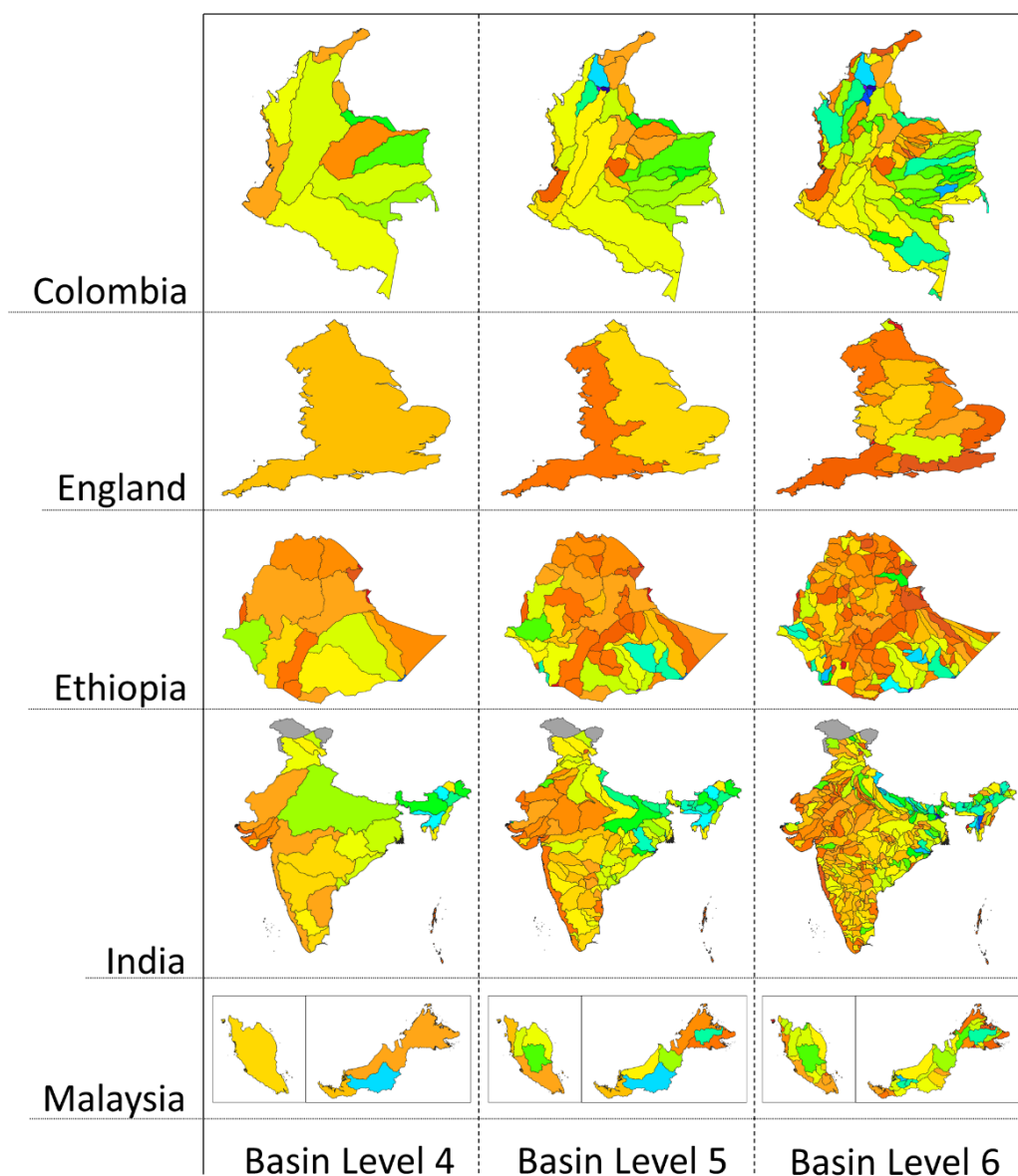
Figure C.13 Basin level WorldPop exposure agreement index scores for HydroAtlas basin levels 4-6.
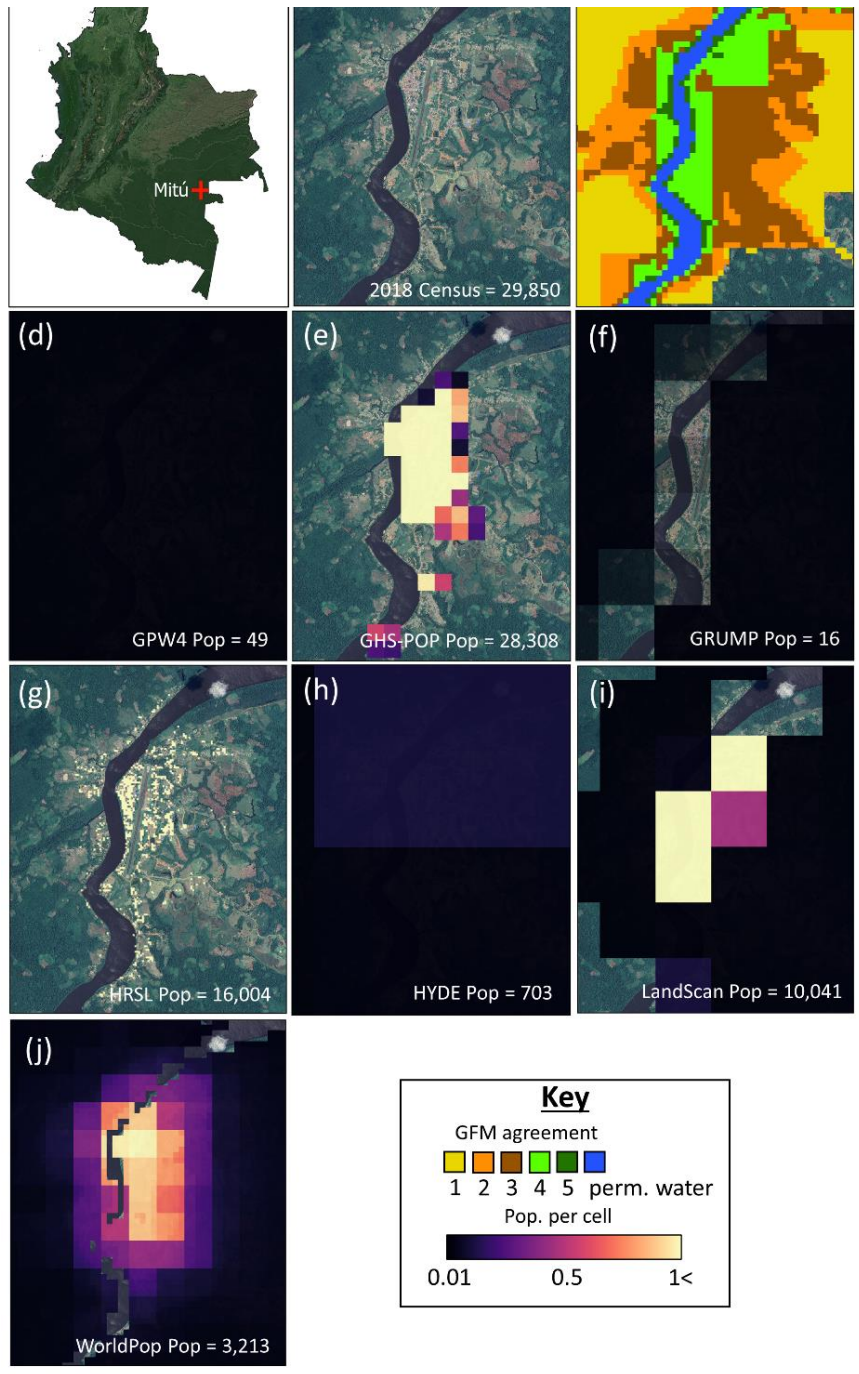
Figure C.14 Comparison of global population datasets in the town of Mitú,
   Colombia

(a) Location of Mitú in Colombia. (b) Satellite image of Mitú and offical 2018
census population total. (c) Aggregated GFM flood map in Mitú. (d) GPW4
Mitú population distribution. (e) GHS-POP Mitú population distribution. (f)
GRUMP Mitú population distribution. (g) HRSL Mitú population distribution.
(h) HYDE Mitú population distribution. (i) LandScan Mitú population
distribution. (j) WorldPop Mitú population distribution. All global population
datasets resampled to 1 arcsecond for comparison. All dataset's total national
populations scaled to WorldPop 2020 total national population for comparison.
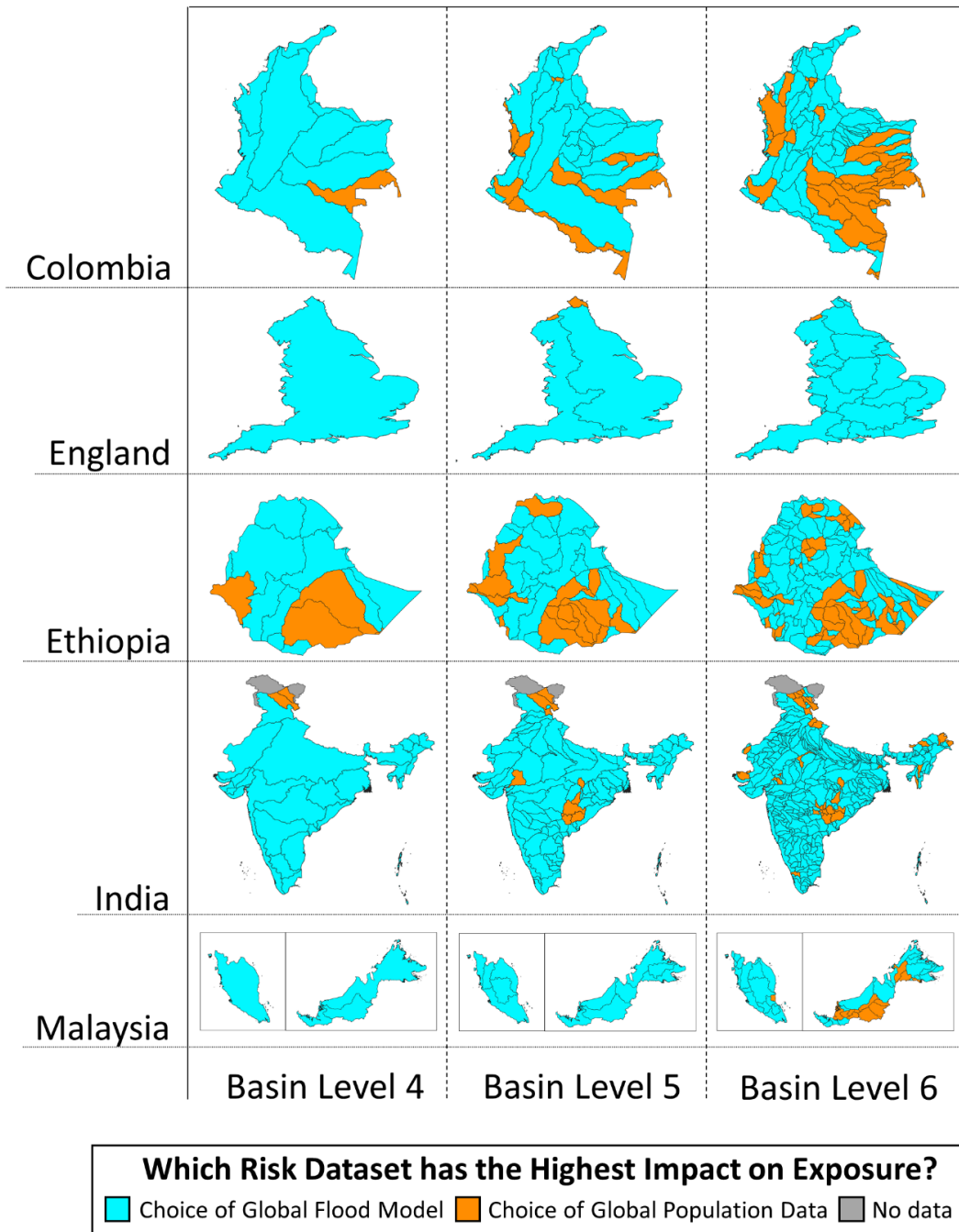Map data: © Google, Maxar Technologies 2021.

Figure C.15 Which dataset has the largest influence on exposure estimates at the basin level (HydroAtlas basins level 4-6)?

Calculated by comparing the average coefficient of variation for exposure estimates when the choice of GFM is held constant to the average coefficient of variation for exposure estimates when the choice of global population dataset is held constant.

References

AERTS, J. P. M., UHLEMANN-ELMER, S., EILANDER, D. & WARD, P. J. 2020. Comparison of estimates of global flood models for flood hazard and exposed gross domestic product: a China case study. *Nat. Hazards Earth Syst. Sci.,* 20**,** 3245-3260.

ALFIERI, L., BISSELINK, B., DOTTORI, F., NAUMANN, G., DE ROO, A., SALAMON, P., WYSER, K. & FEYEN, L. 2017. Global projections of river flood risk in a warmer world. *Earths Future,* 5**,** 171-182.

ALFIERI, L., BUREK, P., DUTRA, E., KRZEMINSKI, B., MURARO, D., THIELEN, J. & PAPPENBERGER, F. 2013. GloFAS - global ensemble streamflow forecasting and flood early warning. *Hydrol. Earth Syst. Sci.,* 17**,** 1161-1175.

ARNELL, N. W. & GOSLING, S. N. 2016. The impacts of climate change on river flood risk at the global scale. *Climatic Change,* 134**,** 387-401.

BALK, D., POZZI, F., YETMAN, G., DEICHMANN, U. & NELSONC, A. 2005. The distribution of people and the dimension of place: Methodologies to improve the global estimation of urban extents. *International Society for Photogrammetry and Remote Sensing, Proceedings of the Urban Remote Sensing Conference.*

BALK, D. L., DEICHMANN, U., YETMAN, G., POZZI, F., HAY, S. I. & NELSON, A. 2006. Determining Global Population Distribution: Methods, Applications and Data. *In:* HAY, S. I., GRAHAM, A. & ROGERS, D. J. (eds.) *Advances in Parasitology.* Academic Press.

BALSAMO, G., ALBERGEL, C., BELJAARS, A., BOUSSETTA, S., BRUN, E., CLOKE, H., DEE, D., DUTRA, E., MUÑOZ-SABATER, J., PAPPENBERGER, F., DE ROSNAY, P., STOCKDALE, T. & VITART, F. 2015. ERA-Interim/Land: a global land surface reanalysis data set. *Hydrol. Earth Syst. Sci.,* 19**,** 389-407.

BALSAMO, G., BELJAARS, A., SCIPAL, K., VITERBO, P., VAN DEN HURK, B., HIRSCHI, M. & BETTS, A. K. 2009. A Revised Hydrology for the ECMWF Model: Verification from Field Site to Terrestrial Water Storage and Impact in the Integrated Forecast System %J Journal of Hydrometeorology. 10**,** 623-643.

BATES, P. D., HORRITT, M. S. & FEWTRELL, T. J. 2010. A simple inertial formulation of the shallow water equations for efficient two-dimensional flood inundation modelling. *Journal of Hydrology,* 387**,** 33-45.

BERNHOFEN, M. V., TRIGG, M. A., SLEIGH, P. A., SAMPSON, C. C. & SMITH, A. M. 2021. Global Flood Exposure from Different Sized Rivers. *Nat. Hazards Earth Syst. Sci. Discuss.,* 2021**,** 1-25.

DEE, D. P., UPPALA, S. M., SIMMONS, A. J., BERRISFORD, P., POLI, P., KOBAYASHI, S., ANDRAE, U., BALMASEDA, M. A., BALSAMO, G., BAUER, P., BECHTOLD, P., BELJAARS, A. C. M., VAN DE BERG, L., BIDLOT, J., BORMANN, N., DELSOL, C., DRAGANI, R., FUENTES, M., GEER, A. J., HAIMBERGER, L., HEALY, S. B., HERSBACH, H., HÓLM, E. V., ISAKSEN, L., KÅLLBERG, P., KÖHLER, M., MATRICARDI, M., MCNALLY, A. P., MONGE-SANZ, B. M., MORCRETTE, J.-J., PARK, B.-K., PEUBEY, C., DE ROSNAY, P., TAVOLATO, C., THÉPAUT, J.-N. &

VITART, F. 2011. The ERA-Interim reanalysis: configuration and performance of the data assimilation system. 137, 553-597.

DOTTORI, F., SALAMON, P., BIANCHI, A., ALFIERI, L., HIRPA, F. A. & FEYEN, L. 2016. Development and evaluation of a framework for global flood hazard mapping. *Advances in Water Resources,* 94, 87-102.

DOTTORI, F., SZEWCZYK, W., CISCAR, J. C., ZHAO, F., ALFIERI, L., HIRABAYASHI, Y., BIANCHI, A., MONGELLI, I., FRIELER, K., BETTS, R. A. & FEYEN, L. 2018. Increased human and economic losses from river flooding with anthropogenic warming. *Nature Climate Change,* 8, 781-+.

DOTTORI, F. & TODINI, E. 2011. Developments of a flood inundation model based on the cellular automata approach: Testing different methods to improve model performance. *Physics and Chemistry of the Earth, Parts A/B/C,* 36, 266-280.

DOXSEY-WHITFIELD, E., MACMANUS, K., ADAMO, S. B., PISTOLESI, L., SQUIRES, J., BORKOVSKA, O. & BAPTISTA, S. R. 2015. Taking Advantage of the Improved Availability of Census Data: A First Look at the Gridded Population of the World, Version 4. *Papers in Applied Geography,* 1, 226-234.

DRYDEN, R., ANAND, M., LEHNER, B. & FLUET-CHOUINARD, E. 2021. Do we prioritize floodplains for development and farming? Mapping global dependence and exposure to inundation. *Global Environmental Change,* 71, 102370.

EILANDER, D., COUASNON, A., IKEUCHI, H., MUIS, S., YAMAZAKI, D., WINSEMIUS, H. C. & WARD, P. J. 2020. The effect of surge on riverine flood hazard and impact in deltas globally. *Environmental Research Letters,* 15, 104007.

ELVIDGE, C., BAUGH, K., HOBSON, V., KIHN, E., KROEHL, H., DAVIS, E. & COCERO, D. 1997. Satellite inventory of human settlements using nocturnal radiation emissions: a contribution for the global toolchest. 3, 387-395.

FREIRE, S., KEMPER, T., PESARESI, M., FLORCZYK, A. & SYRRIS, V. Combining GHSL and GPW to improve global population mapping. 2015 IEEE International Geoscience and Remote Sensing Symposium (IGARSS), 26-31 July 2015 2015. 2541-2543.

FREIRE, S., MACMANUS, K., PESARESI, M., DOXSEY-WHITFIELD, E. & MILLS, J. 2016. *Development of new open and free multi-temporal global population grids at 250 m resolution.*

FREIRE, S., SCHIAVINA, M., FLORCZYK, A. J., MACMANUS, K., PESARESI, M., CORBANE, C., BORKOVSKA, O., MILLS, J., PISTOLESI, L., SQUIRES, J. & SLIUZAS, R. 2020. Enhanced data and methods for improving open and free global population grids: putting 'leaving no one behind' into practice. *International Journal of Digital Earth,* 13, 61-77.

GU, X., ZHANG, Q., LI, J., CHEN, D., SINGH, V. P., ZHANG, Y., LIU, J., SHEN, Z. & YU, H. 2020. Impacts of anthropogenic warming and uneven regional socio-economic development on global river flood risk. *Journal of Hydrology,* 590, 125262.

HAZELEGER, W., WANG, X., SEVERIJNS, C., ŞTEFĂNESCU, S., BINTANJA, R., STERL, A., WYSER, K., SEMMLER, T., YANG, S., VAN DEN HURK, B., VAN NOIJE, T., VAN DER LINDEN, E. & VAN DER WIEL, K. 2012. EC-Earth V2.2: description and validation of a new seamless earth system prediction model. *Climate Dynamics,* 39, 2611-2629.

HIRABAYASHI, Y., MAHENDRAN, R., KOIRALA, S., KONOSHIMA, L., YAMAZAKI, D., WATANABE, S., KIM, H. & KANAE, S. 2013. Global flood risk under climate change. *Nature Climate Change,* 3**,** 816-821.

HIRABAYASHI, Y., TANOUE, M., SASAKI, O., ZHOU, X. & YAMAZAKI, D. 2021. Global exposure to flooding from the new CMIP6 climate model projections. *Scientific Reports,* 11**,** 3740.

JONGMAN, B., WARD, P. J. & AERTS, J. 2012. Global exposure to river and coastal flooding: Long term trends and changes. *Global Environmental Change-Human and Policy Dimensions,* 22**,** 823-835.

KETTNER, A. J., BRAKENRIDGE, G. R., SCHUMANN, G. J. P. & SHEN, X. 2021. Chapter 7 - DFO—Flood Observatory. *In:* SCHUMANN, G. J. P. (ed.) *Earth Observation for Flood Applications.* Elsevier.

KLEIN GOLDEWIJK, K., BEUSEN, A., DOELMAN, J. & STEHFEST, E. 2017. Anthropogenic land use estimates for the Holocene – HYDE 3.2. *Earth Syst. Sci. Data,* 9**,** 927-953.

KLEIN GOLDEWIJK, K., BEUSEN, A. & JANSSEN, P. 2010. Long-term dynamic modeling of global population and built-up area in a spatially explicit way: HYDE 3.1. 20**,** 565-573.

LEHNER, B. & GRILL, G. 2013. Global river hydrography and network routing: baseline data and new approaches to study the world's large river systems. Hydrological Processes.

LEHNER, B., VERDIN, K. & JARVIS, A. 2008. New Global Hydrography Derived From Spaceborne Elevation Data. *Eos, Transactions American Geophysical Union,* 89**,** 93-94.

LEYK, S., GAUGHAN, A. E., ADAMO, S. B., DE SHERBININ, A., BALK, D., FREIRE, S., ROSE, A., STEVENS, F. R., BLANKESPOOR, B., FRYE, C., COMENETZ, J., SORICHETTA, A., MACMANUS, K., PISTOLESI, L., LEVY, M., TATEM, A. J. & PESARESI, M. 2019. The spatial allocation of population: a review of large-scale gridded population data products and their fitness for use. *Earth Syst. Sci. Data,* 11**,** 1385-1409.

LINDERSSON, S., BRANDIMARTE, L., MÅRD, J. & DI BALDASSARRE, G. 2021. Global riverine flood risk – how do hydrogeomorphic floodplain maps compare to flood hazard maps? *Nat. Hazards Earth Syst. Sci.,* 21**,** 2921-2948.

LLOYD, C. T., CHAMBERLAIN, H., KERR, D., YETMAN, G., PISTOLESI, L., STEVENS, F. R., GAUGHAN, A. E., NIEVES, J. J., HORNBY, G., MACMANUS, K., SINHA, P., BONDARENKO, M., SORICHETTA, A. & TATEM, A. J. 2019. Global spatio-temporally harmonised datasets for producing high-resolution gridded population distribution datasets. *Big Earth Data,* 3**,** 108-139.

NEAL, J., HAWKER, L., SAVAGE, J., DURAND, M., BATES, P. & SAMPSON, C. 2021. Estimating River Channel Bathymetry in Large Scale Flood Inundation Models. 57**,** e2020WR028301.

NEAL, J., SCHUMANN, G. & BATES, P. 2012. A subgrid channel model for simulating river hydraulics and floodplain inundation over large and data sparse areas. *Water Resources Research,* 48**,** 16.

PESARESI, M., EHRLICH, D., FLORCZYK, A. J., FREIRE, S., JULEA, A., KEMPER, T. & SYRRIS, V. The global human settlement layer from landsat imagery. 2016 IEEE International Geoscience and Remote Sensing Symposium (IGARSS), 10-15 July 2016 2016. 7276-7279.

PESARESI, M., HUADONG, G., BLAES, X., EHRLICH, D., FERRI, S., GUEGUEN, L., HALKIA, M., KAUFFMANN, M., KEMPER, T., LU, L., MARIN-HERRERA, M. A., OUZOUNIS, G. K., SCAVAZZON, M., SOILLE, P., SYRRIS, V. & ZANCHETTA, L. 2013. A Global Human Settlement Layer From Optical HR/VHR RS Data: Concept and First Results. *IEEE Journal of Selected Topics in Applied Earth Observations and Remote Sensing,* 6**,** 2102-2131.

RENTSCHLER, J. & SALHAB, M. 2020. People in Harm's Way: Flood Exposure and Poverty in 189 Countries. *Policy Research Wokring Paper.* Washington, D.C.: World Bank.

RUDARI, R., SILVESTRO, F., CAMPO, L., REBORA, N., BONI, G. & HEROLD, C. 2015. IMPROVEMENT OF THE GLOBAL FLOOD MODEL FOR THE GAR 2015.

SAMPSON, C. C., SMITH, A. M., BATES, P. B., NEAL, J. C., ALFIERI, L. & FREER, J. E. 2015. A high-resolution global flood hazard model. *Water Resources Research,* 51**,** 7358-7381.

SCHELLEKENS, J., DUTRA, E., MARTINEZ-DE LA TORRE, A., BALSAMO, G., VAN DIJK, A., WEILAND, F. S., MINVIELLE, M., CALVET, J. C., DECHARME, B., EISNER, S., FINK, G., FLORKE, M., PESSENTEINER, S., VAN BEEK, R., POLCHER, J., BECK, H., ORTH, R., CALTON, B., BURKE, S., DORIGO, W. & WEEDON, G. P. 2017. A global water resources ensemble of hydrological models: the eartH2Observe Tier-1 dataset. *Earth System Science Data,* 9**,** 389-413.

SILVESTRO, F., GABELLANI, S., DELOGU, F., RUDARI, R. & BONI, G. 2013. Exploiting remote sensing land surface temperature in distributed hydrological modelling: the example of the Continuum model. *Hydrol. Earth Syst. Sci.,* 17**,** 39-62.

SMITH, A., BATES, P. D., WING, O., SAMPSON, C., QUINN, N. & NEAL, J. 2019. New estimates of flood exposure in developing countries using high-resolution population data. *Nature Communications,* 10**,** 1814.

SMITH, A., SAMPSON, C. & BATES, P. 2015. Regional flood frequency analysis at the global scale. *Water Resources Research,* 51**,** 539-553.

STEVENS, F. R., GAUGHAN, A. E., LINARD, C. & TATEM, A. J. 2015. Disaggregating Census Data for Population Mapping Using Random Forests with Remotely-Sensed and Ancillary Data. *Plos One,* 10**,** 22.

SUTANUDJAJA, E. H., VAN BEEK, R., WANDERS, N., WADA, Y., BOSMANS, J. H. C., DROST, N., VAN DER ENT, R. J., DE GRAAF, I. E. M., HOCH, J. M., DE JONG, K., KARSSENBERG, D., LÓPEZ LÓPEZ, P., PEßENTEINER, S., SCHMITZ, O., STRAATSMA, M. W., VANNAMETEE, E., WISSER, D. & BIERKENS, M. F. P. 2018. PCR-GLOBWB 2: a 5 arcmin global hydrological and water resources model. *Geosci. Model Dev.,* 11**,** 2429-2453.

TANOUE, M., HIRABAYASHI, Y. & IKEUCHI, H. 2016. Global-scale river flood vulnerability in the last 50 years. *Scientific Reports,* 6**,** 36021.

TELLMAN, B., SULLIVAN, J. A., KUHN, C., KETTNER, A. J., DOYLE, C. S., BRAKENRIDGE, G. R., ERICKSON, T. A. & SLAYBACK, D. A. 2021. Satellite imaging reveals increased proportion of population exposed to floods. *Nature,* 596**,** 80-86.

TIECKE, T. G. L., XIANMING ZHANG, AMY GROS, ANDREAS LI, NAN YETMAN, GREGORY KILIC, TALIP MURRAY, SIOBHAN

BLANKESPOOR, BRIAN PRYDZ, ESPEN B. DANG, HAI-ANH H. 2017. *Mapping the World Population One Building at a Time*.

TRENDS 2020. Leaving no one off the map: a guide for gridded population data for sustainable development. Thematic Research Network on Data and Statistics.

TRIGG, M. A., BIRCH, C. E., NEAL, J. C., BATES, P. D., SMITH, A., SAMPSON, C. C., YAMAZAKI, D., HIRABAYASHI, Y., PAPPENBERGER, F., DUTRA, E., WARD, P. J., WINSEMIUS, H. C., SALAMON, P., DOTTORI, F., RUDARI, R., KAPPES, M. S., SIMPSON, A. L., HADZILACOS, G. & FEWTRELL, T. J. 2016. The credibility challenge for global fluvial flood risk analysis. *Environmental Research Letters,* 11**,** 10.

UNDRR 2015. Global Assessment Report 2015, Making Development Sustainable: The Future of Disaster Risk Management. Geneva: UN Office for Disaster Risk Reduction

VAN BEEK, L. P. H., WADA, Y. & BIERKENS, M. F. P. 2011. Global monthly water stress: 1. Water balance and water availability. 47.

WARD, P. J., JONGMAN, B., AERTS, J., BATES, P. D., BOTZEN, W. J. W., LOAIZA, A. D., HALLEGATTE, S., KIND, J. M., KWADIJK, J., SCUSSOLINI, P. & WINSEMIUS, H. C. 2017. A global framework for future costs and benefits of river-flood protection in urban areas. *Nature Climate Change,* 7**,** 642-+.

WARD, P. J., JONGMAN, B., WEILAND, F. S., BOUWMAN, A., VAN BEEK, R., BIERKENS, M. F. P., LIGTVOET, W. & WINSEMIUS, H. C. 2013. Assessing flood risk at the global scale: model setup, results, and sensitivity. *Environmental Research Letters,* 8**,** 10.

WARD, P. J., WINSEMIUS, H. C., KUZMA, S., BIERKENS, M. F. P., BOUWMAN, A., DE MOEL, H., DÍAZ LOAIZA, A., EILANDER, D., ENGLHARDT, J., ERKENS, G., TAFETE GEBTEMEDHIN, E., ICELAND, C., KOOI, H., LIGTVOET, W., MUIS, S., SCUSSOLINI, P., SUTANUDJAJA, E. H., VAN BEEK, R., VAN BEMMEL, B., VAN HUIJSTEE, J., VAN RIJN, F., VAN WESENBEECK, B., VATVANI, D., VERLAAN, M., TIGGELOVEN, T. & LUO, T. 2020. Aqueduct Floods Methodology. Wasington D.C.: World Resources Institute.

WEEDON, G. P., BALSAMO, G., BELLOUIN, N., GOMES, S., BEST, M. J. & VITERBO, P. 2014. The WFDEI meteorological forcing data set: WATCH Forcing Data methodology applied to ERA-Interim reanalysis data. 50**,** 7505-7514.

WEEDON, G. P., GOMES, S., VITERBO, P., SHUTTLEWORTH, W. J., BLYTH, E., ÖSTERLE, H., ADAM, J. C., BELLOUIN, N., BOUCHER, O. & BEST, M. 2011. Creation of the WATCH Forcing Data and Its Use to Assess Global and Regional Reference Crop Evaporation over Land during the Twentieth Century. *Journal of Hydrometeorology,* 12**,** 823-848.

WILLNER, S. N., OTTO, C. & LEVERMANN, A. 2018. Global economic response to river floods. *Nature Climate Change,* 8**,** 594-598.

WING, O. E. J., BATES, P. D., SAMPSON, C. C., SMITH, A. M., JOHNSON, K. A. & ERICKSON, T. A. 2017. Validation of a 30 m resolution flood hazard model of the conterminous United States. *Water Resources Research,* 53**,** 7968-7986.

WINSEMIUS, H. C., AERTS, J., VAN BEEK, L. P. H., BIERKENS, M. F. P., BOUWMAN, A., JONGMAN, B., KWADIJK, J. C. J., LIGTVOET, W.,

LUCAS, P. L., VAN VUUREN, D. P. & WARD, P. J. 2016. Global drivers of future river flood risk. *Nature Climate Change,* 6**,** 381-385.

WINSEMIUS, H. C., VAN BEEK, L. P. H., JONGMAN, B., WARD, P. J. & BOUWMAN, A. 2013. A framework for global river flood risk assessments. *Hydrology and Earth System Sciences,* 17**,** 1871-1892.

YAMAZAKI, D., DE ALMEIDA, G. A. M. & BATES, P. D. 2013. Improving computational efficiency in global river models by implementing the local inertial flow equation and a vector-based river network map. Water Resources Research.

YAMAZAKI, D., IKESHIMA, D., SOSA, J., BATES, P. D., ALLEN, G. H. & PAVELSKY, T. M. 2019. MERIT Hydro: A High-Resolution Global Hydrography Map Based on Latest Topography Dataset. *Water Resources Research,* 55**,** 5053-5073.

YAMAZAKI, D., IKESHIMA, D., TAWATARI, R., YAMAGUCHI, T., O'LOUGHLIN, F., NEAL, J. C., SAMPSON, C. C., KANAE, S. & BATES, P. D. 2017. A high-accuracy map of global terrain elevations. *Geophysical Research Letters,* 44**,** 5844-5853.

YAMAZAKI, D., KANAE, S., KIM, H. & OKI, T. 2011. A physically based description of floodplain inundation dynamics in a global river routing model. *Water Resources Research,* 47**,** 21.

YAMAZAKI, D., SATO, T., KANAE, S., HIRABAYASHI, Y. & BATES, P. D. 2014. Regional flood dynamics in a bifurcating mega delta simulated in a global river model. *Geophysical Research Letters,* 41**,** 3127-3135.

ZHOU, X., MA, W., ECHIZENYA, W. & YAMAZAKI, D. 2020. Uncertainty in flood frequency analysis of hydrodynamic model simulations. *Nat. Hazards Earth Syst. Sci. Discuss.,* 2020**,** 1-31.

ZISCHG, A. P. & BERMÚDEZ, M. 2020. Mapping the Sensitivity of Population Exposure to Changes in Flood Magnitude: Prospective Application From Local to Global Scale. 8.